Assessment of Cyclone Gabrielle and Mangawhai Flash Flood Report

Authors: Duc-Phuoc Vo, Yueyang Chen and Asaad Y. Shamseldin[1†]

Date: 18 June 2026

Client: Northland Regional Council

Project Ref: WRAF contract UOAX2312

[1†] Professor Asaad Y. Shamseldin passed away in February 2026.

Contents

List of Figures

List of Tables

Summary

Northland is New Zealand's most cyclone-prone region, experiencing increasingly frequent and severe cyclones over the past two decades. The region's unique geography and topography contribute to the complexity of storm occurrences, their impacts, and recovery processes. This was demonstrated again in early 2023 when a series of severe storms and floods caused widespread damage across Northland. Cyclone Gabrielle and the Mangawhai flash flood, which occurred just one week apart in February 2023, highlighted the region's vulnerability to significant damage and isolation. These events emphasise the urgent need for a deeper understanding of historical storm patterns to enhance resilience and recovery strategies in preparation for future extreme weather events.

The present study undertakes a statistical analysis of historical rainfall to address the urgency of developing a deeper understanding of historical storms and their impacts. First, a literature review is conducted to identify the key atmospheric circulation variables driving storms in Northland. Historical storm patterns are categorised based on event-based analysis to highlight their direction, duration, severity, and other parameters using weather radar, ground stations, and satellite data. Quantitative analyses estimate rainfall and flood flow for the February 2023 storms, both temporally and spatially, at regional and local scales.

This study uses ground station data across the region by applying event-based analysis to investigate several critical aspects of Northland's storm activity during Cyclone Gabrielle and Mangawhai flash flood. It seeks to determine whether patterns of storms can be identified for the region. Additionally, the project analyses whether Cyclone Gabrielle and the Mangawhai storm followed these patterns. The study focuses on understanding the physical impacts caused by these two events and identifying their unique characteristics.

Furthermore, the impacts of extreme rainfall in February 2023 on Northland's river flooding are quantified. The project also focuses on characterising Cyclone Gabrielle and the Mangawhai flash flood in detail, including mapping rainfall intensity and flood extent for both events. These efforts aim to provide a comprehensive understanding of the storms to inform better planning and resilience-building initiatives for Northland's future.

1. Introduction

In the past 100 years, the New Zealand climate has warmed by 1.1°C. New Zealand is experiencing more hot days and fewer cold days – the year 2021 was the warmest year on record, surpassing the previous record set in 2016 (MoE, 2018b). Higher temperatures change our physical environment and weather patterns, presenting new and greater risks to the wellbeing of people and communities and their ways of life, buildings and infrastructure, our natural environment, and the economy. Sea-level rise is accelerating, with an average rate of rise of 3.7 millimetres per year between 2006 and 2018 (Pearce et al., 2011). By 2100, the median sea-level rise in New Zealand is projected to increase by a further 0.44 metres on average under a low-emissions scenario and 0.83 metres on average under a high-emissions scenario (Masson-Delmotte et al., 2021). Under the worst scenario, the sea-level rise in New Zealand is projected to increase by 1.09 metres on average (Masson-Delmotte et al., 2021).

Extreme weather events, such as storms, heatwaves, and heavy rainfall, are likely to be more frequent and intense due to climate change (MoE, 2018b). Tropical cyclones are likely to have increased wind intensity and rainfall rates, becoming stronger and causing more damage. Projections indicate that New Zealand will have stronger, northeasterly airflows in summer and stronger westerlies in winter, particularly in the south of the South Island, affecting rainfall patterns at the same time (MoE, 2022). Natural hazard management has tended to be static and reactive, taking past events as a proxy for their future likelihood and consequences. Climate change is exacerbating the natural hazards we typically experience, making them more frequent and severe (MoE, 2022). Thus, understanding weather patterns is becoming increasingly important, especially given the impacts of climate change. The World Economic Forum has reported that natural disasters and extreme weather events are the second most severe global risk over the next two years and the third highest global risk over the next ten years (McLennan & Group, 2023).

Considering New Zealand's unique geographic location and climatic conditions, it is important to study storm patterns to improve disaster preparedness, and mitigation, tackle the storm changes under climate change, manage potential hazards to agriculture, protect forests and ecosystems, manage water resources (RSNZ, 2016), and protect indigenous and heritage sites. Several regions within New Zealand, including both North Island and South Island areas, are particularly vulnerable to storms due to their geographic location, topography, and proximity to the coast. Northland is among the

most affected regions because tropical and subtropical storms often hit this region due to its proximity to the subtropics (NRC, 2007). It is one of the first areas to experience the remnants of tropical cyclones, which can bring heavy rain, strong winds, and coastal flooding (CDP, 2023).

The Northland Region is the northernmost of New Zealand's 16 local government regions. The Northland Region occupies the northern 80% of the 330 kilometres long Northland Peninsula, with its southernmost boundary extending into the Auckland Region. It is bounded to the west by the Tasman Sea and to the east by the Pacific Ocean. The land is predominantly rolling hill country (Orange, 2015). It is New Zealand's most cyclone-prone region, with storms becoming more frequent and more severe in the past two decades (NIWA, 2002). The occurrence, frequency, and impacts of this type of extreme weather in Northland are complex due to its unique geography and topography. This was demonstrated in early 2023 by a series of storms and floods with different characteristics and damages at all levels (Trüdinger, 2023). Cyclone Gabrielle and Mangawhai flash flood in February 2023 (a week apart) highlighted how susceptible Northland is to damage and isolation (Olley, 2023). Without understanding the events and their history, effective recovery is not possible, nor is better resilience planning for future occurrence (Gray, 2003). In addition, understanding them is beneficial for climate change adaptation, disaster preparedness and mitigation, water resource management, and potential economic implications (Ferreira, 2024).

This project explores and investigates the cause, formation, and characteristics of events such as Cyclone Gabrielle and Mangawhai flash flood. Some researchers showed that it is essential to use high-resolution space-time rainfall fields provided by weather radars to properly analyse and understand cyclone and cyclone-induced flash flood events (Borga et al., 2008; Bouilloud et al., 2010). Others showed the importance of topography (Norbiato et al., 2009), geology, or the impact of hydraulic routing within the river network and geomorphological controls in understanding these events (Bonnifait et al., 2009). Depending on the conditions, one or several factors, including rainfall intensity and duration (Beven, 2012), land use and vegetation cover (Foley et al., 2005), and antecedent moisture conditions (Uber et al., 2018), can impact the hydrological response significantly. Thus, assessing cyclone and cyclone-induced flash flood susceptibility and understanding the processes further requires a multiple and cross-combined approach. It is important to combine various data sources, including in-situ (gauging station) and observation (satellite and radar), and multiple approaches to provide reliable analysis. By doing so, we can identify the cyclone and flash flood events and quantify the associated effects more quickly and comprehensively.

Furthermore, such work usually involves substantial efforts and inputs from various sectors, providing a platform for scientists, policymakers, and communities to collaborate effectively. Scientists and researchers can contribute valuable insights, such as probabilistic, uncertain, and hypothetical analyses, to support decision-making. Communities have more experience in understanding the role indigenous knowledge plays in facilitating disaster preparedness, risk mitigation and emergency management and so on. In turn, decision-makers can make quicker and more effective decisions in responding to emergencies, as well as in management, planning, and recovery management system development.

The main focuses of the report are to identify the storm patterns, analyse Cyclone Gabrielle and Mangawhai storms, assess their associated physical impacts, and characterise flash floods. The report is organised as follows: Section 2: Literature Review; Section 3: Methodology; Section 4: Identification of Atmospheric Circulation Variables and Categorisation of Historic Storm Patterns; Section 5: Analysis of February 2023 Storm Events; Section 6: Discussion; and Section 7: Conclusion.

2. Literature Review

2.1 Overview of New Zealand Climate

New Zealand is situated between latitudes 34° and 47° S within the prevailing westerlies. Coastal areas in New Zealand frequently experience strong winds, while inland regions generally have lighter breezes. Most areas of New Zealand have between 600 and 1,600 mm of rainfall spread throughout the year, with a dry period during the summer (NIWA, 2024k). Parts of the Southern Alps receive more than 10,000 mm of annual rainfall. In contrast, Central Otago, the country's driest region, records just about 350 mm annually due to sheltering from rain-bearing systems arriving from the west and north. In eastern and inland locations, more than two weeks of dry spells are quite common (Macara, 2015).

Temperatures across New Zealand are generally mild due to the moderating effect of the surrounding sea, which prevents extreme highs and lows. Mean annual temperatures range from 10°C in the south to 16°C in the north of New Zealand. Temperatures exceeding 30°C are not common for most locations nationwide. However, they occur reasonably frequently during summer in low-elevation inland areas and eastern parts of the country. July is generally the coldest month in New Zealand, whereas January and February are the warmest. Seasonal temperature variability is relatively limited across most of the country, although inland regions and areas located east of the mountain

ranges experience greater contrasts, with summer–winter temperature differences of up to 14°C. Temperatures drop by about 0.7°C for every 100 metres altitude (NIWA, 2024k).

Frosts are common in the cooler months for most of the country except for the north of Waikato. Nelson and Marlborough are typically New Zealand's sunniest regions, while parts of the Bay of Plenty receive similarly high sunshine hours (NIWA, 2019). Most of the snow in New Zealand falls in the mountain areas. Snow rarely falls in the coastal areas of the North Island and west of the South Island, although the east and south of the South Island may experience some snow in winter.

New Zealand is divided into six climate zones, taking into account climate data and territorial authority boundaries. **Figure 1** below shows the six climate zones. The climate of New Zealand is also summarised and detailed from the very north of the North Island to the southernmost point of the South Island by selecting locations throughout the country and grouping them into broad climate zones. A brief description of each region across New Zealand and its associated climate zone can be found in the coming sections of this report.

2.1.1 Northern New Zealand

Northern New Zealand is a sub-tropical climate zone, with warm humid summers and mild winters. Typical summer daytime maximum air temperatures range from 22°C to 26°C but seldom exceed 30°C. Winter daytime maximum air temperatures range from 12°C to 17°C. Annual sunshine hours average about 2,000 in many areas. Tauranga is much sunnier with at least 2,200 hours. Southwest winds prevail for much of the year. Sea breezes often occur on warm summer days. Winter usually has more rain and is the most unsettled time of year. In summer and autumn, storms of tropical origin may bring high winds and heavy rainfall from the east or northeast (NIWA, 2023b).

2.1.2 Central North Island

As Central North Island is sheltered by high country to the south and east, it has less wind than many other parts of New Zealand. Being inland, a wide range of temperature is experienced. Warm, dry and settled weather predominates during summer. Typical summer daytime maximum air temperatures range from 21°C to 26°C, rarely exceeding 30°C. Winters are cool and this is normally the most unsettled time of the year. Typical winter daytime maximum air temperatures range from 10°C to 14°C. Frosts occur in clear, calm conditions in winter. Sunshine hours average 2,000 to 2,100 in most places. Lake breezes often occur in Taupo and Rotorua on warm summer days (NIWA, 2024c).

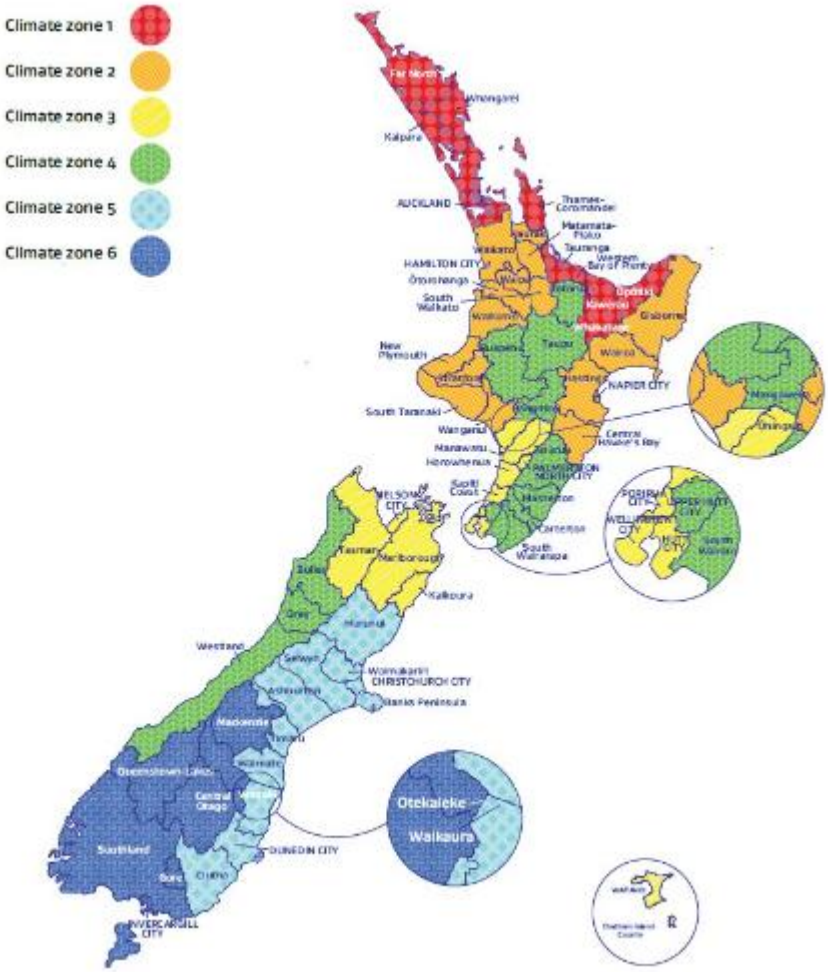

Figure 1: Six climate zones across New Zealand (MBIE, 2021)

2.1.3 South-West North Island

Due to its exposure to disturbed weather systems from the Tasman Sea, the climate zone of South-West North Island is often quite windy but has few climate extremes. The most settled weather occurs during summer and early autumn. Summers are warm. Typical summer daytime maximum air temperatures range from 19°C to 24°C, seldom exceeding 30°C. Winters are relatively mild in New Plymouth and Wanganui, but cooler in Palmerston North and Wellington. This is normally the most unsettled time of the year. Typical winter daytime maximum air temperatures range from 10°C to 14°C. Frost occurs inland during clear calm conditions in winter. Annual sunshine hours average about 2,000 hours, but inland at Palmerston North it is much cloudier. North-westerly airflows prevail. Sea breezes occasionally occur along the coast during summer (NIWA, 2024i).

2.1.4 Eastern North Island

Sheltered by high country to the west, this region enjoys a dry, sunny climate. Warm dry settled weather predominates in summer. Frosts may occur in winter. Typical summer daytime maximum air temperatures range from 20°C to 28°C, occasionally rising above

30°C. High temperatures are frequent in summer, which may be accompanied by strong dry foehn winds from the northwest. Extreme temperatures as high as 39°C have been recorded. Winter is mild in the north of this region and cooler in the south. Typical winter daytime maximum air temperatures range from 10°C to 16°C. Annual hours of bright sunshine average about 2,200 in Gisborne and Napier. Heavy rainfall can occur from the east or southeast. Westerly winds prevail. Sea breezes often occur in coastal areas on warm summer days (NIWA, 2024d).

2.1.5 Northern South Island

As much of this climate zone is sheltered by high country to the west, south and in some areas to the east, it is the sunniest region of New Zealand. Warm, dry and settled weather predominates during summer. Winter days often start with frost but are usually mild overall. Typical summer daytime maximum air temperatures range from 20°C to 26°C but occasionally rise above 30°C. Late winter and early spring are normally the most unsettled time of the year. Typical winter daytime maximum air temperatures range from 10°C to 15°C. Annual hours of sunshine average at least 2,300 hours. North-northeast winds prevail in Nelson, while southwesterlies prevail about Blenheim. Nelson has less wind than many other urban areas and its temperatures are often moderated by sea breezes. High temperatures are frequent in Blenheim and may be accompanied by foehn winds from the northwest (NIWA, 2024g).

2.1.6 Western South Island

The climate of Western South Island is greatly dependent on its exposure to weather systems from the Tasman Sea and the line of the Southern Alps to the east. Although mean annual rainfall is very high, dry spells do occur, especially in late summer and during winter. Heavy rainfall occurs from the northwest. Summers are mild. Typical summer daytime maximum air temperatures range from 17°C to 22°C and seldom exceed 25°C. Winter days often start with frost. Typical winter daytime maximum air temperatures range from 10°C to 14°C. North-northeast winds prevail along the coast in Westport and Hokitika while southwesterlies prevail in coastal areas further south. Sea breezes can occur on warm summer days (NIWA, 2024j).

2.1.7 Eastern South Island

The climate of Eastern South Island is greatly dependent on the lie of the massive Southern Alps to the west. Summer temperatures are warm, with the highest temperatures occurring when hot dry foehn north westerlies blow over the Alps and plains. Mean annual rainfall is low, and long dry spells can occur, especially in summer. For much of the time summer temperatures are moderated by a cool northeasterly sea breeze. Typical summer daytime maximum air temperatures range from 18°C to 26°C but

may rise to more than 30°C. A temperature of 42°C has been recorded in Christchurch. Winters are cold with frequent frost. Typical winter daytime maximum air temperatures range from 7°C to 14°C. Northeasterlies prevail about the coast for much of the year. Southwesterlies are more frequent during winter (NIWA, 2024e).

2.1.8 Inland South Island

The climate of Inland South Island is largely dependent on the lie of the Southern Alps to the west, but many areas are also sheltered by high country to the south and east. Mean rainfall is low, and long dry spells can occur, especially in summer. Summer afternoons are very warm, with high temperatures occurring when hot dry foehn north-westerlies blow over the Alps. Typical summer daytime maximum air temperatures range from 20°C to 26°C, occasionally rising above 30°C. Winters are very cold with frequent, often severe frosts, and occasional snowfalls. In severe cases, snow may lie for several days or longer. Typical winter daytime maximum air temperatures range from 3°C to 11°C. Wind flow is dependent on topography; however, the strongest winds are often from the northwest (NIWA, 2024f).

2.1.9 Mountainous and Alpine Regions

Mountainous areas are subject to heavy snowfalls, high winds, and low temperatures. Semi-permanent snow and ice fields exist at about 1,000-1,100 metres during winter. Anticyclones often bring settled weather in summer, but clear cold conditions in winter with severe frost. Winter and spring are usually more unsettled than summer and autumn (NIWA, 2024b).

2.1.10 Southern New Zealand

Most of this climate zone is characterised by cool coastal breezes and the absence of shelter from the unsettled weather that moves over the sea from the south and southwest. Hot north-westerly conditions in summer can occasionally bring high temperatures. Typical summer daytime maximum air temperatures range from 16°C to 23°C, occasionally rising above 30°C. Winters are cold with infrequent snowfall and frequent frost. Typical winter daytime maximum air temperatures range from 8°C to 12°C. Hours of bright sunshine average about 1,600 hours annually and are often affected by low coastal clouds or by high clouds in foehn wind conditions. South-westerlies prevail for much of the time about Southland, but north-easterlies are more frequent from Dunedin north (NIWA, 2024h).

2.2 Overview of Northland and its Climatology

The Northland Region is the northernmost of New Zealand's 16 local government regions. The climate in the Northland Region is mild throughout the year. It has an estimated

population of 203,900 as of June 2023 and the main population centre is the city of Whangārei; the largest town is Kerikeri. At the 2018 New Zealand census, Northland recorded a population growth rate of 18.1% since the previous 2013 census, placing it among the fastest-growing regions in New Zealand, ahead of other strong growth regions such as the Bay of Plenty Region (2nd with 15%) and Waikato (3rd with 13.5%) (Ali, 2019; Stats-NZ, 2020).

The Northland Region covers the northern 80% (265 kilometres) of the Northland Peninsula, with the southernmost section lying in the Auckland Region. The region features mostly rolling hill country bordered by the Tasman Sea to the west and the Pacific Ocean to the east. Farming and forestry dominate the landscape, accounting for more than half of the land use and serving as two of the region's key industries (Orange, 2015).

The western coast of Northland is characterised by long, straight beaches, most notably the famous Ninety Mile Beach, though it spans only 88 kilometres. Further south is the slightly longer Ripiro Beach. This coast is also home to two large inlets: the vast Kaipara Harbour in the south, shared with the Auckland Region, and the intricate inlets of Hokianga Harbour. In contrast, the east coast is more rugged, with numerous bays and peninsulas. Several large natural harbours are found here, including Parengarenga near the northern tip, Whangaroa Harbour, and the well-known Bay of Islands, extending down to Whangārei Harbour, where the region's largest population centre is located. The coastline is dotted with many islands, such as the Cavalli Islands, Hen and Chicken Islands, Aorangaia Island, and the Poor Knights Islands (Orange, 2015).

Due to Northland's latitude, the tracks of anticyclone centres moving across New Zealand often pass to the south of the region. As a result, winds tend to shift to the southeast after a trough moves through and as the next anticyclone approaches. Once the anticyclone shifts east and a new trough nears, the winds turn northeast. These northeast winds travel over warm ocean waters to the north of New Zealand, becoming very moist. As the air cools when moving southward over the sea, cloud formation occurs, and upward motion from the trough often leads to rain. In some cases, subtropical depressions form in these troughs and move close to Northland, bringing heavy rainfall. When anticyclones pass north of New Zealand, the following trough often brings a wind shift from north-westerly to south-westerly. The cold fronts in these troughs tend to bring less rain to Northland compared to areas further south (Chappell, 2013).

Tropical cyclones that reach Northland with extremely low pressure and hurricane-force winds are quite rare. However, other storms of tropical origin, even if they never fully develop into cyclones, impact Northland about once or twice a year, mostly between

December and April. These storms typically bring heavy rain and strong easterly winds (Chappell, 2013).

According to NIWA's regional report, there are four main characteristic weather sequences in Northland. They are fine weather spells, brief periods of rain, showery weather and prolonged rainfall (Chappell, 2013).

A prolonged period of fine weather, lasting five days or more, often occurs when a large anticyclone slowly moves over the Northland region. For instance, if the centre of an anticyclone settles over the South Island, with a ridge of high pressure extending north or northwest from its centre, Northland can experience clear skies. In summer, Northland sometimes enjoys two to three weeks of mostly fine weather due to a process called anticyclone replacement. In this process, an anticyclone becomes stationary east of Australia and gradually weakens (Chappell, 2013). A cold front then moves along the southern edge of the anticyclone and crosses New Zealand, bringing cloud cover but little or no rainfall. As the original anticyclone fades, it is replaced by another, repeating the cycle. This process can continue for several cycles, resulting in long stretches of fine weather in Northland. During these periods, temperatures are normal or slightly above normal, except for brief interruptions caused by weak fronts (Chappell, 2013).

When a cold front oriented northwest to southeast crosses Northland, it is typically preceded by north to northwest winds and followed by south-westerlies. In such cases, rainfall is usually brief and often light. Conversely, when a depression forms in the trough between two anticyclones and moves over central and southern New Zealand, Northland experiences brief rainfall that may be heavier (Chappell, 2013).

Prolonged periods of changeable weather, featuring frequent and sometimes heavy showers, typically arise from two main scenarios. The first is that, following the passage of a depression or cyclonic storm that moves over Northland from the northwest or west, the region may experience cold conditions with moderate to fresh south-westerly or southerly winds, accompanied by frequent showers that can last for two to three days. The second case is when an anticyclone is situated well to the south of Northland, the region may be subject to prolonged easterly winds. In such cases, a trough of low pressure can develop to the north of Northland. The winds to the east of the trough are typically northeast, while those to the west are south-easterly. Once established, these troughs tend to move slowly, resulting in several days of showery weather in Northland, with rainfall generally higher in the east than in the west (Chappell, 2013).

Most prolonged periods of rain in Northland occur when a stationary anticyclone is located to the east or southeast of New Zealand. These anticyclones are often elliptic in

shape, with their major axis extending far to the north or northeast of the country. Under these conditions, warm, moist air flows from low latitudes over Northland. When this flow is lifted by vertical motion associated with a trough in the northern Tasman Sea, it can result in several days of rainfall, with totals often reaching up to 100 mm or more (Chappell, 2013).

The airflow over Northland predominantly comes from the southwest, especially during winter and spring. However, in summer, the proportion of winds from the easterly quarter, particularly in eastern districts, nearly matches that of the southwest. This shift is due to the seasonal movement of the high-pressure belt, which is positioned further south in summer and early autumn compared to winter and spring. Additionally, sea breezes contribute to the increase in easterly winds in eastern areas during summer and early autumn. Table 1 below shows the mean annual wind frequencies based on hourly surface wind observations from selected stations (Chappell, 2013). Mean wind speed data (calculated as the average speed over the 10 minutes before each hour) is available for several sites in Northland, highlighting the region's diverse wind patterns. Exposed coastal areas tend to be very windy, with some of the highest mean annual wind speeds in New Zealand. For instance, Cape Reinga and Mokohinau Islands report mean annual wind speeds of around 30 km/h. Locations like Kaitaia Airport, which are somewhat sheltered but still exposed to most winds, typically experience speeds between 15 and 20 km/h. Conversely, inland and sheltered areas, such as Kaikohe and Kerikeri, are among the least windy, with mean annual wind speeds of about 10 km/h. Table 1 below presents the mean monthly wind speeds for selected Northland stations (Chappell, 2013).

Table 1: Mean monthly and annual wind speed (km/hr) (Chappell, 2013)

Location	Jan	Feb	Mar	Apr	May	Jun	Jul	Aug	Sep	Oct	Nov	Dec	Ann
Cape Reinga	29	28	28	29	32	34	33	33	30	32	30	28	31
Kaitaia Airport	16	15	15	15	15	16	17	16	17	18	17	16	16
Kaikohe AWS	11	10	10	9	10	11	12	12	13	14	13	12	11
Kerikeri EWS	7	7	6	6	6	7	7	7	7	8	8	7	7
Whangarei Airport	12	12	11	10	10	10	11	11	12	13	13	12	11
Mokohinau Islands	24	24	24	25	28	30	31	29	27	28	28	25	27

Northland is a narrow peninsula, with no area more than 50 kilometres from the sea, resulting in moist winds and abundant rainfall across the region. Rainfall distribution is

closely tied to the area's orography: low-lying coastal areas receive around 1,000 mm of rain annually, while higher elevations can receive up to 2,000 mm. Figure 2 illustrates the distribution of median annual rainfall based on data from the 1981–2010 period. Seasonal influences on rainfall are also well-defined. Table 2 shows the monthly rainfall normal and percentages of the annual total for selected stations during the 1981–2010 period. The northern and eastern parts of the region receive 35 to 40 percent of their annual rainfall between June and August (winter months), while southern and western areas receive around 30 to 35 percent during these winter months. In contrast, 18 to 20 percent of Northland's annual rainfall occurs during the summer months (December to February) (Chappell, 2013).

One of the most notable features of Northland's rainfall pattern is its significant variability from month to month and year to year. This variability is often measured using the coefficient of variation, which is the ratio of the standard deviation to the mean, expressed as a percentage. Table 3 presents the seasonal and the annual rainfall variability for various stations across Northland, along with selected sites from other regions for comparison.

Table 2: Monthly/annual rainfall normal (a; mm); percentage of annual total for each month (b; %) (Chappell, 2013)

Location		Jan	Feb	Mar	Apr	May	Jun	Jul	Aug	Sep	Oct	Nov	Dec	Ann
Cape Reinga Aws	a	58	65	56	109	96	103	128	95	85	61	57	76	988
	b	6	7	6	11	10	10	13	10	9	6	6	8	
Kaitaia Observatory	a	85	93	81	96	135	151	169	144	128	99	87	100	1367
	b	6	7	6	7	10	11	12	11	9	7	6	7	
Kaitaia Aero Ews	a	69	121	86	119	138	125	136	104	93	93	73	99	1253
	b	5	10	7	9	11	10	11	8	7	7	6	8	
Kaeo Northland	a	88	102	120	140	144	169	200	170	148	113	102	100	1596
	b	6	6	8	9	9	11	12	11	9	7	6	6	
Rawene 2	a	78	72	89	98	128	145	164	142	118	91	83	91	1299
	b	6	6	7	8	10	11	13	11	9	7	6	7	
Opononi	a	86	65	93	94	124	144	133	116	105	93	92	88	1234
	b	7	5	8	8	10	12	11	9	8	8	7	7	
Kaikohe Aws	a	110	106	109	140	139	152	188	159	124	100	96	109	1532
	b	7	7	7	9	9	10	12	10	8	6	6	7	
Kerikeri Airport	a	122	117	138	145	154	185	205	182	162	127	114	123	1775
	b	7	7	8	8	9	10	12	10	9	7	6	7	
Russell	a	91	87	116	117	130	144	172	146	121	97	89	90	1400
	b	7	6	8	8	9	10	12	10	9	7	6	6	
Waipoua Visitor Centre	a	89	82	103	97	146	177	166	153	132	110	93	94	1443
	b	6	6	7	7	10	12	11	11	9	8	6	7	
Whangarei Airport	a	78	98	117	103	110	132	169	127	110	84	76	97	1300
	b	6	8	9	8	8	10	13	10	8	6	6	7	
Dargaville 2	a	64	69	102	107	97	121	141	109	109	82	63	74	1137
	b	6	6	9	9	9	11	12	10	10	7	6	7	

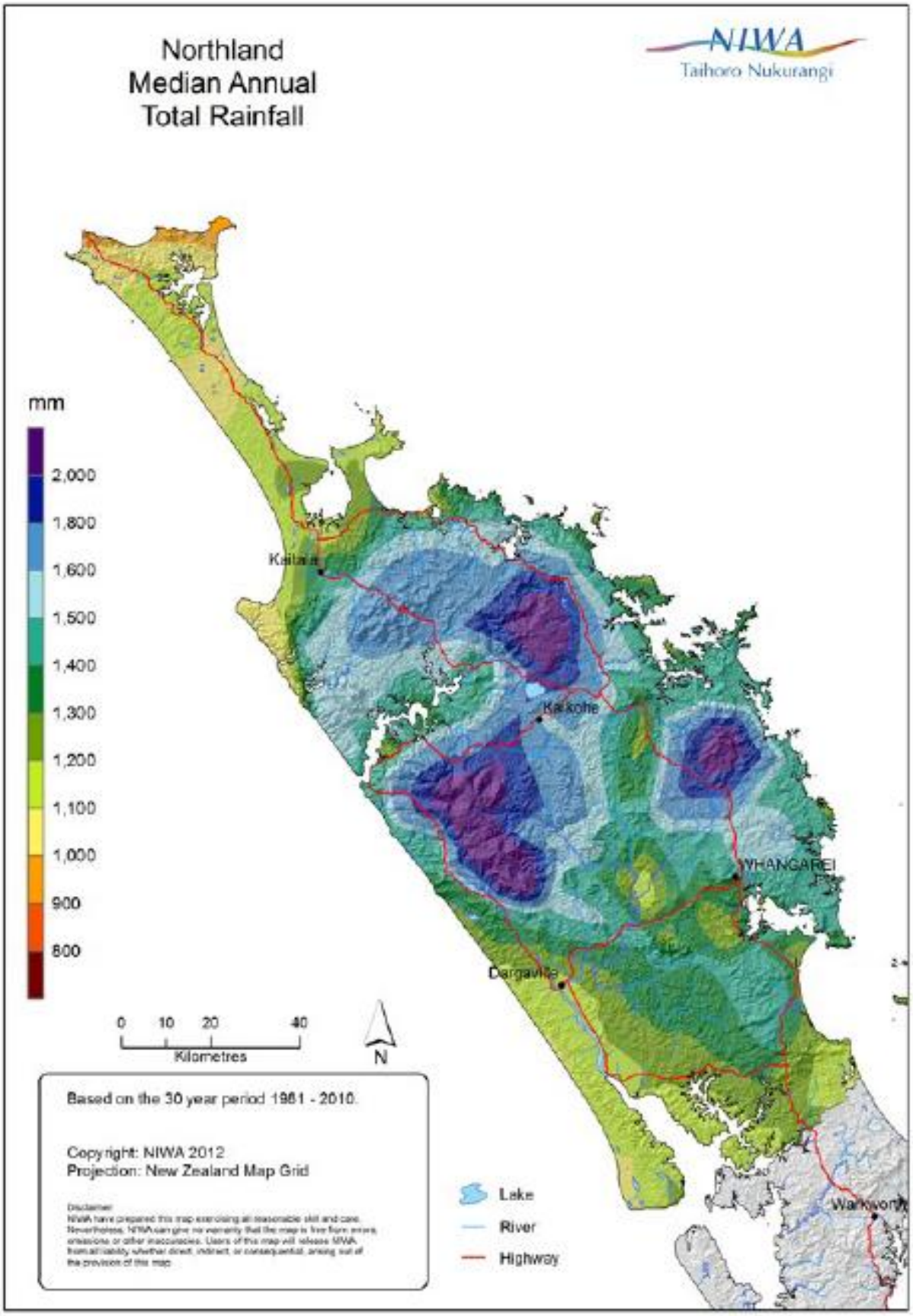

Figure 2: Northland median annual rainfall, 1981-2010 (Chappell, 2013)

Table 3: Seasonal variability of rainfall (Coefficient of variation) (Chappell, 2013)

Location	Summer	Autumn	Winter	Spring
Cape Reinga	46	75	25	45
Kaitaia Observatory	41	34	24	19
Kaeo Northland	50	45	30	31
Rawene 2	42	32	29	25
Kaikohe AWS	47	45	38	33
Kerikeri EWS	46	39	28	32
Waipoua Visitor Centre	42	25	23	31
Whangarei Aero AWS	37	41	33	31
Dargaville 2	37	21	24	17
Auckland	47	24	27	25
Wellington	42	38	30	36
Christchurch	37	27	42	32
Westport	24	28	20	17

Mean annual temperatures in Northland range from around 15.5°C to 16.5°C on the Aupouri Peninsula, north of Kaitaia, and between 14°C and 16°C in other areas. The region north of Auckland City has the highest mean annual temperatures in New Zealand. Although other parts of the country may experience higher temperatures in February, no area south of Auckland has higher mean July temperatures. Figure 3 below illustrates the median annual average temperature for Northland based on data from 1981–2010 (Chappell, 2013).

Solar radiation data is available for several locations in Northland, including Kaitaia, Kaikohe, and Whangārei, covering the 1981–2010 normal period. Solar insolation reaches its peak during December and January, while it is at its lowest in June. Table 4 presents the mean daily solar radiation for each month at these three stations (Chappell, 2013).

Table 4: Mean daily global solar radiation (MJ/m^2/day). (Chappell, 2013)

Location	Jan	Feb	Mar	Apr	May	Jun	Jul	Aug	Sep	Oct	Nov	Dec	Ann
Kaitaia Observatory	21.7	19.4	16.4	11.6	8.5	7.0	7.7	10.1	13.5	16.9	19.9	22.1	14.5
Kaikohe AWS	20.5	18.2	15.3	11.0	8.2	7.1	7.5	9.8	13.3	16.5	19.2	20.6	13.9
Whangarei Aero AWS	21.4	18.2	15.5	11.1	8.2	7.0	7.4	10.1	13.6	17.0	19.6	20.4	14.1

2.3 Overview of Atmospheric Circulation Variables Influencing Storms

Atmospheric circulation refers to the large-scale movement of air across the planet, playing a crucial role in the distribution of heat and the formation of storm systems. This process governs how thermal energy and weather patterns shift across the Earth's surface (NOAA, 2023). In the absence of factors such as the Earth’s rotation, axial tilt, and surface water, global circulation would be straightforward. With the Sun positioned directly above the equator, the ground and atmosphere in this region would warm more

intensely than elsewhere. This would lead to a continuous belt of rising warm air, generating low pressure around the equator (Lutgens & Tarbuck, 1998). The warm air would then flow directly northward toward the poles, cooling as it travelled and eventually sinking to form high-pressure zones near the poles. The resulting temperature and pressure differences would drive the cold air back toward the equator, creating a basic global circulation pattern (NOAA, 2023).

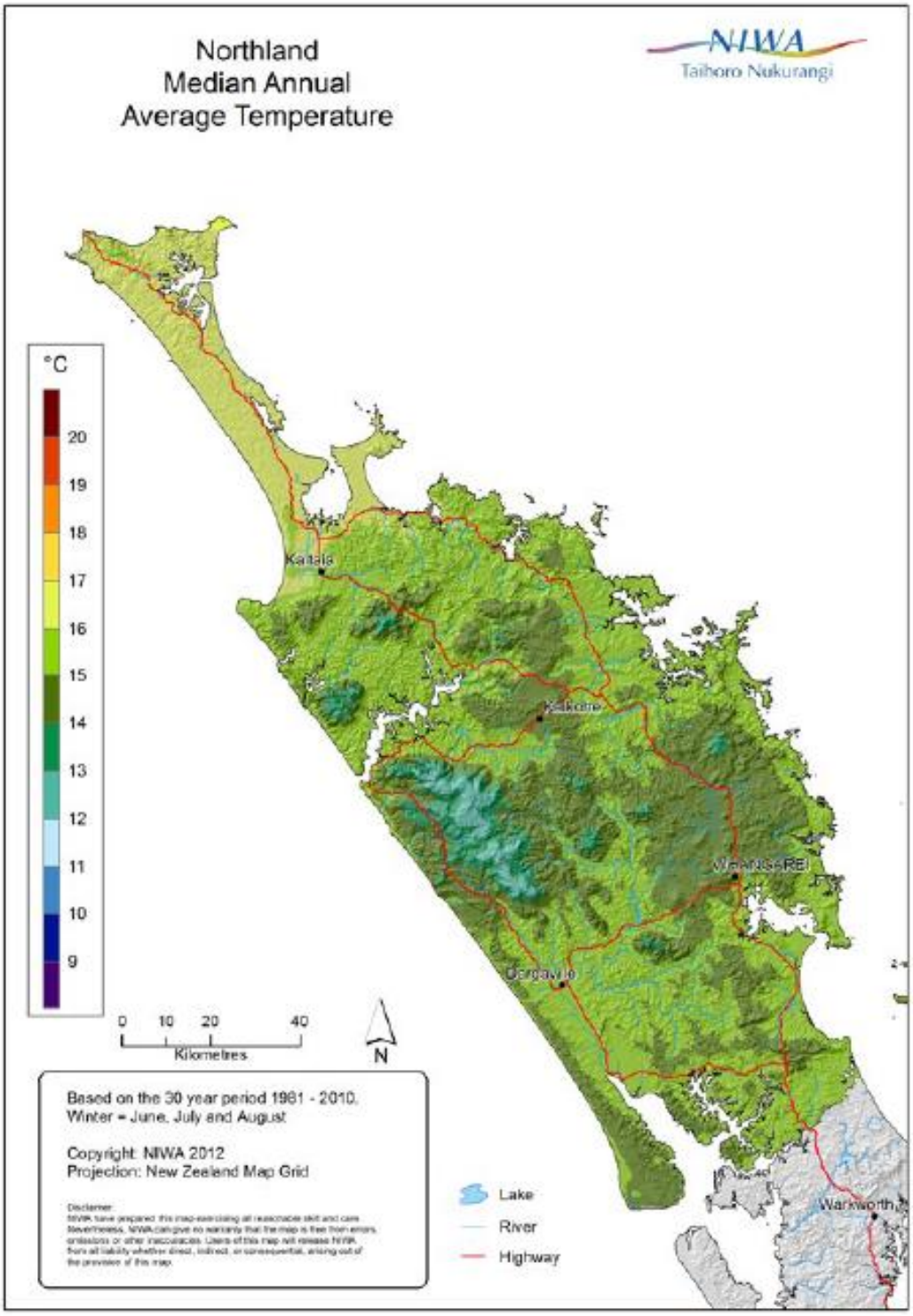

Figure 3: Northland median annual average temperature, 1981-2010. (Chappell, 2013)

Solar radiation that reaches Earth passes through the atmosphere, where it is either absorbed or reflected by the atmosphere and the planet's surface. Most absorption occurs at the Earth's surface, heating the land and water. A small amount of heat is transferred to the first few centimetres of the atmosphere through conduction, the process by which energy is transferred through molecular collisions. However, because air molecules are spaced farther apart than those in liquids or solids, they collide less frequently, making air a poor conductor of heat. Instead, most heat in the atmosphere is transferred via radiation and convection. When sunlight is absorbed by the Earth's surface, it is re-radiated as heat, warming the atmosphere from the bottom up. Greenhouse gases in the atmosphere absorb and re-radiate this heat, leading to the greenhouse effect (Wallace & Hobbs, 2006). As warm air expands and becomes less dense than cool air, it rises, while cooler air sinks and moves horizontally to replace the rising warm air. This movement, experienced as wind, results from the transfer of heat due to density differences in the air, known as convection (Lutgens & Tarbuck, 1998).

The major atmospheric circulation patterns in the tropics (between latitudes of 30°N and 30°S) are driven by convection, as areas near the equator receive more sunlight than higher latitudes. The resulting Hadley Cells transport heat and moisture away from the equator toward the poles. Earth's rotation further complicates air movement patterns. Air moving from the equator toward the poles is deflected due to the Coriolis effect, adding complexity to global atmospheric circulation. Variations in solar radiation absorption and heat re-radiation create temperature differences in the air over different terrains. For example, sea breezes arise because land heats and cools faster than water, causing air to flow inland from the sea during the day and reverse direction at night as the land cools more quickly than the ocean (Lutgens & Tarbuck, 1998).

Atmospheric circulation plays a crucial role in heat transport across Earth's surface, impacting the water cycle by influencing cloud formation and precipitation. These air mass movements shape our daily weather, while long-term circulation patterns influence regional climates and ecosystems. Wind-driven surface ocean currents also transport heat, and changes in atmospheric and ocean circulation, driven by human-induced increases in greenhouse gases, are altering environments worldwide (California, 2024). Storm formation, development, and behaviour are highly influenced by atmospheric circulation variables. Some key variables impacting storms include pressure systems, jet streams, wind shear, Coriolis effect, humidity and moisture content, temperature gradients, sea surface temperature (SST), atmospheric instability, tropical waves and disturbances, monsoonal winds, and El Niño-La Niña (ENSO) (Ahrens, 2007). The following paragraphs will illustrate the variables in detail.

Low-pressure systems are typically associated with storm formation. In these areas, air rises, cools, and condenses, leading to cloud formation and precipitation. High-pressure systems are usually linked to fair weather, as they suppress vertical air movement, which inhibits storm development (Lutgens & Tarbuck, 1998).

Jet streams are fast-moving air currents found in the upper levels of the atmosphere. They influence the movement and intensity of storm systems, steering them across the globe. A strong jet stream can deepen a storm system, leading to more intense storms, while a weaker jet stream might slow storm development (Holton, 2004). Wind shear is the change in wind speed and/or direction with height. It can either enhance or inhibit storm development. Vertical wind shear is particularly important for the formation of severe thunderstorms and tropical cyclones. Too much shear can tear a storm apart, but moderate shear can help storms organise and intensify (Ahrens, 2007). The Coriolis effect is caused by Earth's rotation and influences the direction of wind and storm systems. It causes storms to rotate counterclockwise in the Northern Hemisphere and clockwise in the Southern Hemisphere. This effect is crucial for the development of large-scale storm systems, like cyclones, by helping air circulate around low-pressure centres (Wallace & Hobbs, 2006).

Storms rely on moisture in the atmosphere to develop. Higher humidity levels provide more fuel for storms, leading to more intense precipitation and storm development. The latent heat release from the condensation of water vapor into clouds plays a significant role in powering storms, especially tropical cyclones (Trenberth et al., 2015). Temperature differences between different regions create pressure gradients that drive winds and atmospheric circulation. The contrast between warm and cold air masses (such as in frontal systems) can trigger storms. For example, warm air rising over cold air can lead to thunderstorms and cyclogenesis (storm formation) (Bluestein, 1992). Warmer sea surface temperatures (SST) provide more energy for tropical storms and hurricanes. Storms feed off the heat and moisture from warm ocean waters. Increases in SST are directly linked to the intensity and duration of tropical storms (Emanuel, 1987). Instability in the atmosphere, where warmer air lies below cooler air, allows for strong updrafts and the development of storms. Convective available potential energy (CAPE) is a measure of atmospheric instability, and higher CAPE values are associated with stronger storms (Holton, 2004). Tropical waves or disturbances often serve as the seeds for tropical storm formation. These are areas of low pressure with increased thunderstorm activity that can develop into larger storm systems under the right conditions. In certain regions, seasonal monsoon winds bring changes in atmospheric circulation patterns that lead to periods of heavy rainfall and storm formation (Wang & LinHo, 2002).

2.4 Key Variables Driving Northland Storms

The Northland region of New Zealand is influenced by several atmospheric circulation variables that impact its climate and weather patterns. Some of the most significant variables include westerly winds, band of subtropical anticyclones, El Niño-Southern Oscillation, Southern Annular Mode, tropical cyclones, Tasman Sea temperatures and blocking highs (Salinger & Mullan, 1999). The band of subtropical anticyclones and the westerly band dominate weather and climate in this region. Westerly winds, especially those associated with the mid-latitude westerly wind belt, significantly impact Northland. These winds can bring moist air from the Tasman Sea, leading to precipitation, especially when interacting with topography. On the other hand, the tracks of anticyclone centres crossing New Zealand which are often to the south of the region may lead the region to experience settled, dry, and warm conditions (Chappell, 2013).

In the Northland region of New Zealand, rainfall is primarily influenced by four key mechanisms. Rainfall can result from uplift within cold fronts, which are common during periods of disturbed westerlies and are often accompanied by occasional depressions and unstable post-frontal airstreams (Salinger, 1980). The region's topography plays a significant role, with orographic uplift greatly enhancing rainfall on the windward sides of mountain ranges (Griffiths, 2007). Additionally, during the summer months, the heating of dry inland and eastern regions can generate enough convection to trigger cumulus cloud development, leading to showers (Chappell, 2013; Griffiths, 2007). Lastly, subtropical depressions, characterised by a complex interaction of warm and cold fronts, frequently drift across New Zealand, contributing to the region's diverse rainfall patterns (Griffiths, 2011).

Northland's weather patterns are significantly shaped by various atmospheric circulation factors. For instance, atmospheric rivers (ARs), which are narrow corridors of concentrated moisture, can lead to intense rainfall and flooding, especially when they coincide with cyclones (Ummenhofer et al., 2009). The El Niño-Southern Oscillation (ENSO) also plays a crucial role, with El Niño typically bringing stronger westerly winds and drier conditions, while La Niña results in more easterly winds and increased rainfall (Mosley, 2000; Ummenhofer et al., 2009). The Southern Annular Mode (SAM) further influences the region, with positive phases bringing more stable weather, and negative phases leading to more stormy conditions (Thompson, 2006). Additionally, tropical cyclones, although often on the periphery of Northland, can bring heavy rainfall and strong winds, with their impact potentially intensified by the presence of atmospheric rivers (NIWA, 2024l).

The interaction between low-pressure systems (troughs) and high-pressure systems (anticyclones) significantly influences storm development (Kidson, 2000). Troughs can bring unstable air and precipitation, while anticyclones typically lead to settled weather (Griffiths, 2011; Kidson, 2000). Additionally, the temperatures of surrounding waters, particularly the Tasman Sea and Pacific Ocean, play a crucial role. Warmer sea surface temperatures can enhance storm intensity by providing more moisture and energy to the atmosphere (Rampal et al., 2022).

Tropical cyclones are rotating storms that originate in tropical regions. In the southwest Pacific and Indian Ocean, they are called tropical cyclones. In the Southern Hemisphere, these storms rotate clockwise. Tropical cyclones form near the equator and derive their energy from the heat released when water vapor condenses into rain (Terry, 2007). Typically, they span about 500 kilometres and feature a central area known as the "eye," where clouds are sparse, and winds are light. As these cyclones approach New Zealand, they tend to weaken due to cooler sea temperatures, which provide less heat (NIWA). The most severe cyclones usually occur between December and April, as autumn brings higher sea surface temperatures that allow the storms to maintain their intensity, increasing the likelihood of interacting with cold air fronts from Antarctica. As the atmosphere attempts to balance pressure differences, winds develop, blowing from areas of high pressure to low pressure. When air reaches the centre of a low-pressure area, it is forced upward into the colder atmosphere, causing water vapor to condense into rain. Northland is occasionally affected by tropical cyclones, especially during the Southern Hemisphere summer. The path and intensity of these cyclones can bring heavy rainfall and strong winds (NIWA, 2024l).

Local conditions also make a significant contribution to forming precipitation in the area. The region's rolling hills and mountainous terrain play a significant role in enhancing rainfall through orographic lift, where moist air is forced to rise over elevated areas, causing increased precipitation (Griffiths, 2011). Atmospheric moisture, influenced by prevailing winds and oceanic conditions, is also critical for storm development, with high humidity often leading to more intense storms and rainfall. Winds, especially from the northeast, can carry additional moisture into the region, intensifying storm activity. Climate change further contributes to these dynamics, leading to more frequent and severe weather patterns, altering historical norms, and increasing the risk of flooding (Griffiths, 2007; Payne et al., 2020). Additionally, in the summer months, localised heating can trigger convection, leading to thunderstorms. These storms often produce intense, localised heavy rainfall, particularly in the afternoons.

2.4.1. El Niño-Southern Oscillation (ENSO)

Rainfall in the Northland Region has a strong correlation with global climate drivers. An investigation into local precipitation (as represented by Standardised Precipitation Index, SPI) and global climate drivers (as represented by the Southern Oscillation Index, SOI) (Mosley, 2000) has been conducted in the region. SOI fluctuations have a noticeable impact on the standardised precipitation index (SPI), consistent with established climate phenomena where El Niño and La Niña influence regional rainfall patterns.

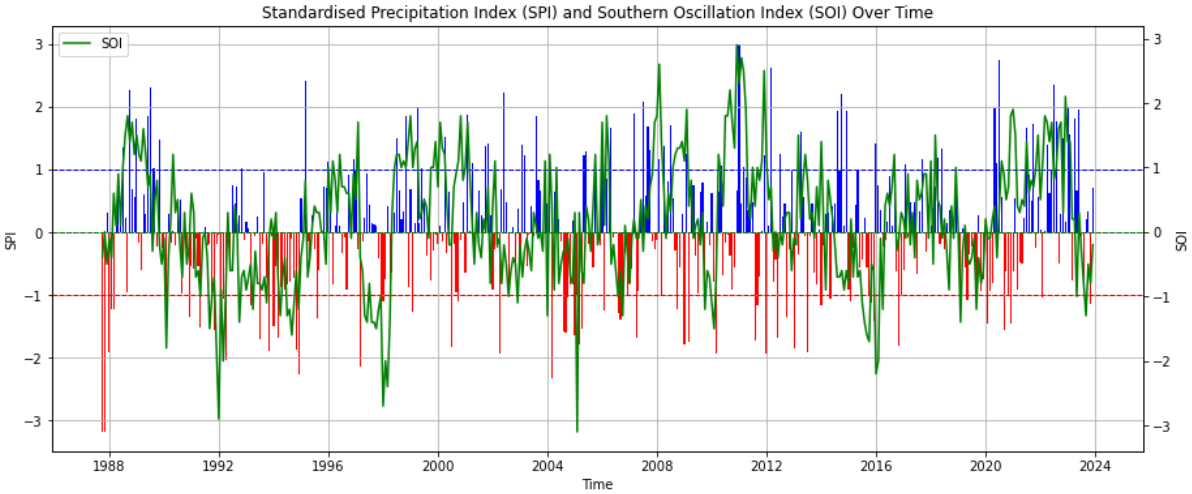

Figure 4: Standardised Precipitation Index (SPI) and the Southern Oscillation Index (SOI) from 1988 to 2023 at Hatea at Glenbervie Forest. The SPI values are depicted as bars, where blue bars represent positive SPI values (above-average precipitation) and red bars represent negative SPI values (below-average precipitation or drought conditions). The SOI values are shown as a green line, with higher values typically indicating La Niña conditions and lower values indicating El Niño conditions (Source: https://www.cpc.ncep.noaa.gov/data/indices/soi)

Figure 4 effectively illustrates the interplay between Southern Oscillation Index fluctuations and Standardised Precipitation Index (SPI) over time. There has been a correlation between SPI and SOI, where positive SOI values (La Niña conditions) are often associated with positive SPI values (wetter conditions), and negative SOI values (El Niño conditions) with negative SPI values (drier conditions). This relationship appears consistent throughout the timeline, indicating that large-scale climate patterns like El Niño and La Niña significantly influence local precipitation as measured by SPI.

2.4.2 Atmospheric River

Precipitation in the region has been significantly impacted by Atmospheric Rivers. Atmospheric Rivers (ARs) are narrow corridors of concentrated moisture in the atmosphere, often likened to "rivers in the sky" (Guan & Waliser, 2015; Zhu & Newell, 1998). They typically form when warm, moist air from tropical or subtropical regions is transported by strong winds toward mid-latitudes (Gimeno et al., 2014). The vast majority of total annual rainfall in the region has been correlated with the landfall of ARs (Shu et al., 2021). The trend is most significant in the east side of the region following the

movement of extratropical cyclones (Shu et al., 2021). ARs events have contributed over 40 percent of the total rainfall in the region (see Figure 5). The alternation between years dominated by AR or Non-AR rainfall suggests that the influence of AR events on annual precipitation is not constant and may be influenced by broader climatic patterns or localised weather conditions. In several years, AR events contribute over 50% of the annual rainfall, indicating their importance in driving extreme precipitation in certain periods. These years may correspond to seasons with strong AR activity, possibly influenced by large-scale atmospheric conditions such as El Niño or La Niña events (Diamond et al., 2013).

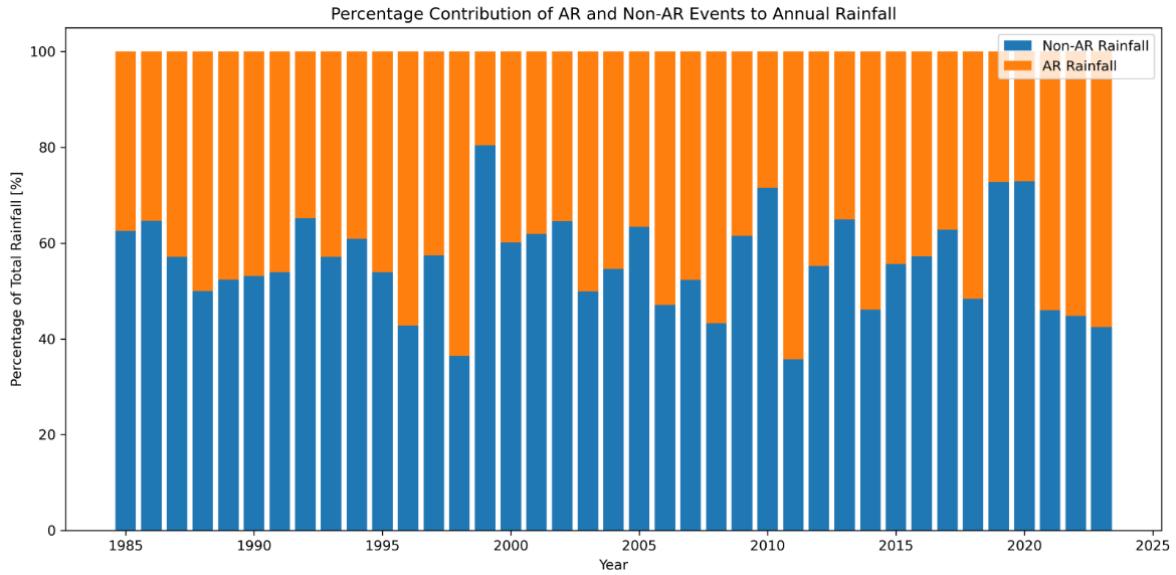

Figure 5: Annual percentage contribution of Atmospheric River (AR) (orange) events and Non-AR events (blue) to total rainfall over the years

ARs have significantly contributed to heavy rain. We subsequently investigated the majority of rainfall events to identify the predominant weather regimes responsible for heavy rainfall in the Northland region. By tracing these events back through historical records and correlating them with various sources of investigation, we discovered that most extreme rainfall events in the Northland region are associated with atmospheric rivers (ARs). This finding is consistent with previous research which emphasised the contribution of AR to intense rainfall in the region (Reid et al., 2021). Table 5 shows the total rainfall (in mm) for the ten heaviest precipitation events recorded at three stations, along with the correlation of Atmospheric Rivers (ARs) identified as true (i.e., ARs present for over 50% of the event duration) and correlation between ARs. The results indicate that many extreme events at selected rainfall gauging stations in the region are associated with ARs. Notably, all of the top three extreme events at these stations were linked to ARs.

Table 5. Summary of influence of ARs to heavy rain in three stations in the Northland region.

Hatea at Glenbervie Forest		Okarika at Rowland Rd		Waitangi at McDonald Road	
Total Rainfall [mm]	AR Correlation	Total Rainfall [mm]	AR Correlation	Total Rainfall [mm]	AR Correlation
341.5	TRUE	214.0	TRUE	350.0	TRUE
340.6	TRUE	206.0	TRUE	276.0	TRUE
334.5	TRUE	201.4	TRUE	232.5	TRUE
315.7	FALSE	184.1	TRUE	221.4	TRUE
298.0	TRUE	164.7	FALSE	203.0	TRUE
257.0	TRUE	155.9	FALSE	200.0	TRUE
254.8	TRUE	153.1	FALSE	197.5	TRUE
239.0	TRUE	151.5	TRUE	189.5	TRUE
229.1	TRUE	148.0	TRUE	186.5	TRUE
228.2	TRUE	147.7	TRUE	182.0	FALSE

2.4.3. Tropical Cyclone

Northland, located in latitudes between 34° S and 36° S, is frequently struck by tropical cyclones that have caused severe damage to the region. Between 1985 and 2023, a total of 65 tropical cyclones affected the Northland region, highlighting its exposure to these events (Knapp et al., 2018; Knapp et al., 2010). They usually bring heavy rain and strong easterly winds. Cyclones such as Gabrielle (2023), Bola (1988), and Pam (2015) have led to significant damage to the Northland Region Tropical cyclones are revolving storms that begin in the tropics (Harrington et al., 2023). These tropical cyclones form near the equator and gain their energy from the heat that is released when water vapour condenses into rain. They are about 500 km in width and may have a central region with relatively little cloud and light winds called the eye. In the tropical region, these tropical cyclones often travel from east to west before curving southward toward New Zealand.

Tropical cyclones weaken as they move towards New Zealand because the cooler seas provide less heat and moisture. However, the strength of these storms still leads to much damage to Northland Region (NIWA, 2024l). The worst cyclones usually occur from December to April (Chandra & Kumar, 2021). In autumn, the sea surface temperatures remain high, allowing the tropical cyclones to retain their intensity, and the chance of meeting a cold air front from the Antarctic increases as autumn progresses. Tropical cyclones that reach Northland and still retain very low pressures and hurricane force winds are very rare. However, other storms of tropical origin (which may never have been fully developed tropical cyclones) affect Northland about once or twice each year, mainly between December and April (Terry, 2007). Figure 6 shows tropical storms that have influenced Northland Region (in a buffer zone of 5 degrees).

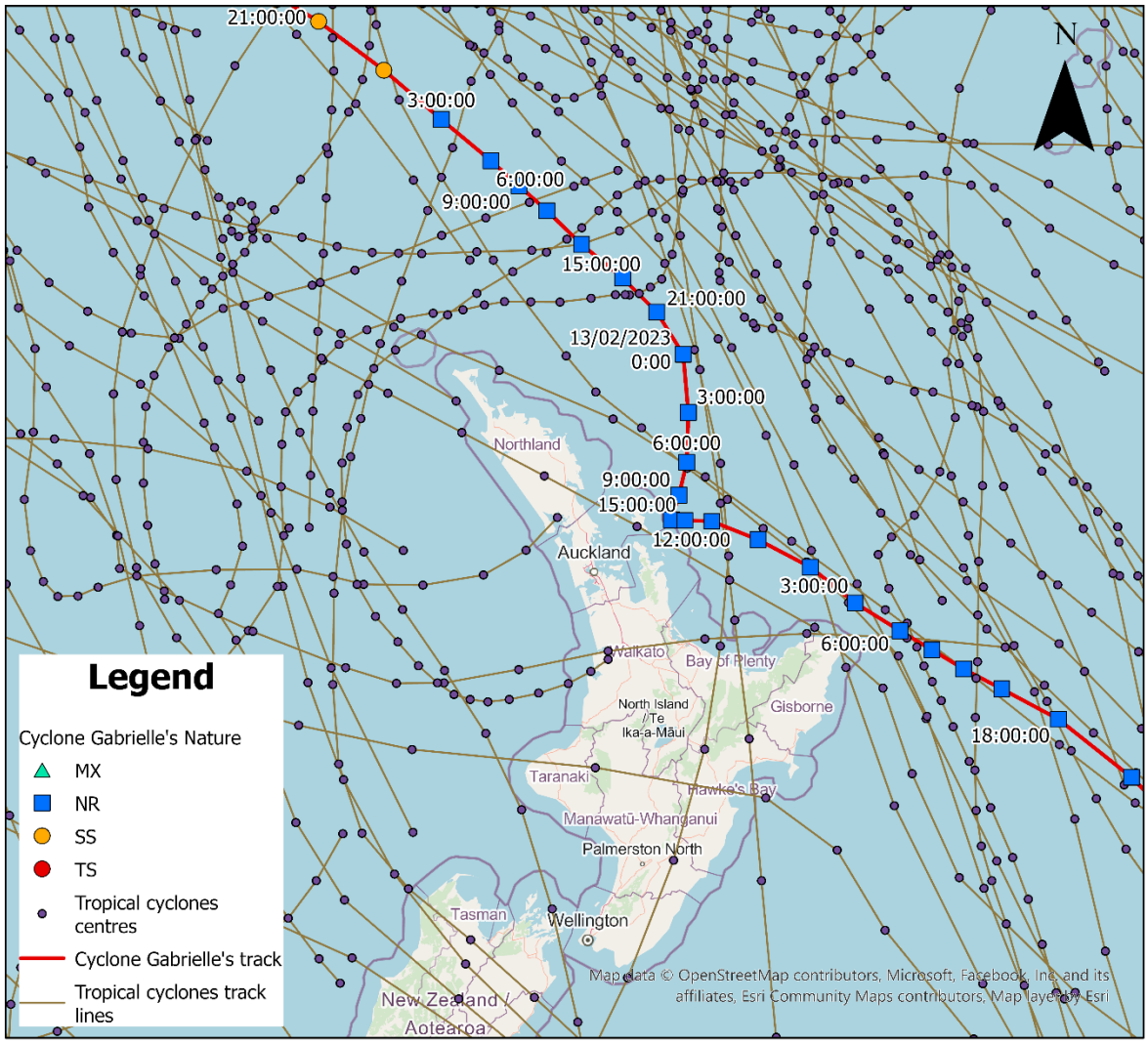

Figure 6. Storms that have influenced New Zealand from 1980 to 2023 using storm track from IBTrACS (dot, 3 hours or 6 hours centre of the storm) (source: https://www.ncei.noaa.gov/products/international-best-track-archive)

Tropical cyclones, though distinct from systems with classic frontal structures, exhibit atmospheric processes that are influenced by dynamics like those of cold, warm, and stationary fronts. A cold front, for instance, forces warm air to rise over advancing cold air, leading to condensation and intense precipitation. Similarly, within a tropical cyclone, warm, moist air is drawn toward the low-pressure centre and rapidly lifted into the cooler upper atmosphere, where it condenses and releases latent heat, fuelling the storm's energy. In some cases, as a tropical cyclone moves into mid-latitudes, interactions with cold or stationary fronts can significantly enhance rainfall, as the cyclone's moisture-rich environment converges with the lifting mechanisms at the frontal boundary (Emanuel, 2003). This results in prolonged and extreme precipitation. Furthermore, the low-pressure core of the cyclone drives winds from surrounding high-pressure areas, intensifying moisture inflow (Liu et al., 2023). These dynamics, coupled with the inherent

instability of the system, create the torrential rains and strong winds characteristic of tropical cyclones.

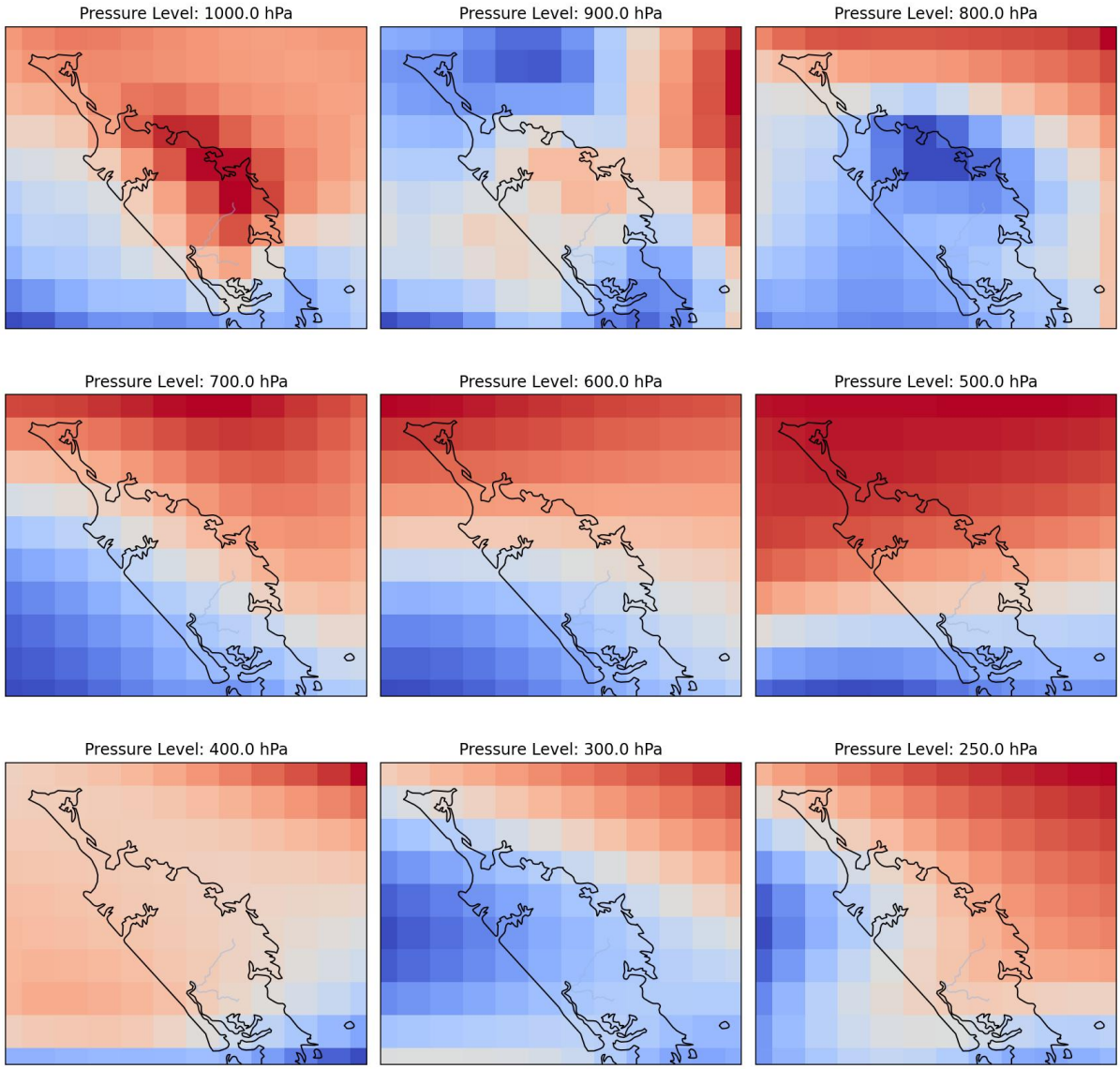

Figure 7: Spatial distribution of mean air temperature (°C) at multiple pressure levels (1000–250 hPa) over the Northland region, New Zealand, from 00:00 UTC to 07:00 UTC on 24th February 2023. *Each panel represents the horizontal temperature structure at a given pressure level derived from ERA5 reanalysis data. Warmer shades indicate higher temperatures, while cooler shades represent lower temperatures, illustrating the vertical thermal gradient and synoptic-scale temperature patterns associated with the analysed storm period.*

2.4.4 Summer heat and local moisture

Additionally, during the summer months, the heating of dry inland and eastern regions can generate enough convection to trigger cumulus cloud development, leading to showers (Chappell, 2013; Griffiths, 2007). Lastly, subtropical depressions, characterised by a complex interaction of warm and cold fronts, frequently drift across New Zealand, contributing to the region's diverse rainfall patterns (Griffiths, 2011).

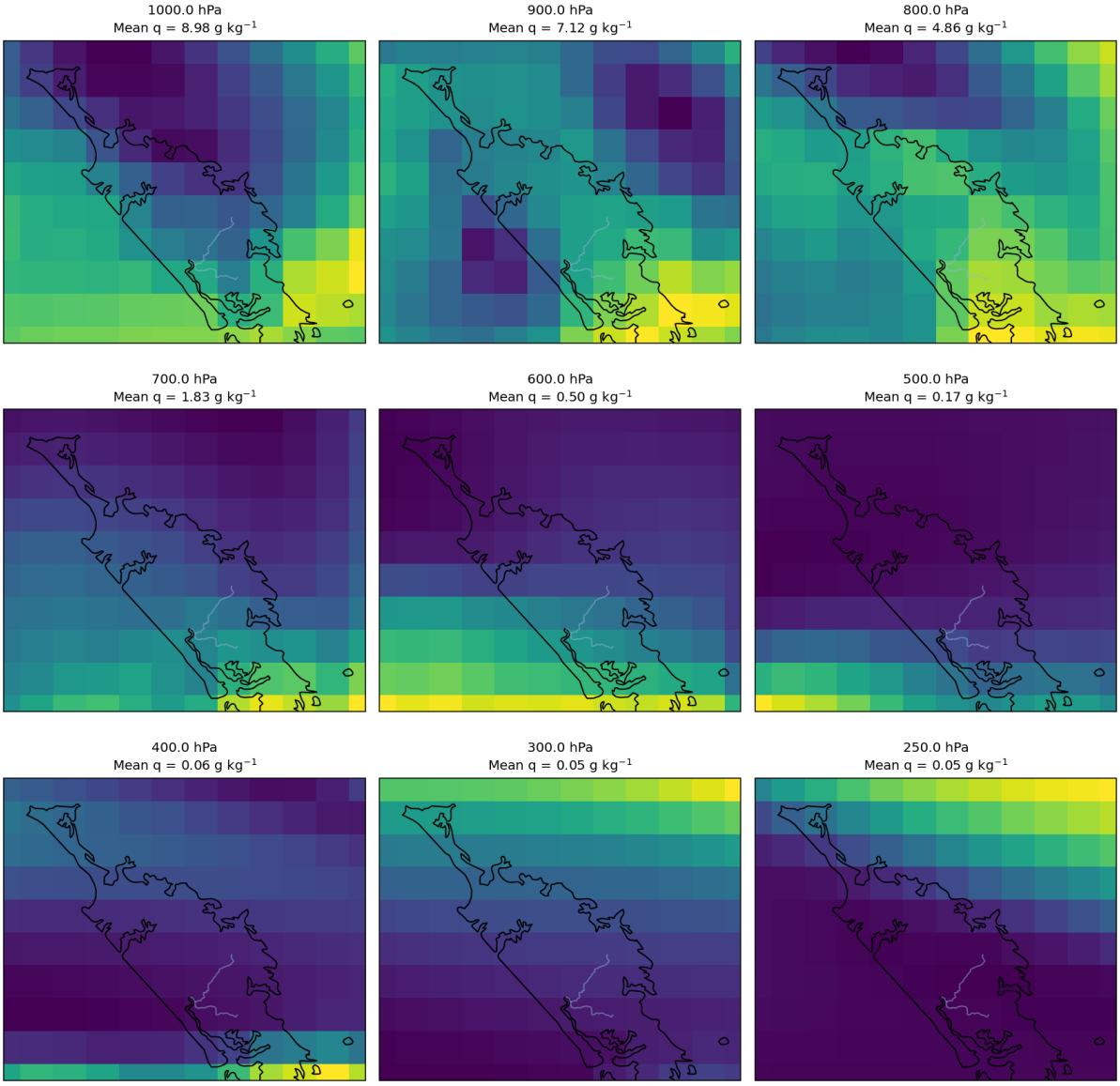

Figure 8: Spatial distribution of mean specific humidity (g kg^{-1}) across nine atmospheric pressure levels (1000–250 hPa) over the Northland Region during the early hours of 24th February 2023. The colour shading represents the spatial distribution of moisture at each level. *The figure highlights a strong vertical gradient, with the highest moisture concentrated near the surface (8.98 g kg^{-1} at 1000 hPa) and rapidly decreasing with altitude, reaching less than 0.1 g kg^{-1} above 400 hPa. This demonstrates that the rainfall event at Mangawhai was supported primarily by moisture in the lower troposphere, with much drier conditions aloft.*

During the Mangawhai extreme rainfall event, the vertical thermodynamic structure of the atmosphere revealed strong instability and abundant moisture throughout the troposphere. At low levels (1000–850 hPa), temperatures were markedly warmer, while the mid- to upper troposphere (700–300 hPa) exhibited substantially colder air. This pronounced temperature gradient indicates a highly unstable atmospheric column (Figure 7), favouring vigorous upward motion and deep convective development. Complementing this, the specific humidity distribution shows an extensive layer of moisture extending from the surface up to approximately 500 hPa (Figure 8), signifying a deep and moist air mass. The combination of warm, moist air near the surface and cold, dry air aloft provided ideal conditions for condensation and latent heat release, further

amplifying convection. Moreover, the elevated specific humidity over the coastal zone suggests a continuous inflow of moist maritime air. When this moisture-laden air encountered the orographic lifting along the Mangawhai–Auckland coastal terrain, it produced intense and sustained rainfall. Therefore, the observed temperature instability, high column moisture content, and dynamic moisture convergence collectively explain the extreme precipitation observed in the Mangawhai region during the event.

2.5 Previous Studies on Storm Patterns in Northland and New Zealand

MoE (2018a) examined how climate change might influence storm patterns in New Zealand. Using global and regional climate models, the researchers projected an increase in the frequency and intensity of extreme storms, particularly in the west and south of New Zealand. They highlighted that these changes are associated with shifts in the position and strength of the Southern Hemisphere westerlies, which are influenced by warming trends (MoE, 2018a).

Lorrey et al. (2014) explored the occurrence of extratropical cyclones and their impact on New Zealand. The study outlined that while these cyclones are rare, they can cause severe flooding, high winds, and significant damage to infrastructure. The study emphasised the need for better preparedness, given the increasing unpredictability of tropical systems reaching New Zealand due to climate change (Lorrey et al., 2014).

NIWA has produced extensive analyses of Cyclone Bola (1988), one of the most destructive storms in New Zealand's history. The event caused extreme rainfall and flooding, especially in the North Island. These reports serve as a valuable case study on the effects of tropical storms on New Zealand’s environment, infrastructure, and economy (NIWA, 2018).

Lee (2020) and Weather (2024) focused on the relationship between low-pressure systems and extreme rainfall events. The studies found that most extreme rainfall events in New Zealand are linked to strong low-pressure systems, particularly those from the Tasman Sea. These systems tend to cause widespread flooding and storm damage, especially in the western and northern regions of the country (Lee, 2020; Weather, 2024).

NIWA (2024m) discussed the synoptic weather patterns commonly associated with major flooding events in New Zealand. It also categorised storm systems and analysed how they have led to significant rainfall and flooding.

NIWA (2024a) provided insights into storm surges and their effects on coastal flooding in New Zealand. It identified the areas that are most vulnerable to these storm-induced floods, particularly in low-lying coastal regions such as Northland, Auckland, and the eastern Bay of Plenty (NIWA, 2024a).

These studies collectively show that New Zealand's storm patterns are influenced by a combination of tropical cyclones, extratropical storms, and shifts in large-scale climate systems like the Southern Hemisphere westerlies. Climate change is likely to intensify these patterns, increasing the risk of extreme weather events across the country.

2.6 Impacts of Extreme Rainfall Events on River Flooding and Infrastructure

Extreme rainfall events can have significant impacts on river flooding and infrastructure, particularly in regions such as Northland, New Zealand. Below are some key points regarding these impacts.

Extreme rainfall events can result in river flooding through increased runoff, flash flooding and associated erosion and sediment. Heavy rainfall can lead to rapid surface runoff, overwhelming rivers and streams. This results in higher water levels, which can cause flooding in surrounding areas. Short-duration, high-intensity rainfall can lead to flash floods, which occur with little warning and can inundate areas quickly, especially in urban settings where drainage systems may be inadequate. Flooding can cause significant erosion of riverbanks and the surrounding landscape, leading to increased sedimentation in rivers, which can affect water quality and aquatic habitats (Talbot et al., 2018).

Impacts caused by extreme rainfall events on infrastructure are equally significant. Floodwater can wash away roads and bridges, making them impassable and posing risks to vehicles and pedestrians. Infrastructure damage can disrupt transportation and emergency services. Flooding can also lead to property damage, particularly in low-lying areas. Homes and businesses may be inundated, leading to costly repairs and potential loss of livelihood. During extreme rainfall events, water and sewer systems can be compromised, leading to contamination and service outages. This poses public health risks and complicates recovery efforts (FAY et al., 2008).

Economic impacts associated with extreme rainfall events can be substantial. The financial burden of repairing damaged infrastructure and providing assistance to affected communities can be significant. Flooding can disrupt local economies by closing businesses, leading to lost income for owners and employees. Recovery can take time, further impacting the local economy (Svetlana et al., 2015). Additionally, investing in flood-resistant infrastructure, such as levees, floodwalls, and improved drainage systems, can help mitigate the impacts of extreme rainfall.

Beyond the direct impacts described above, repeated flooding can alter river morphology and significantly affect ecosystems over the long term. It may also lead to long-term changes in sediment transport and habitat availability for wildlife. Areas repeatedly

affected by flooding may become more vulnerable over time, especially if climate change leads to more frequent and intense rainfall events (N. LeRoy Poff, 2002).

The impacts of extreme rainfall events on river flooding and infrastructure are profound, affecting not only the physical environment but also the economy and communities. Understanding these impacts is crucial for effective planning and response strategies to mitigate future risks (Smith, 2013).

3. Data and Methodology

3.1. Data Collection

To accomplish the research objectives, a diverse set of data types has been employed, ensuring comprehensive analysis and robustness of findings. The selected data sources are widely recognised for their reliability, having been extensively validated and utilised in numerous prior studies across various scientific disciplines, providing a sturdy foundation for this research. Table 6 provides a summary of the data sources used in the present study.

Table 6: Source of used data

Data type	Spatial resolution	Temporal resolution	Sources
Rainfall	Station based	Hourly, sub-hourly and daily	NRC
Hydrology (flow data)	Station based	Hourly, sub-hourly	NRC environmental data hub
GIS data			Online from NRC: https://localmaps.nrc.govt.nz/LocalMapsGallery/
Climate Radar	1km x 1km, 0.5 km x 0.5 km	1 minute	NRC via Mott MacDonald API https://api.moata.com/v1
Satellite rainfall	0.1 x 0.1 degree	30 minutes (later run)	NASA IMERG: Integrated Multi-satellitE Retrievals for GPM Final run. https://gpm.nasa.gov/data/imerg
Storm data	Event base	three hourly, six hourly	NOAA Historical Storm Track International Best Track Archive for Climate Stewardship (IBTrACS) (Knapp et al., 2010)
AR data	0.25 x 0.25 degree	6 hourly	https://dataverse.ucla.edu/dataverse/ar
SOI index	Nan	Monthly	https://www.cpc.ncep.noaa.gov/data/indices/soi

3.2. Rainfall Data

3.2.1 Ground Base Data

Rainfall data for this study is sourced from three primary categories: gauging data, satellite observations, and climate datasets. Gauging data serves as the primary source for in-depth analysis in this research. Specifically, rainfall data was obtained from 43

stations across Northland, as shown in Figure 9. Of these, 40 stations are managed by the Northland Regional Council, while the remaining three are operated by NIWA (National Institute of Water and Atmospheric Research). Most of the regional stations record rainfall data in sub-hourly intervals, whereas the NIWA stations provide hourly data. Ground-based data was provided by Northland Regional Council at sub-hourly temporal resolution, which is sufficient for analysis of intensity and distribution of rainfall.

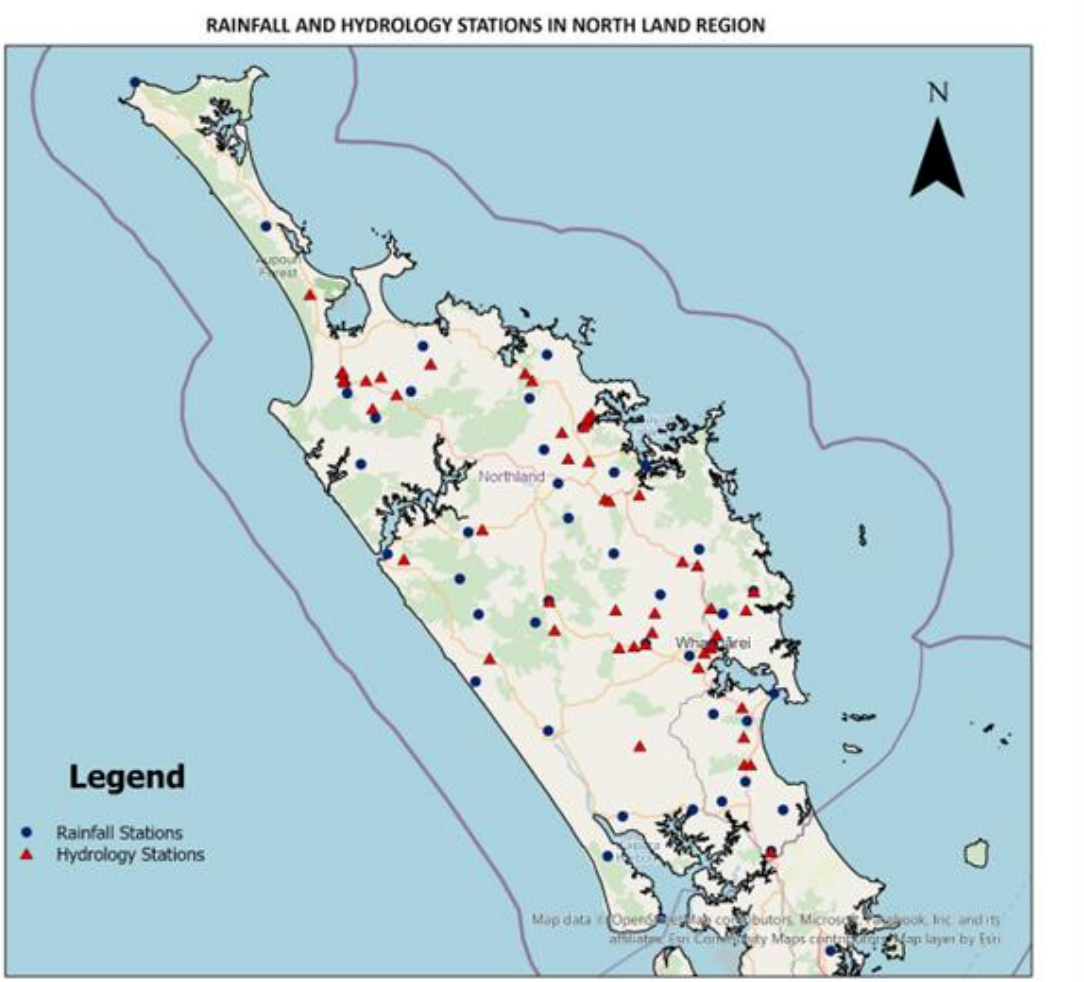

Figure 9: Rainfall (blue Circles) and river (Red Triangles) stations in the Northland region

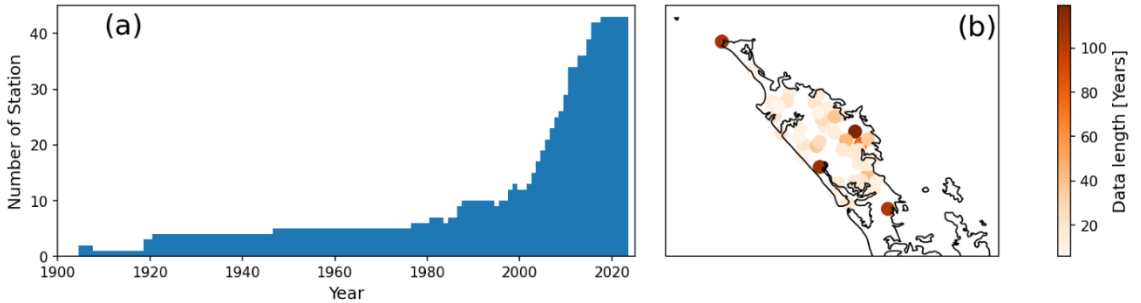

Figure 10: (a) Data length (in years) for rainfall gauging stations in Northland; (b) the geographical locations and corresponding data length (colour dots) of the 43 stations used in our study across Northland

Figure 10a illustrates the number of gauging stations with recorded rainfall data over time (years). Starting from the early 1900s, there has been a noticeable increase in the number

of stations from the mid-20th century, with a sharp rise in station numbers after the 1980s. By 2020, the number of stations in the dataset reaches around 40. This suggests that rainfall monitoring in Northland has become more intensive over time. This increase in data availability is likely due to technological advancements and growing environmental monitoring efforts.

In addition, Figure 9 displays the geographical distribution of the 43 rainfall stations across Northland. The stations are represented as coloured dots, where the colour gradient reflects the length of the data records (in years) from each station. Stations with darker red or brown dots have longer data records (up to 100 years), while lighter dots represent stations with shorter data records. Most of the longer-record stations are in the southern parts of the region; however, these stations are adequate to analyse North-South, east-west gradient.

One of the main issues with the data is that the total number of available data before 1980 is very rare (as shown in Figure 10a) and data started accumulating after the time, partially due to the better cover of stations and the wider use of satellite observations. In terms of rainfall analysis, the main problems lie in the time step, consistency, and start and end date. We applied different techniques to offset the difference so that the data is consistent and fit to proceed with any calculation we have later to analyse the storm and corresponding influence it may exert on.

3.2.2 Weather Radar Data

Weather radar is a technologically advanced tool that has been used to enhance rainfall analysis by providing insights into precipitation characteristics and the physical processes underlying its formation. Unlike rain gauges, which offer point-based measurements, weather radar provides real-time observations with high spatial and temporal resolution. In the Northland region, high-resolution radar data are available at a temporal resolution of one minute and a spatial resolution of 0.5 km, enabling detailed analysis of rainfall intensity and distribution (see **Table** 7). In addition, weather radar can capture the three-dimensional structure of precipitation and estimate rainfall over the sea surface, which is not possible using ground-based gauges alone. However, due to data accessibility limitations, radar data were used in this study only to investigate precipitation associated with Cyclone Gabrielle and the Mangawhai flash flood.

Table 7: Data quality of Northland weather data

Data quality	Total data cells	Spatial resolution	Time resolution
Coarse	37975	1km x 1km	1 minute
Finer	110024	0.5 km x 0.5 km	1 minute

3.2.3 Satellite Image

Satellite systems provide significant data for many atmospheric parameters at regular intervals. One of the main advantages of satellite techniques is that they can provide long records of global, homogeneous, precipitation measurements data in remote areas and over oceans. Sensors onboard satellites can be classified into three categories: visible/IR (VIS/IR) sensors on geostationary (GEO) and low Earth orbit (LEO) satellites, passive MW (PMW) sensors on LEO satellites, and active MW sensors on LEO satellites.

As a result of these satellite missions, a wide range of precipitation products has been developed and is widely used for different applications. Examples include the Climate Prediction Center Morphing Technique (CMORPH) (Joyce et al., 2004) and NASA's Integrated Multi-satellitE Retrievals for GPM (IMERG) (Huffman et al., 2020), as well as the Precipitation Estimation from Remotely Sensed Information using Artificial Neural Networks (PERSIANN) (Hong et al., 2004). In New Zealand, a study by Vishwanathan et al. (2023) reported that IMERG products perform well in capturing precipitation intensity.

Table 8: Product of IMERG products

No.	Product	Latency
1	Early Run	30 minutes
2	Late Run	One day
3	Final Run	One month

NASA Integrated Multi-Satellite Retrievals for GPM (IMERG) algorithm combines information from the GPM satellite constellation to estimate precipitation over the majority of the Earth's surface. IMERG fuses precipitation estimates collected during the TRMM satellite's operation (2000 - 2015) with recent precipitation estimates collected by the GPM mission (2014 - present) creating a continuous precipitation dataset spanning over two decades. IMERG provides various products with distinguishing latency and accuracy (see Table 8). NASA has suggested that Final Run is the most recommended product for research activities.

3.3. Flow Data

The flow data were provided from the online database of Northland Regional Council (NRC) environmental data hub. The data provide river flow rate (m^3/s) and water level (Stage (mm)) at 50 stations around the Northland region. The dataset provides hourly temporal resolution over the full record, with sub-hourly data available for approximately the past five years, which is sufficient for analysis.

However, some limitations still exist in the data. There are gaps in flow data at multiple stations such as Hikurangi at Moengawahine, Hatea at Whareora road (see Figure 11).

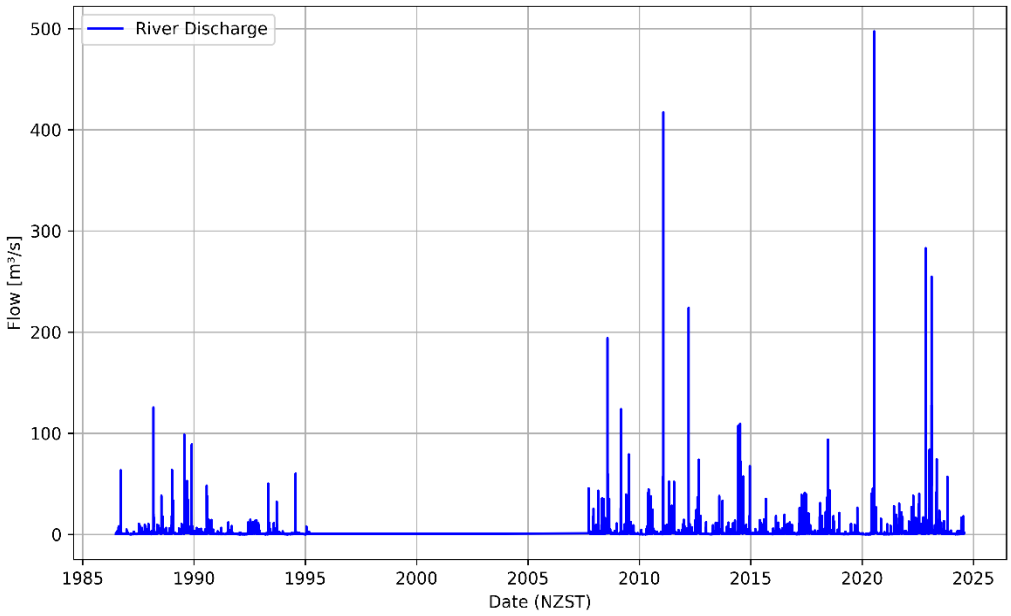

Figure 11: Flow data [m³/s] at station of Hatea at Whareora road

In the present study, the precipitation associated with Cyclone Gabrielle and Mangawhai flash flood was investigated using three distinct rainfall data types which are ground-based data, satellite data, and weather radar data. Ground-based data was provided by Northland Regional council in sub-hourly temporal resolution, which is sufficient for analysis of intensity and distribution of rainfall. In terms of satellite data, the NASA IMERG (Integrated Multi-satellite Retrievals for GPM) Final Run product is used. This product is part of the Global Precipitation Measurement (GPM) mission, which provides high-resolution precipitation estimates by integrating data from multiple satellite sources.

3.4. Analysis Methodology

To understand the atmospheric variables that commonly lead to heavy rainfall in the Northland region, a statistical analysis was conducted to identify the correlation between atmospheric conditions and precipitation. Key atmospheric variables such as wind patterns, pressure systems, and temperature fluctuations were analysed to determine their relationship with storm occurrences in Northland.

To analyse the precipitation characteristics of Cyclone Gabrielle and the Mangawhai flash flood, an event-based rainfall analysis approach was applied. This method isolates individual rainfall events based on the onset and cessation of precipitation exceeding defined thresholds, allowing each storm to be examined as a discrete hydrometeorological unit. Event identification is carried out using criteria such as rainfall intensity, duration, and total accumulation, ensuring that significant storms are separated from background rainfall. This approach is particularly suited for

extreme-event studies because it provides detailed temporal structure of rainfall, supports assessment of flood-generating mechanisms, and helps quantify the stress imposed on infrastructure during high-impact events. By focusing on the most intense and hydrologically relevant events, the analysis enables a clearer understanding of the processes that lead to flooding and damage across the region.

Event-based rainfall analysis requires well-defined event definition criteria, where thresholds such as minimum rainfall intensity or duration are established to identify significant rainfall events. These thresholds help differentiate between minor rainfall and events that could pose risks like flooding. In this project, the events with a total rainfall greater than 2.5 mm were selected for further investigation. After defining the criteria, event segmentation was conducted, often using algorithms that can break down continuous rainfall data into distinct, measurable events. This segmentation allows for a more granular analysis of each event's characteristics. Storm event temporal properties are defined using the inter-event time definition (IETD) (see Figure 12). The IETD can be formally defined as the minimum time without rainfall between two successive rainfall periods. Two successive rainfall periods separated by a time interval greater than the chosen IETD value are regarded as two separate storm rainfall events. Conversely, if the separation time is less than or equal to the chosen IETD value, then the two successive rainfall periods are considered as a single storm rainfall event. Statistical analysis was then applied to examine the frequency, intensity, and distribution of rainfall events.

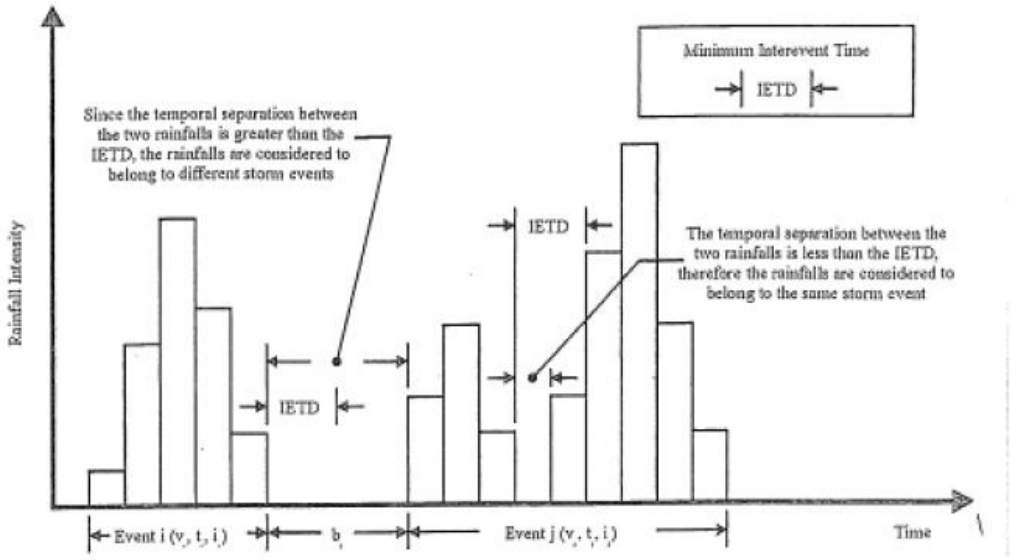

Figure 12: Identification of discrete rainfall events for a continuous rainfall record based on IETD (Source Adams and Papa (2001).

To assess the quantitative impact of the February 2023 storm, rainfall and flood flow estimates were conducted using a combination of radar and ground station data. By analysing these sources, the total precipitation for the event was accurately calculated,

providing insight into the scale of the storm. In addition, spatial analysis was performed using GIS tools to evaluate the geographical distribution of rainfall and the extent of flooding. This approach allowed for a detailed understanding of how the storm affected different regions, highlighting areas of intense rainfall and significant flood risk.

To quantify the impacts of extreme rainfall on river flooding in Northland, a statistical analysis of flood frequency and magnitude related to storm events was conducted. This analysis aimed to help establish relationships between intense rainfall and subsequent flooding, providing a clearer picture of how different storm events influence river behaviour. Additionally, data from Cyclone Gabrielle and the Mangawhai flash flood were analysed in detail to assess their specific characteristics, such as intensity and duration. By examining these events in comparison to historical storm patterns, we gained valuable insights. This comparison contributed to a deeper understanding of the unique factors driving flood risk during extreme storms in Northland.

The time distributions of rainfall events were expressed as cumulative percentages of storm rainfall and storm duration to facilitate accurate comparisons between storms and to simplify data analysis and presentation. This methodology was initially introduced by Huff (1967) and later refined in 1990 (Huff, 1990). Rainfall distributions were categorised based on the timing of the heaviest rainfall, occurring in either the first, second, third, or fourth quarter of a storm. Figure 13 presents the median of the four quartiles and the time distribution for Cyclone Gabrielle, using the Huff approach. For each quartile group, a family of curves (median, 15th percentile, and 85th percentile) was generated to quantify the expected inter-storm variability. This variability was subsequently compared to extreme events in the region to assess the dominant precipitation patterns.

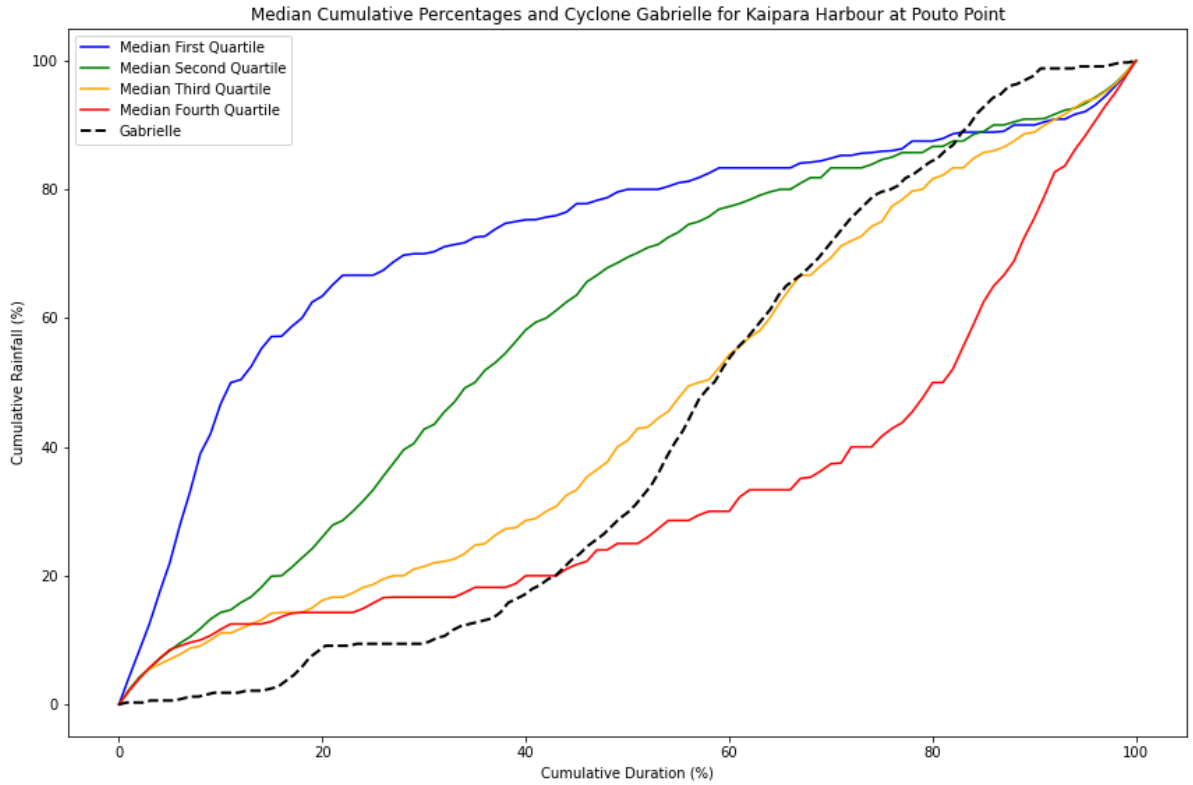

Figure 13: Median cumulative percentages of rainfall for four quartiles of storms, alongside data from Cyclone Gabrielle at Kaipara Harbour (Pouto Point)

Cyclone Gabrielle displays rainfall patterns that align with storms where the most intense rainfall occurs in the second half of the event (Figure 13). The curve indicates considerable inter-storm variability, especially when compared to the more evenly distributed rainfall of storms in the third and second quartiles. Cyclone Gabrielle's peak rainfall occurs earlier than storms in the fourth quartile but later than those in the second quartile, suggesting it shares characteristics of both mid- and late-storm intensifications. Overall, Cyclone Gabrielle most closely resembles storms in the third quartile, with the heaviest rainfall occurring in the latter half of the event. The sharp increase in rainfall between 40% and 60% of the storm's duration underscores the variability and intensity that defined this storm.

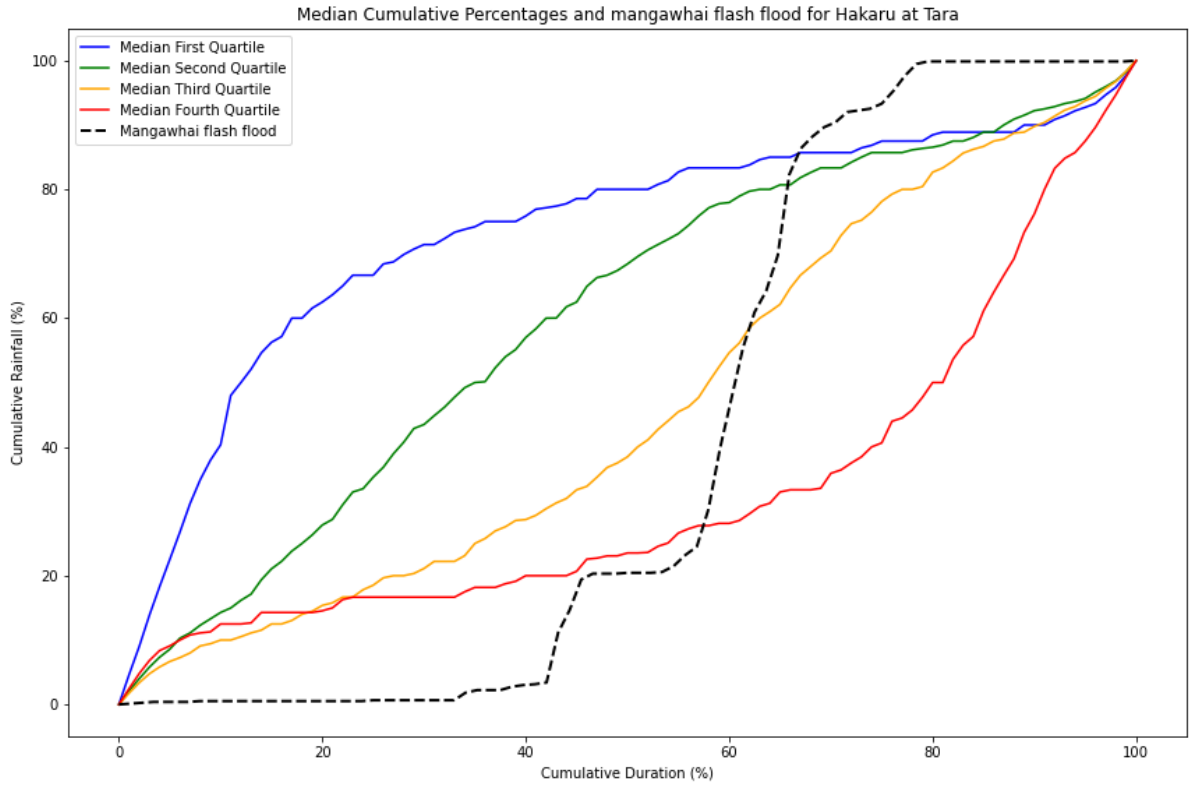

Figure 14: Median cumulative percentages of rainfall for four quartiles of storms, alongside data from Mangawhai flash flood at Hakaru at Tara

Figure 14 illustrates the median cumulative rainfall percentages for four quartiles and a Mangawhai flash flood event as a function of cumulative duration. The Mangawhai flash flood (black dashed line) has been categorised in the third quartile group, and displays an extremely concentrated rainfall accumulation, where nearly all rainfall occurs between 40% and 60% of the duration, emphasising the sudden and intense nature of flash flood events. These patterns underscore the variability in rainfall distributions, with early-peaking storms in the first quartile, back-loaded storms in the fourth quartile, and flash floods exhibiting extreme short-term intensity, highlighting the importance of understanding rainfall timing for effective hazard prediction and flood risk management.

4. Categorisation of Historic Storm Patterns

4.1. Annual Mean Rainfall

Figure 15 represents the spatial distribution of mean annual rainfall in the Northland region. Higher rainfall areas are represented by red and dark orange circles, which are clustered mainly in the northern and central parts of the region. These areas, receiving over 1,600 mm of rainfall annually, may be influenced by topography, where orographic lifting or proximity to windward sides of elevation increases rainfall accumulation. Lower rainfall regions, shown by blue and green circles, are primarily found in southern and southwestern coastal areas. These regions experience mean annual rainfall of 1,000 to

1,400 mm; the annual rainfall pattern agrees with the pattern reported by NIWA in 2013 (Chappell, 2013).

Figure 15 highlights clear spatial contrasts in rainfall across Northland. While parts of the northern region show clusters of stations with relatively high rainfall, the Cape Reinga itself records noticeably lower totals. Southern areas exhibit more variability in rainfall, but generally show lower mean annual values compared to the centre of the region, indicating less consistent moisture influx or possibly different climate regimes. Despite the general patterns, there is significant localised variability between nearby stations. Some stations within the same latitude or proximity show noticeable differences in mean annual rainfall. This localised variability could be due to microclimatic factors, such as small changes in elevation, land use (e.g., urban vs. rural), or specific localised wind patterns. More recently, a study has confirmed that Atmospheric Rivers have a significant influence on rainfall distribution in Northland (Shu et al., 2021).

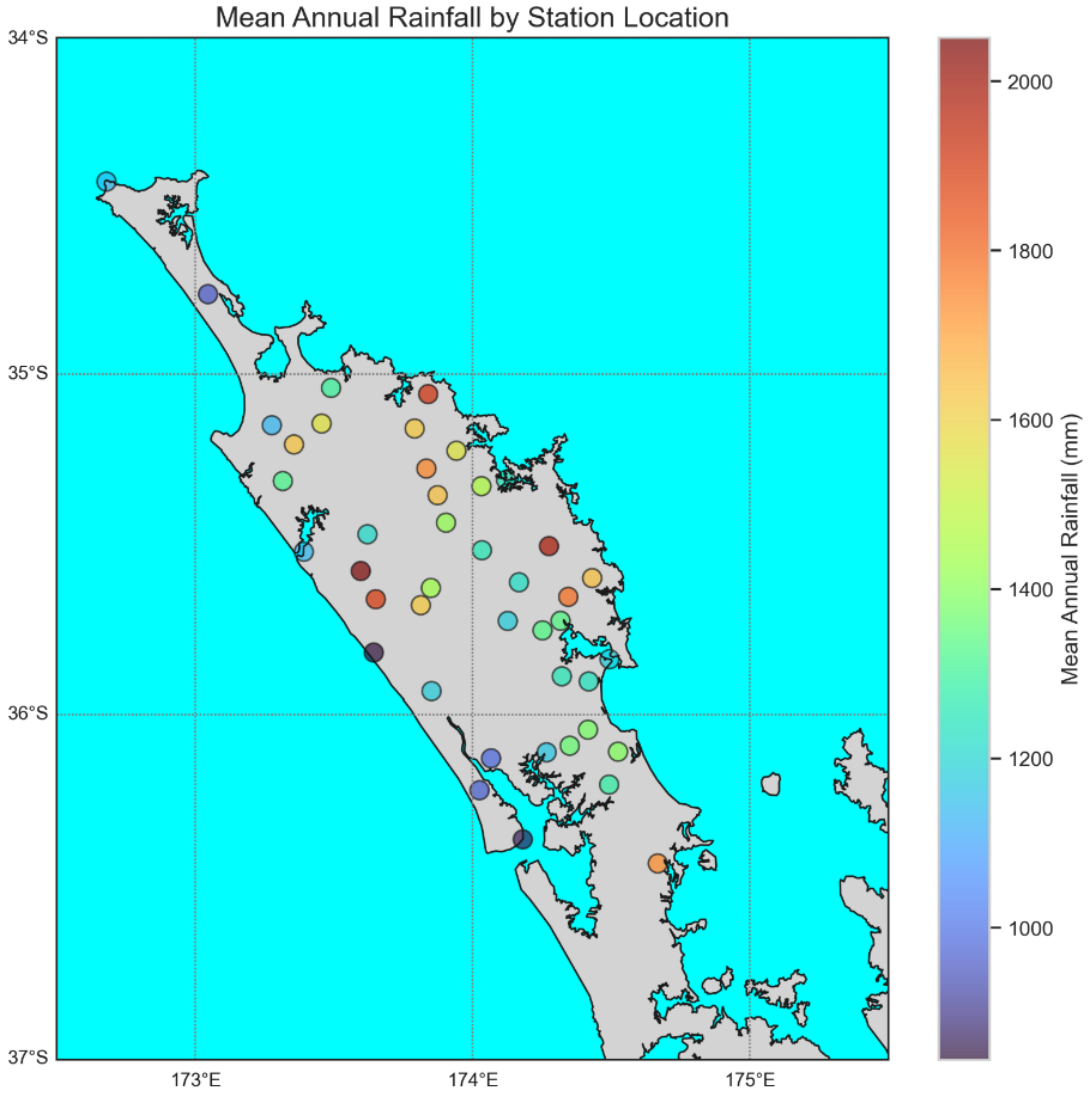

Figure 15: Mean annual rainfall (in mm) across different station locations in a region, likely in the Northland region

Figure 15 shows that rainfall distribution in Northland is heavily influenced by the region's orography. Precipitation levels range from around 1,000 mm in the low-lying coastal zones to approximately 2,000 mm in the elevated areas. The eastern coastal areas generally receive more rainfall compared to the western coast. Topography plays a critical role in this pattern, with higher elevations and proximity to mountain ranges leading to increased rainfall due to orographic lifting, where moist air is forced to rise over terrain, cooling and condensing to form precipitation.

4.2. Seasonal and Temporal Rainfall

Seasonal and temporal rainfall patterns were assessed using long-term data from gauging stations across the region. Figure 16 illustrates an example from the Waitangi at McDonald Road station, showing both the monthly distribution of rainfall and the corresponding monthly mean values. Plots for the remaining stations are provided in Appendix 1. The data show a strong seasonal pattern in rainfall, with higher amounts in the winter months and lower in the summer. There is clear seasonality in the rainfall pattern, with more rainfall occurring during the winter months (June, July, and August), and relatively lower rainfall during the late spring and summer months (October to March). The summer months (January, February, and December) generally show lower rainfall. In particular, July (Month 7) consistently shows higher rainfall compared to other months, both in terms of the median and overall range. Months such as January, February, and November exhibit lower total rainfall and smaller variability, suggesting a drier season.

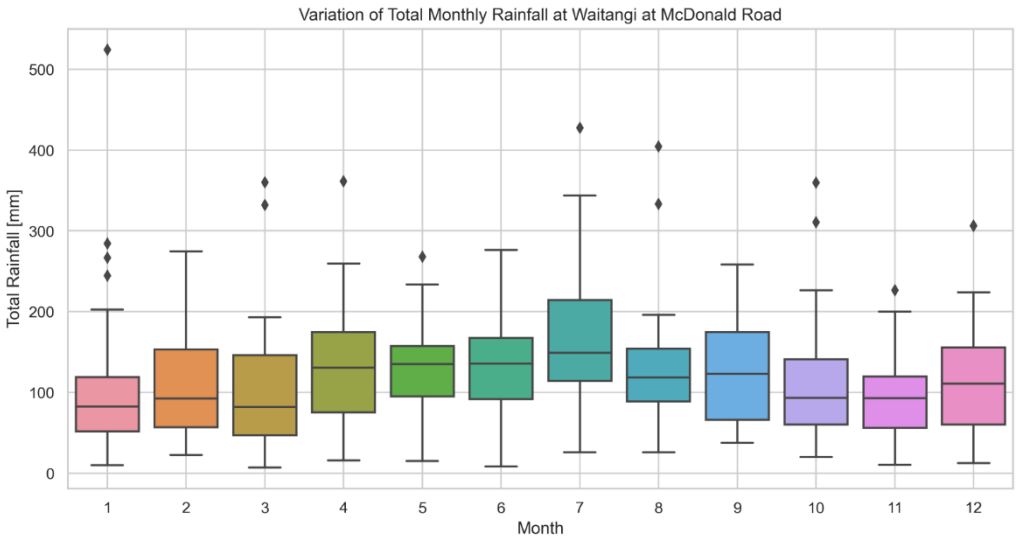

Figure 16: Variation in total monthly rainfall for each month at the "Waitangi at McDonald Road" station

4.3. Rainfall Event Characteristic

Event-based analysis was conducted to determine the duration and severity of rainfall in the region. Storm event temporal properties are defined using inter-event time definition (IETD) (Adams & Papa, 2001).

Table 9: Percentage of rainfall event in the different quartiles based on extreme rainfall storms (> 100 mm/ 24h)

Station	First Quartile (%)	Second Quartile (%)	Third Quartile (%)	Fourth Quartile (%)	Number of events (%)
Whangarei Harbour at Marsden Point Oil Refinery	0	27	64	9	11
Paparoa at Maungaturoto	17	25	50	8	12
Otiria at Ngapipito	0	38	54	8	13
Waiarohia at NRC Water St	0	23	69	8	13
Veronica Channel at Opua Wharf	0	29	50	21	14
Te Puhi at Mangakawakawa Trig	0	36	64	0	14
Waiwarawara at Wilsons Dam	0	33	67	0	15
Hakaru at Tara	0	44	44	13	16
Waitangi at Wiroa Road 2	0	38	44	19	16
Kerikeri at BOI Golf club	0	41	53	6	17
Waipao at Draffin Road Rain	12	35	41	12	17
Okarika at Rowland Rd	11	33	44	11	18
Mangakahia at Twin Bridges	0	42	42	16	19
Opouteke at Brookvale	4	38	46	13	24
Waihoihoi at Brynderwyn	8	28	44	20	25
Kaeo at Bramleys	0	33	56	11	27
Touwai at Weta	0	48	41	10	29
Waitangi at Ohaeawai	6	28	64	3	36
Waitangi at McDonald Road	0	39	55	7	44
Hatea at Glenbervie Forest HQ	2	28	66	4	47
Ngunguru at Dugmores Rock	3	31	49	17	59
Whakapara at Puhipuhi	2	38	52	7	81

Table 9 provides information on the percentage of extreme rainfall events associated with four different quartiles, along with the total number of rainfall events recorded for different rainfall gauging station. Most stations exhibit very little rainfall in the first quartile (Early load Rainfall), indicating that the onset of storms is typically marked by low rainfall intensity. Mid-Event Rainfall (Second and Third Quartiles) is generally the peak periods of rainfall for most stations, with percentages ranging from 23% to 69%. The fourth quartile generally has lower percentages, reflecting that storms tend to taper off towards the end, except in a few stations where prolonged rainfall is evident.

Rainfall distribution across quartiles for extreme precipitation events shows that, for many stations, the bulk of rainfall occurs during the second and third quartiles, which represent the mid-event period. Stations such as Whangarei Harbour, Waiarohia, and Waiwarawara exhibit a particularly high number of events in the third quartile, signifying

peak rainfall during this phase of storms. In contrast, the first quartile, representing the early phase of storms, often shows minimal rainfall, with values at or near 0%, indicating that storms in these regions typically begin with low intensity and build up as they progress.

In the fourth quartile, many stations show a significant drop in rainfall compared to the mid-event periods. For example, Te Puhi at Mangakawakawa Trig and Waiwarawara at Wilsons Dam both have very little rainfall in the fourth quartile, illustrating a sharp decrease in intensity towards the end of storms. However, certain stations, such as Waihoihoi at Brynderwyn (20%) and Veronica Channel at Opua Wharf (21%), display higher proportions of rainfall in the fourth quartile, suggesting prolonged rainfall at the end of events. Stations with higher event counts, such as Whakapara at Puhipuhi and Ngunguru at Dugmores Rock, still follow this general pattern, with most rainfall concentrated in the second and third quartiles. However, stations such as Hakaru at Tara and Waitangi at Wiroa Road 2 also show distinctive fourth quartile trends, indicating varying storm behaviours across the region.

4.4. Time Distribution of rainfall events

The time distribution of rainfall at gauging stations in Northland has been analysed to understand how rainfall is distributed during storm events, including the distribution of the top five largest rainfall events. This analysis follows the method proposed by Huff (1990). Event-based rainfall characteristics across the Northland region have been investigated to determine how rainfall patterns have changed during the rainfall event.

Figure 17 presents the time distribution of cumulative rainfall for extreme events at the Ngunguru station at Dugmores Rock, with corresponding plots for other stations shown in Appendix 2. Precipitation has been divided into four quartiles, each representing how rainfall accumulates over the duration of an event. The analysis indicates that rainfall is predominantly concentrated in the second and third quartiles, reflecting peak accumulation during the middle stages of storm events. These mid-event quartiles exhibit more consistent and sustained rainfall, which is more likely to generate higher flow rates as catchments progressively approach saturation. In contrast, the first and fourth quartiles generally show lower rainfall contributions, indicating limited early-stage accumulation and tapering rainfall toward the end of events. Most extreme rainfall events across the region fall within the second and third quartiles, a pattern consistently observed across multiple stations. This distribution highlights the importance of mid-event rainfall intensity and duration in driving runoff generation and flood response, although some events display atypical behaviour with rainfall concentrated toward the beginning or end of the storm.

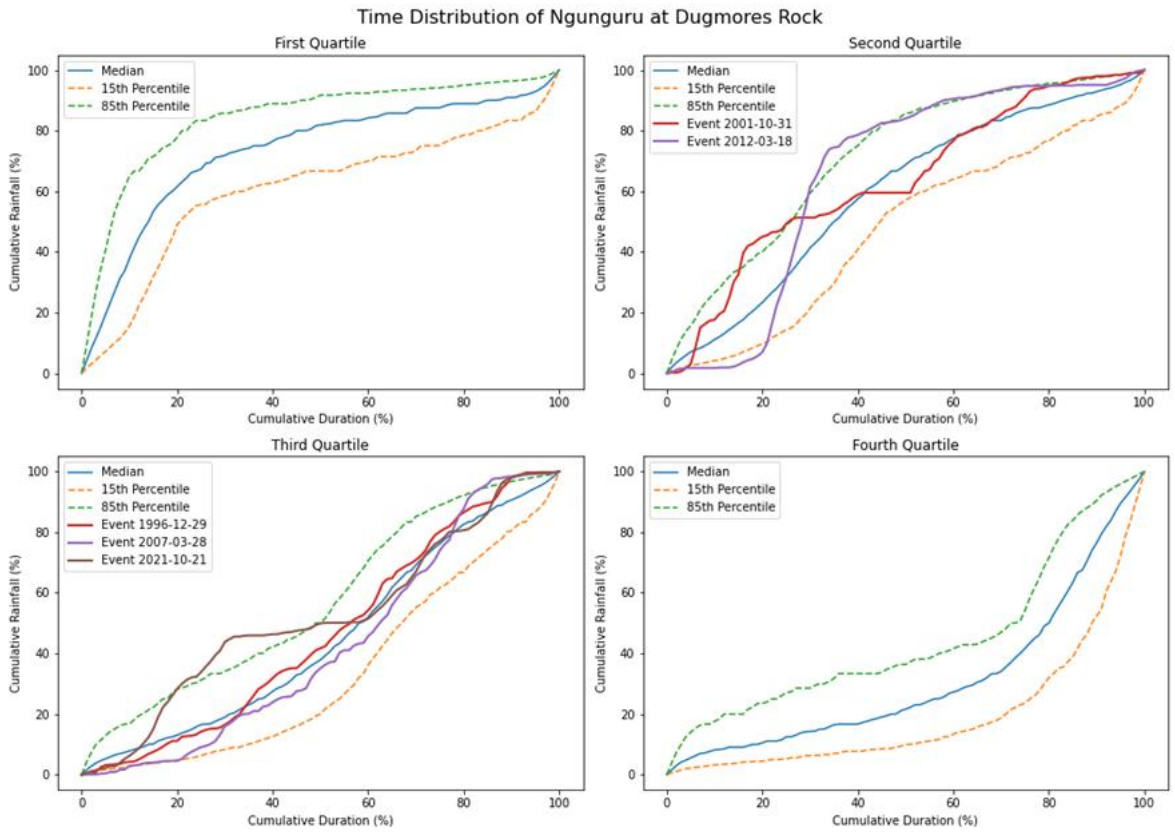

Figure 17: Time distribution of Ngunguru at Dugmores Rock and five heaviest events.

4.5 Common Storm Types in Northland

In the present study, the results indicate that the most extreme rainfall events, recorded over 12-hour, 24-hour, and 48-hour periods, are strongly correlated with atmospheric river (AR) events (see Table 10). The total rainfall amounts during AR events are significantly higher than those during non-AR events. Table 10 shows the association of extreme rainfall for three stations for three rainfall durations, namely 12-, 24- and 48 hours durations. The table shows that at the Waitangi at McDonald Road station, both 12-hour and 24-hour analyses show considerably higher rainfall amounts during AR events compared to non-AR events.

Table 10: Maximum of 12 hours, 24 hours and 48 hours rainfall and their association with AR

Period	12 Hours		24 Hours		48 Hours	
Station	AR rainfall	Non-AR Rainfall	AR rainfall	Non-AR Rainfall	AR rainfall	Non-AR Rainfall
Okarika at Rowland Rd	180.6	122.3	190.0	135.1	198.6	147.0
Hatea at Glenbervie Forest	268.2	246.9	308.7	291.1	338.0	303.2
Waitangi at McDonald Road	255.5	168.8	308.5	180.8	348.0	215.5

4.6 Change in the Future of Rainfall

In the present study, linear regression analysis was applied to analyse trends in annual rainfall at stations with more than 30 years of continuous records. Ten rainfall gauging stations met this criterion. The results of the trend analysis are shown in Figure 18 in which stations with an increasing trend are shown in red, and stations with a decreasing trend are shown in blue. Examination of the figure shows that there is an increasing trend in most of the stations (eight out of ten). However, there is a decreasing trend in two stations, namely, Dargaville 2 and Hatea at Glenbervie Forest.

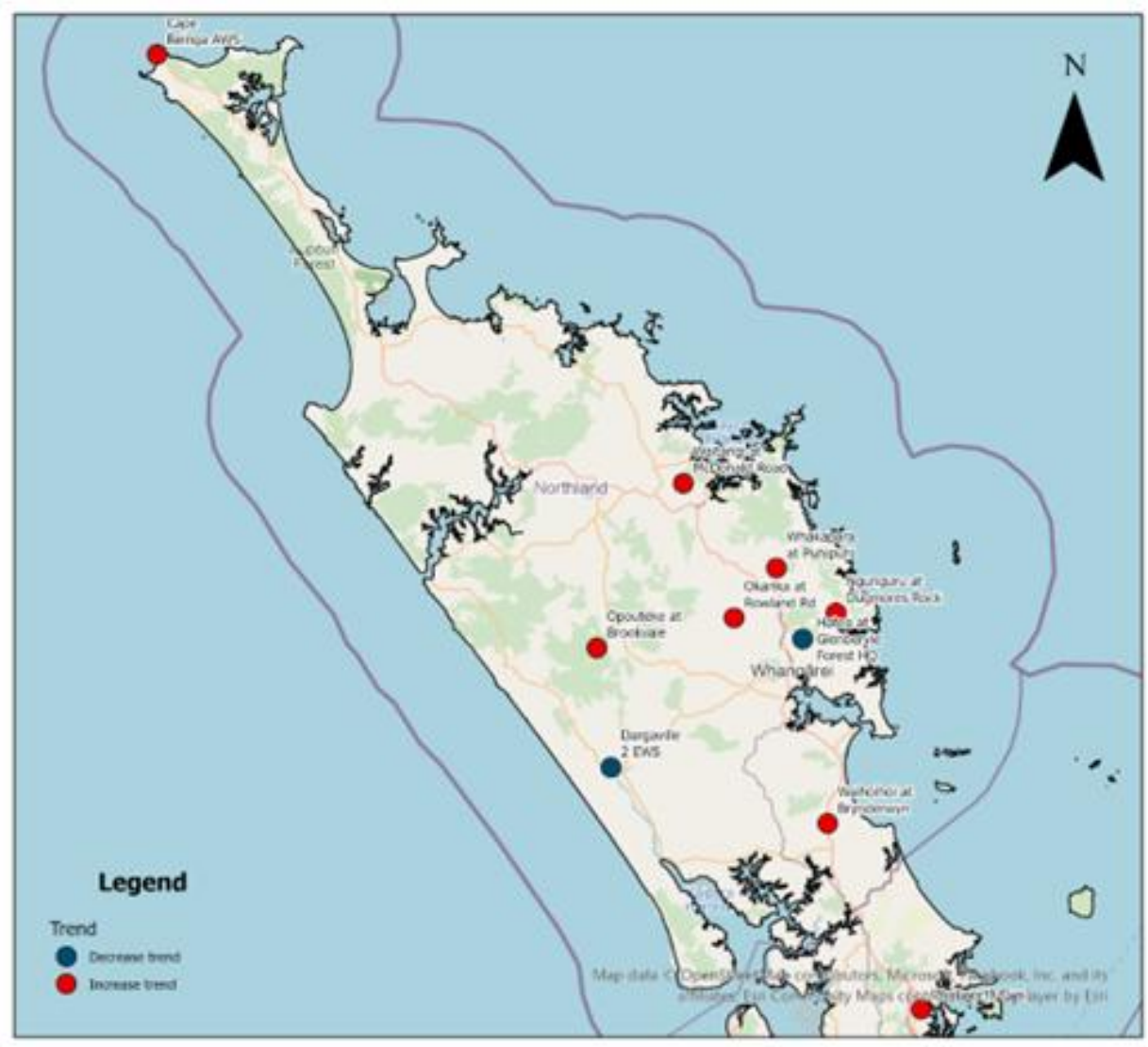

Figure 18: Trend over recording time of annual rainfall at stations in the Northland regions.

The trend suggests a potential increase in rainfall intensity in the future. Figure 19 below shows the trend analysis for the stations of Waitangi at McDonald Road and Waihoihoi at Brynderwyn in the Northland region from 1920 to 2023. The data reveal significant interannual variability in rainfall, with sharp peaks and troughs throughout the record. Despite this variability, the linear trend line indicates a gradual increase in annual rainfall

over the period, suggesting a long-term upward trend. In the early decades (1920–1950), rainfall totals were relatively low and less variable, while from the mid-20th century onward, the magnitude and frequency of extreme rainfall events increased. Notably, recent years (post-2000) exhibit several instances of exceptionally high rainfall, surpassing 2500 mm, interspersed with occasional dry years, including the notable decline around 2020.

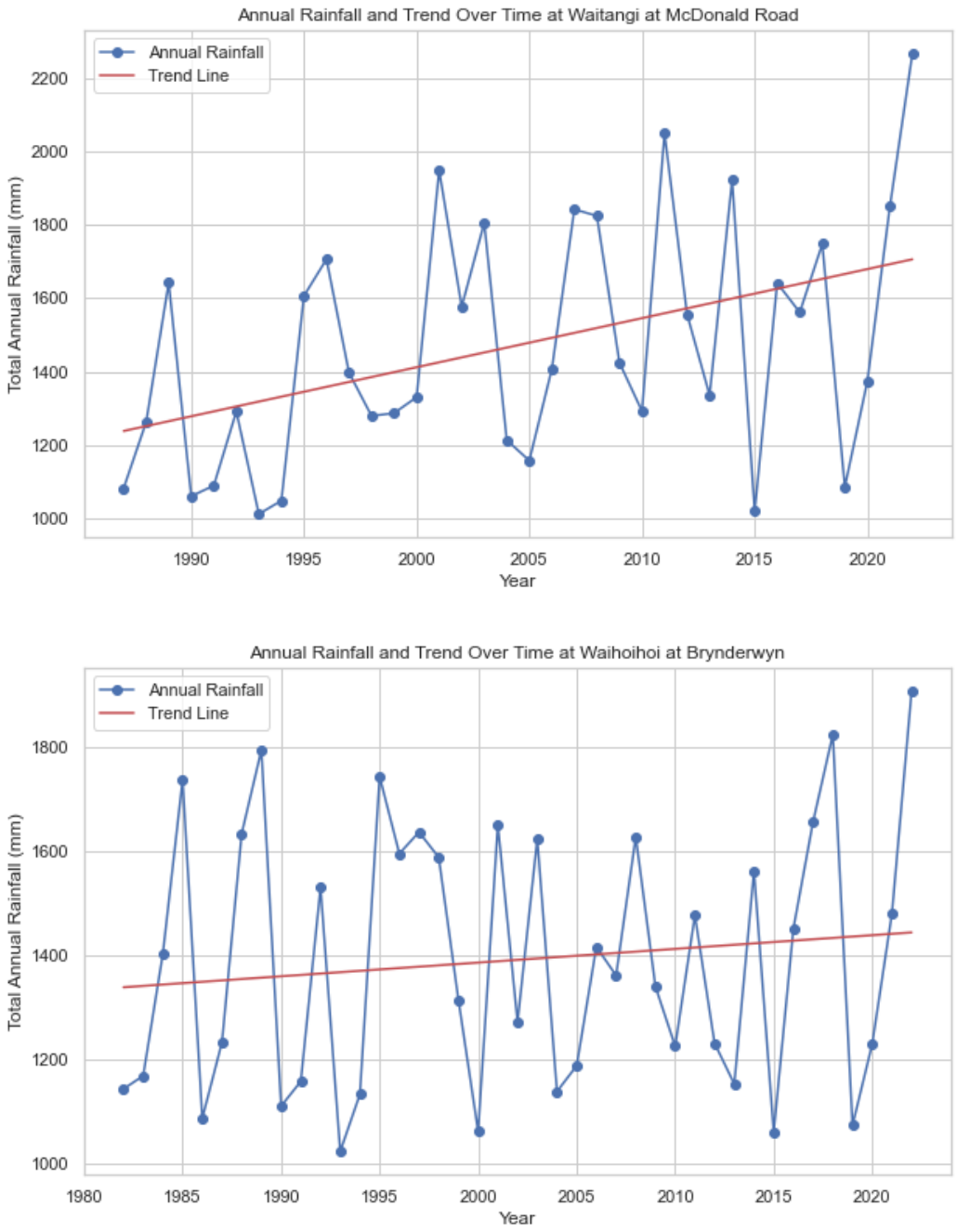

Figure 19: Trend analysis of annual rainfall at station of Waitangi at McDonald Road and Waihoihoi at Brynderwyn.

4.7. Rainfall in February

Summer months usually have the least rainfall compared to winter months. However, due to the influence of tropical cyclones and local heat, Northland could experience many heavy rain events in February. Figure 20 presents the maximum historical daily rainfall recorded at each station in February, alongside the rainfall associated with Cyclone Gabrielle and the Mangawhai flash flood. These two events clearly exceed the historical maxima at several locations, highlighting the potential for extreme summer rainfall despite the season's usual dryness.

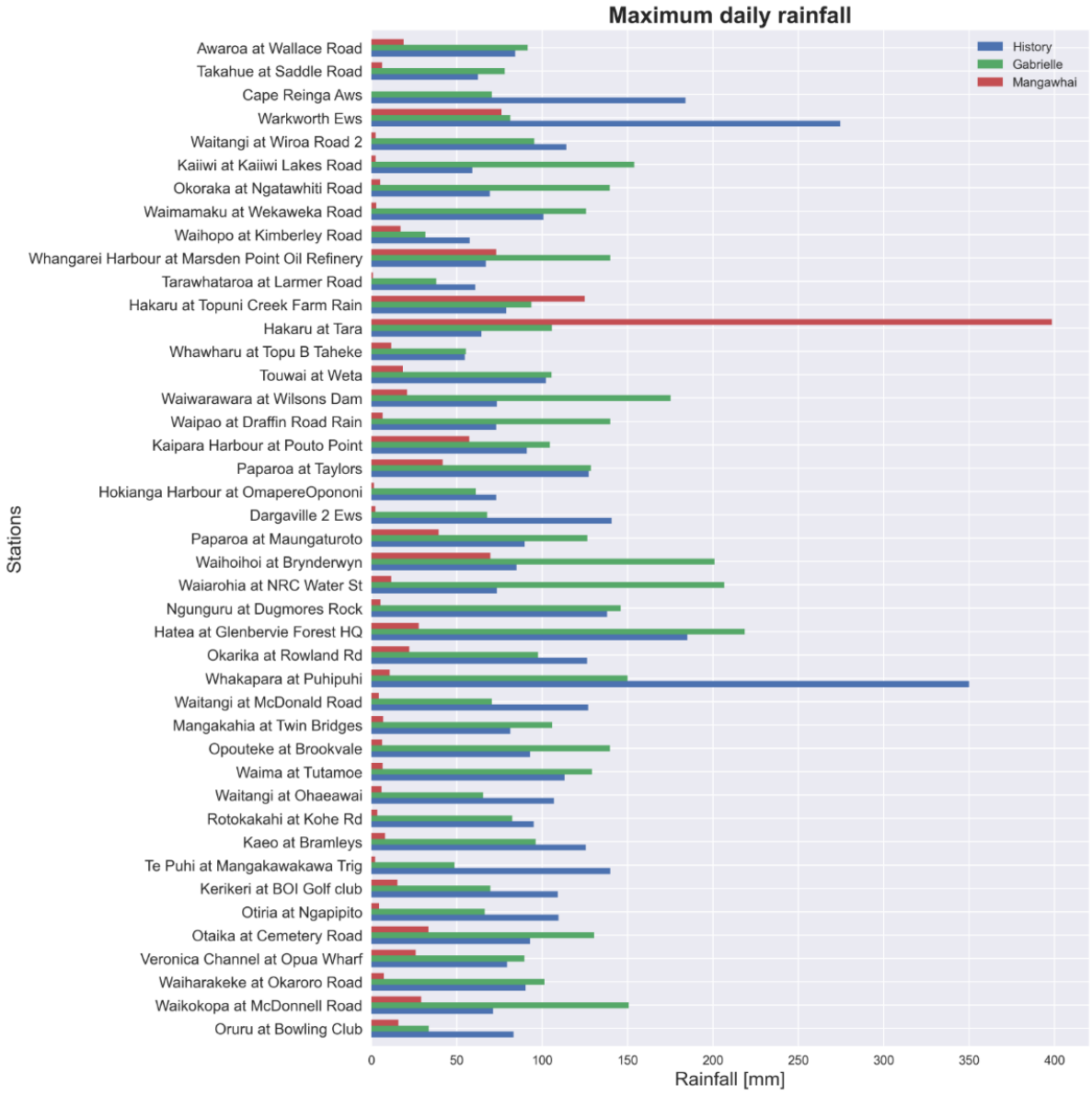

Figure 20: Maximum daily rainfall (mm) in 43 stations in February in the Northland region, (Blue bars: recorded data (to the end of 2022), Red bar: Mangawhai flash flood, Green: Cyclone Gabrielle)

Figure 20 shows that many stations recorded exceptionally high daily rainfall during Cyclone Gabrielle, with several locations exceeding their historical February maxima. In contrast, the Mangawhai flash flood produced a much more localised rainfall pattern. At

most stations across Northland, rainfall during the Mangawhai event remained well below the historical February extremes. Only the two Hakaru stations—Hakaru at Topuni Creek Farm and Hakaru at Tara—recorded rainfall amounts that approached or exceeded their historical maxima, reflecting the highly concentrated nature of the Mangawhai storm. The Hakaru at Tara station recorded nearly 400 mm of rainfall, and it stands out compared to other stations. This value exceeded the highest daily precipitation recorded at Whakapara at Puhipuhi, which had a historical maximum of over 350 mm.

There is a significant spatial variability in rainfall, with certain stations experiencing much heavier downpours than others during these events. Historical data indicates the past maximum rainfall values recorded are in the range of 100 to 200 mm, but some stations may exceed this. Rainfall from the Cyclone Gabrielle event (Green bars) varies across stations. In some cases, such as Mangakahia at Twin Bridges, this event caused more rainfall than the historical maximum. Cyclone Gabrielle seems to have caused significant rainfall at several stations ranging from 100 to 250 mm. The Mangawhai flash flood (Red bars) rainfall appears lower compared to the historical data and the Gabrielle event at most stations, with some stations recording little or no rainfall.

5. Analysis of February 2023 Storm Events

5.1 Cyclone Gabrielle Event

5.1.1 Rainfall

In this study, the temporal and spatial rainfall variability during Cyclone Gabrielle is analysed by using gauging station data, satellite data and weather radar data. The temporal and spatial patterns of rainfall during Cyclone Gabrielle are shown in **Figure** 21.

Figure 21 illustrates the temporal and the spatial distribution of rainfall during Cyclone Gabrielle in the Northland region. The plot illustrates a temporal pattern where rainfall intensity builds up from 11th to 13th of February 2023, with the peak rainfall occurring on 13th February, followed by a decrease on the 14th of February. The rainfall progression followed the movement of the cyclone through the region, intensifying and gradually weakening after the passage of Cyclone Gabrielle. The central region consistently shows higher rainfall on 12th and 13th February 2023, which could indicate the path of the weather system or localised orographic effects. The northernmost and southernmost regions tend to receive less rainfall, suggesting that the central area might be more prone to heavy rainfall during this event.

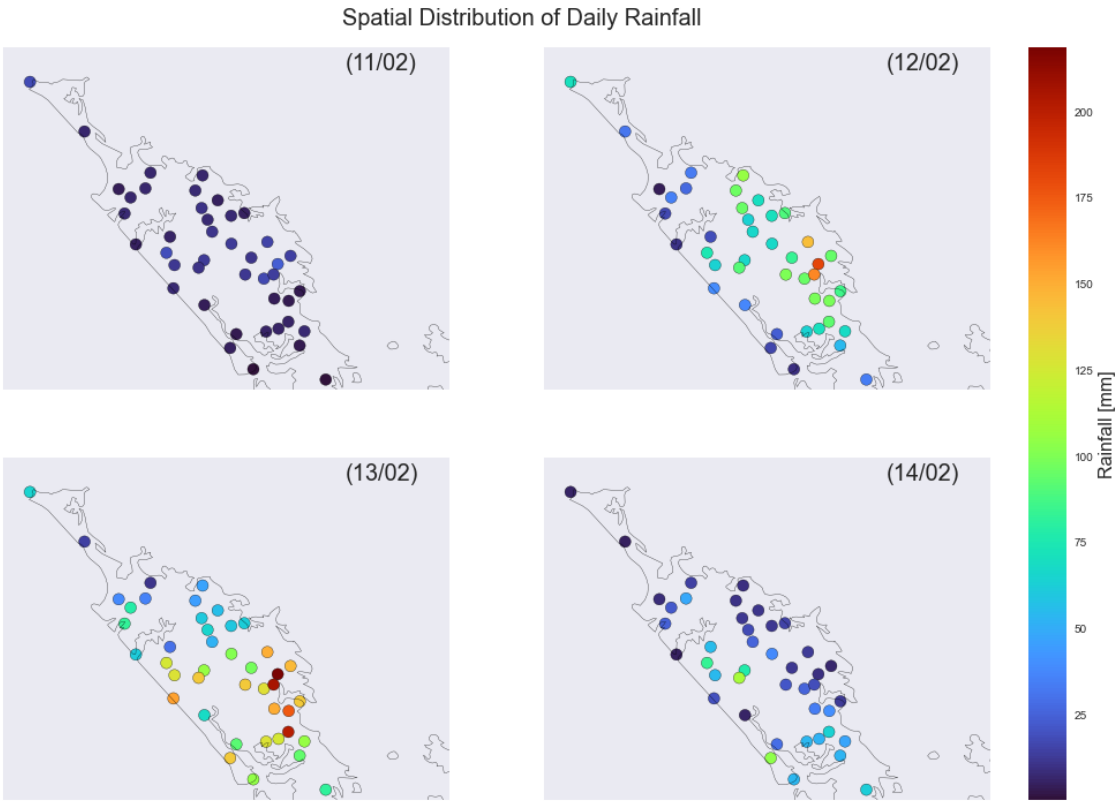

Figure 21: Spatial distribution of daily rainfall across the Northland region for four consecutive days: 11th to 14th February 2023 (NZST) during the Cyclone Gabrielle.

On 11th February, the rainfall across the region was generally low, as indicated by the prevalence of dark purple colours at most stations, suggesting that the rainfall amounts were likely below 25 mm. On 12th February, a noticeable increase in rainfall was observed, particularly in the central region, where the colours shifted from green to orange, indicating moderate to higher rainfall amounts, approximately between 100 and 175 mm. By 13th February, the rainfall distribution became more widespread, with some central and northern areas experiencing the highest levels, as shown by the red and orange colours, suggesting amounts exceeding 175 mm. However, by 14th February, the rainfall decreased across most stations, returning to lower amounts like those recorded on 11th February.

Figure 22 shows the daily rainfall during Cyclone Gabrielle from 11th February to 14th February 2023, as recorded by IMERG satellite rainfall data (New Zealand Standard Time). The data reveal a distinct temporal distribution of rainfall, with rainfall commencing on 11th February, peaking on 13th February, and diminishing by 14th February. Notably, the southern parts of the region experienced the highest rainfall during the peak on 13th February, reflecting the area most severely impacted by the cyclone. However, the spatial distribution of the IMERG data exhibits significant biases when compared to ground-based gauging stations, particularly on 13th February.

The progression of the storm is evident, with increasing rainfall from February 11th to 13th February, followed by a marked reduction on 14th February as the cyclone dissipated or moved away. On 11th February, the rainfall was moderate to light across most regions, with heightened rainfall observed slightly offshore and to the west, while inland areas received relatively lower amounts. On 12th February, the rainfall intensified and extends over a broader area, particularly in the central and northern regions, indicating the storm's progression and intensification. The most substantial rainfall occurs on 13th February, with extensive heavy rainfall, especially concentrated in the central and southern areas. The southern portion near 36°S experiences the peak intensity of rainfall, signifying the cyclone's most severe impact on this day. By 14th February, the rainfall decreases substantially compared to the previous day, with lighter precipitation confined to a smaller area, suggesting the storm is weakening and moving away from the region.

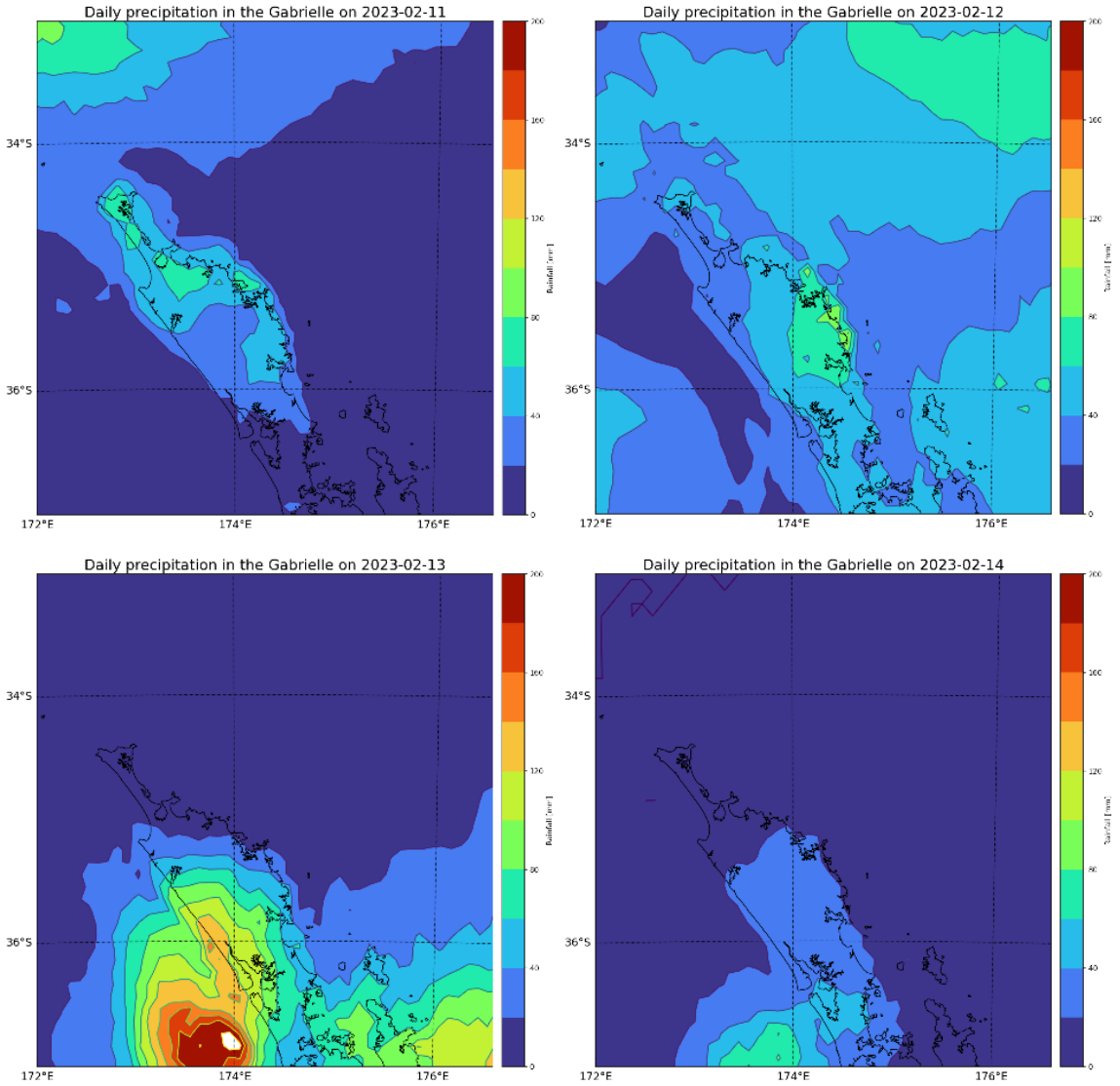

Figure 22: Daily rainfall during Cyclone Gabrielle (NZST) from IMERG Satellite rainfall data

The radar data show a similar rainfall pattern to that obtained from the satellite data (see Figure 23). The figure shows that rainfall intensity increased from 11th February to 13th February, peaking on 13th February, followed by a rapid decrease on 14th February. This pattern suggests the passage of cyclone which intensifies as it approaches and then weakens or moves away. The rainfall distribution varied across the region, with different parts experiencing varying levels of intensity. The southern part of the region appears to be more affected on 13th February, while the central part is more affected on 12th February.

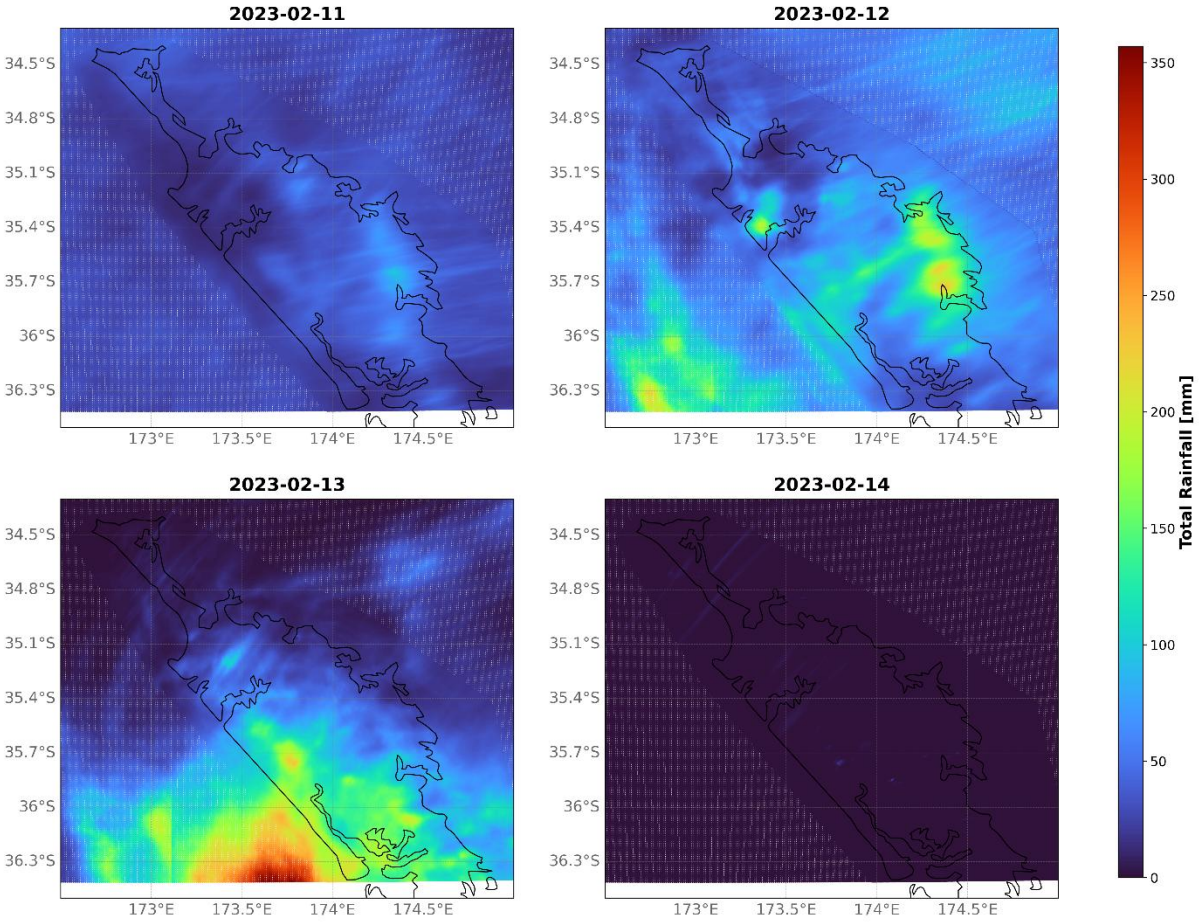

Figure 23: Spatial distribution of daily rainfall (Weather Radar data) during Cyclone Gabrielle in the Northland Region (February 11-14, 2023).

Figure 24 compares rainfall estimates from gauges, the IMERG satellite product, and radar data for 13th February 2023. Clear differences are evident between the three datasets. The figure shows a strong north–south gradient, with the highest rainfall occurring in the southern part of the region and substantially lower amounts in the north. However, the east–west pattern reveals a notable discrepancy: IMERG indicates heavy rainfall over the western areas, whereas both the gauge network and radar data show that the most intense rainfall was concentrated along the eastern coastal zone. This mismatch suggests that the satellite product underestimates or misplaces extreme

rainfall during cyclonic events, likely due to its limited ability to resolve orographic enhancement. The intense rainfall in the southern catchments on 13th February produced significant hydrological impacts, including widespread flooding across parts of Northland. Accurately understanding these spatial rainfall patterns is therefore essential for effective water-resource management and flood-risk preparedness.

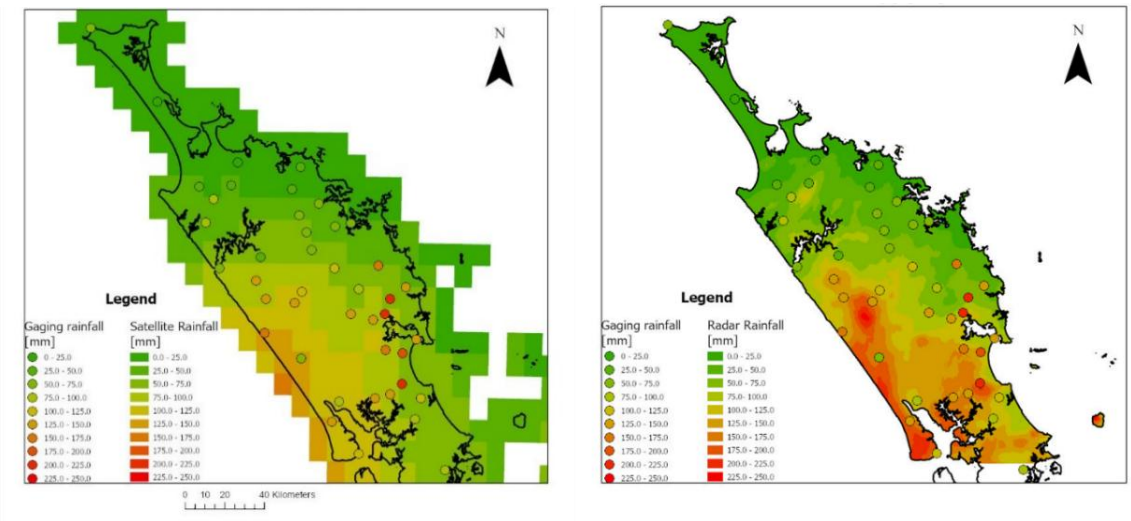

(a) (b)

Figure 24: Comparison of precipitation on February 13th (NZST) using three types of rainfall data: (a) NASA IMERG Final Run and gauging station data; (b) Climate Radar and gauging station data.

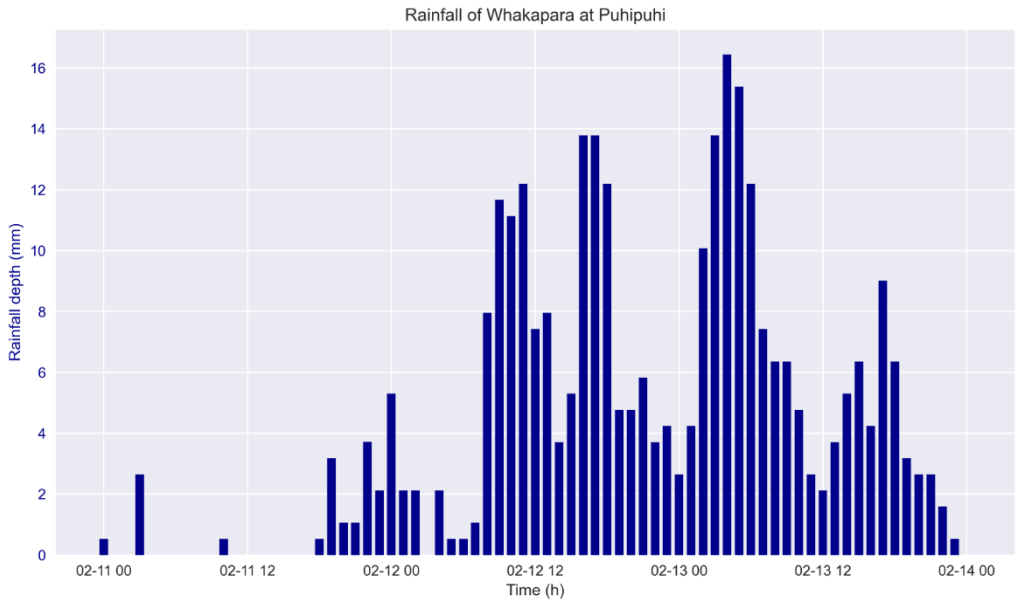

Figure 25: Hourly rainfall depth (mm) at Whakapara at Puhipuhi in Cyclone Gabrielle (11th February to 14th February 2023).

Figure 25 shows a rainfall pattern at the Whakapara at Puhipuhi station, where the largest rainfall during Cyclone Gabrielle was recorded. During Cyclone Gabrielle, the rainfall began at around 11th February with small, sporadic rainfall events below 2 mm, until around 12th February at 00:00. The most significant rainfall occurs between 12th February

12:00 and 13th February 12:00, where there are several spikes in rainfall depth exceeding 10 mm, with the peak rainfall reaching close to 16 mm around 13th February 00:00. This indicates a period of consistent and intense rainfall. There were fluctuations in rainfall throughout the period, with multiple peaks and declines, suggesting intermittent heavy rain and periods of reduced rainfall. After the peak rainfall at around 13th February 05:00, the rainfall gradually decreased on 14th February 00:00, though there were still moderate rain events following the main peaks.

Cyclone Gabrielle led to severe flooding mainly because many locations experienced long duration rainfall with daily rainfall amounts exceeding 100 mm/day, whereas the Mangawhai flash flood was extreme and due to localised heavy rainfall occurring over a short period of time.

Table 11 gives a comparison of rainfall intensity for all recorded data over 40 regional stations (three NIWA stations were not included) under normal conditions and during Cyclone Gabrielle. They show significant differences in precipitation. From historical records, rainfall intensities were substantially higher across all durations, ranging from 10 minutes to 24 hours, compared to those observed during the cyclone. For example, short-duration rainfall intensities (10 to 30 minutes) often exceeded 100 mm/hour under normal conditions but were significantly reduced during Cyclone Gabrielle, frequently falling below 40 mm/hour. Similarly, long-duration rainfall intensities (6 to 24 hours) were considerably lower during the cyclone, with values rarely exceeding 10 mm/hour, as opposed to historically recorded data where these intensities often surpassed 20 mm/hour. This stark contrast highlights Cyclone Gabrielle's moderate rainfall rates spread over longer durations, unlike the more intense and localised rainfall typically recorded in non-cyclonic events. These findings underline Cyclone Gabrielle’s unique precipitation dynamics, emphasising widespread, sustained rainfall rather than the extreme short-term intensities seen under normal storm conditions.

Table 11: Rainfall Intensity (mm/hr) across 40 Regional Stations in Northland: Historical Data (a) vs. Cyclone Gabrielle (b)

Stations	10 min		30 min		1 hr		3 hr		6 hr		9 hr		12 hr		18 hr		24 hr	
	a	b	a	b	a	b	a	b	a	b	a	b	a	b	a	b	a	b
Oruru at Bowling Club	108.0	12.2	68.3	7.1	56.4	5.6	27.5	3.2	20.0	2.9	14.5	2.4	12.5	2.0	10.6	1.8	7.9	1.6
Waikokopa at McDonnell Road	126.7	21.5	83.5	14.3	58.8	12.8	31.8	11.4	22.1	10.8	14.3	7.2	12.2	7.0	10.4	7.0	7.9	6.3
Waiharakeke at Okaroro Road	116.4	18.6	99.8	13.5	95.9	12.4	64.3	9.7	35.8	7.3	18.8	5.3	15.0	5.6	12.5	5.3	9.4	4.4
Veronica Channel at Opua Wharf	129.0	18.0	84.0	12.0	53.5	10.5	27.3	7.5	24.8	6.4	18.1	5.9	15.4	5.3	13.2	5.3	9.9	5.1
Otaika at Cemetery Road	108.0	26.7	64.0	15.6	46.0	15.0	23.9	12.1	14.8	11.0	9.8	7.1	8.4	6.9	7.7	6.5	6.0	5.5
Otiria at Ngapipito	122.1	17.8	66.8	12.9	56.9	10.4	33.1	6.8	22.4	5.5	12.7	4.2	10.2	3.8	9.1	3.4	7.9	3.3
Kerikeri at BOI Golf club	113.3	23.1	61.2	12.1	52.5	10.4	35.0	6.8	20.4	5.6	15.1	4.6	12.6	4.2	10.7	3.9	9.0	3.8
Te Puhi at Mangakawakawa Trig	79.1	10.9	56.5	8.2	37.0	6.8	21.3	5.6	15.9	4.9	11.6	4.7	10.7	4.2	9.2	3.6	7.5	2.9
Kaeo at Bramleys	96.8	21.1	69.4	14.1	52.5	11.6	32.5	7.7	22.9	6.8	20.6	6.2	17.8	5.6	15.2	5.1	12.2	4.8
Rotokakahi at Kohe Rd	90.0	21.5	59.9	15.4	47.3	10.8	23.0	7.3	13.6	6.0	9.5	4.8	7.9	4.2	7.0	4.0	5.5	3.4
Waitangi at Ohaeawai	122.5	22.5	86.1	16.1	66.8	12.3	27.6	7.5	24.0	5.3	17.1	4.2	14.5	4.0	12.4	3.9	9.9	3.6
Waima at Tutamoe	138.8	15.3	65.0	14.3	47.0	12.2	24.8	9.2	15.8	7.8	10.6	7.0	9.7	6.8	8.5	6.6	6.8	6.3
Opouteke at Brookvale	104.7	20.3	75.4	18.0	43.3	15.8	31.5	13.7	24.8	12.0	14.2	9.6	11.7	8.5	10.5	8.4	8.4	8.4
Mangakahia at Twin Bridges	92.5	25.9	64.9	18.4	58.0	15.7	25.2	11.9	17.3	8.3	12.6	6.6	10.7	5.7	9.2	5.5	7.9	5.3
Waitangi at McDonald Road	134.1	25.4	80.8	20.1	61.7	16.4	35.3	9.5	29.7	5.3	21.3	4.7	18.0	4.1	15.3	3.7	12.9	3.6
Whakapara at Puhipuhi	183.5	28.6	110.8	20.2	80.2	18.6	42.0	15.2	32.0	12.6	23.5	9.3	20.7	9.2	18.3	8.8	16.0	8.9
Okarika at Rowland Rd	146.1	24.1	126.0	11.1	80.4	10.1	28.6	7.9	22.3	6.9	15.8	5.5	13.4	4.9	11.4	4.8	8.6	5.0
Hatea at Glenbervie Forest HQ	154.3	36.9	120.4	23.6	73.3	21.0	44.5	17.6	34.0	15.6	22.5	11.9	19.0	11.7	15.9	10.8	13.0	11.0
Ngunguru at Dugmores Rock	144.0	32.5	110.4	18.7	74.0	14.3	37.2	12.0	27.3	10.7	20.5	8.8	19.3	7.8	17.6	7.3	15.9	6.7
Waiarohia at NRC Water St	165.6	30.0	101.2	26.4	76.0	24.0	38.0	18.3	27.7	15.6	18.8	10.6	15.6	10.7	13.3	10.4	10.3	10.1

Waihoihoi at Brynderwyn	174.3	26.8	124.4	23.4	114.2	22.3	59.2	18.6	34.5	16.4	21.5	12.0	17.9	10.8	15.7	10.2	12.2	9.0
Paparoa at Maungaturoto	138.0	20.4	102.0	17.5	78.4	16.5	36.6	14.6	25.5	12.2	15.6	8.9	13.0	8.4	10.9	7.8	8.3	6.5
Hokianga Harbour at Omapere Opononi	120.0	12.0	86.0	9.0	67.5	7.0	32.3	6.1	16.7	4.9	9.5	3.8	8.8	3.3	7.8	2.9	6.0	2.6
Paparoa at Taylors	113.5	21.3	97.7	17.3	74.5	15.7	37.6	14.2	20.9	12.4	12.1	9.2	10.2	8.4	8.6	8.3	6.8	6.8
Kaipara Harbour at Pouto Point	111.0	17.3	47.0	15.4	39.0	14.4	22.3	12.3	13.4	10.6	8.8	8.8	8.2	8.2	7.6	7.6	6.3	6.3
Waipao at Draffin Road Rain	141.0	16.6	96.0	15.5	81.0	12.7	47.3	11.2	27.0	10.2	15.5	7.0	12.4	7.0	10.4	6.8	7.8	6.0
Waiwarawara at Wilsons Dam	131.2	25.9	95.9	21.6	78.9	19.4	34.0	15.6	32.1	12.5	19.8	7.8	16.6	8.0	14.1	8.2	10.6	7.4
Touwai at Weta	116.0	21.0	72.3	16.0	47.7	12.5	29.7	9.5	29.2	7.9	21.1	6.2	18.1	5.6	15.5	5.5	11.8	5.2
Whawharu at Topu B Taheke	141.1	9.5	81.5	8.4	43.4	7.9	20.5	6.7	13.0	5.8	8.0	4.8	6.9	4.4	6.0	3.7	4.6	3.0
Hakaru at Tara	222.6	15.7	157.8	14.6	133.3	14.1	89.0	11.5	57.3	9.0	33.0	7.8	26.4	6.8	22.1	5.9	16.6	5.1
Hakaru at Topuni Creek Farm Rain	149.9	19.5	127.1	14.1	105.9	13.5	42.0	11.4	22.8	10.0	12.0	9.0	10.2	7.8	9.0	6.7	6.9	5.4
Tarawhataroa at Larmer Road	101.6	8.8	55.0	7.8	46.2	5.9	21.2	4.4	11.6	2.8	7.4	2.4	6.5	2.1	5.9	2.0	4.8	1.6
Whangarei Harbour at Marsden Point Oil Refinery	117.0	27.0	74.0	16.0	48.5	12.5	23.3	10.7	14.3	9.0	8.0	7.2	6.8	6.4	6.5	6.5	5.9	5.9
Waihopo at Kimberley Road	87.4	12.8	55.1	7.5	40.8	4.3	23.2	3.0	16.9	2.0	9.6	1.9	7.7	1.6	7.7	1.6	6.9	1.6
Waimamaku at Wekaweka Road	112.8	18.8	69.2	15.7	49.8	14.1	21.9	11.8	13.1	9.7	9.4	9.4	8.8	8.8	7.9	7.9	7.5	7.5
Okoraka at Ngatawhiti Road	162.0	162.0	94.0	94.0	55.7	55.7	23.6	21.6	14.0	13.9	9.3	9.3	9.1	9.1	9.7	9.7	9.0	9.0
Kaiiwi at Kaiiwi Lakes Road	70.1	31.2	45.6	22.9	43.9	16.6	18.1	15.6	14.1	14.1	10.3	10.3	8.8	8.8	7.7	7.7	6.5	6.5
Waitangi at Wiroa Road 2	126.8	21.2	97.9	13.1	76.8	11.1	31.7	8.9	19.1	7.4	12.3	6.4	10.4	5.7	9.7	5.1	8.7	5.1
Takahue at Saddle Road	89.5	18.0	49.5	15.0	38.3	12.0	19.6	8.0	13.9	6.3	8.6	4.3	7.0	3.9	6.4	3.7	5.8	3.3
Awaroa at Wallace Road	87.5	10.8	60.8	9.9	41.6	9.4	29.8	8.1	19.1	7.3	10.5	5.9	8.4	5.1	7.3	4.8	6.5	4.2

5.1.2 Flow

In the present study, the flow rates that occurred in the region during Cyclone Gabrielle have been analysed in conjunction with the rainfall data. The flow data can be essential for hydrological modelling and understanding the dynamics of rainfall and runoff across the region. Areas with high flow values, especially in 2023, could be prioritised for flood mitigation efforts or water resource planning. Additionally, the geographical distribution of stations would highlight deficiencies in the spatial distribution of flow gauging stations in the region. Figure 26 shows the maximum flow values recorded during cyclone Gabrielle and the maximum historical flow values. The figure shows that several stations experienced flows close to or exceeding their historical maxima, particularly in the southern and eastern catchments, indicating the severity of the event. In contrast, some northern stations recorded flows well below their historical peaks, reflecting the spatial variability of the cyclone's hydrological impact. These differences highlight areas where flood risk is highest and where additional monitoring or mitigation measures may be needed.

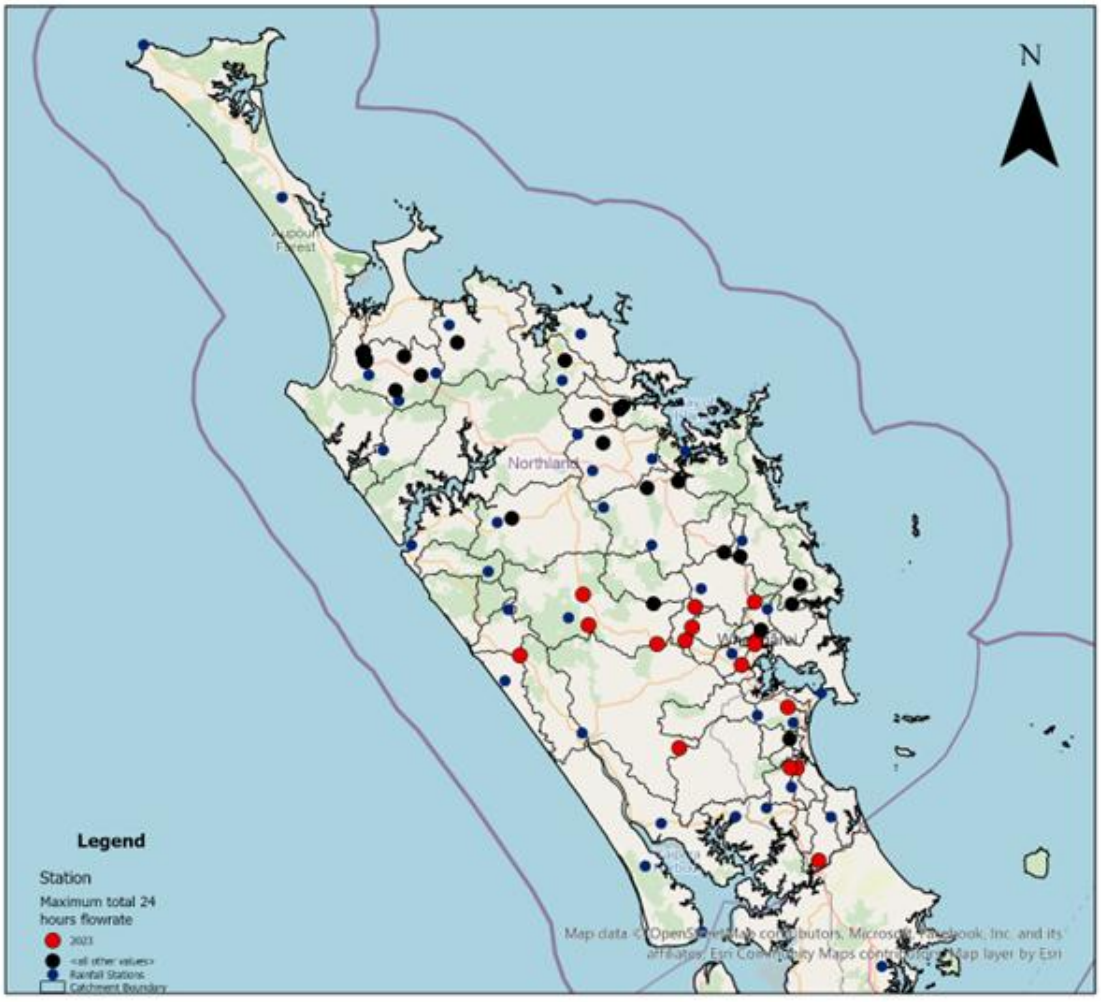

Figure 26: Comparison of maximum 24-hour flow rates during Cyclone Gabrielle and historical events. (Red dots represent stations where the flow rate during Cyclone Gabrielle exceeded historical records, Black dots indicate stations where historical events recorded higher flow rates than Cyclone Gabrielle.)

Figure 27 demonstrates an example of the relationship between intense rainfall and river flow during Cyclone Gabrielle from 11th to 16th February. The figure highlights the rapid hydrological response of the Ngunguru catchment at Dugmores Rock, while similar plots for other stations are provided in Appendix 3. The data reveal a strong connection between rainfall and river flow, with a noticeable lag between the peak rainfall and the peak river flow. The highest rainfall intensity, recorded on February 13 at over 12 mm/hour, corresponds to the maximum flow rate of more than 50 m^3/s observed shortly afterward. This lag reflects the time required for rainwater to travel through the catchment before contributing to river discharge.

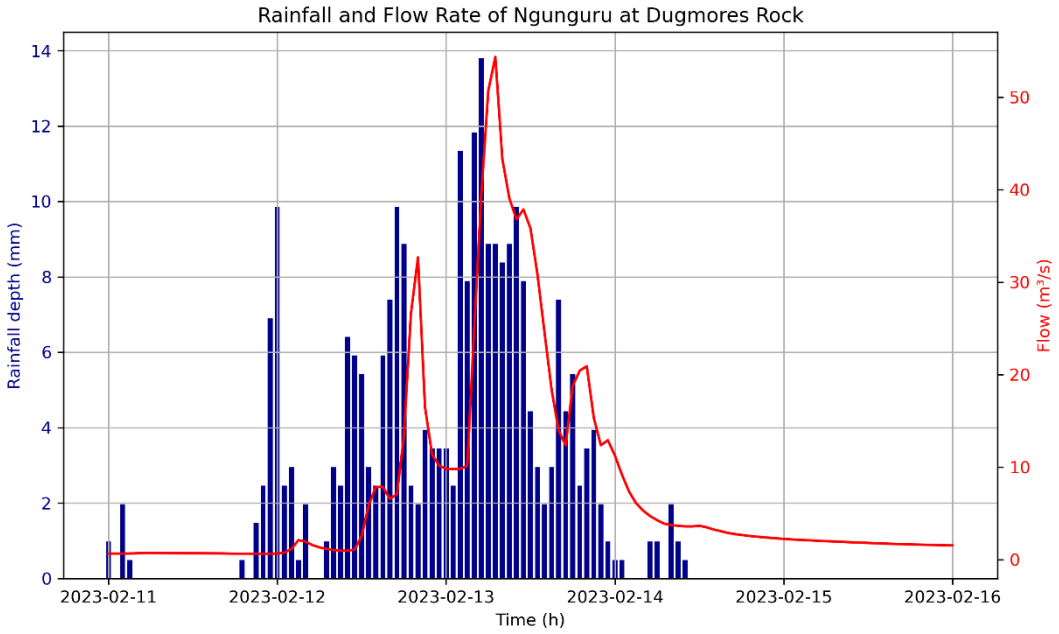

Figure 27: Rainfall depth (blue bars) and river flow rate (red line) at Ngunguru at Dugmores Rock from 11th to 16th February 2023.

The hydrograph shows a rapid rise in flow beginning on 12th February, coinciding with the onset of intense rainfall (**Figure 27**). The sharp peak on 13th February followed by a gradual recession indicates a highly responsive catchment with limited storage capacity. Differences in the spatial distribution of rainfall and flow-gauging stations create varying time lags between sites, making it difficult for any single station to fully represent the regional impact of Cyclone Gabrielle. The event also caused data-recording anomalies at several stations, particularly during longer durations.

Analysis of peak flow metrics shows that Cyclone Gabrielle did not produce the highest hourly flows at most locations—only two stations recorded their maximum hourly values during the event. In contrast, 40% of stations reached their highest 24-hour flow totals, primarily in the southern part of the region. This proportion increased to 47.5% for

48-hour flows, highlighting the prolonged and widespread hydrological impact of the cyclone.

In this study, we visually assessed the performance of five frequency distributions in fitting the annual maximum flow data. These distributions are the GEV, Log-Normal, Weibull, Gumbel, and Pearson Type III distributions. We have fitted and plotted various distributions on the frequency curve. Figure 28 shows an example of the probability plots using these five distributions for the Waihoihoi at St Marys Rd flow gauging station. Examination of the figure shows that the Gumbel fit, the GEV fit, and the Log-Normal fit all match the observed data points very well across the entire range of exceedance probabilities. These distributions offer a strong fit, particularly in the middle range where the majority of data points are concentrated. In contrast, the Pearson Type III fit exhibits noticeable deviations at both extremes of the distribution, rendering it less suitable for accurately capturing the full range of flow rate variability. Similarly, the Weibull fit shows more significant deviations at lower exceedance probabilities (corresponding to higher flow rates).

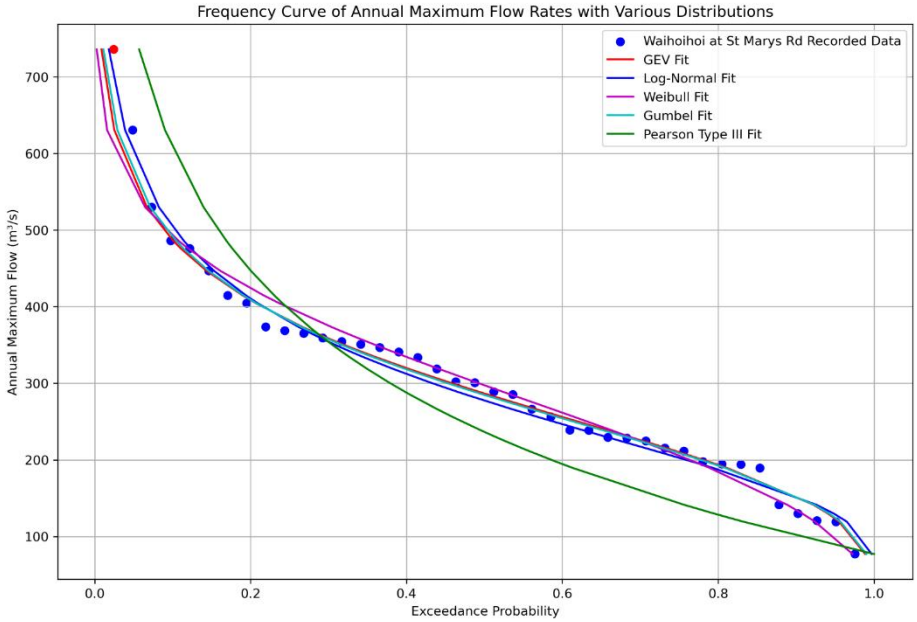

Figure 28: Frequency Curve of Annual Maximum Flow Rates for Waihoihoi at St Marys Rd with various distribution (Red dot: flow rate during Cyclone Gabrielle; Blue dots: peak flow rates from other years).

The Gumbel fit and GEV fit emerge as the most accurate models, providing a close match to the observed flow rates across the entire spectrum of exceedance probabilities. Of these, the Gumbel fit appears slightly more aligned with the data, especially at lower exceedance probabilities, positioning it as the strongest candidate for overall fit quality. Notably, the GEV fit demonstrates significant deviations at many stations, particularly where the data record spans less than 14 years. Therefore, for subsequent analysis and

statistical assessments in the Northland region, the Gumbel distribution was selected as the preferred model.

Figure 29 shows that Cyclone Gabrielle resulted in flow values that exceeded previously recorded maximum flows. For example, at the Manganui at Permanent station, the flow recorded during Cyclone Gabrielle exceeded the largest historical value, corresponding to an exceedance probability of 0.01, which is equivalent to a return period of approximately 100 years.

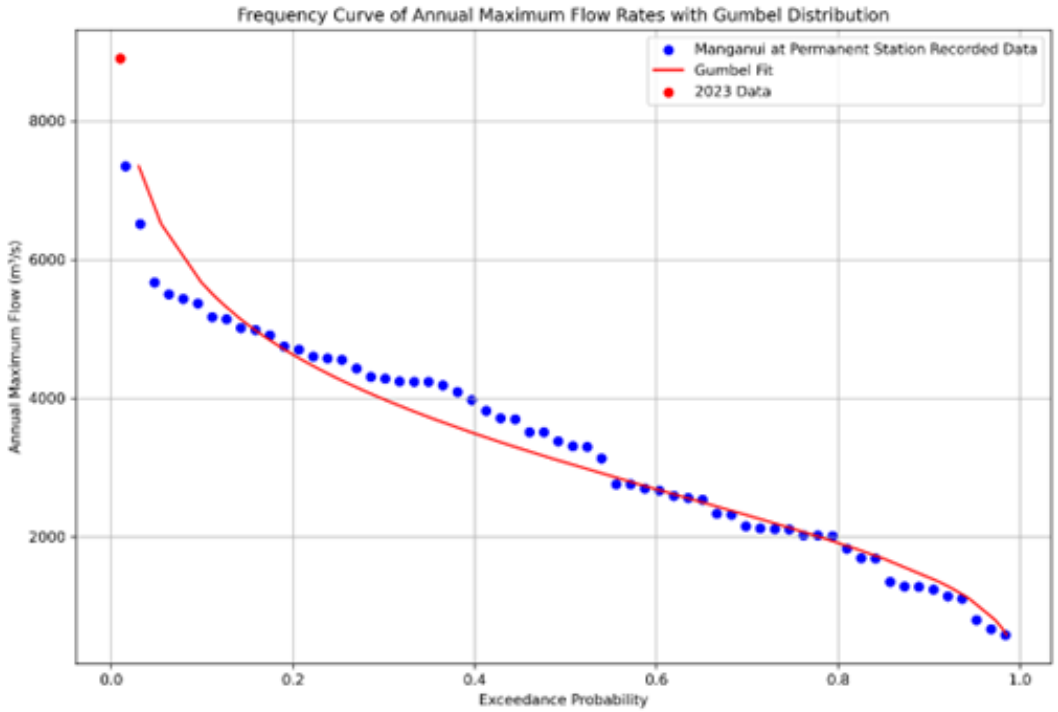

Figure 29: Frequency curve of annual maximum flow rates, modelled with the Gumbel distribution.

The frequency curve of annual maximum flow rates indicates that the Gumbel distribution provides a good fit to the recorded data from the Manganui Permanent Station. The majority of the data points align well with the Gumbel fit, suggesting that the distribution effectively captures the general trend of extreme flow events. However, the 2023 data point significantly deviates from the expected trend, indicating an exceptionally high flow event in that year, which may be due to unusual meteorological conditions. This outlier highlights the potential impact of extreme events on flow rates, emphasising the importance of considering such anomalies in future risk assessments and infrastructure planning.

The findings indicate that Cyclone Gabrielle had an exceptionally high impact on river flow rates in the southern part of the Northland region, with the Ahuroa at Braigh Flats station experiencing a record-breaking flow rate. This would have some implications related to flood risk management.

5.2 The Mangawhai Flash Flood

5.2.1 Rainfall

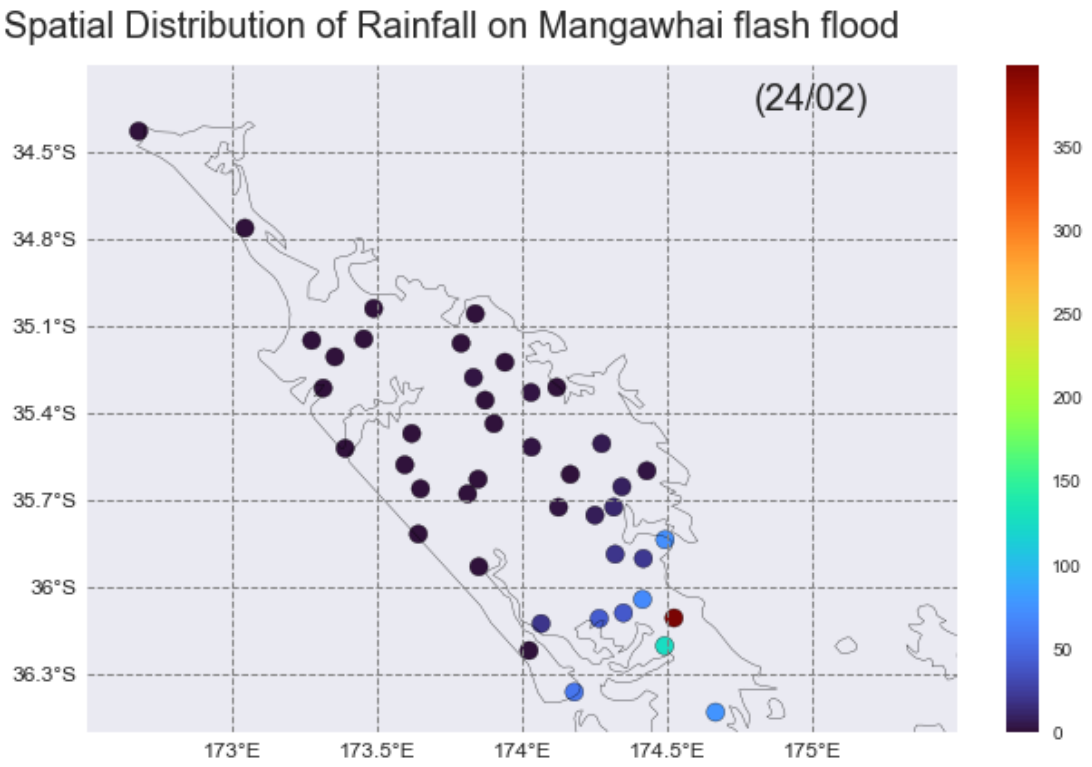

Figure 30: Spatial distribution of rainfall during the Mangawhai flash flood event on 24th February 2023 based on gauging station.

Figure 30 illustrates the spatial distribution of rainfall during the Mangawhai flash flood on 24th February 2023, covering the Northland region of New Zealand. The rainfall data is mapped across various monitoring stations, with the colour scale indicating rainfall intensity, ranging from 0 to over 400 mm. Most stations across the region recorded relatively low rainfall amounts, with darker colours (purple and blue) representing values between 0 and 50 mm. However, there were a few notable locations, particularly in the southern part of the region near Mangawhai, where rainfall intensities increased sharply, with values between 100 mm and 350 mm indicated by green, red, and cyan colours. This suggests that while most of the region experienced light to moderate rainfall, there were localised areas of heavy downpours.

The concentration of intense rainfall around 174.5°E and -36°S corresponds to the location of the Mangawhai area, which appears to have been the hardest hit. The sharp gradient in rainfall, with significant differences over a small area, likely contributed to the flash flood event. In contrast, northern and western areas experienced much lighter rainfall, showing the localised nature of the storm. Overall, the plot highlights how a few stations recorded significantly higher rainfall levels than the rest of the region, leading to the flash flood, despite relatively modest rainfall across most areas.

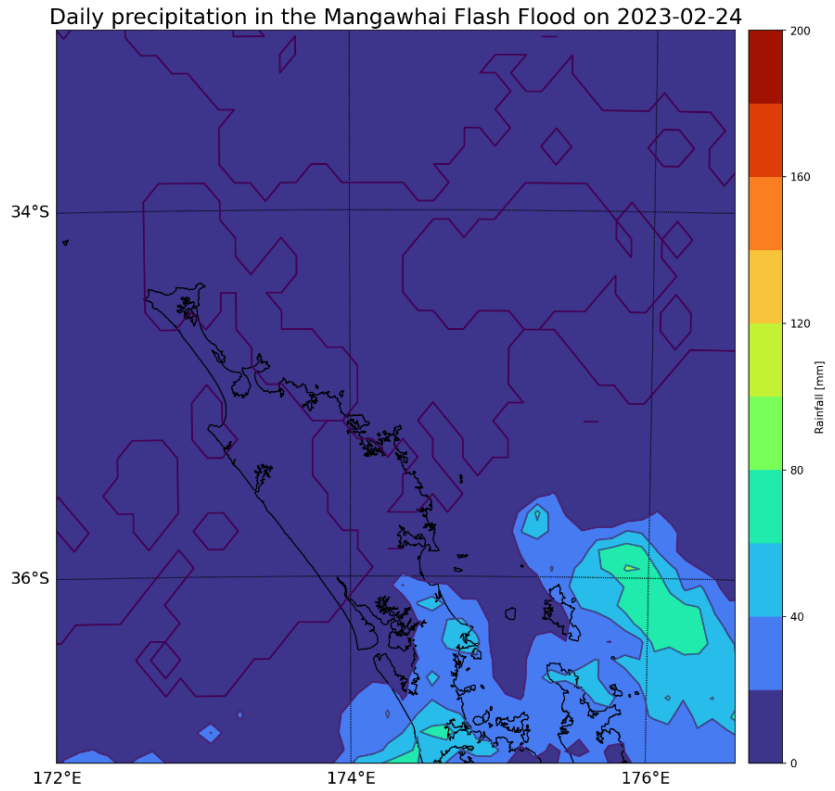

Figure 31: Spatial distribution of daily rainfall during the Mangawhai flash flood event on 24/02 based on IMERG satellite data.

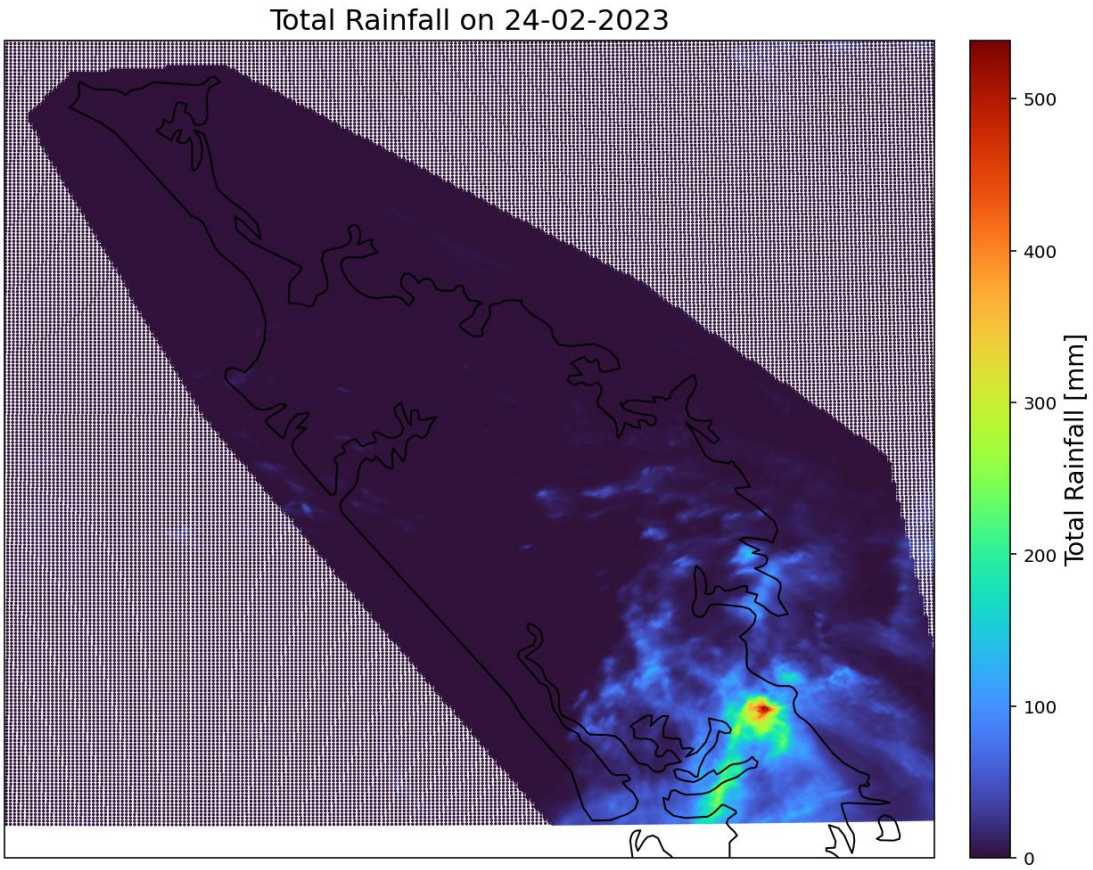

Figure 32: ***Spatial distribution of daily rainfall during the Mangawhai flash flood event on 24th February, derived from weather Radar data***

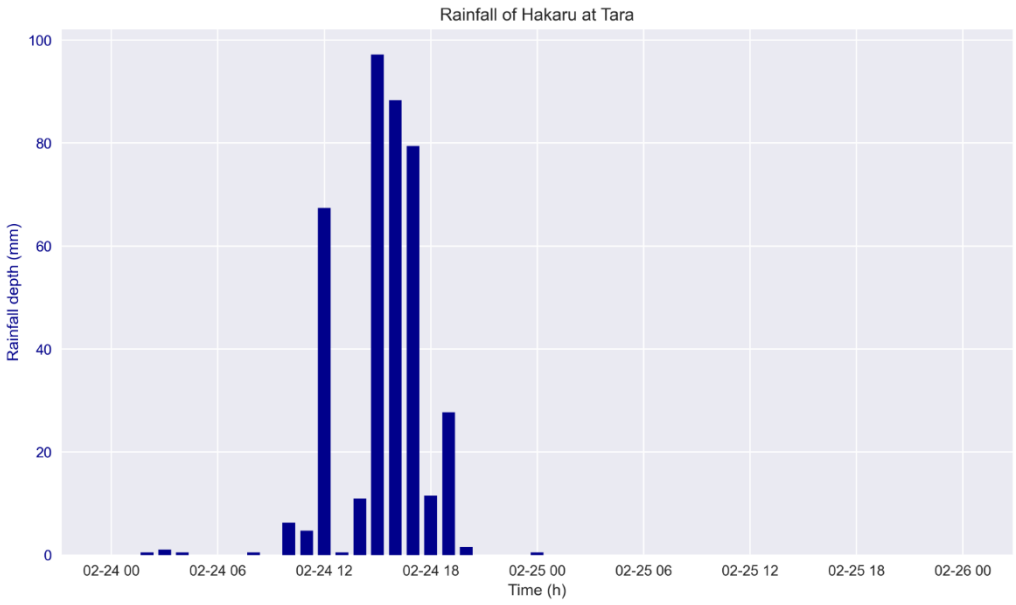

Figure 33: Rainfall depth (mm) over time at Hakaru Tara during Mangawhai flash flood.

Rainfall records from multiple data sources reveal inconsistencies in capturing high-intensity precipitation. The IMERG final run shows an underestimation of precipitation compared to gauging recorded data. While the gauge-recorded value reached up to 400 mm, the maximum value obtained from IMERG is only up to 80mm on 24th Feb 2023 (Figure 31). In contrast, the Radar data overestimate precipitation, showing a maximum of 530 mm (see Figure 32). Despite these discrepancies in magnitude, the spatial distribution patterns from Radar data align reasonably well with ground-based observations.

Figure 33 shows the hourly rainfall at the station of Hakaru at Tara from 24th February to 26th February. The rainfall depth spikes quickly with high intensity, indicating that a large amount of rain fell within a one-hour window of time, followed by a rapid decline. The most significant rainfall occurred between 24th February 12:00 and 24th February 18:00, with the rainfall depth exceeding 80 mm, peaking close to 100 mm. This period experienced intense rainfall in a relatively short span, indicating a very heavy rain event. There are minor showers later in the day, particularly on 24th February 18:00 and 25th February 00:00, but no significant rainfall after the primary peak event.

5.2.2 Flow

Due to the localised nature of rainfall, flow rates exhibited correspondingly localised patterns. Rainfall and flow data related to the Mangawhai flash flood are analysed based on the Hakaru at Topuni Creek Farm monitoring station. Even though the distribution of rainfall in the station shows differences compared to the station at Hakaru at Tara, it recorded the second-largest precipitation in this event. The relationship between rainfall

and flow rates at the Hakaru at Topuni Creek Farm monitoring station is shown in Figure 34.

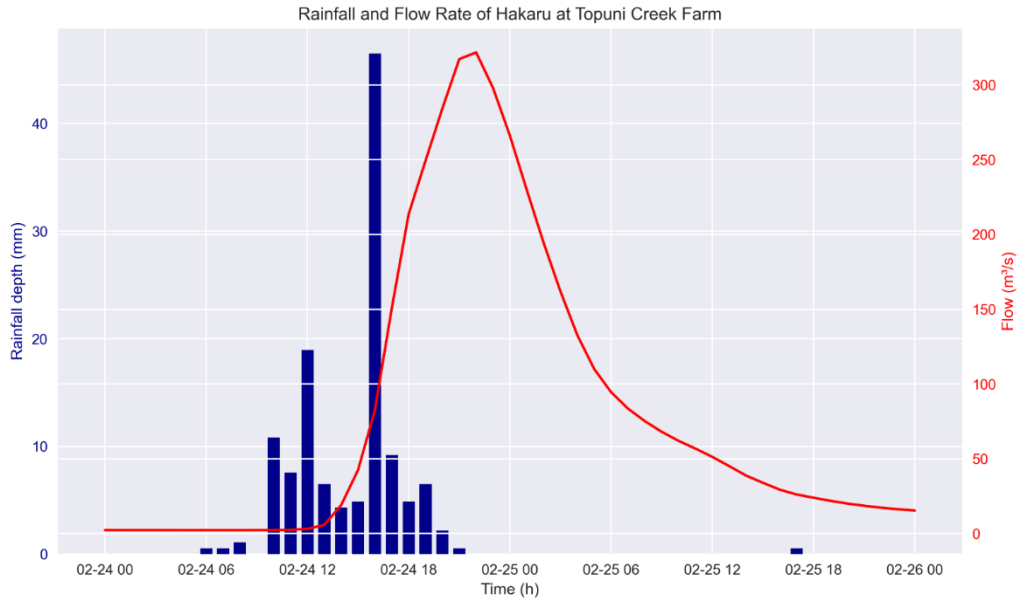

Figure 34: Time series analysis of rainfall depth and flow rate data for Hakaru at Topuni Creek Farm.

The rainfall depth, indicated by blue bars on the left y-axis, is measured in mm over time. Rainfall begins to increase around 24th February 06:00, with notable spikes occurring after 24th February 12:00, reaching a peak of over 40 mm at approximately 24th February 18:00. This pattern suggests a period of intense rainfall within a relatively short duration. In response, the flow rate, shown by the red line on the right y-axis and measured in cubic metres per second (m^3/s), rose sharply shortly after the rainfall peak. The flow rate reached its maximum of approximately 300 m^3/s between 24th February 18:00 and 25th February 00:00, demonstrating the catchment's rapid response to the heavy rainfall event.

There is a noticeable lag between peak rainfall and peak flow rate. The rainfall reaches its highest point around 18:00 on 24th February, while the flow rate peaks several hours later, between 00:00 and 02:00 on 25th February. This delay is expected as it takes time for runoff from the rainfall to accumulate and move into the creek system. Following the rainfall event, the flow rate declines gradually rather than immediately, indicating that the watershed continues to drain water even after the rainfall has ceased. The sharp rise in flow rate following the peak rainfall reflects the watershed's strong hydrological response to intense rainfall which represents flash flooding during extreme weather conditions.

5.3 Impact Quantification

Severe Tropical Cyclone Gabrielle struck parts of New Zealand's North Island, as well as areas in Vanuatu and Australia, in February 2023. It became the costliest tropical cyclone

ever recorded in the Southern Hemisphere, with total damages estimated to be at least NZ$14.5 billion, including insured damages of at least NZ$3.18 billion (Nick Wilson, 2024). In the Hawke's Bay alone, costs are estimated to exceed NZ$5 billion (Pocock, 2023). Cyclone Gabrielle was also the deadliest cyclone and weather event to affect New Zealand since Cyclone Giselle in 1968, surpassing the impact of Cyclone Bola in 1988. Gabrielle was the fifth named storm of the 2022–23 Australian cyclone season and the first severe tropical cyclone of the South Pacific season. It was first noted as a developing tropical low on 6th February 2023, while positioned south of the Solomon Islands. It was subsequently classified as a tropical cyclone and named Gabrielle by the Australian Bureau of Meteorology. The system peaked as a Category 3 cyclone before moving into the South Pacific basin and rapidly weakening into a subtropical low on 11th February 2023. As Cyclone Gabrielle approached, Norfolk Island was placed under a red alert, and heavy rain and wind warnings were issued for New Zealand's North Island. Existing states of emergency in Auckland and the Coromandel, due to recent flooding, were extended, and new states of emergency were declared in additional areas. The cyclone impacted New Zealand from 11th February to 17th February, with a national state of emergency declared on 14th February 2023. All states of emergency were lifted by 14th March (Gourley, 2023).

February 2023 will go into the record books as a month during which Aotearoa New Zealand experienced one of its worst weather disasters in modern history, in the form of an ex-tropical cyclone. The major event was Cyclone Gabrielle, which had a historic impact on the North Island of Aotearoa New Zealand. The impact can be divided into different aspects and is discussed below.

Overall, the February rainfall was exceptional in the North Island. Most areas experienced above-normal or well-above-normal rainfall. Parts of southern Northland, Auckland, Gisborne, Hawke's Bay, and coastal Wairarapa received at least 400% of the normal February rainfall. For instance, Napier received a total of 359 mm of rain, which is approximately 45% of its annual normal rainfall. This made it the town's third wettest month overall since records began in 1870. For temperature, the northern part of North Island had temperatures generally near average. For soil moisture, soil moisture levels were well above normal across most of the North Island. Cyclone Gabrielle had a significant impact. On 13th-14th February, Cyclone Gabrielle caused historic extreme rainfall, river flooding, catastrophic wind damage and substantial storm surges across the North Island, with the most significant damage occurring in Northland, Auckland, the Coromandel Peninsula, Gisborne, Hawke's Bay, and east-coastal Manawatū-Whanganui. The recovery from this storm is expected to take years and be very costly, particularly along the North Island's east coast. Gabrielle's impact is comparable to

other historically significant storms like Cyclone Bola (1988), Giselle (1968), and the "Cyclone of 1936". In summary, Cyclone Gabrielle left an indelible mark on New Zealand's weather history, with devastating consequences and a long road to recovery ahead (NIWA, 2023a).

Despite the significant human and economic impacts of Cyclone Gabrielle, there has been no national inquiry into the disaster. While there have been inquiries into issues like slash and land use and ongoing reviews of the Hawke's Bay Civil Defence response, the central government has not committed to a comprehensive assessment of the cyclone's effects. This oversight is concerning; without a thorough evaluation of the overall situation, we cannot adequately prepare for future extreme weather events exacerbated by climate change. In this report, we aim to provide a brief overview of this major disaster by highlighting key quantifiable impacts, drawing from media reports, government statements, Official Information Act requests, and data from private companies.

5.3.1. Widespread Impact

A National State of Emergency was declared on 14th February, covering six regions severely affected by the cyclone: Northland, Auckland, Tairāwhiti, Bay of Plenty, Waikato, and Hawke's Bay, marking only the third time in New Zealand's history that such a declaration was made (Beehive, 2023). The state of emergency was lifted in Northland, Auckland, Waikato, and Tararua on 3rd March, while Hawke's Bay and Tairāwhiti saw it end on 14th March (Council, 2023).

5.3.2. Human and Economic Toll

Cyclone Gabrielle has been classified as one of New Zealand’s mass fatality events, claiming 11 lives and injuring nearly 2,000 people, according to ACC claims data (Kerr, 2023). Many of these injuries, such as concussions, can lead to prolonged health issues. The Treasury estimates the cyclone’s economic impact could reach up to $14.5 billion, with costs likely to rise due to ongoing repair needs exacerbated by subsequent weather events. Vulnerable populations, including low-income households and marginalised groups, are disproportionately affected by flooding and disasters, compounding existing inequalities.

5.3.3. Housing Damage

More than 300 homes received red-placards (designated as unsafe) post-cyclone, with two-thirds of these located in Auckland. Approximately 700 properties deemed to be at risk of future severe weather have received buyout offers from the government and local councils (Sharpe, 2023). The Insurance Council of New Zealand reports that the combined impacts of the Auckland Anniversary Weekend floods and Cyclone Gabrielle

have led to over 100,000 claims, totalling an estimated cost of over $3.18 billion (Gibbens, 2023).

5.3.4. Road Infrastructure Damage

At the time the National State of Emergency was declared, over 30 sections of state highway were closed. This included critical routes serving Northland, Auckland, Coromandel, and other areas. State Highway 2, between Wairoa and Napier, experienced the longest closure, with access restored three months later through a temporary bridge.

5.3.5. Loss of Electrical Power

During the storm, 332,000 households lost power, with 200,000 affected at the peak. The Northpower company described the event as the most significant in their staff's memory. While 60% of affected customers were reconnected within 24 hours, a small percentage experienced prolonged outages due to severe damage.

5.3.6. Cell Phone Connectivity Issues

The power outages led to significant disruptions in cellphone coverage and landline services, affecting EFTPOS transactions as well. Although only two out of over 1,600 mobile towers were damaged, the storm knocked more than 660 towers offline nationally. In Tairāwhiti, approximately 90% of towers were out of service during the storm's peak.

5.3.7. Water Infrastructure Damage

Water infrastructure faced severe strain during the cyclone, resulting in at least eight boil-water notices in the North Island, lasting an average of 19 days. Some wastewater treatment plants were inundated, leading to environmental concerns as raw sewage was discharged into the sea for months.

In summary, Cyclone Gabrielle starkly highlighted New Zealand’s lack of resilient infrastructure, increasing the region’s vulnerability to climate change-driven storms and other disasters. The government has pledged $6 billion for a National Resilience Plan, including $100 million for a new infrastructure delivery agency. However, there remains an urgent need for both central and local governments to enhance infrastructure resilience while preparing for increasingly disruptive weather patterns. This critical long-term planning should not be overshadowed by the election cycle or potential changes in government (PHCC, 2023).

6. Discussion

6.1 Spatial and Temporal Variation in Rainfall

The data illustrate a significant spatial variation in rainfall distribution across the Northland Region during Cyclone Gabrielle and the Mangawhai flash flood. During Cyclone Gabrielle, the highest rainfall intensities were concentrated in specific areas such as the southern areas around Whangarei and Dargaville, particularly on 13th February, which suggests that certain regions within Northland were more susceptible to extreme rainfall and potential flooding. The Mangawhai flash flood event demonstrates highly localised intense rainfall in the southeast near Mangawhai. Such disparities emphasise the need for localised monitoring and prediction systems capable of capturing these high-intensity events to enable precise and effective response strategies. The spatial distribution of rainfall during Cyclone Gabrielle exhibited significant daily variations, with peak intensities observed on specific dates. For example, regions with third quartile loading of rainfall intensity reflected spatial agreement between ground-based observations and other data sources. These patterns underline the complex interplay between geography, atmospheric dynamics, and storm progression, which dictates rainfall distribution during such extreme weather events.

The temporal analysis of rainfall during Cyclone Gabrielle and the Mangawhai flash flood event demonstrates a dynamic progression in intensity and distribution. Daily rainfall patterns from February 11th to February 14th show a clear temporal evolution, with peak rainfall occurring on February 13th, followed by a decline. This progression mirrors the lifecycle of Cyclone Gabrielle, where varying storm intensities influenced the timing and magnitude of rainfall impacts. The temporal distribution during the Mangawhai flash flood shows extreme intensities of precipitation throughout the event. Precipitation mostly reached 100 mm/hour, which is the main factor leading to flash flooding in the region.

Understanding this temporal evolution is crucial for forecasting and preparedness. It enables the identification of critical periods during a storm when the risk of flooding, landslides, and other hazards is highest. The intense rainfall concentrated over specific periods and areas underscores the importance of integrating spatial and temporal analysis for comprehensive risk assessment and mitigation planning.

6.2 Comparison of Rainfall Data Sources

The comparison between NASA IMERG data, Climate Radar data, and ground-based gauging station measurements reveals discrepancies in the observed rainfall intensities. The IMERG data, being satellite-based, provides broad coverage but may lack the fine

resolution needed for precise, localised assessments. In contrast, the Climate Radar data, although more localised, may still have variations when compared to on-ground measurements. This could imply the need for more accurate, localised measurements for better flood prediction and response planning.

These discrepancies underline the challenges in relying on a single data source for understanding rainfall patterns during extreme weather events. This suggests that integrating multiple data sources can provide a more comprehensive and accurate picture, essential for effective disaster management. Further investigation is needed to understand why this difference still exists and the mechanisms underlying the observed data discrepancies. This discrepancy arises from limitations in data sources. Although the rainfall gauging station network in the Northland region is robust enough to support the development of various models, there is a pressing need for high-resolution, more accurate gridded products. Future research should therefore focus on more comprehensive integration of diverse rainfall data sources to improve the accuracy and spatial resolution of gridded rainfall products for the region.

6.3 Flow

The extreme rainfall associated with Cyclone Gabrielle and the Mangawhai event was a key driver of flooding. As the cyclone moved toward New Zealand, it brought significant moisture from the tropics, causing very high rainfall rates in a short period. The Northland region, especially around Whangarei and Dargaville, experienced intense rainfall, with some areas receiving over 200 mm in just 24 hours. This rainfall led to the highest recorded flow rates in the region, highlighting the intense nature of the storm. The flooding caused by Cyclone Gabrielle was not a short-lived event; due to continuous rainfall over multiple days, the flow rates in rivers and streams remained high for an extended period, leading to prolonged flooding. Riverbanks were breached, and floodwaters lingered in the affected areas, with recovery taking days or even weeks in some regions.

On the other hand, the Mangawhai flash flood, which occurred on February 24, 2023, was a localised but intense event that resulted from extreme rainfall in a short period. Mangawhai experienced a rapid accumulation of rainfall that overwhelmed drainage systems, rivers, and streams, leading to flash flooding in the area. The Mangawhai flash flood serves as a reminder of the dangers posed by intense rainfall and rapid runoff, particularly in areas with steep topographical features. It underscores the need for better flood prediction systems, infrastructure planning, and risk management strategies for communities in flood-prone areas.

The intense rainfall and flow surges caused widespread flooding, from rural farmland to urban regions. Major roads and infrastructure were flooded, leading to significant transportation disruptions, while communities in flood-prone areas were particularly hard-hit. The flow dynamics during Cyclone Gabrielle resulted in high flow rates and significant flooding, primarily driven by the combination of heavy rainfall, rapid runoff, and overwhelmed river systems. The varying flow rates and flood extents were influenced by regional topography and the intensity of the cyclone's rainfall. This resulted in localised flash floods and widespread river flooding that caused major disruptions in affected communities. The event underscores the need for more accurate modelling and enhanced flood risk management strategies to mitigate the impact of future extreme weather events.

This research primarily focuses on rainfall and its characteristics, but it is important to recognise that numerous other factors significantly influence rainfall-runoff generation, including land cover, soil properties, and topography. Understanding the interactions among these factors is essential for determining the extent and severity of flooding and should be incorporated into integrated watershed management strategies. Future research should delve deeper into these interactions by developing and applying hydrological models to understand comprehensively the mechanisms of rainfall-runoff generation and flow dynamics in the region.

6.4 Implications for Infrastructure and Flood Management

The findings suggest that areas with the highest rainfall intensities were at the greatest risk for infrastructure damage, particularly in regions with inadequate stormwater management systems. The observed rainfall intensities likely exceeded the design capacity of existing infrastructure in some areas, leading to urban flooding and potential damage to roads, bridges, and other critical facilities.

This interpretation highlights the need for upgrading and adapting stormwater systems to handle such extreme events, particularly in regions prone to cyclones and intense rainfall.

6.5 Regional Vulnerability and Resilience

The data point to a varying degree of vulnerability across different parts of the Northland Region. Areas that experienced the highest rainfall intensities were likely more vulnerable to the impacts of Cyclone Gabrielle, suggesting the need for targeted resilience-building measures in these areas.

The findings also imply that future resilience strategies should consider not only the amount of rainfall but also its spatial and temporal distribution. This approach would help in identifying the most vulnerable areas and prioritising them for interventions.

The intense and varying rainfall patterns suggest a heightened risk for damage to infrastructure, particularly in areas that received higher precipitation levels. Roads, bridges, and stormwater systems in the Northland Region might have been particularly vulnerable, especially if they were not designed to handle such extreme events.

6.6 Climate Change and Future Projections

The extreme rainfall associated with Cyclone Gabrielle may be indicative of broader trends related to climate change, which is expected to increase the frequency and intensity of such weather events. The findings suggest that climate change adaptation strategies in the Northland Region should incorporate projections of more frequent and intense cyclonic events. This highlights the need for integrating climate change projections into regional planning efforts to ensure that both the built and natural environments can withstand future challenges.

The extreme rainfall associated with Cyclone Gabrielle could be indicative of more frequent and intense weather events in the future, as suggested by many climate models. The observed data support the argument for proactive planning and infrastructure development that can accommodate future changes in climate patterns, thereby reducing the long-term risks to communities and the economy.

Overall, the results suggest that Cyclone Gabrielle and the Mangawhai flash flood had a significant impact on the Northland Region, with important implications for infrastructure, stormwater management, and regional preparedness. These findings underscore the importance of using a combination of satellite and ground-based data to inform decision-making and improve resilience against future cyclonic events.

7. Conclusion

The analysis successfully identified key atmospheric circulation variables that significantly influence storm events in Northland, such as tropical cyclones, atmospheric rivers, and ENSO, highlighting the importance of these factors in predicting severe weather.

Using an event-based analysis approach to categorise historic storm patterns, the research provides a comprehensive framework for understanding the typical behaviours of Northland storms, especially the temporal distribution of precipitation. The vast

majority of extreme precipitation events occur during the second and third quartiles. Precipitation during Cyclone Gabrielle was primarily concentrated in the third quartile, corresponding to the large proportion of rainfall recorded on 13th February 2023. Spatial distribution of rainfall during the cyclone has shown that eastern regions were more significantly impacted by Cyclone Gabrielle than western regions due to prevailing wind direction.

The study yielded robust quantitative estimates of rainfall and flood flow from the February 2023 storm, illustrating its unprecedented impact on local hydrology and helping to inform flood management practices. The quantification of the February extreme rainfall's effects on river flooding in Northland underscores the vulnerability of the region's waterways to heavy precipitation events, emphasising the need for enhanced flood risk assessment and mitigation strategies, especially in the southern part of the region.

The detailed characterisation of Cyclone Gabrielle and the Mangawhai flash flood offers valuable insights into the specific conditions that contributed to these events. The interaction between Cyclone Gabrielle and atmospheric rivers appears to be a significant factor in generating substantial rainfall across extensive areas, driven by global general circulation patterns. While short-duration, high-intensity precipitation events were not widespread, prolonged rainfall emerged as the primary contributor to flooding in many regions. Conversely, the Mangawhai flash flood was localised, driven by summer heat and local moisture. This produced extremely high-intensity rainfall over a short period, rapidly elevating river water levels and causing flash flooding.

The findings underscore the urgent need for climate adaptation measures in Northland, given the heightened frequency and intensity of storms associated with climate change (Carey-Smith et al., 2010; Griffiths, 2007; Salinger & Griffiths, 2001), which present substantial risks to both the region's ecosystems and communities. Observations from various monitoring stations throughout the region confirm an increase in flood vulnerability. Consequently, it is imperative for central and local authorities to develop new strategies aimed at preparing for the anticipated rise in extreme rainfall and flooding events in the future.

This research establishes a foundation for future studies focused on long-term climate trends in Northland, facilitating the development of more resilient urban and rural planning strategies to address increasing weather extremes. Future investigations should delve deeper into the impacts of atmospheric rivers and tropical cyclones in the region. Additionally, further research into the influence of local surface conditions on rainfall-runoff response is needed, as this could significantly enhance our understanding of flood mechanisms and inform preparedness and resilience strategies.

8. Acknowledgement:

*Outcomes of this research have partially contributed to two scholarly outputs: a conference paper presented at the IAHR Conference in Korea titled "**Contrasting Hydrometeorological Drivers of Extreme Flooding in New Zealand: Cyclone Gabrielle and the Mangawhai Flash Flood**"* and a journal manuscript currently under review, ***"The Role of Integrated Vapor Transport Dynamics within Atmospheric Rivers in Enhancing Precipitation During Tropical Cyclones: A Case Study of Cyclone Gabrielle – 2023"*.

9. References

Adams, B. J., & Papa, F. (2001). Urban stormwater management planning with analytical probabilistic models. *Canadian Journal of Civil Engineering*, *28*(3), 545.

Ahrens, C. D. (2007). *Meteorology today : an introduction to weather, climate, and the environment*. Eighth edition. Belmont, CA : Thomson/Brooks/Cole, [2007] ©2007.

Ali, I. (2019). *Northland's population is the fastest growing in NZ*. Retrieved 03.10 from https://www.nzherald.co.nz/northern-advocate/news/northlands-population-is-the-fastest-growing-in-nz/JYTKIBIP6SJMJDYCSXG22FN4UQ/

Beehive. (2023). *State of National Emergency Declared*. Beehive.govt.nz. Retrieved 1 November 2024 from https://www.beehive.govt.nz/release/state-national-emergency-declared

Beven, K. (2012). Down to Basics: Runoff Processes and the Modelling Process. In *Rainfall-Runoff Modelling* (pp. 1–23). https://doi.org/https://doi.org/10.1002/9781119951001.ch1

Bluestein, H. B. (1992). *Synoptic-Dynamic Meteorology in Midlatitudes: Volume 1*.

Bonnifait, L., Delrieu, G., Lay, M. L., Boudevillain, B., Masson, A., Belleudy, P., Gaume, E., & Saulnier, G.-M. (2009). Distributed hydrologic and hydraulic modelling with radar rainfall input: Reconstruction of the 8–9 September 2002 catastrophic flood event in the Gard region, France. *Advances in Water Resources*, *32*(7), 1077–1089. https://doi.org/https://doi.org/10.1016/j.advwatres.2009.03.007

Borga, M., Gaume, E., Creutin, J. D., & Marchi, L. (2008). Surveying flash floods: gauging the ungauged extremes. *Hydrological Processes*, *22*(18), 3883–3885. https://doi.org/https://doi.org/10.1002/hyp.7111

Bouilloud, L., Delrieu, G., Boudevillain, B., & Kirstetter, P.-E. (2010). Radar rainfall estimation in the context of post-event analysis of flash-flood events. *Journal of Hydrology*, *394*(1), 17–27. https://doi.org/https://doi.org/10.1016/j.jhydrol.2010.02.035

California, U. o. (2024). *Atmospheric circulation*. Retrieved 03.10 from https://ugc.berkeley.edu/background-content/atmospheric-circulation/

Carey-Smith, T., Dean, S., Vial, J., & Thompson, C. (2010). Changes in precipitation extremes for New Zealand: climate model predictions. *Weather and Climate*, *30*, 23–48.

CDP. (2023). *2023 New Zealand Floods and Cyclone Gabrielle*. Retrieved 01-11-2024 from https://disasterphilanthropy.org/disasters/2023-new-zealand-floods/

Chandra, A., & Kumar, S. (2021). Sea surface temperature and ocean heat content during Tropical cyclones Pam (2015) and Winston (2016) in the Southwest Pacific region. *Monthly Weather Review*, *149*(4), 1173–1187.

Chappell, P. R. (2013). *The climate and weather of Northland* (3rd ed.). NIWA.

Council, N. C. (2023). *Cyclone Gabrielle*. Napier City Council. Retrieved 1 November 2024 from https://www.napier.govt.nz/our-council/cyclone-gabrielle

Diamond, H. J., Lorrey, A. M., & Renwick, J. A. (2013). A Southwest Pacific Tropical Cyclone Climatology and Linkages to the El Niño–Southern Oscillation. *Journal of Climate*, *26*(1), 3–25. https://doi.org/10.1175/jcli-d-12-00077.1

Emanuel, K. (2003). Tropical cyclones. *Annual review of earth and planetary sciences*, *31*(1), 75–104.

Emanuel, K. A. (1987). The dependence of hurricane intensity on climate. *Nature*, *326*(6112), 483–485. https://doi.org/10.1038/326483a0

Fay, P. A., Kaufman, D. M., Nippert, J. B., Carlisle, J. D., & Harper, C. W. (2008). Changes in grassland ecosystem function due to extreme rainfall events: Implications for responses to climate change. *Global Change Biology, 14*(7), 1600–1608. https://doi.org/https://doi.org/10.1111/j.1365-2486.2008.01605.x

Ferreira, S. (2024). Extreme Weather Events and Climate Change: Economic Impacts and Adaptation Policies. *Annual Review of Resource Economics*, *16*(Volume 16, 2024), 207–231. https://doi.org/https://doi.org/10.1146/annurev-resource-101623-095314

Foley, J. A., DeFries, R., Asner, G. P., Barford, C., Bonan, G., Carpenter, S. R., Chapin, F. S., Coe, M. T., Daily, G. C., Gibbs, H. K., Helkowski, J. H., Holloway, T., Howard, E. A., Kucharik, C. J., Monfreda, C., Patz, J. A., Prentice, I. C., Ramankutty, N., & Snyder, P. K. (2005). Global Consequences of Land Use. *Science*, *309*(5734), 570–574. https://doi.org/doi:10.1126/science.1111772

Gibbens, K. (2023). *More than 400,000 residential buildings in flood prone areas*. RNZ. Retrieved 01.11 from https://www.rnz.co.nz/news/national/493223/more-than-400-000-residential-buildings-in-flood-prone-areas

Gimeno, L., Nieto, R., VÃ¡zquez, M., & Lavers, D. A. (2014). Atmospheric rivers: a mini-review. *Frontiers in Earth Science*, *2*. https://doi.org/10.3389/feart.2014.00002

Gourley, E. (2023). *Cyclone Gabrielle: National state of emergency ends on Tuesday*. Stuff. Retrieved 01.11 from https://www.stuff.co.nz/national/hawkes-bay/131480932/cyclone-gabrielle-national-state-of-emergency-ends-on-tuesday

Gray, W. (2003). *Overview of weather and coastal hazards in the Northland region*. chrome-

extension://efaidnbmnnnibpcajpcglclefindmkaj/https://www.nrc.govt.nz/media/0lqkpymm/weatherhazardsniwa.pdf
Griffiths, G. (2007). Changes in New Zealand daily rainfall extremes 1930-2004. *Weather and Climate*, *27*, 3–44.
Griffiths, G. (2011). Drivers of extreme daily rainfalls in New Zealand. *Weather and Climate*, *31*, 24–49.
Guan, B., & Waliser, D. E. (2015). Detection of atmospheric rivers: Evaluation and application of an algorithm for global studies. *Journal of Geophysical Research: Atmospheres*, *120*(24), 12514–12535. https://doi.org/10.1002/2015jd024257
Harrington, L. J., Dean, S. M., Awatere, S., Rosier, S., Queen, L., Gibson, P. B., Barnes, C., Zachariah, M., Philip, S., & Kew, S. (2023). The role of climate change in extreme rainfall associated with Cyclone Gabrielle over Aotearoa New Zealand's East Coast.
Holton, J. R. (2004). *Introduction to Dynamic Meteorology* (4th ed.). Elsevier.
Hong, Y., Hsu, K.-L., Sorooshian, S., & Gao, X. (2004). Precipitation estimation from remotely sensed imagery using an artificial neural network cloud classification system. *Journal of Applied Meteorology*, *43*(12), 1834–1853.
Huff, F. A. (1967). Time distribution of rainfall in heavy storms. *Water Resources Research*, *3*(4), 1007–1019.
Huff, F. A. (1990). Time distributions of heavy rainstorms in Illinois. *Circular no. 173*.
Huffman, G. J., Bolvin, D. T., Braithwaite, D., Hsu, K.-L., Joyce, R. J., Kidd, C., Nelkin, E. J., Sorooshian, S., Stocker, E. F., & Tan, J. (2020). Integrated multi-satellite retrievals for the global precipitation measurement (GPM) mission (IMERG). In *Satellite precipitation measurement: Volume 1* (pp. 343–353). Springer.
Joyce, R. J., Janowiak, J. E., Arkin, P. A., & Xie, P. (2004). CMORPH: A method that produces global precipitation estimates from passive microwave and infrared data at high spatial and temporal resolution. *Journal of Hydrometeorology*, *5*(3), 487–503.
Kerr, J., Thomson, G., & Wilson, N. (2023). *Cyclone Gabrielle joins list of Aotearoa NZ's 'sudden mass fatality events'*. Public Health Expert Briefing. Retrieved 01.11 from https://www.phcc.org.nz/briefing/cyclone-gabrielle-joins-list-aotearoa-nzs-sudden-mass-fatality-events
Kidson, J. W. (2000). An analysis of New Zealand synoptic types and their use in defining weather regimes. *International Journal of Climatology*, *20*(3), 299–316. https://doi.org/10.1002/(sici)1097-0088(20000315)20:3<299::Aid-joc474>3.0.Co;2-b
Knapp, K. R., Diamond, H. J., Kossin, J. P., Kruk, M. C., & Schreck, C. J. (2018). International best track archive for climate stewardship (IBTrACS) project, version 4. *NOAA National Centers for Environmental Information*, *10*.
Knapp, K. R., Kruk, M. C., Levinson, D. H., Diamond, H. J., & Neumann, C. J. (2010). The international best track archive for climate stewardship (IBTrACS) unifying tropical cyclone data. *Bulletin of the American Meteorological Society*, *91*(3), 363–376.
Lee, J. (2020). *Landslides triggered by the "Tasman Tempest" rainfall event*.
Liu, T., Chen, Y., Chen, S., Li, W., & Zhang, A. (2023). Mechanisms of the transport height of water vapor by tropical cyclones on heavy rainfall. *Weather and Climate Extremes*, *41*, 100587.

Lorrey, A., Griffiths, G., Fauchereau, N., Diamond, H., Pearce, P., & Renwick, J. (2014). An ex-tropical cyclone climatology for Auckland, New Zealand. *International Journal of Climatology*, *34*. https://doi.org/10.1002/joc.3753

Lutgens, F. K., & Tarbuck, E. J. (1998). *The atmosphere : an introduction to meteorology* (7th ed ed.). Prentice Hall.

Macara, G. R. (2015). *The climate and weather of Otago*. chrome-extension://efaidnbmnnnibpcajpcglclefindmkaj/https://docs.niwa.co.nz/library/public/NIWAsts67.pdf

Masson-Delmotte, V., Zhai, P., Pirani, A., Connors, S. L., Péan, C., Berger, S., Caud, N., Chen, Y., Goldfarb, L., Gomis, M. I., Huang, M., Leitzell, K., Lonnoy, E., Matthews, J. B. R., Maycock, T. K., Waterfield, T., Yelekçi, O., R. Yu, & Zhou, B. (2021). *Climate change 2021: the physical science basis*. (Contribution of working group I to the sixth assessment report of the intergovernmental panel on climate change, Issue.

MBIE. (2021). *New Zealand climate zones*.

McLennan, M., & Group, Z. I. (2023). *The Global Risks Report 2023*.

MoE. (2018a). *Climate Change Projections for New Zealand: Atmosphere Projections Based on Simulations from the IPCC Fifth Assessment*.

MoE. (2018b). *Climate Change Projections for New Zealand: Atmosphere Projections Based on Simulations from the IPCC Fifth Assessment, 2nd Edition*.

MoE. (2022). *Aotearoa New Zealand's first national adaptation plan*. .

Mosley, M. P. (2000). Regional differences in the effects of El Niño and La Niña on low flows and floods. *Hydrological Sciences Journal*, *45*(2), 249–267.

N. LeRoy Poff, M. M. B., John W. Day, Jr. (2002). *Potential Impacts on Inland Freshwater and Coastal Wetland Ecosystems in the United States*. chrome-extension://efaidnbmnnnibpcajpcglclefindmkaj/https://www.pewtrusts.org/-/media/legacy/uploadedfiles/wwwpewtrustsorg/reports/protecting_ocean_life/envclimateaquaticecosystemspdf.pdf

Nick Wilson, A. B. a. J. K. (2024). *The long shadow of Cyclone Gabrielle: Brief review at 12 months*. Retrieved 01.11 from https://www.phcc.org.nz/briefing/long-shadow-cyclone-gabrielle-brief-review-12-months

NIWA. *Storms and cyclones*. Retrieved 27/07 from https://niwa.co.nz/atmosphere/storms-and-cyclones

NIWA. (2002). *How often is New Zealand hit by tropical cyclones?* chrome-extension://efaidnbmnnnibpcajpcglclefindmkaj/https://niwa.co.nz/sites/default/files/import/attachments/cyclone.pdf

NIWA. (2018). *March 1988 North Island Ex-tropical Cyclone Bola (1988-03-06)*. Retrieved 03.10 from https://hwe.niwa.co.nz/event/March_1988_North_Island_Ex-tropical_Cyclone_Bola

NIWA. (2019). *Annual Climate Summary 2018*. Retrieved 03.10 from https://niwa.co.nz/climate-and-weather/annual/annual-climate-summary-2018#:~:text=During%202018%2C%20temperatures%20were%20above,western%20and%20southern%20South%20Island.

NIWA. (2023a). *Aotearoa New Zealand Climate Summary: February 2023* chrome-extension://efaidnbmnnnibpcajpcglclefindmkaj/https://niwa.co.nz/sites/default/files/Climate_Summary_February_2023_NIWA-web.pdf

NIWA. (2023b). *Map North*. Retrieved 03.10 from https://niwa.co.nz/climate-and-weather/map-north

NIWA. (2024a). *Coastal storm inundation*. Retrieved 03.10 from https://niwa.co.nz/hazards/coastal-storm-inundation
NIWA. (2024b). *Map Alpine*. Retrieved 03.10 from https://niwa.co.nz/map-alpine
NIWA. (2024c). *Map C North*. Retrieved 03.10 from https://niwa.co.nz/map-c-north
NIWA. (2024d). *Map E North*. Retrieved 03.10 from https://niwa.co.nz/climate-and-weather/map-e-north
NIWA. (2024e). *Map E South*. Retrieved 03.10 from https://niwa.co.nz/map-e-south
NIWA. (2024f). *Map I South*. Retrieved 03.10 from https://niwa.co.nz/map-i-south
NIWA. (2024g). *Map N South*. Retrieved 03.10 from https://niwa.co.nz/map-n-south
NIWA. (2024h). *Map South*. Retrieved 03.10 from https://niwa.co.nz/map-south
NIWA. (2024i). *Map Sw North*. Retrieved 03.10 from https://niwa.co.nz/map-sw-north
NIWA. (2024j). *Map W South*. Retrieved 03.10 from https://niwa.co.nz/map-w-south
NIWA. (2024k). *Overview of New Zealand's climate*. Retrieved 03.10 from https://niwa.co.nz/climate-and-weather/overview-new-zealands-climate
NIWA. (2024l). *Storms and cyclones*. Retrieved 03.10 from https://niwa.co.nz/atmosphere/storms-and-cyclones#:~:text=Tropical%20cyclones%20weaken%20as%20they,occur%20from%20December%20to%20April.
NIWA. (2024m). *Synoptic types*. Retrieved 03.10 from https://niwa.co.nz/climate-and-weather/climate-present-and-past/new-zealand-climate/synoptic-types
NOAA. (2023). *Global Atmospheric Circulations*. Retrieved 03.10 from https://www.noaa.gov/jetstream/global/global-atmospheric-circulations
Norbiato, D., Borga, M., Merz, R., Blöschl, G., & Carton, A. (2009). Controls on event runoff coefficients in the eastern Italian Alps. *Journal of Hydrology*, *375*(3), 312–325. https://doi.org/https://doi.org/10.1016/j.jhydrol.2009.06.044
NRC, N. R. C. (2007). *State of the Environment Report*
Olley, S. (2023). *Mangawhai residents face long clean-up job after deluge*. Retrieved 01.11 from https://www.rnz.co.nz/news/national/484906/mangawhai-residents-face-long-clean-up-job-after-deluge
Orange, C. (2015). *'Northland region - Geography', Te Ara - the Encyclopedia of New Zealand*. Retrieved 03.10 from http://www.TeAra.govt.nz/en/northland-region/page-2
Payne, A. E., Demory, M.-E., Leung, L. R., Ramos, A. M., Shields, C. A., Rutz, J. J., Siler, N., Villarini, G., Hall, A., & Ralph, F. M. (2020). Responses and impacts of atmospheric rivers to climate change. *Nature Reviews Earth & Environment*, *1*(3), 143–157. https://doi.org/10.1038/s43017-020-0030-5
Pearce, H. G., J., K., A., C., B., M., D., A., T., C.-S., & E., Y. (2011). *Improved estimates of the effect of climate change on NZ fire danger*.
PHCC. (2023). *Cyclone Gabrielle by the numbers – A review at six months*. Retrieved 03.10 from https://www.phcc.org.nz/briefing/cyclone-gabrielle-numbers-review-six-months
Pocock, J. (2023). *Estimated cost of Cyclone Gabrielle for Hawke's Bay over $5 billion so far*. Hawkes Bay Today. Retrieved 01.11 from https://www.nzherald.co.nz/hawkes-bay-today/news/estimated-cost-of-cyclone-gabrielle-for-hawkes-bay-over-5-billion-so-far/HW6WO46MBJDIPPANQSXOTUARH4/
Rampal, N., Lorrey, A., & Fauchereau, N. (2022). An Objective Weather Regime Classification for Aotearoa New Zealand Using a Two-Tiered K-Means Clustering

Approach. *Monthly Weather Review*, *150*(11), 3103–3122. https://doi.org/10.1175/mwr-d-22-0059.1

Reid, K. J., Rosier, S. M., Harrington, L. J., King, A. D., & Lane, T. P. (2021). Extreme rainfall in New Zealand and its association with Atmospheric Rivers. *Environmental Research Letters*, *16*(4). https://doi.org/10.1088/1748-9326/abeae0

RSNZ, R. S. o. N. Z. (2016). *Climate Change Implications for New Zealand* Retrieved 01-11-2024 from https://www.royalsociety.org.nz/what-we-do/our-expert-advice/all-expert-advice-papers/climate-change-implications-for-new-zealand/

Salinger, M. (1980). New Zealand climate: I. precipitation patterns. *Monthly Weather Review*, *108*(11), 1892–1904.

Salinger, M., & Griffiths, G. (2001). Trends in New Zealand daily temperature and rainfall extremes. *International Journal of Climatology: A Journal of the Royal Meteorological Society*, *21*(12), 1437–1452.

Salinger, M., & Mullan, A. (1999). New Zealand climate: temperature and precipitation variations and their links with atmospheric circulation 1930–1994. *International Journal of Climatology: A Journal of the Royal Meteorological Society*, *19*(10), 1049–1071.

Sharpe, M. (2023). *Hundreds of homeowners to get voluntary buyout offers for cyclone-hit properties*. Stuff. Retrieved 01.11 from https://www.stuff.co.nz/national/300894282/hundreds-of-homeowners-to-get-voluntary-buyout-offers-for-cyclonehit-properties

Shu, J., Shamseldin, A. Y., & Weller, E. (2021). The impact of atmospheric rivers on rainfall in New Zealand. *Sci Rep*, *11*(1), 5869. https://doi.org/10.1038/s41598-021-85297-0

Smith, K. (2013). *Environmental hazards: Assessing risk and reducing disaster* (6th ed.). Routledge.

Stats-NZ. (2020). *Northern regions lead population growth*. Retrieved 03.10 from https://www.stats.govt.nz/news/northern-regions-lead-population-growth

Svetlana, D., Radovan, D., & Ján, D. (2015). The Economic Impact of Floods and their Importance in Different Regions of the World with Emphasis on Europe. *Procedia Economics and Finance*, *34*, 649–655. https://doi.org/https://doi.org/10.1016/S2212-5671(15)01681-0

Talbot, C. J., Bennett, E. M., Cassell, K., Hanes, D. M., Minor, E. C., Paerl, H., Raymond, P. A., Vargas, R., Vidon, P. G., Wollheim, W., & Xenopoulos, M. A. (2018). The impact of flooding on aquatic ecosystem services. *Biogeochemistry*, *141*(3), 439–461. https://doi.org/10.1007/s10533-018-0449-7

Terry, J. P. (2007). *Tropical cyclones: climatology and impacts in the South Pacific*. Springer Science & Business Media.

Thompson, D. (2006). The southern annular mode and New Zealand climate. *Water & Atmosphere*, *14*(2), 24–25.

Trenberth, K. E., Fasullo, J. T., & Shepherd, T. G. (2015). Attribution of climate extreme events. *Nature Climate Change*, *5*(8), 725–730. https://doi.org/10.1038/nclimate2657

Trüdinger, M. (2023). *Cyclone Gabrielle and Tai Tokerau Northland: Stories of community resilience and messages of support for the rest of Aotearoa New Zealand*. . chrome-extension://efaidnbmnnnibpcajpcglclefindmkaj/https://www.nrc.govt.nz/media/dqvgudn5/cyclone-gabrielle-stories-of-resilience_uvn_1.pdf

Uber, M., Vandervaere, J. P., Zin, I., Braud, I., Heistermann, M., Legoût, C., Molinié, G., & Nord, G. (2018). How does initial soil moisture influence the hydrological response? A case study from southern France. *Hydrol. Earth Syst. Sci.*, *22*(12), 6127–6146. https://doi.org/10.5194/hess-22-6127-2018

Ummenhofer, C. C., Gupta, A. S., & England, M. H. (2009). Causes of late twentieth-century trends in New Zealand precipitation. *Journal of Climate*, *22*(1), 3–19.

Vishwanathan, G., McDonald, A., Stone, D. A., Rosier, S., Rana, S., & Noble, C. (2023). Mean and extreme precipitation over Aotearoa New Zealand: A comparison across multiple different estimation techniques. *International Journal of Climatology*, *43*(7), 3072–3093. https://doi.org/10.1002/joc.8017

Wallace, J. M., & Hobbs, P. V. (2006). *Atmospheric Science: An Introductory Survey* (2nd ed.).

Wang, B., & LinHo. (2002). Rainy Season of the Asian–Pacific Summer Monsoon. *Journal of Climate*, *15*(4), 386–398. https://doi.org/https://doi.org/10.1175/1520-0442(2002)015<0386:RSOTAP>2.0.CO;2

Weather, N. S. (2024). *Tasman Low To Bring Significant Rain Accumulation*. Retrieved 03.10 from https://www.severeweather.co.nz/weather-news/tasman-low-to-bring-significant-rain-accumulation

Zhu, Y., & Newell, R. E. (1998). A Proposed Algorithm for Moisture Fluxes from Atmospheric Rivers. *Monthly Weather Review*, *126*(3), 725–735. https://doi.org/https://doi.org/10.1175/1520-0493(1998)126<0725:APAFMF>2.0.CO;2

APPENDIX 1: Monthly variation of total rainfall (in mm) at stations in the Northland region.

These boxplots show the distribution of total monthly rainfall for each month of the year. The boxes represent the interquartile range (IQR), the line inside each box indicates the median, and the whiskers extend to 1.5 times the IQR. Outliers are displayed as individual points beyond the whiskers.

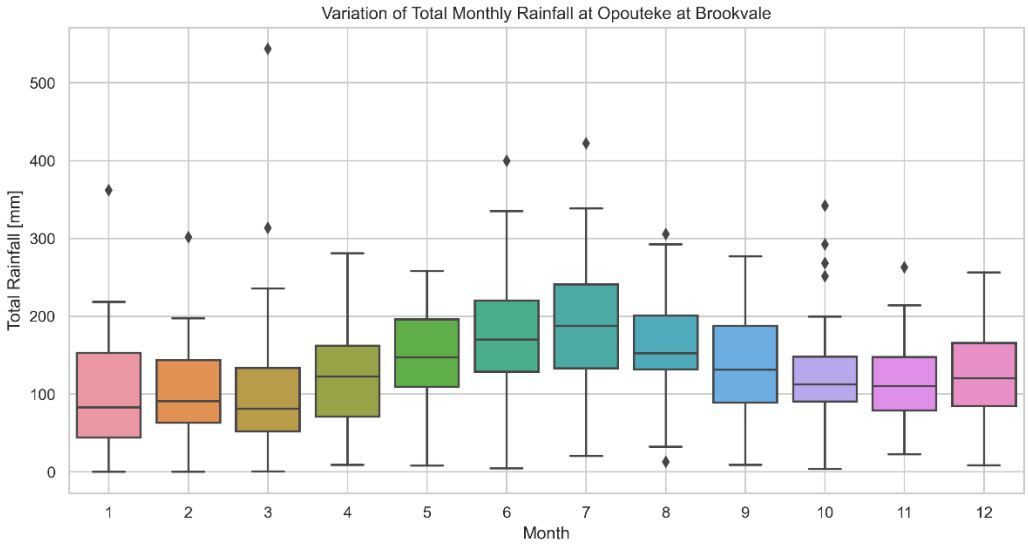

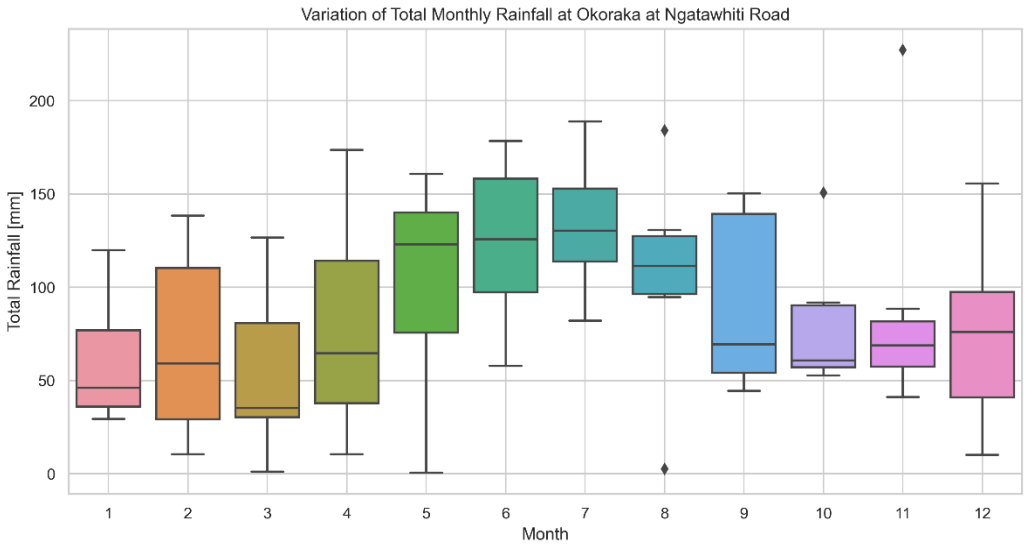

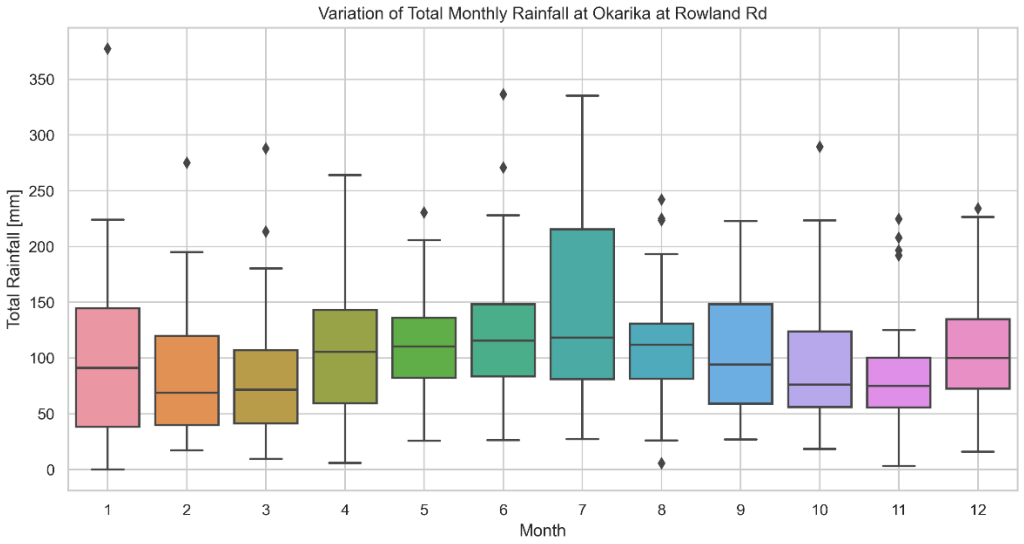
Variation of Total Monthly Rainfall at Okarika at Rowland Rd
Total Rainfall [mm]
0
50
100
150
200
250
300
350
1
2
3
4
5
6
7
8
9
10
11
12
Month

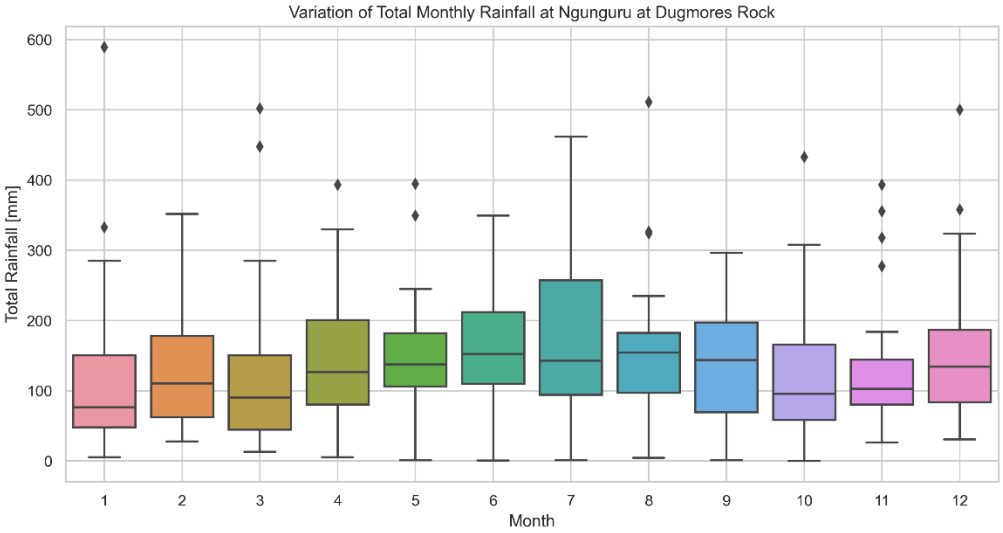
Variation of Total Monthly Rainfall at Ngunguru at Dugmores Rock
Total Rainfall [mm]
0
100
200
300
400
500
600
1
2
3
4
5
6
7
8
9
10
11
12
Month

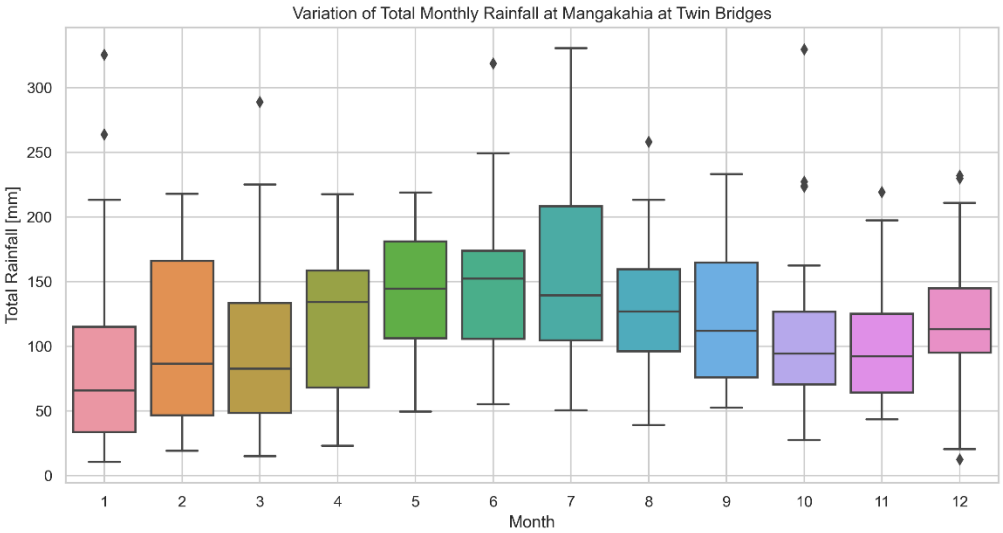
Variation of Total Monthly Rainfall at Mangakahia at Twin Bridges
Total Rainfall [mm]
0
50
100
150
200
250
300
1
2
3
4
5
6
7
8
9
10
11
12
Month

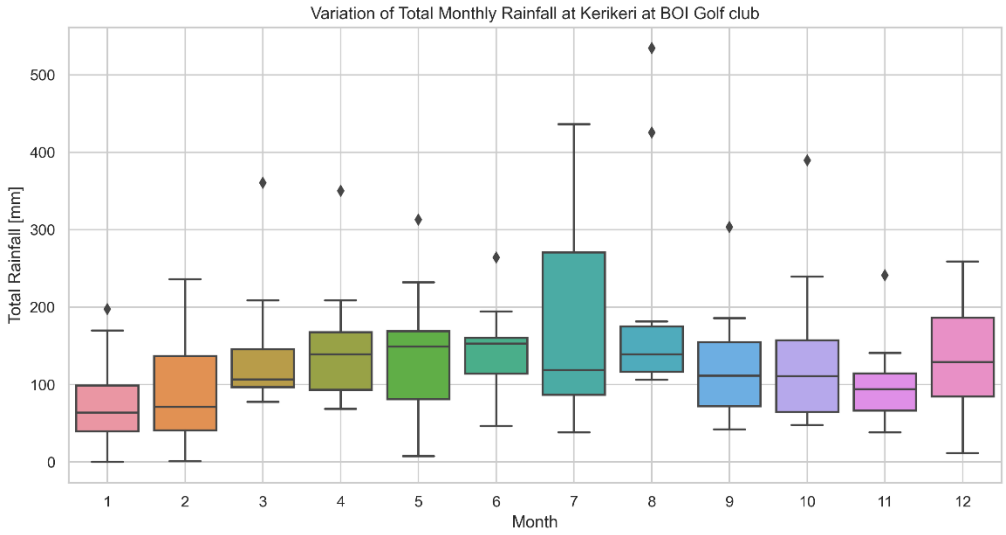
Variation of Total Monthly Rainfall at Kerikeri at BOI Golf club
Total Rainfall [mm]
0
100
200
300
400
500
1
2
3
4
5
6
7
8
9
10
11
12
Month

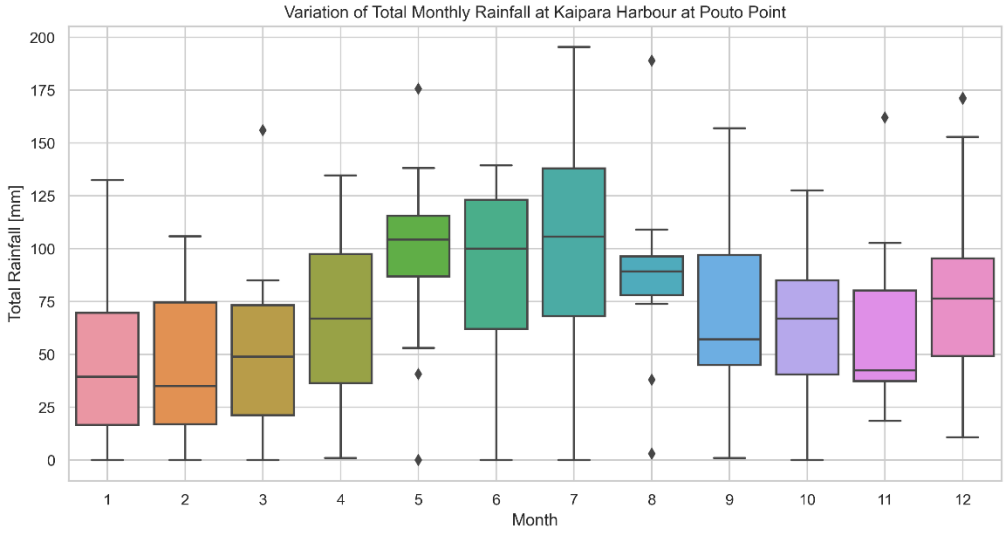
Variation of Total Monthly Rainfall at Kaipara Harbour at Pouto Point
Total Rainfall [mm]
0
25
50
75
100
125
150
175
200
1
2
3
4
5
6
7
8
9
10
11
12
Month

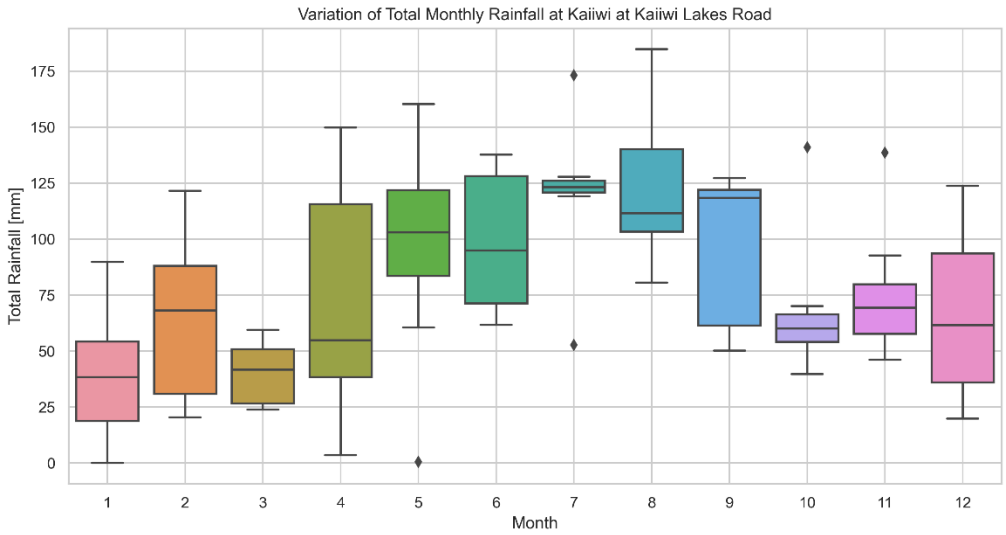
Variation of Total Monthly Rainfall at Kaiiwi at Kaiiwi Lakes Road
Total Rainfall [mm]
0
25
50
75
100
125
150
175
1
2
3
4
5
6
7
8
9
10
11
12
Month

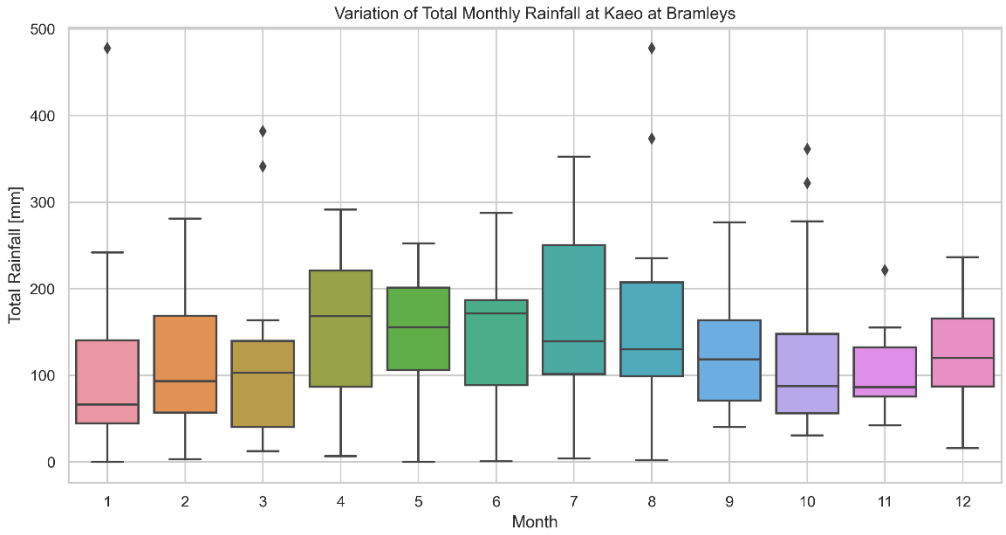
Variation of Total Monthly Rainfall at Kaeo at Bramleys
Total Rainfall [mm]
0
100
200
300
400
500
1
2
3
4
5
6
7
8
9
10
11
12
Month

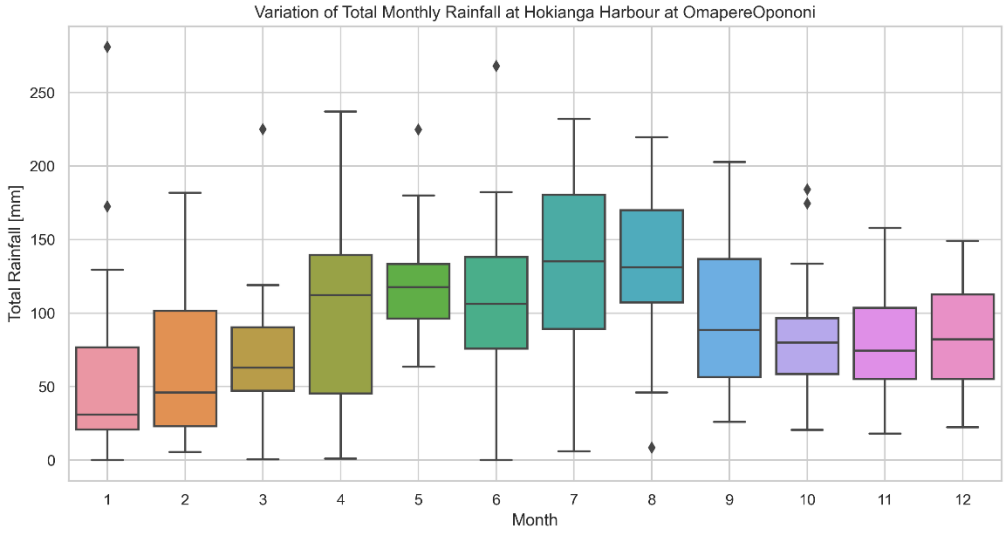
Variation of Total Monthly Rainfall at Hokianga Harbour at OmapereOpononi
Total Rainfall [mm]
0
50
100
150
200
250
1
2
3
4
5
6
7
8
9
10
11
12
Month

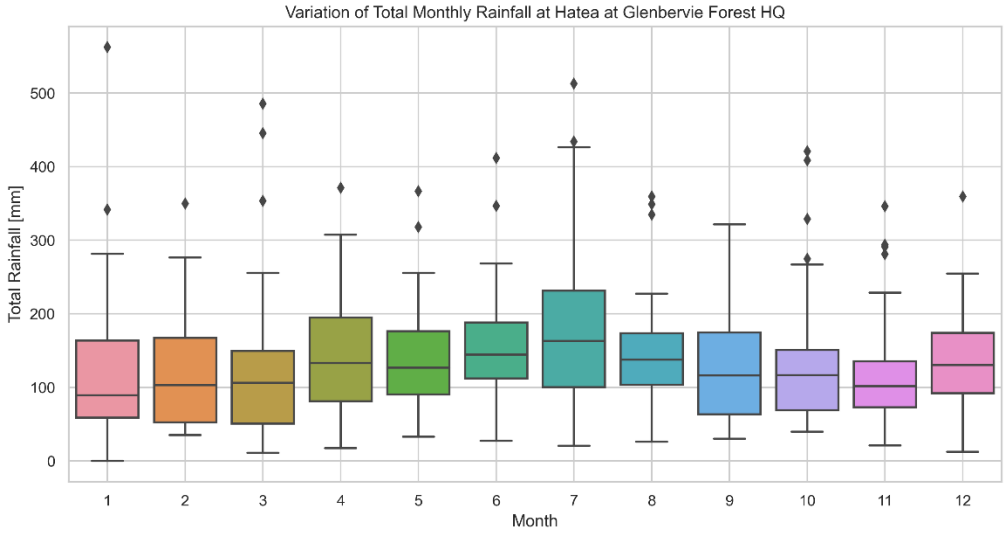
Variation of Total Monthly Rainfall at Hatea at Glenbervie Forest HQ
Total Rainfall [mm]
0
100
200
300
400
500
1
2
3
4
5
6
7
8
9
10
11
12
Month

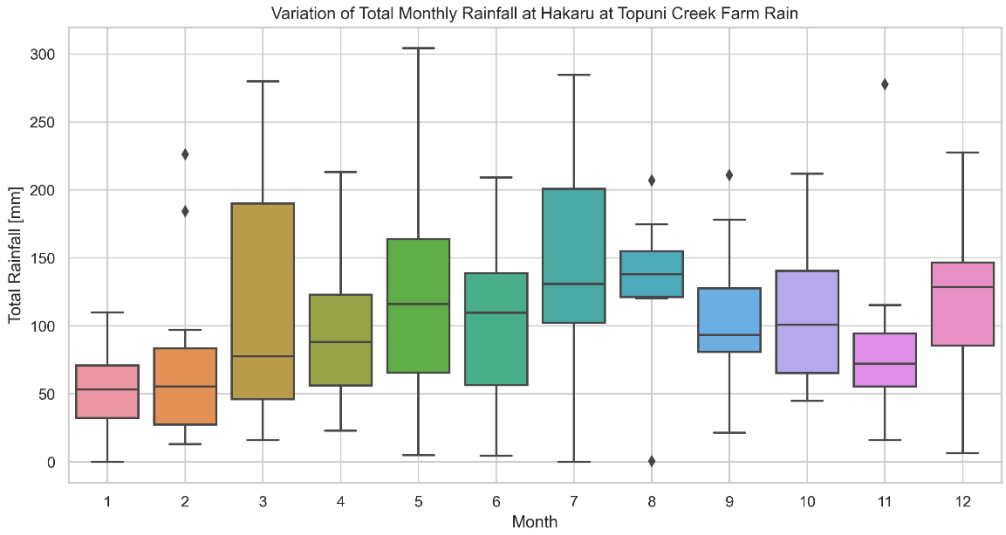
Variation of Total Monthly Rainfall at Hakaru at Topuni Creek Farm Rain
Total Rainfall [mm]
0
50
100
150
200
250
300
1
2
3
4
5
6
7
8
9
10
11
12
Month

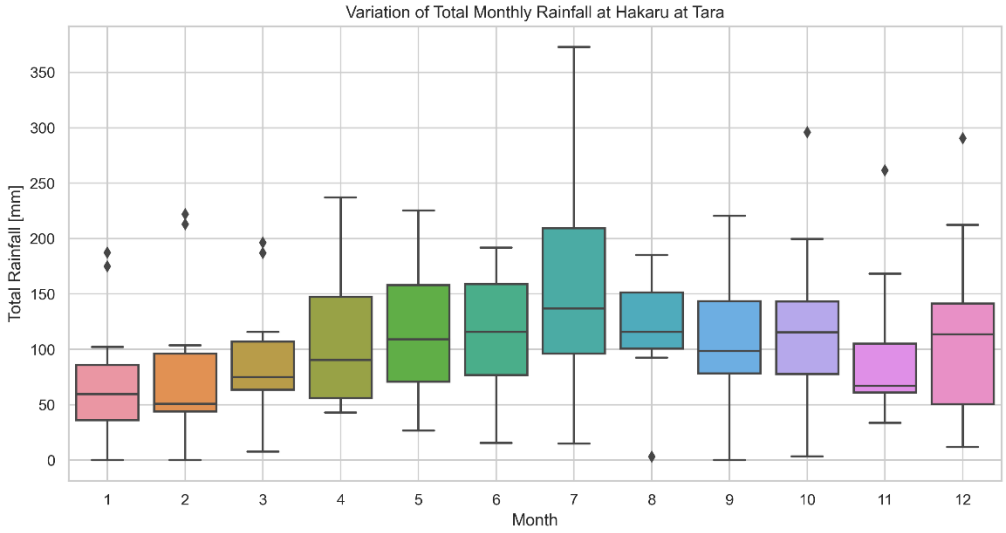
Variation of Total Monthly Rainfall at Hakaru at Tara
Total Rainfall [mm]
0
50
100
150
200
250
300
350
1
2
3
4
5
6
7
8
9
10
11
12
Month

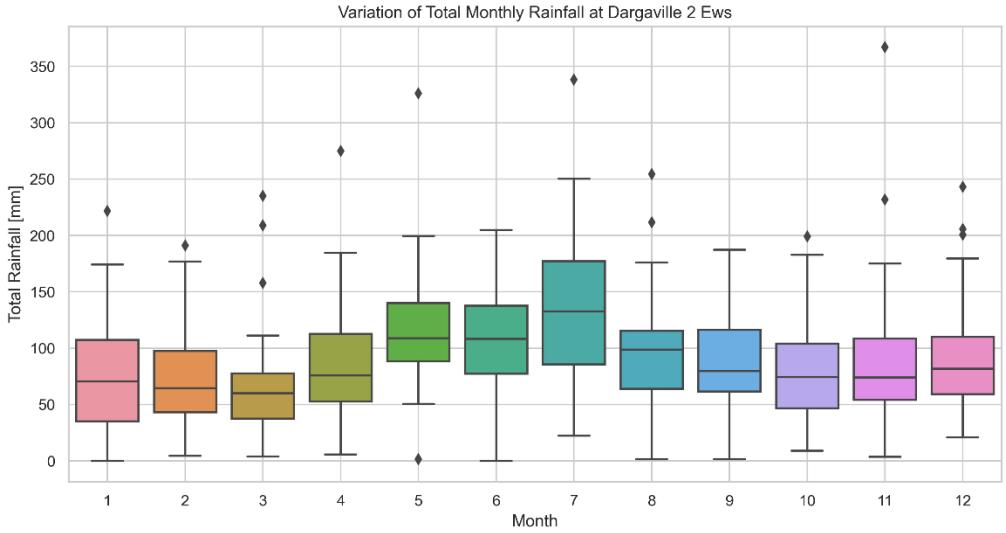
Variation of Total Monthly Rainfall at Dargaville 2 Ews
Total Rainfall [mm]
0
50
100
150
200
250
300
350
1
2
3
4
5
6
7
8
9
10
11
12
Month

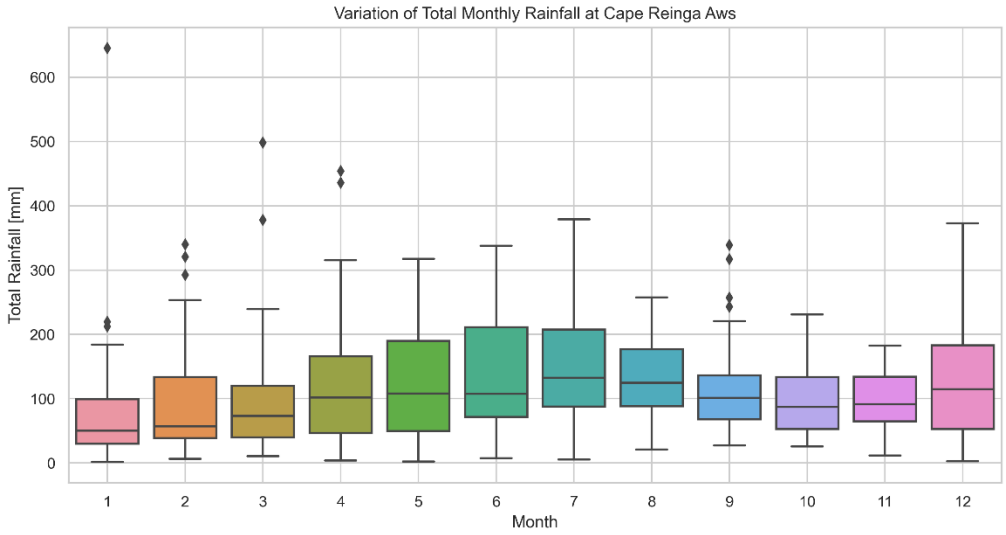
Variation of Total Monthly Rainfall at Cape Reinga Aws
Total Rainfall [mm]
0
100
200
300
400
500
600
1
2
3
4
5
6
7
8
9
10
11
12
Month

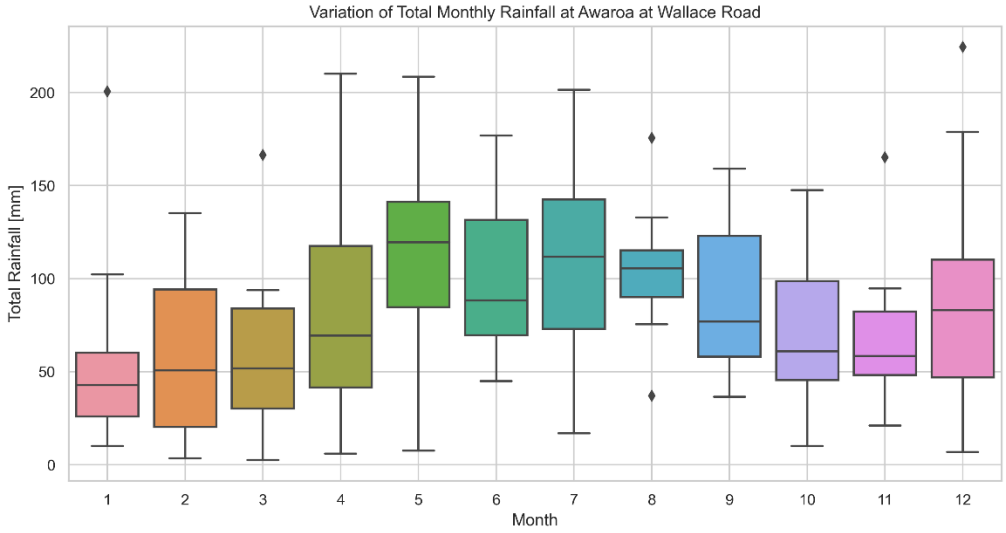
Variation of Total Monthly Rainfall at Awaroa at Wallace Road
Total Rainfall [mm]
0
50
100
150
200
1
2
3
4
5
6
7
8
9
10
11
12
Month

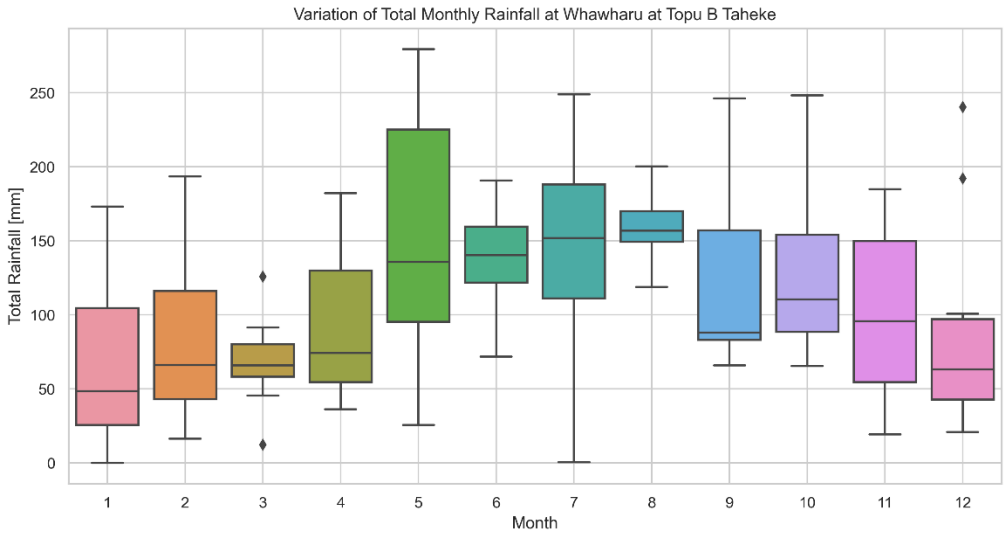
Variation of Total Monthly Rainfall at Whawharu at Topu B Taheke
Total Rainfall [mm]
0
50
100
150
200
250
1
2
3
4
5
6
7
8
9
10
11
12
Month

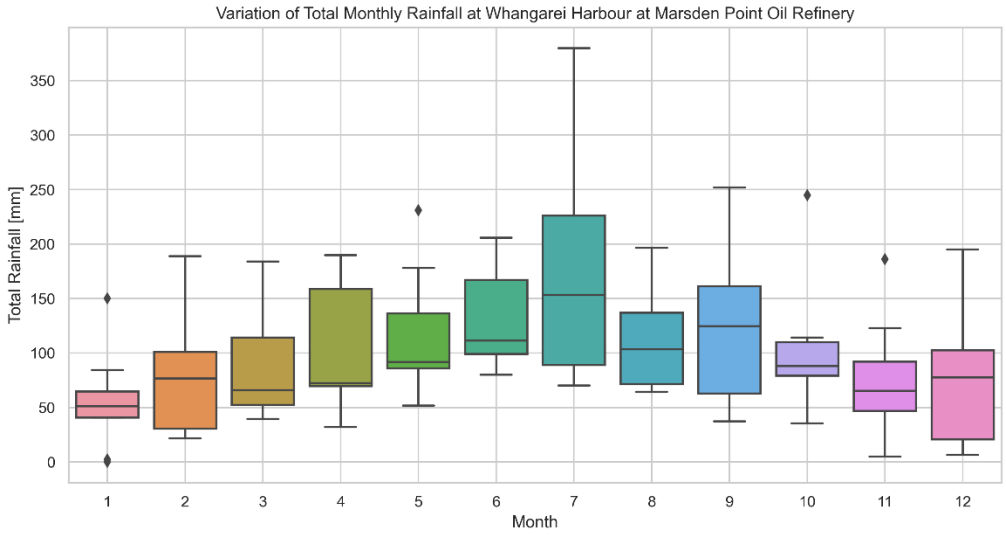
Variation of Total Monthly Rainfall at Whangarei Harbour at Marsden Point Oil Refinery
Total Rainfall [mm]
0
50
100
150
200
250
300
350
1
2
3
4
5
6
7
8
9
10
11
12
Month

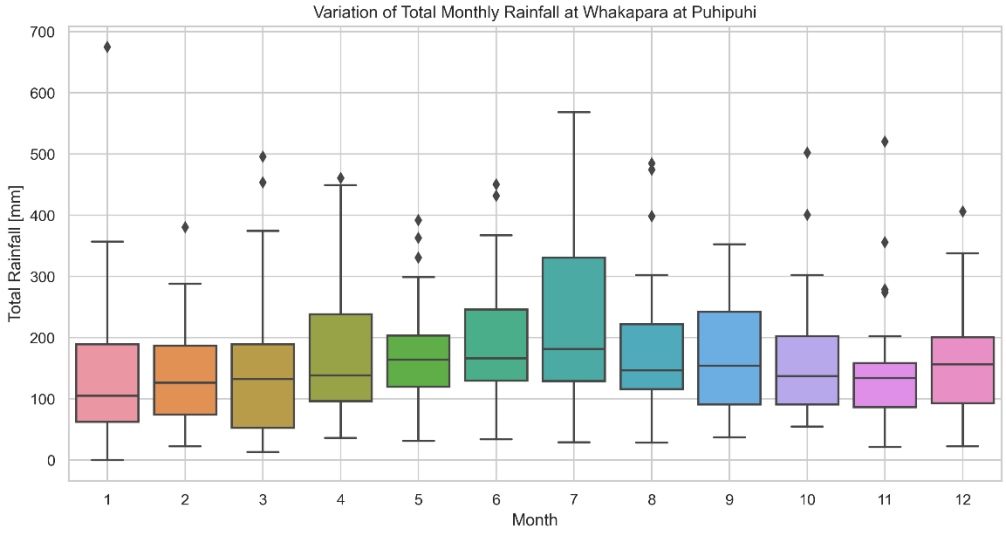
Variation of Total Monthly Rainfall at Whakapara at Puhipuhi
Total Rainfall [mm]
0
100
200
300
400
500
600
700
1
2
3
4
5
6
7
8
9
10
11
12
Month

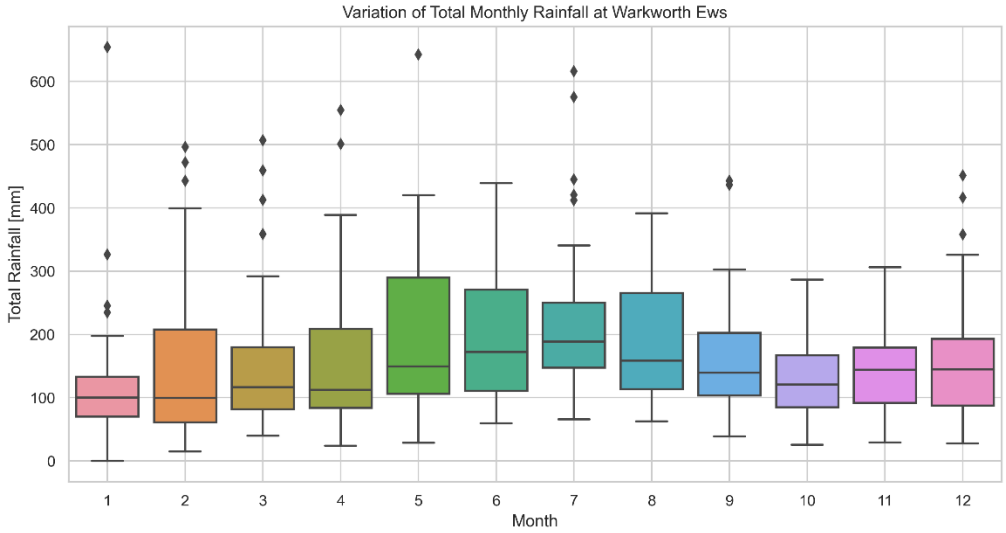
Variation of Total Monthly Rainfall at Warkworth Ews
Total Rainfall [mm]
0
100
200
300
400
500
600
1
2
3
4
5
6
7
8
9
10
11
12
Month

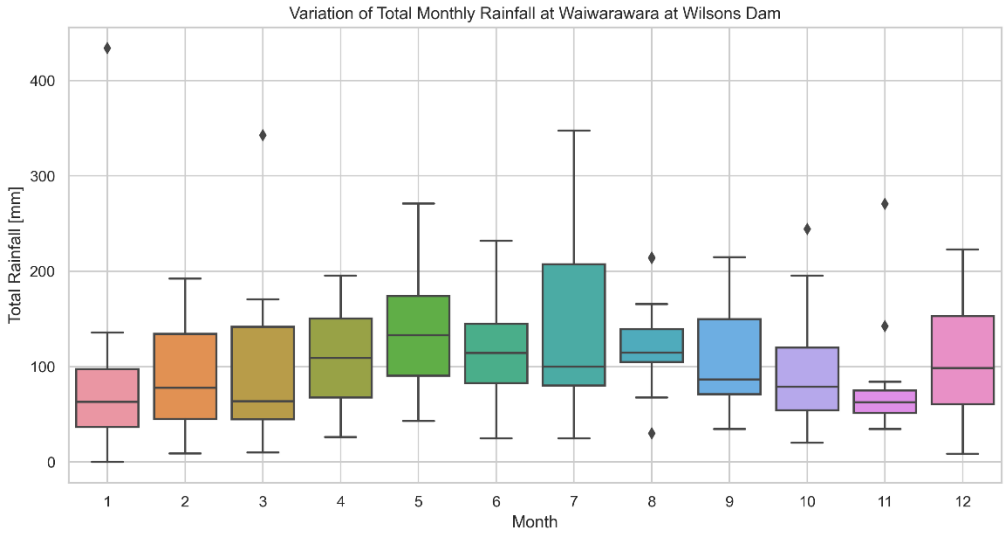
Variation of Total Monthly Rainfall at Waiwarawara at Wilsons Dam
Total Rainfall [mm]
0
100
200
300
400
1
2
3
4
5
6
7
8
9
10
11
12
Month

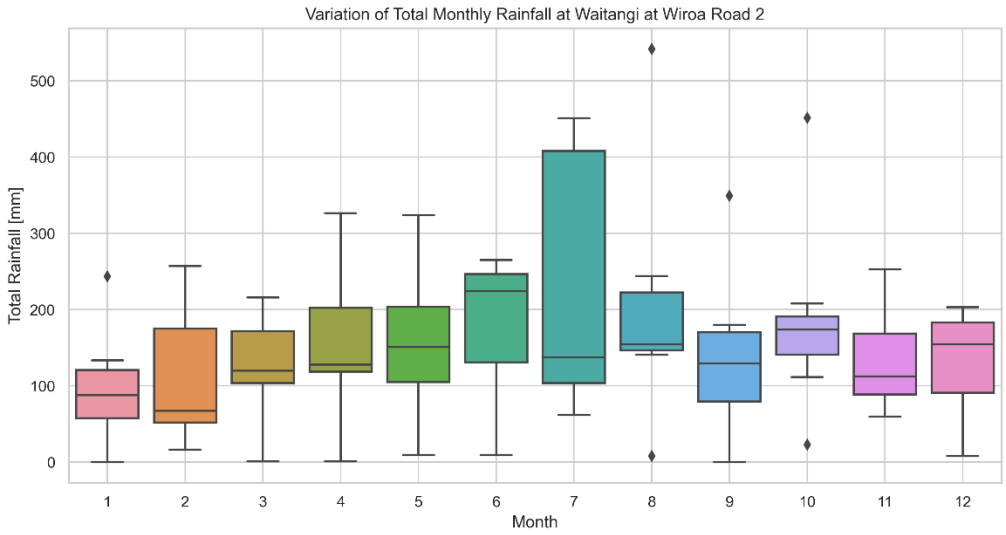
Variation of Total Monthly Rainfall at Waitangi at Wiroa Road 2
Total Rainfall [mm]
0
100
200
300
400
500
1
2
3
4
5
6
7
8
9
10
11
12
Month

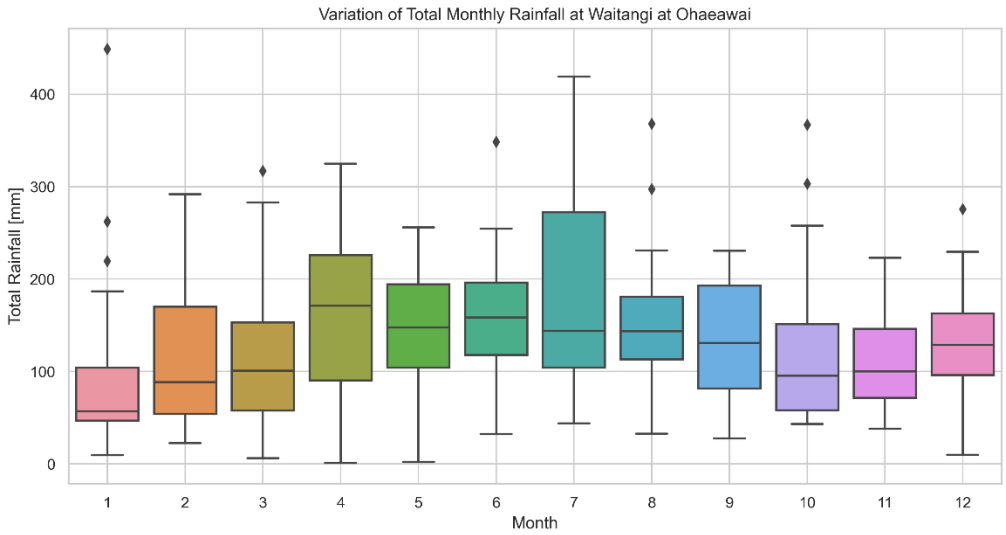
Variation of Total Monthly Rainfall at Waitangi at Ohaeawai
Total Rainfall [mm]
0
100
200
300
400
1
2
3
4
5
6
7
8
9
10
11
12
Month

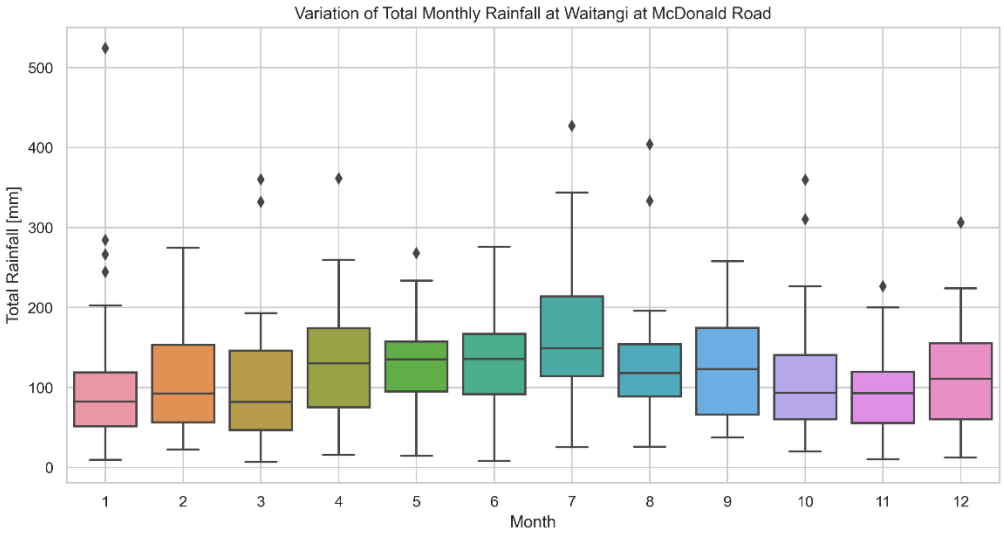
Variation of Total Monthly Rainfall at Waitangi at McDonald Road
Total Rainfall [mm]
0
100
200
300
400
500
1
2
3
4
5
6
7
8
9
10
11
12
Month

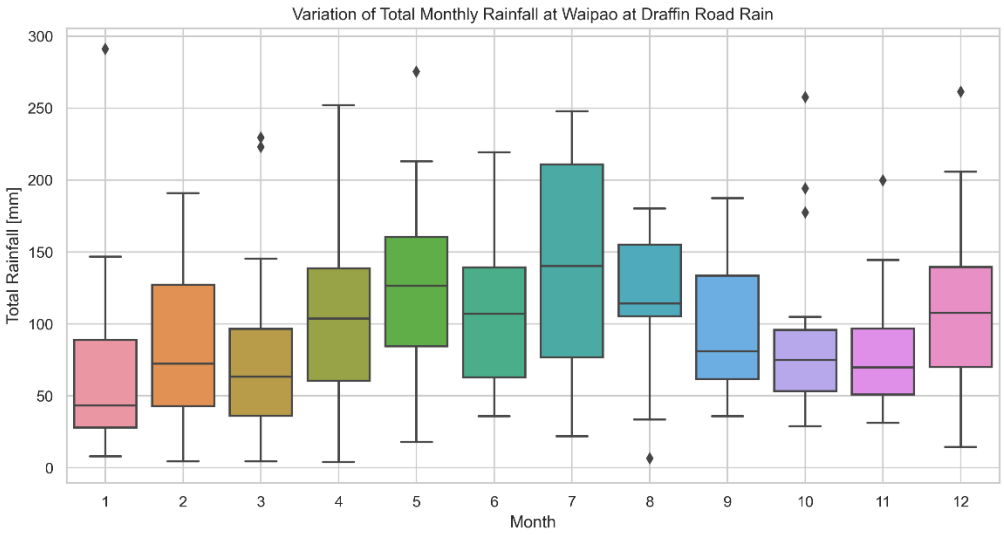
Variation of Total Monthly Rainfall at Waipao at Draffin Road Rain
Total Rainfall [mm]
0
50
100
150
200
250
300
1
2
3
4
5
6
7
8
9
10
11
12
Month

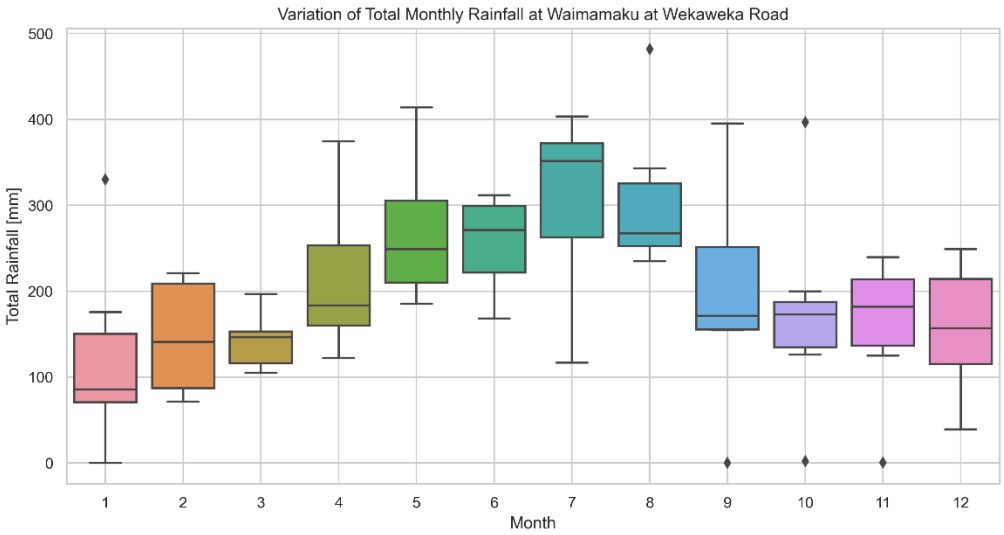
Variation of Total Monthly Rainfall at Waimamaku at Wekaweka Road
Total Rainfall [mm]
0
100
200
300
400
500
1
2
3
4
5
6
7
8
9
10
11
12
Month

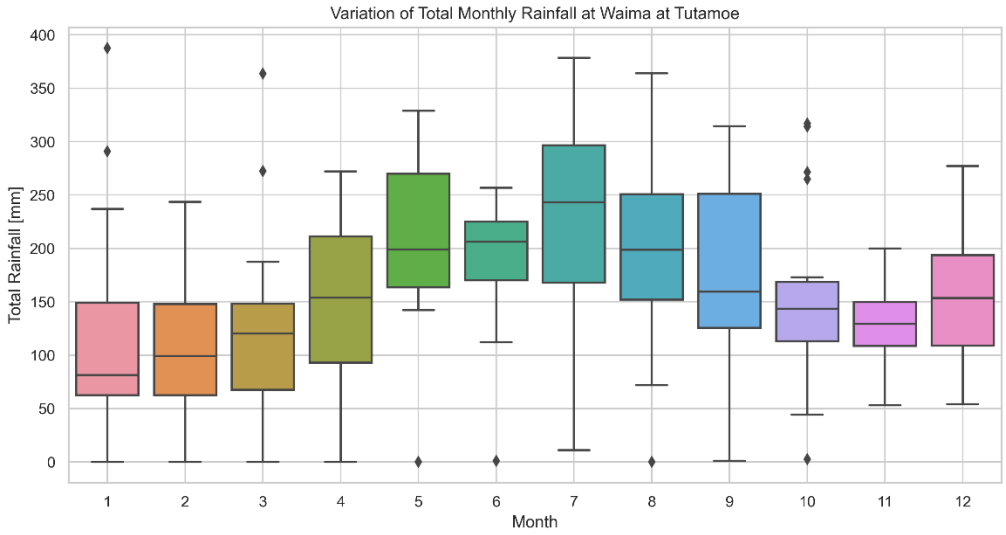
Variation of Total Monthly Rainfall at Waima at Tutamoe
Total Rainfall [mm]
Month

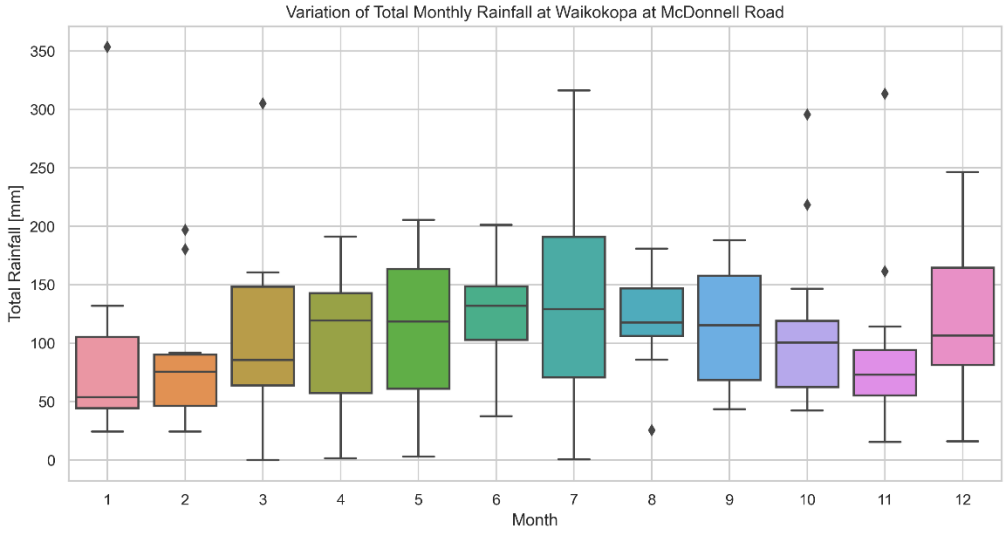
Variation of Total Monthly Rainfall at Waikokopa at McDonnell Road
Total Rainfall [mm]
Month

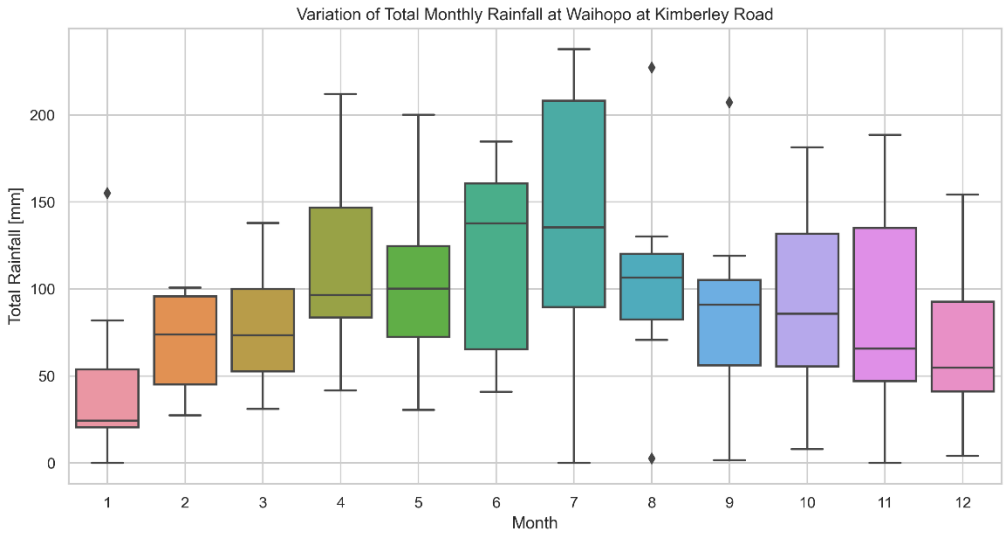
Variation of Total Monthly Rainfall at Waihopo at Kimberley Road
Total Rainfall [mm]
Month

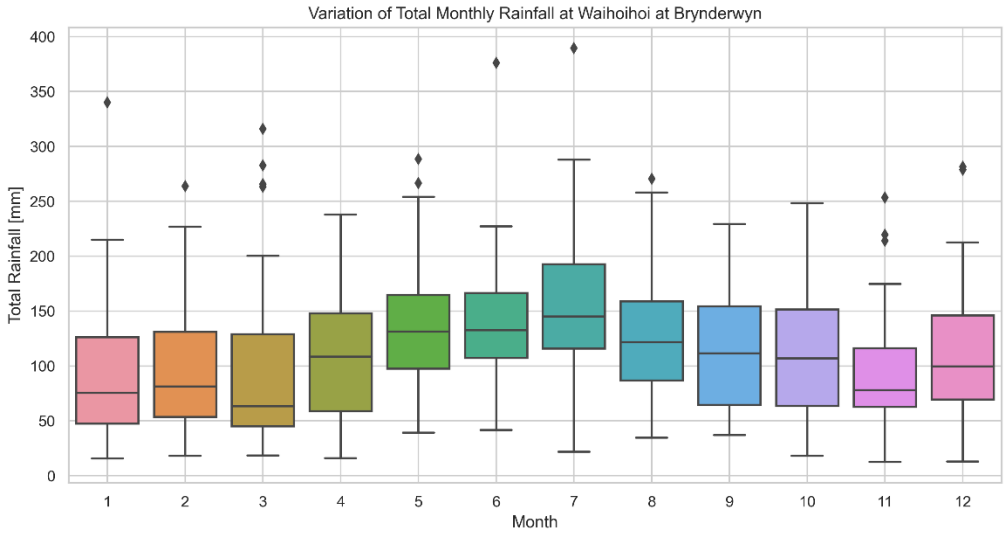
Variation of Total Monthly Rainfall at Waihoihoi at Brynderwyn
Total Rainfall [mm]
0
50
100
150
200
250
300
350
400
1
2
3
4
5
6
7
8
9
10
11
12
Month

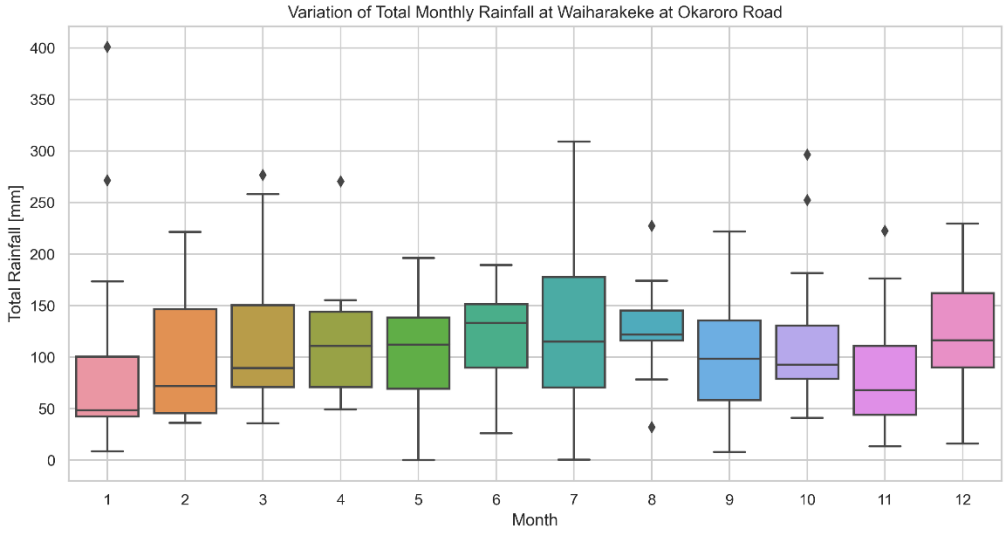
Variation of Total Monthly Rainfall at Waiharakeke at Okaroro Road
Total Rainfall [mm]
0
50
100
150
200
250
300
350
400
1
2
3
4
5
6
7
8
9
10
11
12
Month

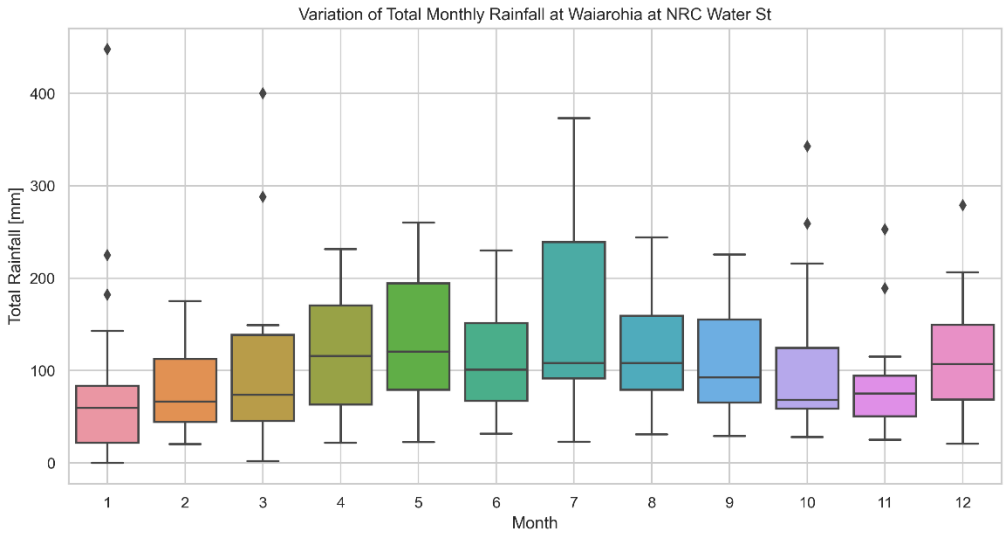
Variation of Total Monthly Rainfall at Waiarohia at NRC Water St
Total Rainfall [mm]
0
100
200
300
400
1
2
3
4
5
6
7
8
9
10
11
12
Month

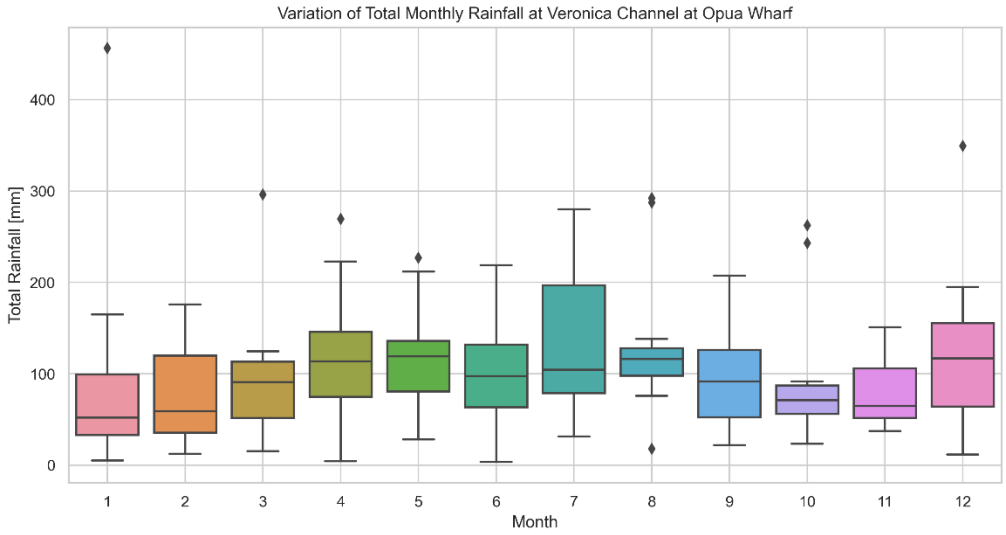
Variation of Total Monthly Rainfall at Veronica Channel at Opua Wharf
Total Rainfall [mm]
0
100
200
300
400
1
2
3
4
5
6
7
8
9
10
11
12
Month

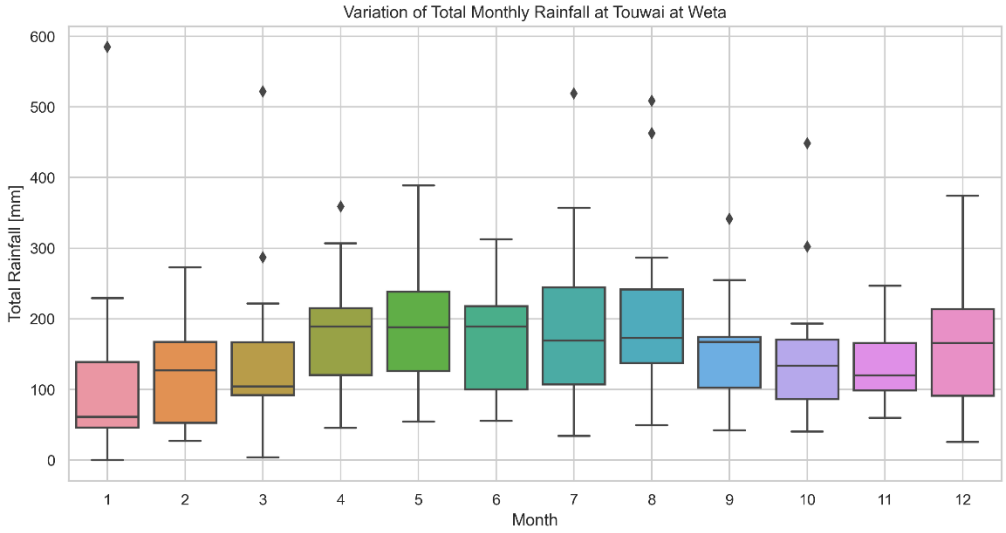
Variation of Total Monthly Rainfall at Touwai at Weta
Total Rainfall [mm]
0
100
200
300
400
500
600
1
2
3
4
5
6
7
8
9
10
11
12
Month

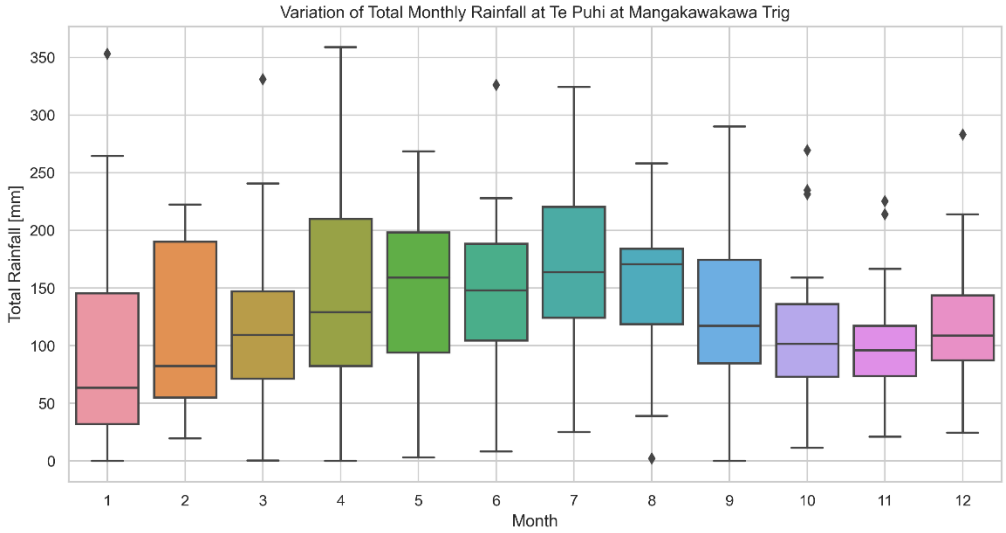
Variation of Total Monthly Rainfall at Te Puhi at Mangakawakawa Trig
Total Rainfall [mm]
0
50
100
150
200
250
300
350
1
2
3
4
5
6
7
8
9
10
11
12
Month

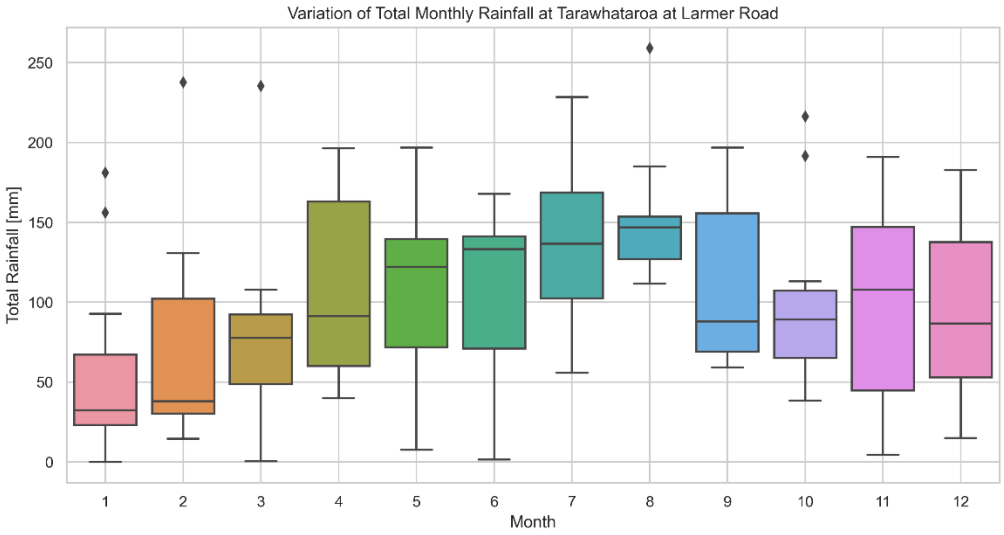
Variation of Total Monthly Rainfall at Tarawhataroa at Larmer Road
Total Rainfall [mm]
0
50
100
150
200
250
1
2
3
4
5
6
7
8
9
10
11
12
Month

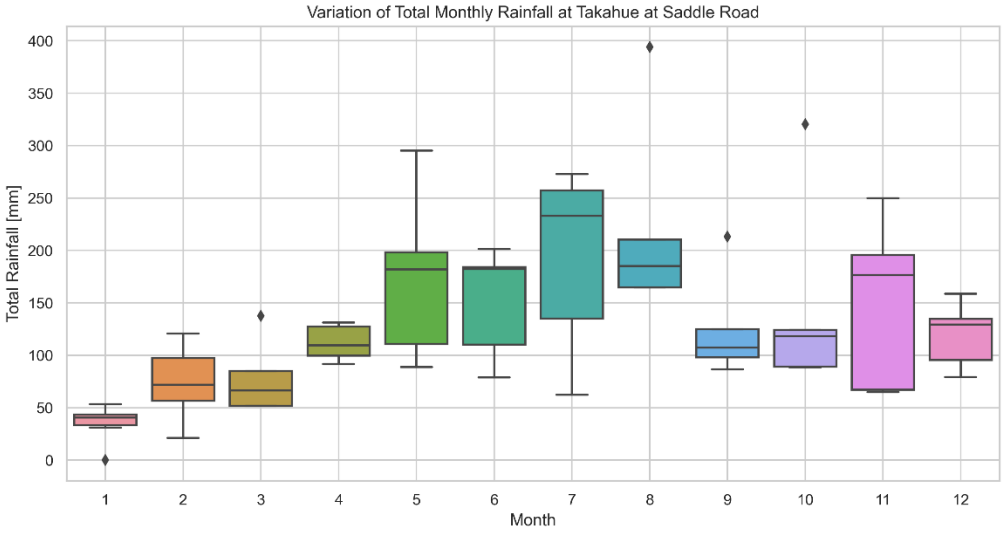
Variation of Total Monthly Rainfall at Takahue at Saddle Road
Total Rainfall [mm]
0
50
100
150
200
250
300
350
400
1
2
3
4
5
6
7
8
9
10
11
12
Month

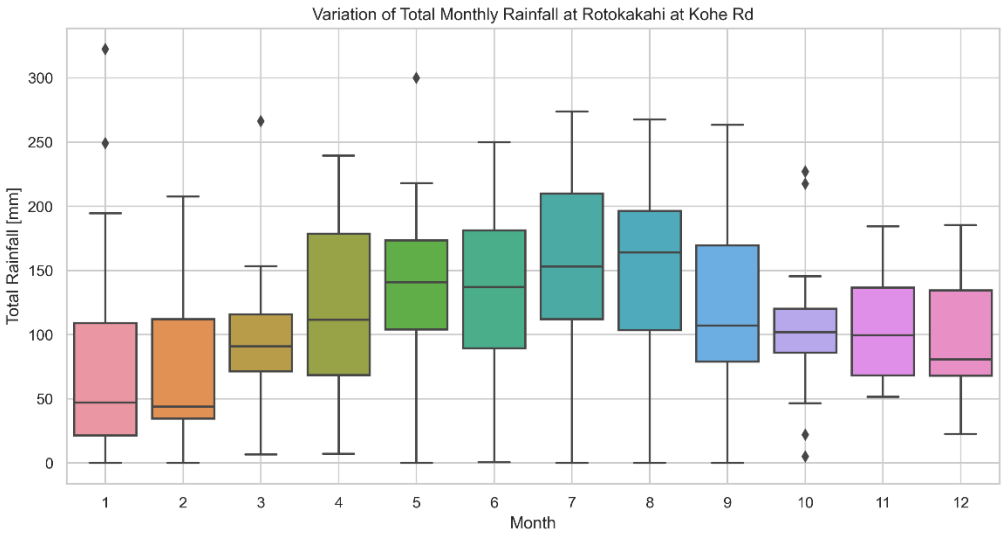
Variation of Total Monthly Rainfall at Rotokakahi at Kohe Rd
Total Rainfall [mm]
0
50
100
150
200
250
300
1
2
3
4
5
6
7
8
9
10
11
12
Month

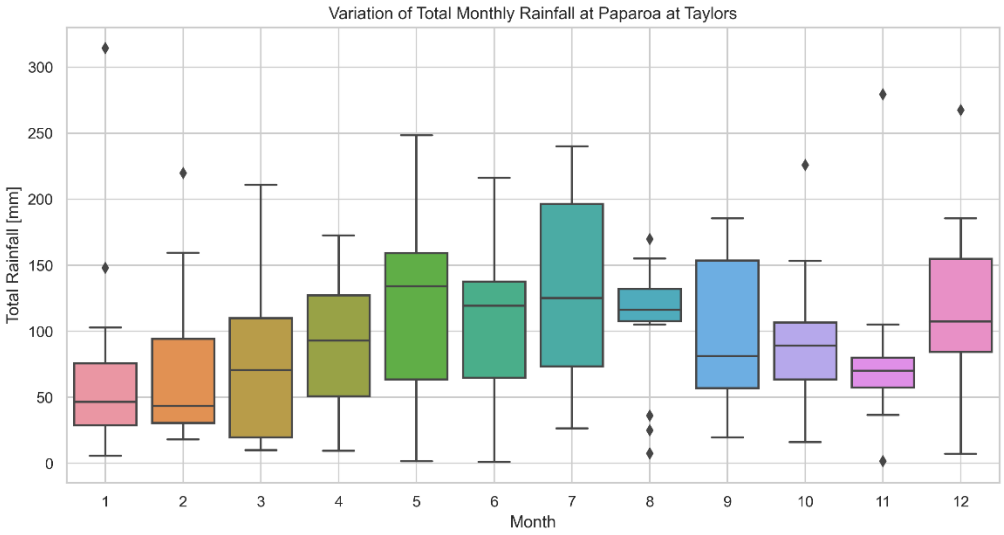
Variation of Total Monthly Rainfall at Paparoa at Taylors
Total Rainfall [mm]
0
50
100
150
200
250
300
1
2
3
4
5
6
7
8
9
10
11
12
Month

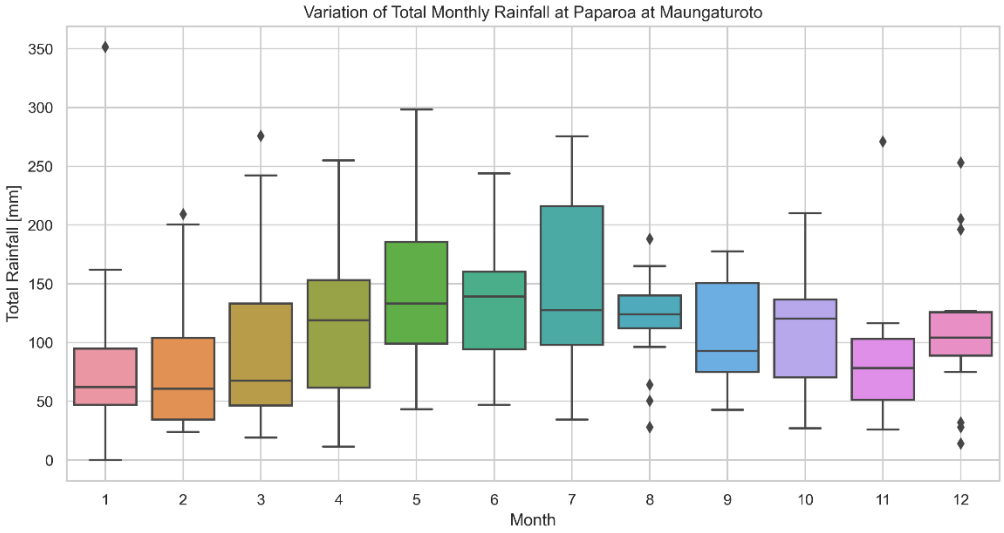
Variation of Total Monthly Rainfall at Paparoa at Maungaturoto
Total Rainfall [mm]
0
50
100
150
200
250
300
350
1
2
3
4
5
6
7
8
9
10
11
12
Month

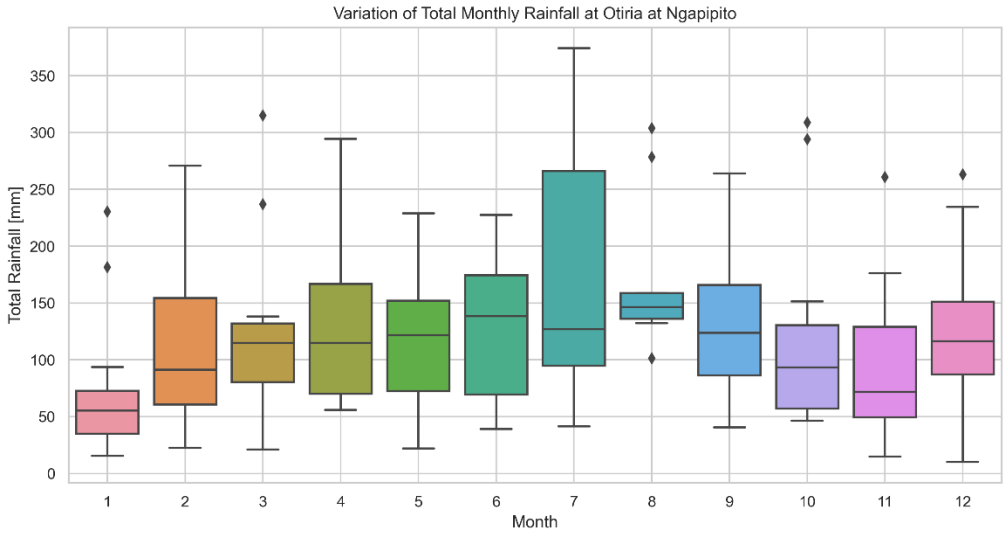
Variation of Total Monthly Rainfall at Otiria at Ngapipito
Total Rainfall [mm]
0
50
100
150
200
250
300
350
1
2
3
4
5
6
7
8
9
10
11
12
Month

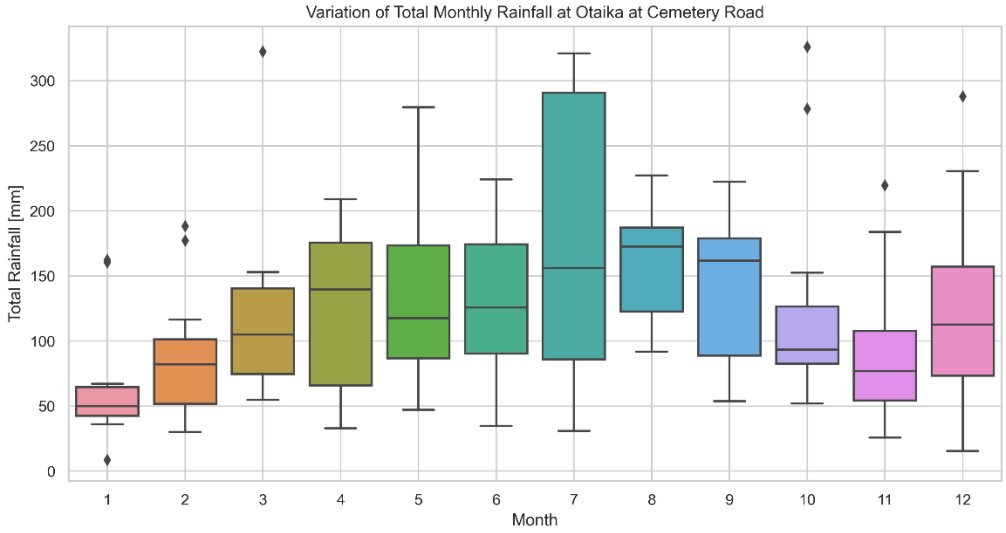
Variation of Total Monthly Rainfall at Otaika at Cemetery Road
Total Rainfall [mm]
0
50
100
150
200
250
300
1
2
3
4
5
6
7
8
9
10
11
12
Month

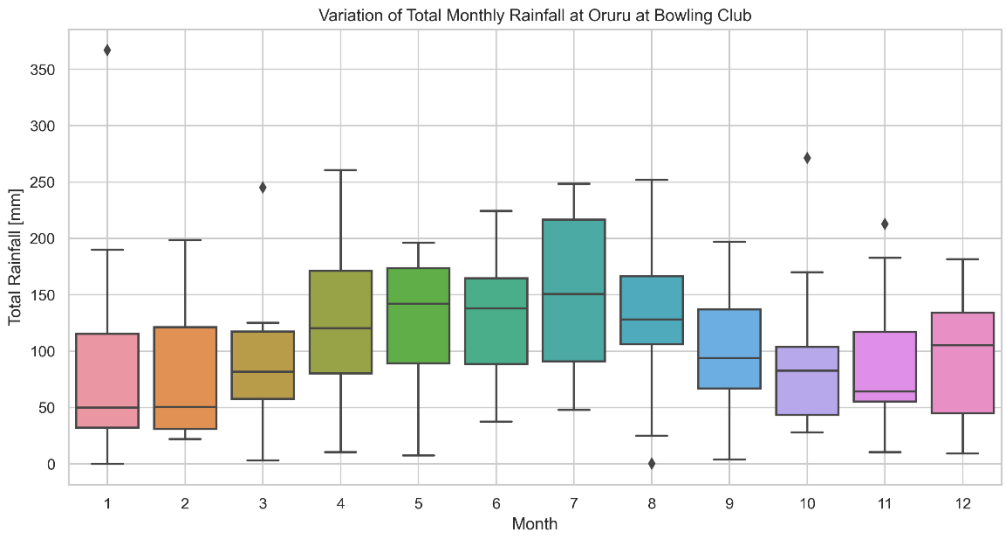
Variation of Total Monthly Rainfall at Oruru at Bowling Club
Total Rainfall [mm]
0
50
100
150
200
250
300
350
1
2
3
4
5
6
7
8
9
10
11
12
Month

APPENDIX 2: Time distribution of rainfall events at recorded stations, categorised by quartiles.

Panels show how rainfall accumulates over time for each quartile of total event rainfall. Median, 15th, and 85th percentile curves (blue, orange, and green) represent typical distribution patterns, with selected events overlaid to highlight variability. Higher quartile events often show delayed or back-loaded rainfall.

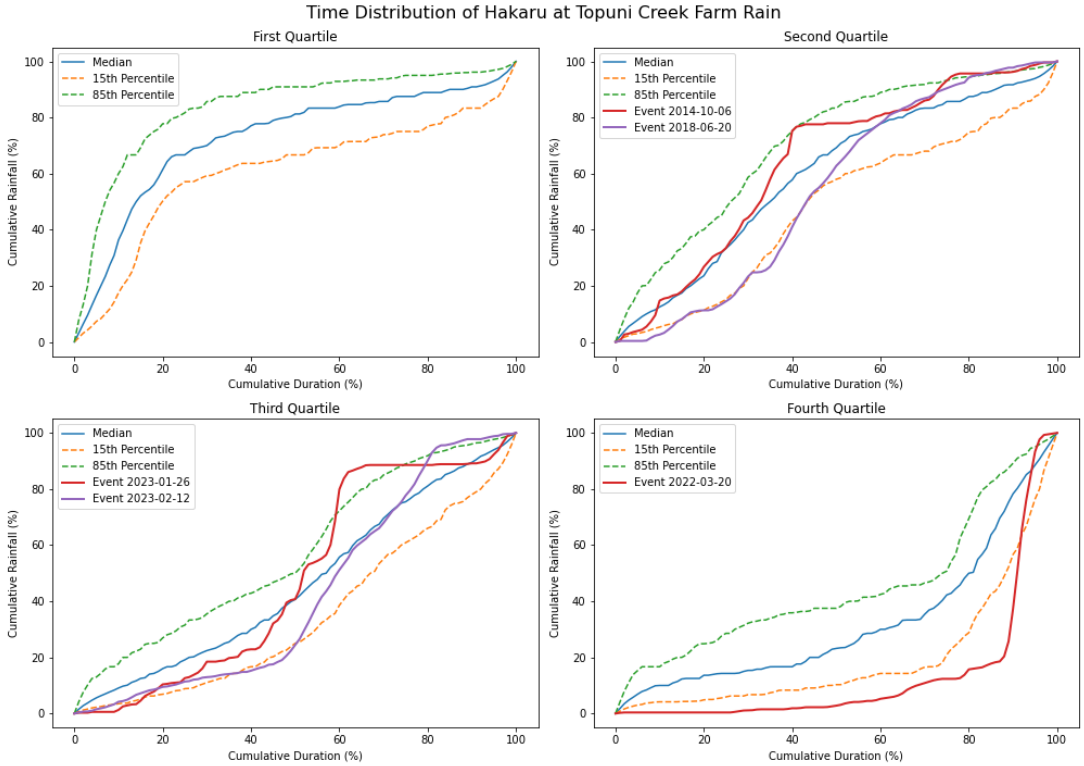

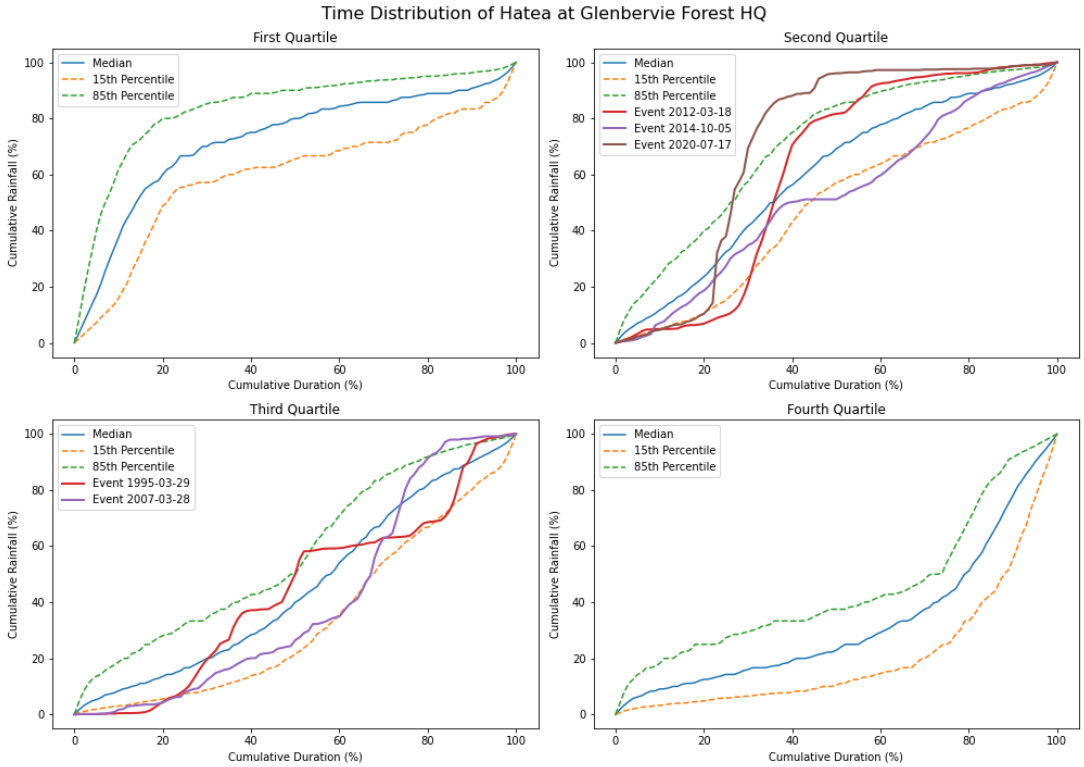

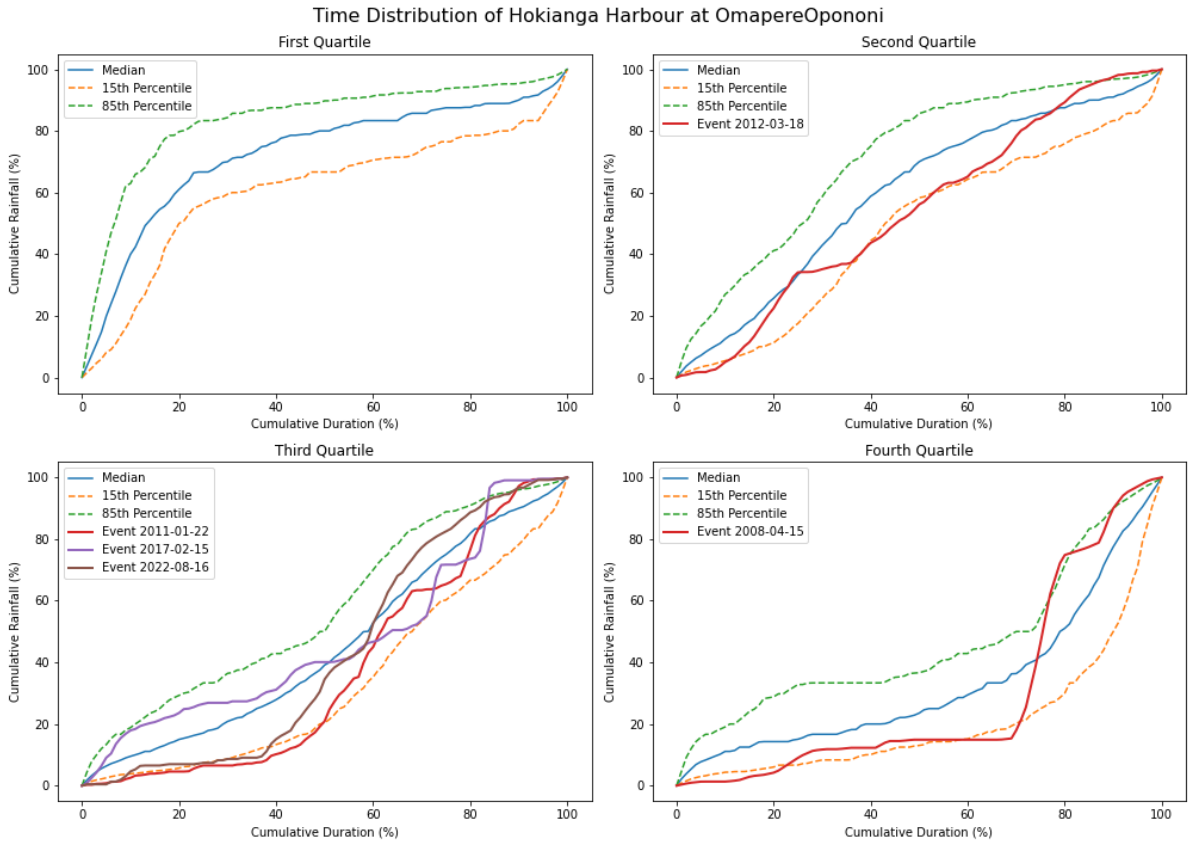
Time Distribution of Hokianga Harbour at OmapereOpononi
First Quartile
Median
15th Percentile
85th Percentile
Cumulative Rainfall (%)
Cumulative Duration (%)
Second Quartile
Median
15th Percentile
85th Percentile
Event 2012-03-18
Cumulative Rainfall (%)
Cumulative Duration (%)
Third Quartile
Median
15th Percentile
85th Percentile
Event 2011-01-22
Event 2017-02-15
Event 2022-08-16
Cumulative Rainfall (%)
Cumulative Duration (%)
Fourth Quartile
Median
15th Percentile
85th Percentile
Event 2008-04-15
Cumulative Rainfall (%)
Cumulative Duration (%)

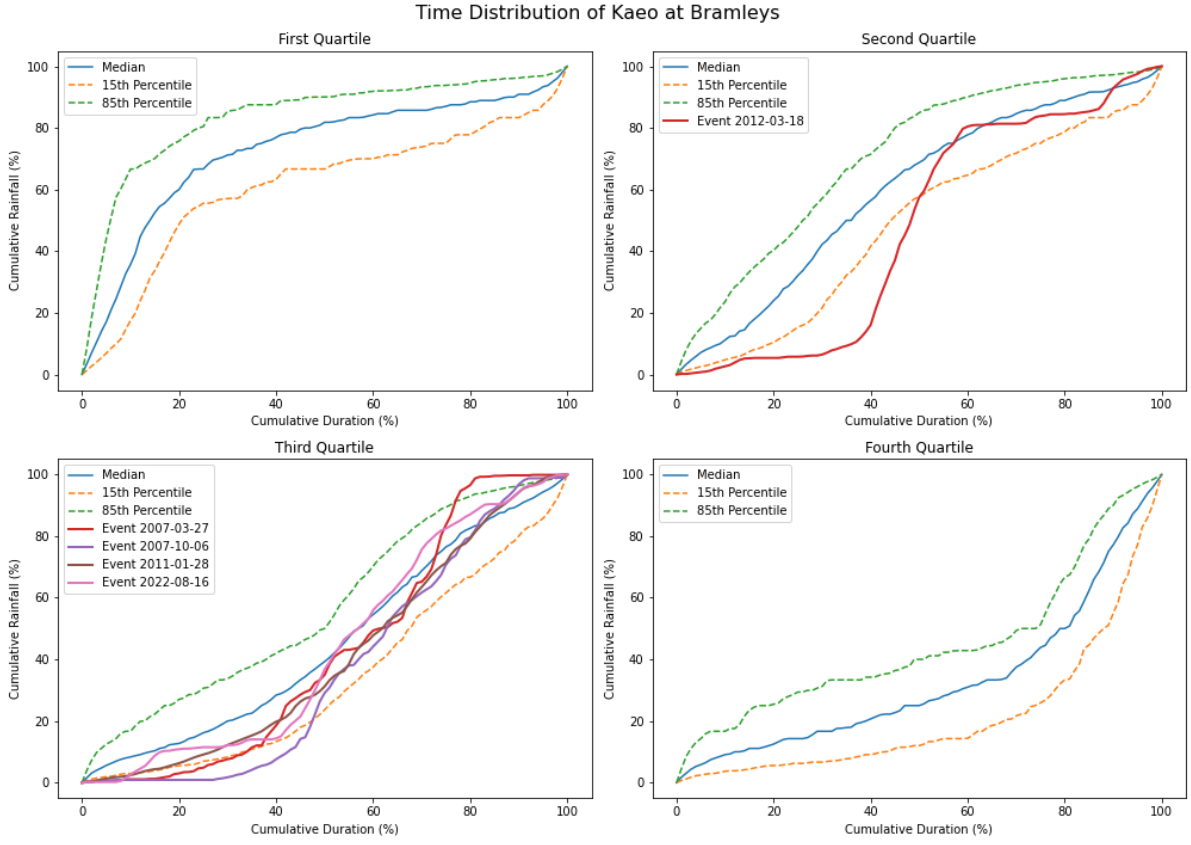
Time Distribution of Kaeo at Bramleys
First Quartile
Median
15th Percentile
85th Percentile
Cumulative Rainfall (%)
Cumulative Duration (%)
Second Quartile
Median
15th Percentile
85th Percentile
Event 2012-03-18
Cumulative Rainfall (%)
Cumulative Duration (%)
Third Quartile
Median
15th Percentile
85th Percentile
Event 2007-03-27
Event 2007-10-06
Event 2011-01-28
Event 2022-08-16
Cumulative Rainfall (%)
Cumulative Duration (%)
Fourth Quartile
Median
15th Percentile
85th Percentile
Cumulative Rainfall (%)
Cumulative Duration (%)

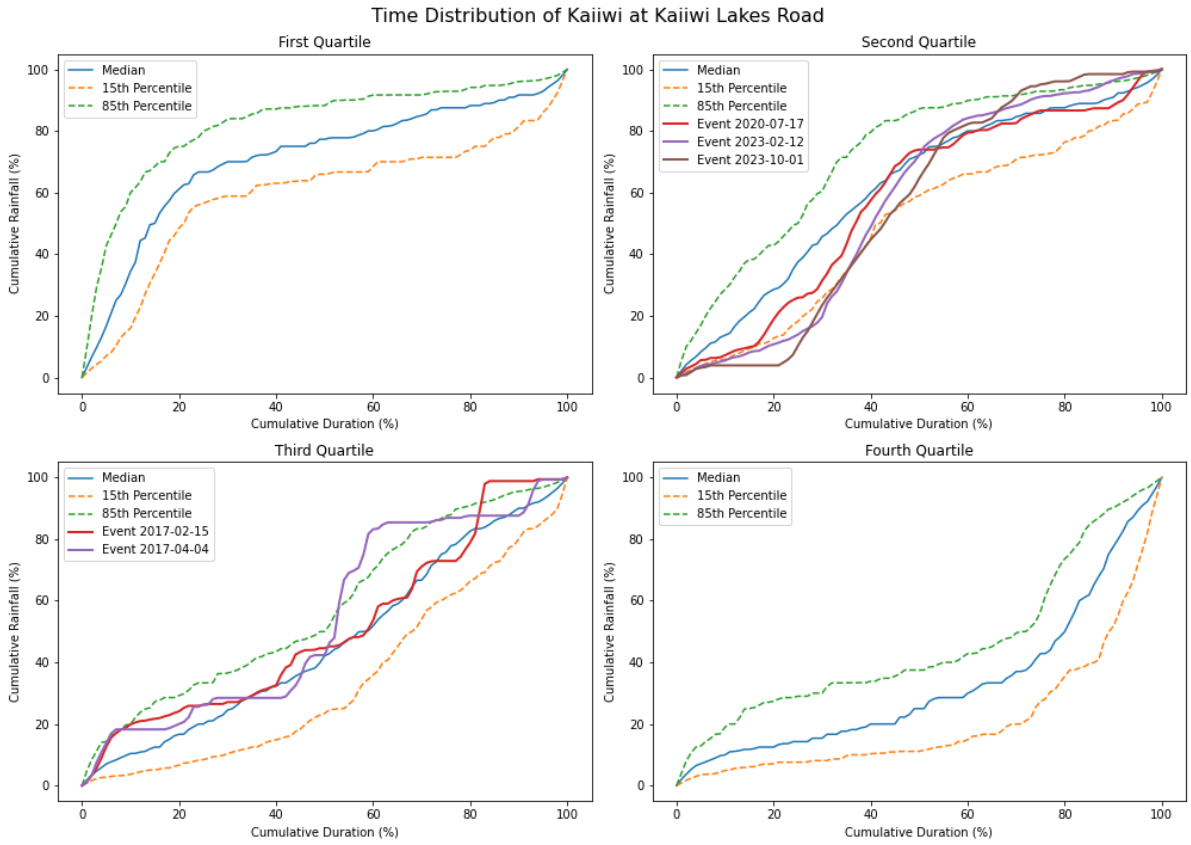
Time Distribution of Kaiiwi at Kaiiwi Lakes Road
First Quartile
Second Quartile
Third Quartile
Fourth Quartile
Median
15th Percentile
85th Percentile
Event 2020-07-17
Event 2023-02-12
Event 2023-10-01
Event 2017-02-15
Event 2017-04-04
Cumulative Rainfall (%)
Cumulative Duration (%)

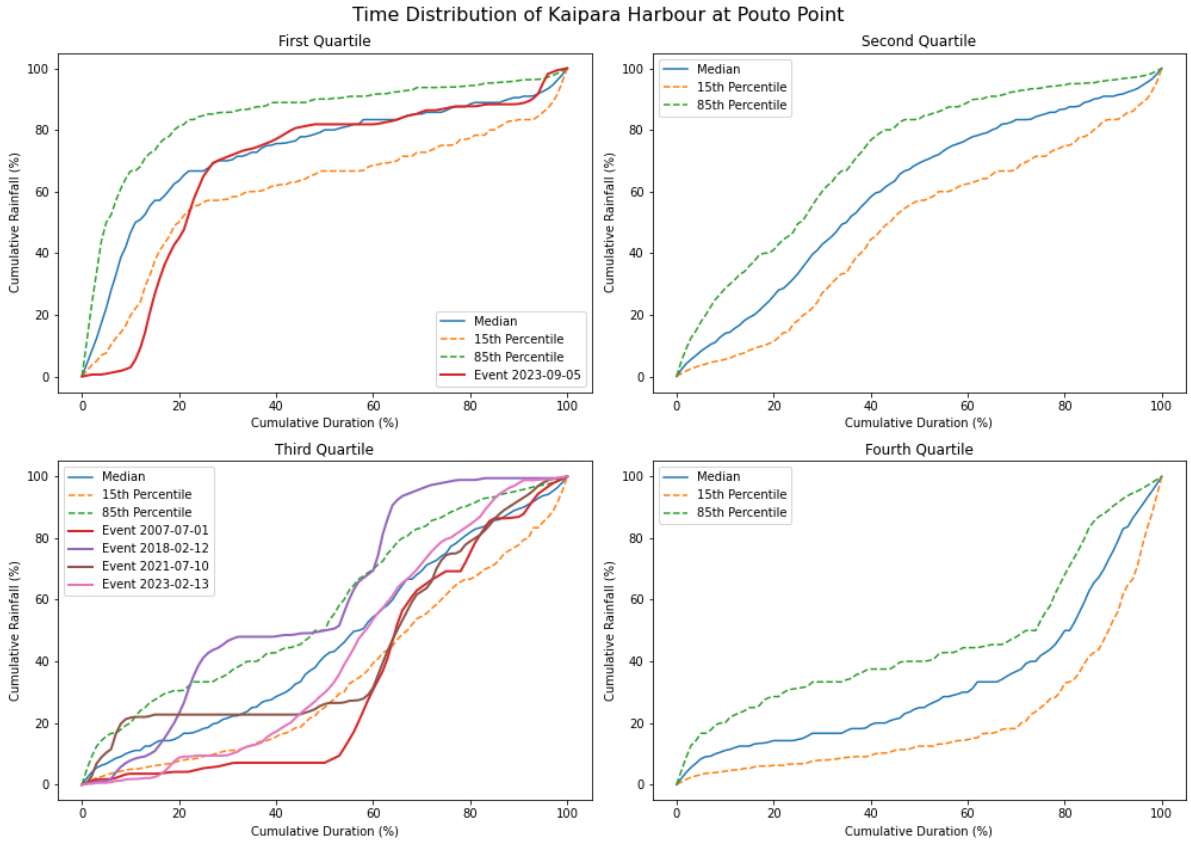
Time Distribution of Kaipara Harbour at Pouto Point
First Quartile
Second Quartile
Third Quartile
Fourth Quartile
Median
15th Percentile
85th Percentile
Event 2023-09-05
Event 2007-07-01
Event 2018-02-12
Event 2021-07-10
Event 2023-02-13
Cumulative Rainfall (%)
Cumulative Duration (%)

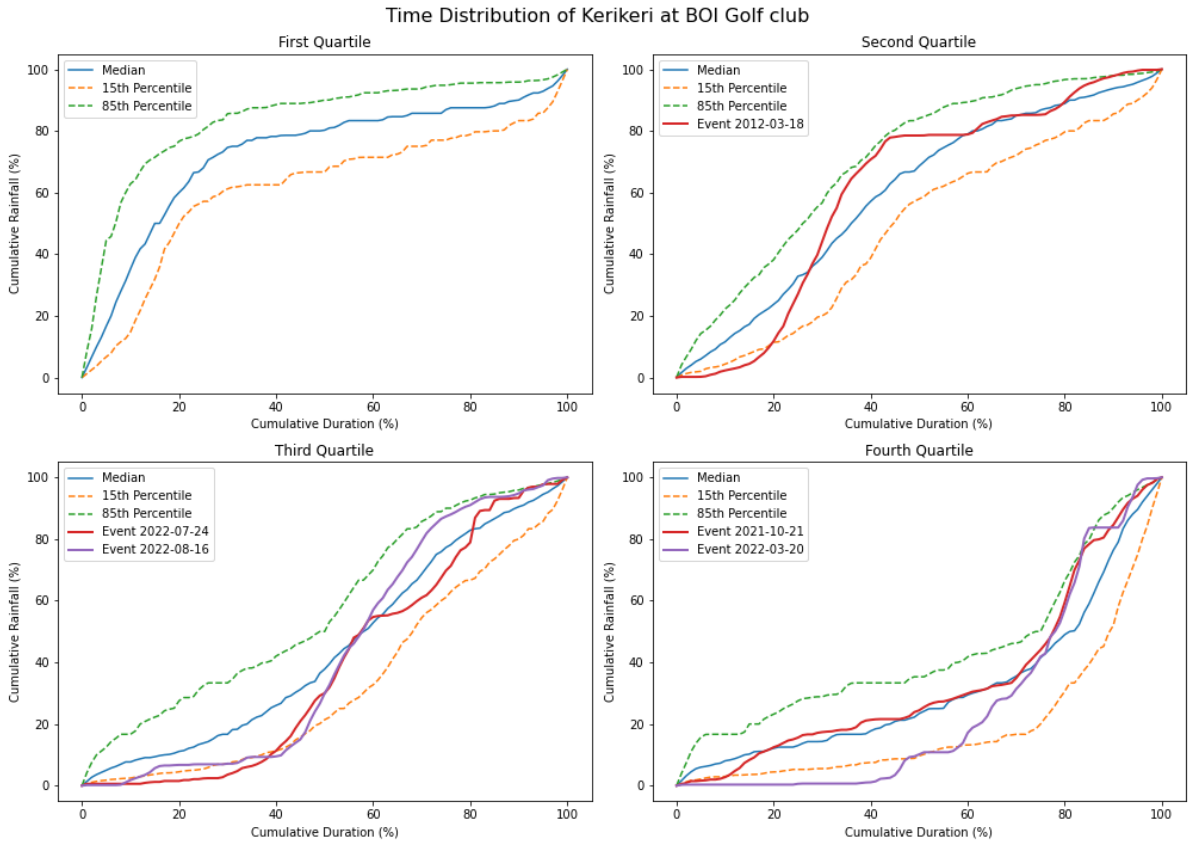
Time Distribution of Kerikeri at BOI Golf club
First Quartile
Median
15th Percentile
85th Percentile
Second Quartile
Median
15th Percentile
85th Percentile
Event 2012-03-18
Third Quartile
Median
15th Percentile
85th Percentile
Event 2022-07-24
Event 2022-08-16
Fourth Quartile
Median
15th Percentile
85th Percentile
Event 2021-10-21
Event 2022-03-20
Cumulative Rainfall (%)
Cumulative Duration (%)

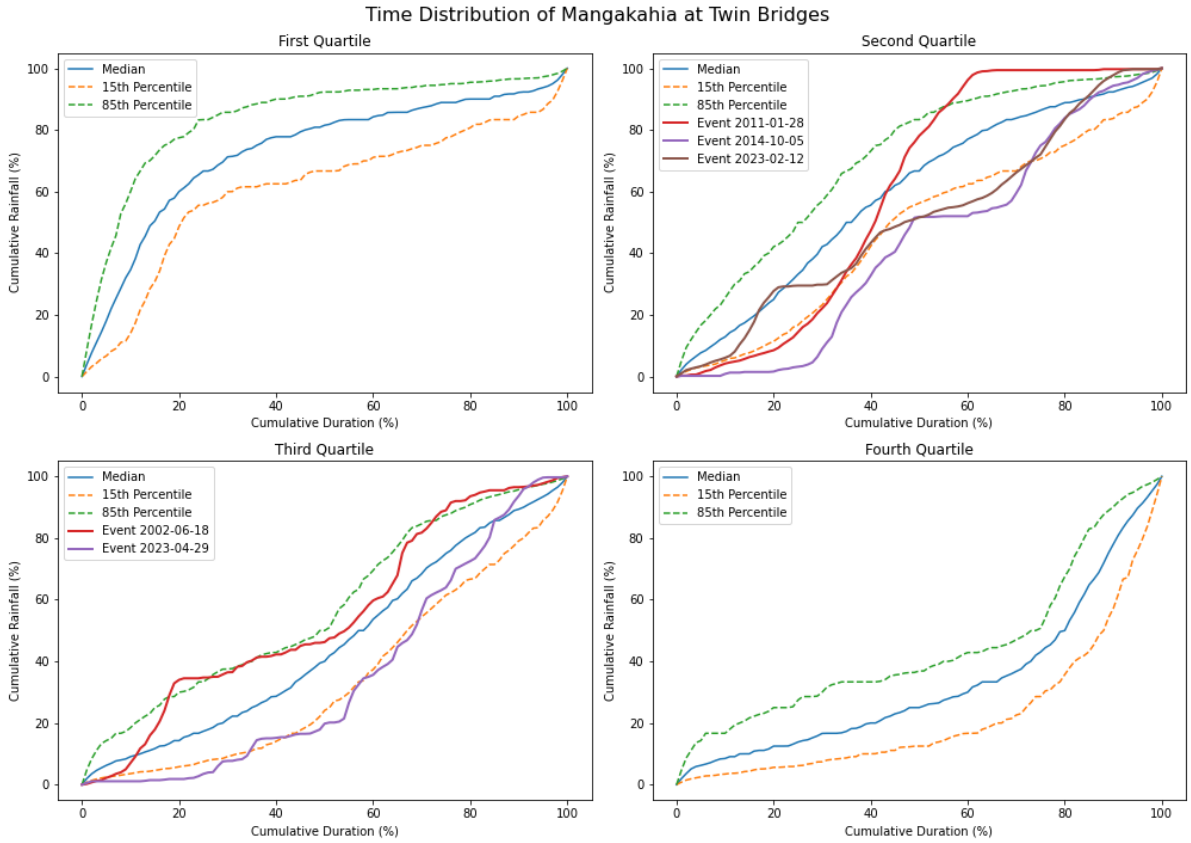
Time Distribution of Mangakahia at Twin Bridges
First Quartile
Median
15th Percentile
85th Percentile
Second Quartile
Median
15th Percentile
85th Percentile
Event 2011-01-28
Event 2014-10-05
Event 2023-02-12
Third Quartile
Median
15th Percentile
85th Percentile
Event 2002-06-18
Event 2023-04-29
Fourth Quartile
Median
15th Percentile
85th Percentile
Cumulative Rainfall (%)
Cumulative Duration (%)

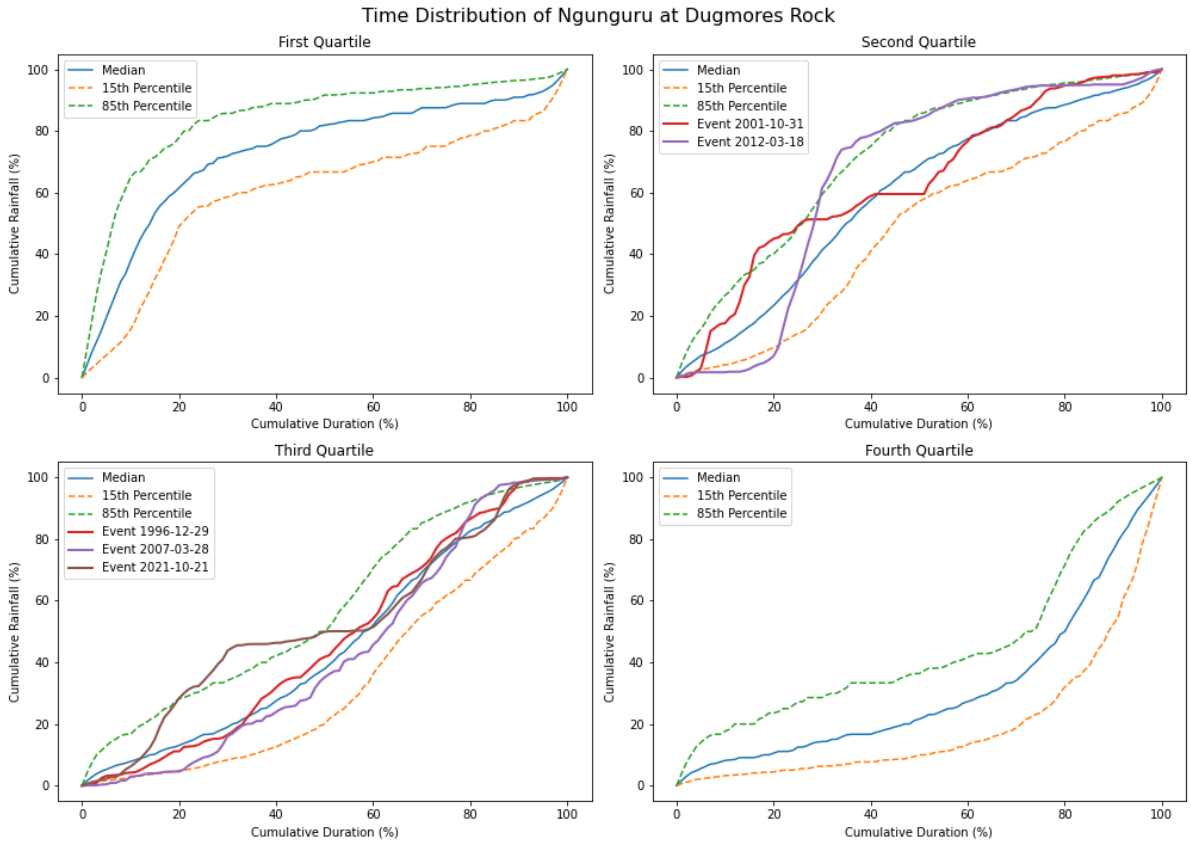
Time Distribution of Ngunguru at Dugmores Rock
First Quartile
Median
15th Percentile
85th Percentile
Second Quartile
Median
15th Percentile
85th Percentile
Event 2001-10-31
Event 2012-03-18
Third Quartile
Median
15th Percentile
85th Percentile
Event 1996-12-29
Event 2007-03-28
Event 2021-10-21
Fourth Quartile
Median
15th Percentile
85th Percentile
Cumulative Rainfall (%)
Cumulative Duration (%)

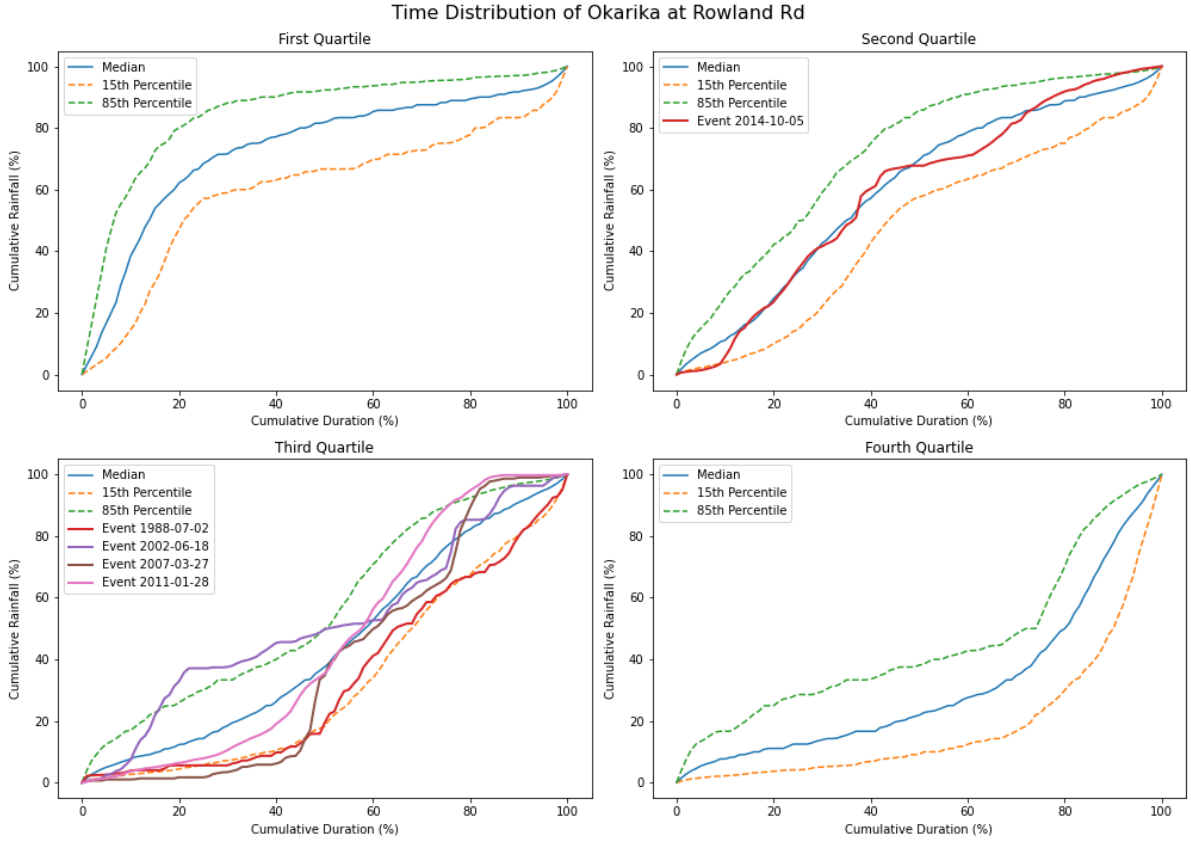
Time Distribution of Okarika at Rowland Rd
First Quartile
Median
15th Percentile
85th Percentile
Second Quartile
Median
15th Percentile
85th Percentile
Event 2014-10-05
Third Quartile
Median
15th Percentile
85th Percentile
Event 1988-07-02
Event 2002-06-18
Event 2007-03-27
Event 2011-01-28
Fourth Quartile
Median
15th Percentile
85th Percentile
Cumulative Rainfall (%)
Cumulative Duration (%)

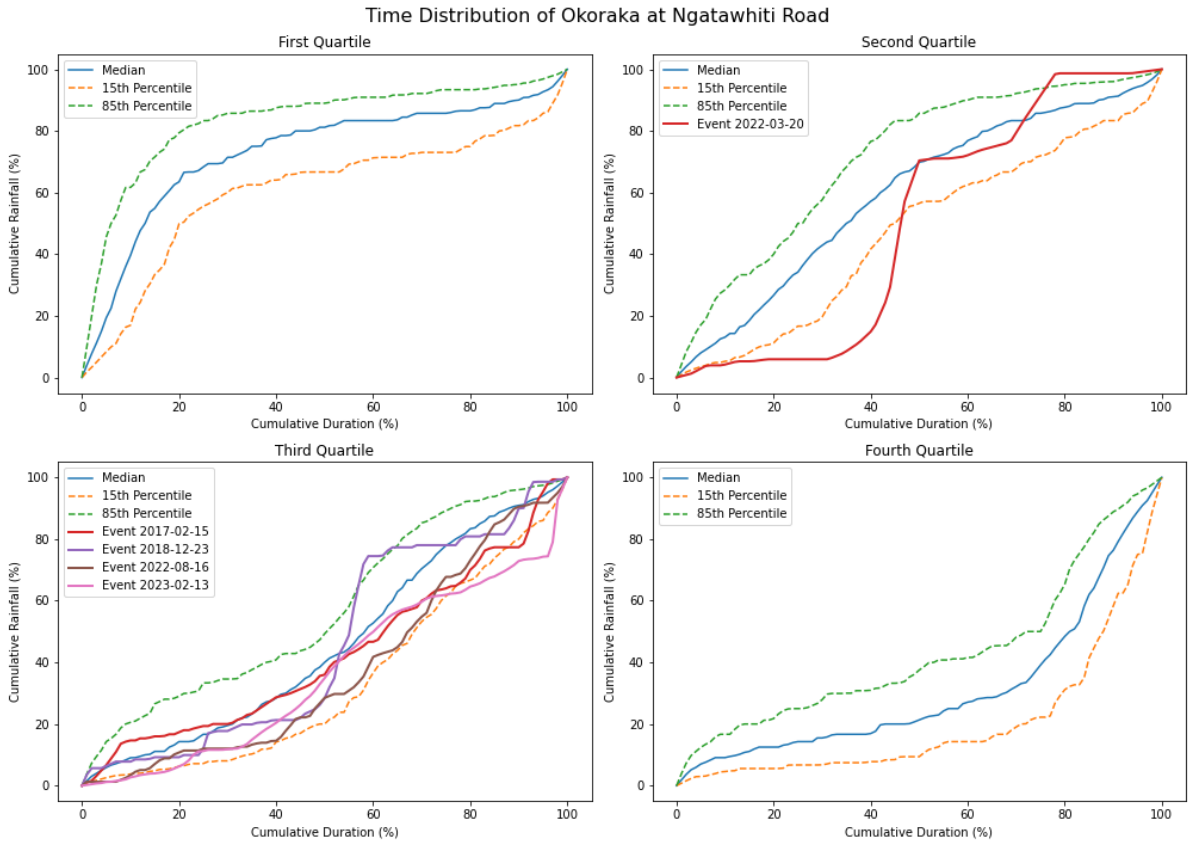
Time Distribution of Okoraka at Ngatawhiti Road
First Quartile
Median
15th Percentile
85th Percentile
Second Quartile
Median
15th Percentile
85th Percentile
Event 2022-03-20
Third Quartile
Median
15th Percentile
85th Percentile
Event 2017-02-15
Event 2018-12-23
Event 2022-08-16
Event 2023-02-13
Fourth Quartile
Median
15th Percentile
85th Percentile
Cumulative Rainfall (%)
Cumulative Duration (%)

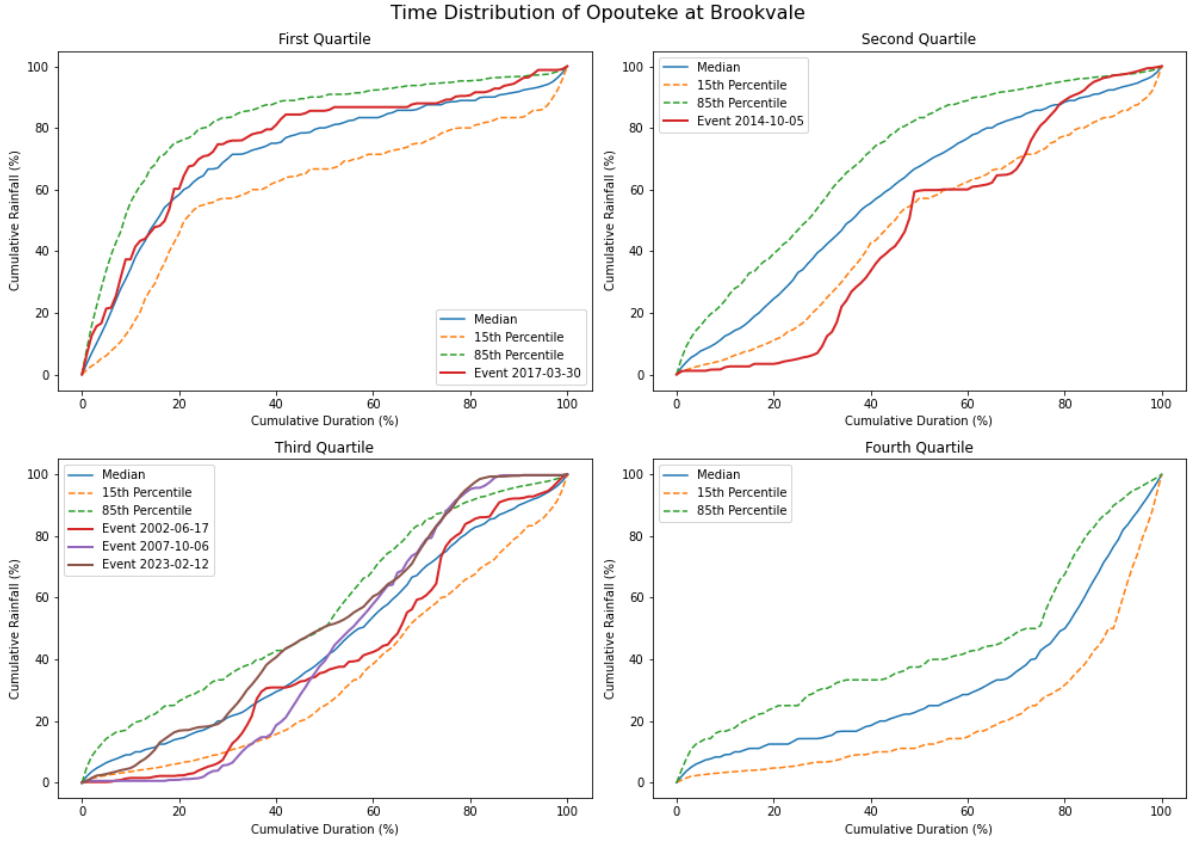
Time Distribution of Opouteke at Brookvale
First Quartile
Median
15th Percentile
85th Percentile
Event 2017-03-30
Second Quartile
Median
15th Percentile
85th Percentile
Event 2014-10-05
Third Quartile
Median
15th Percentile
85th Percentile
Event 2002-06-17
Event 2007-10-06
Event 2023-02-12
Fourth Quartile
Median
15th Percentile
85th Percentile
Cumulative Rainfall (%)
Cumulative Duration (%)

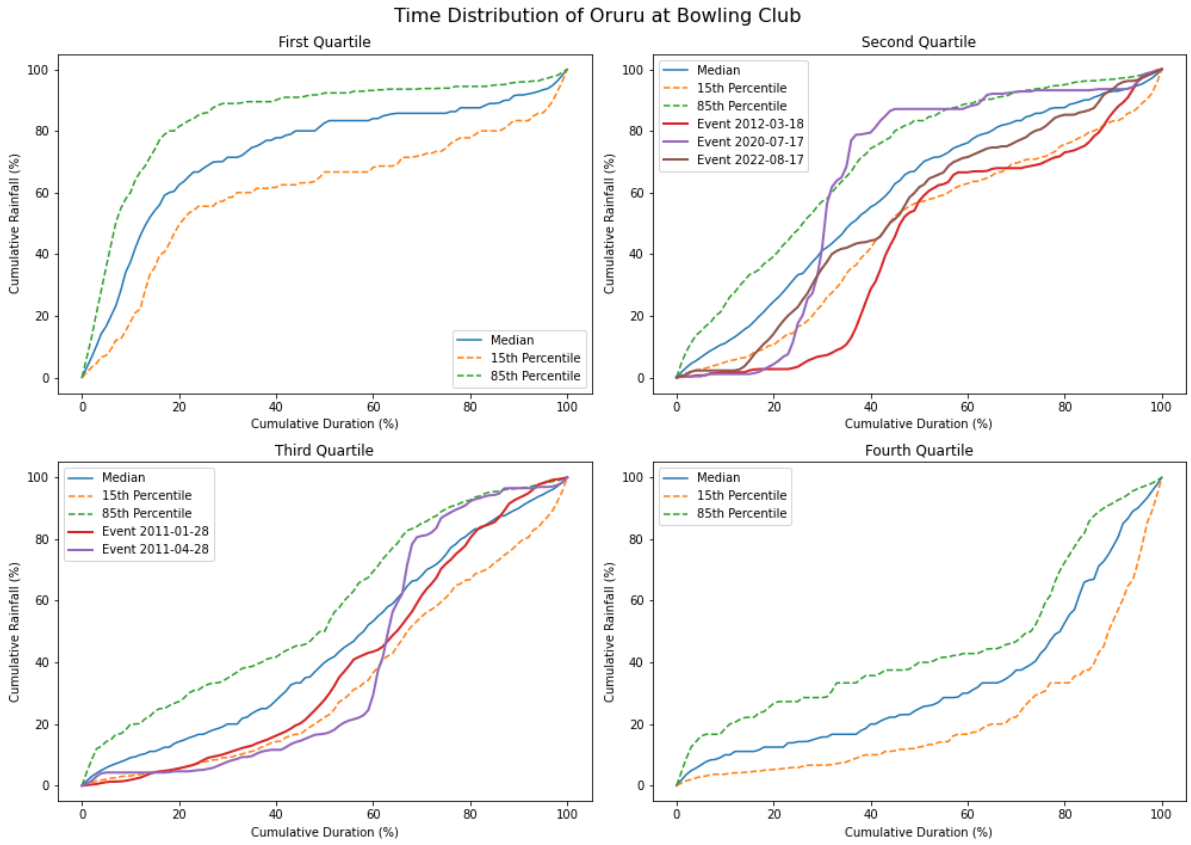
Time Distribution of Oruru at Bowling Club
First Quartile
Second Quartile
Third Quartile
Fourth Quartile
Cumulative Rainfall (%)
Cumulative Duration (%)
Median
15th Percentile
85th Percentile
Event 2012-03-18
Event 2020-07-17
Event 2022-08-17
Event 2011-01-28
Event 2011-04-28

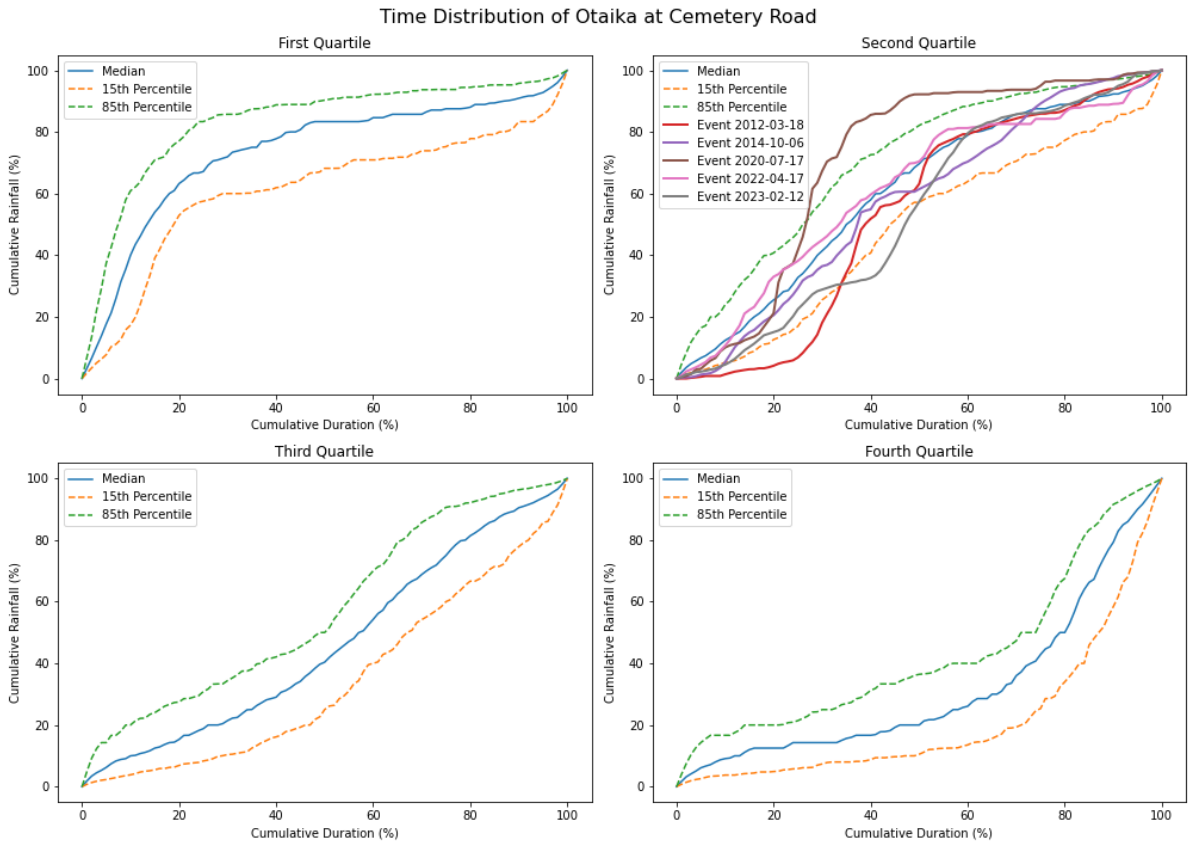
Time Distribution of Otaika at Cemetery Road
First Quartile
Second Quartile
Third Quartile
Fourth Quartile
Cumulative Rainfall (%)
Cumulative Duration (%)
Median
15th Percentile
85th Percentile
Event 2012-03-18
Event 2014-10-06
Event 2020-07-17
Event 2022-04-17
Event 2023-02-12

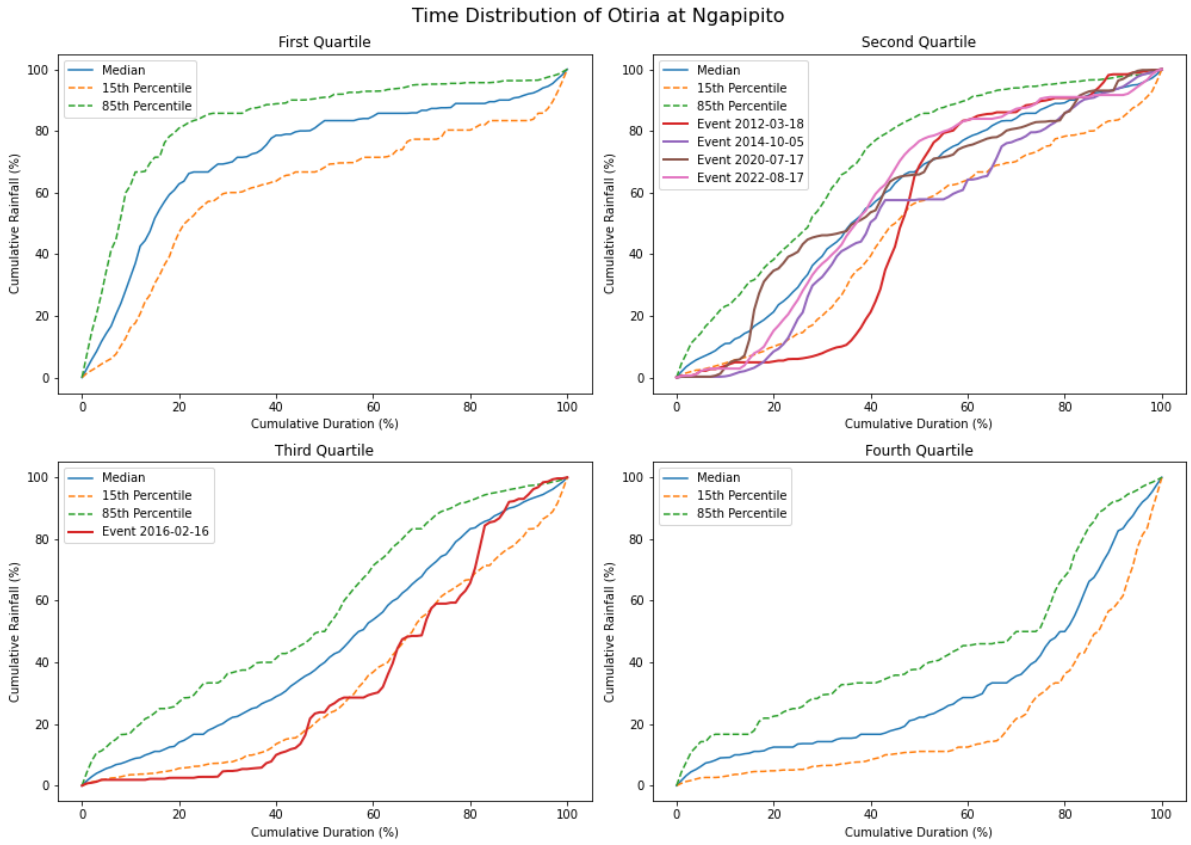
Time Distribution of Otiria at Ngapipito
First Quartile
Median
15th Percentile
85th Percentile
Second Quartile
Median
15th Percentile
85th Percentile
Event 2012-03-18
Event 2014-10-05
Event 2020-07-17
Event 2022-08-17
Third Quartile
Median
15th Percentile
85th Percentile
Event 2016-02-16
Fourth Quartile
Median
15th Percentile
85th Percentile
Cumulative Rainfall (%)
Cumulative Duration (%)

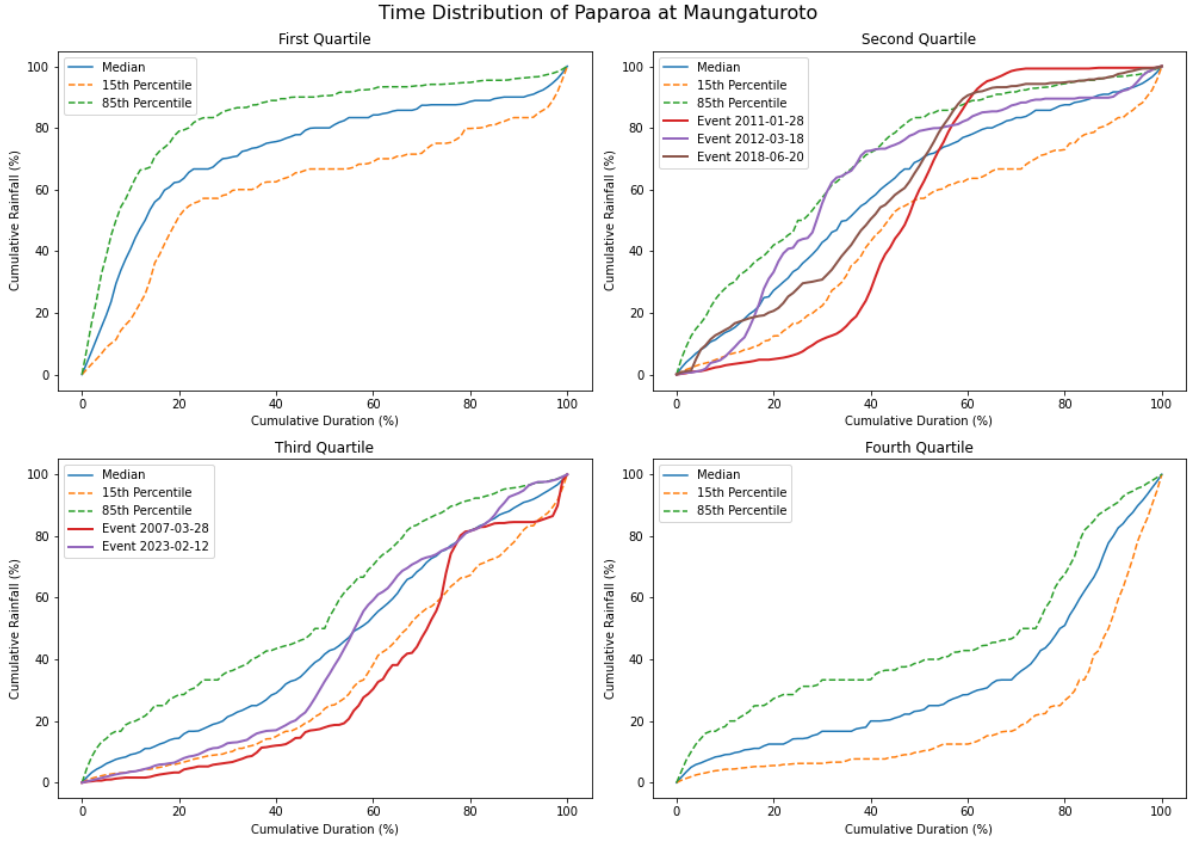
Time Distribution of Paparoa at Maungaturoto
First Quartile
Median
15th Percentile
85th Percentile
Second Quartile
Median
15th Percentile
85th Percentile
Event 2011-01-28
Event 2012-03-18
Event 2018-06-20
Third Quartile
Median
15th Percentile
85th Percentile
Event 2007-03-28
Event 2023-02-12
Fourth Quartile
Median
15th Percentile
85th Percentile
Cumulative Rainfall (%)
Cumulative Duration (%)

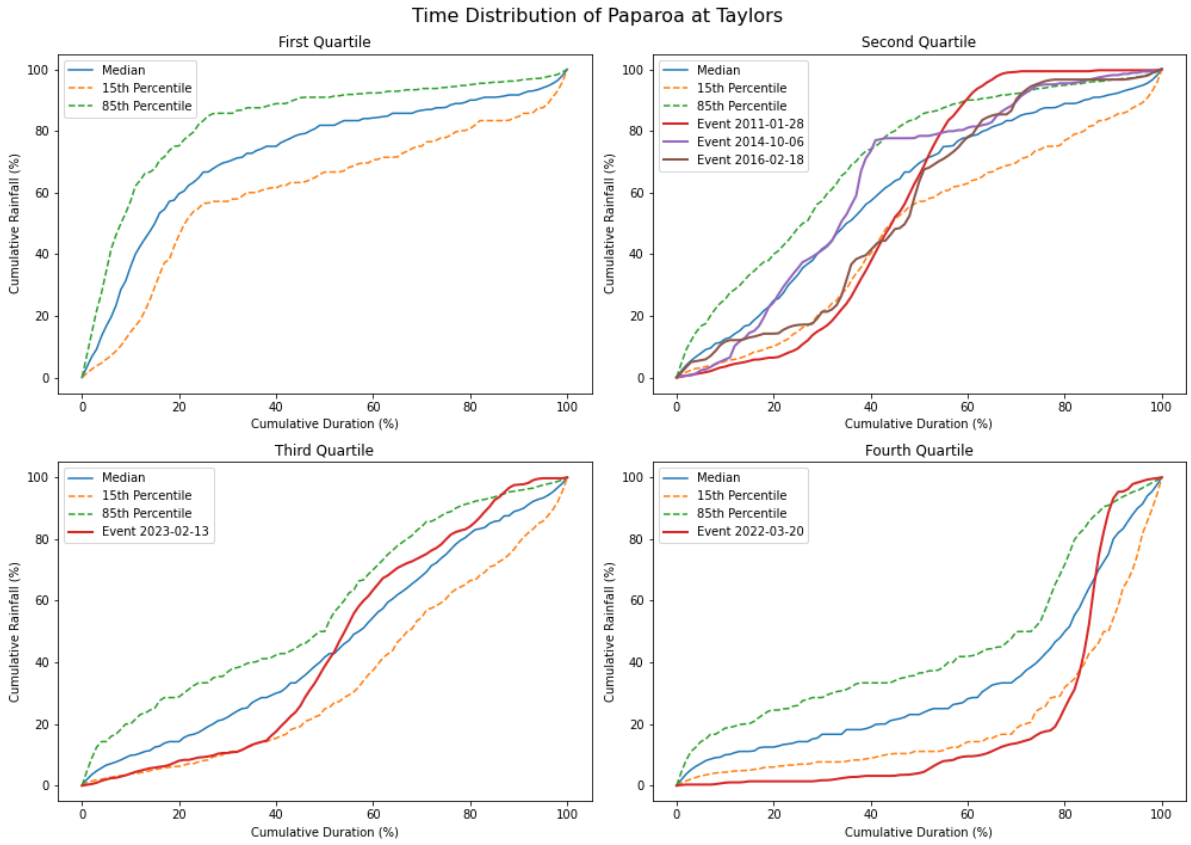
Time Distribution of Paparoa at Taylors
First Quartile
Median
15th Percentile
85th Percentile
Second Quartile
Median
15th Percentile
85th Percentile
Event 2011-01-28
Event 2014-10-06
Event 2016-02-18
Third Quartile
Median
15th Percentile
85th Percentile
Event 2023-02-13
Fourth Quartile
Median
15th Percentile
85th Percentile
Event 2022-03-20
Cumulative Rainfall (%)
Cumulative Duration (%)

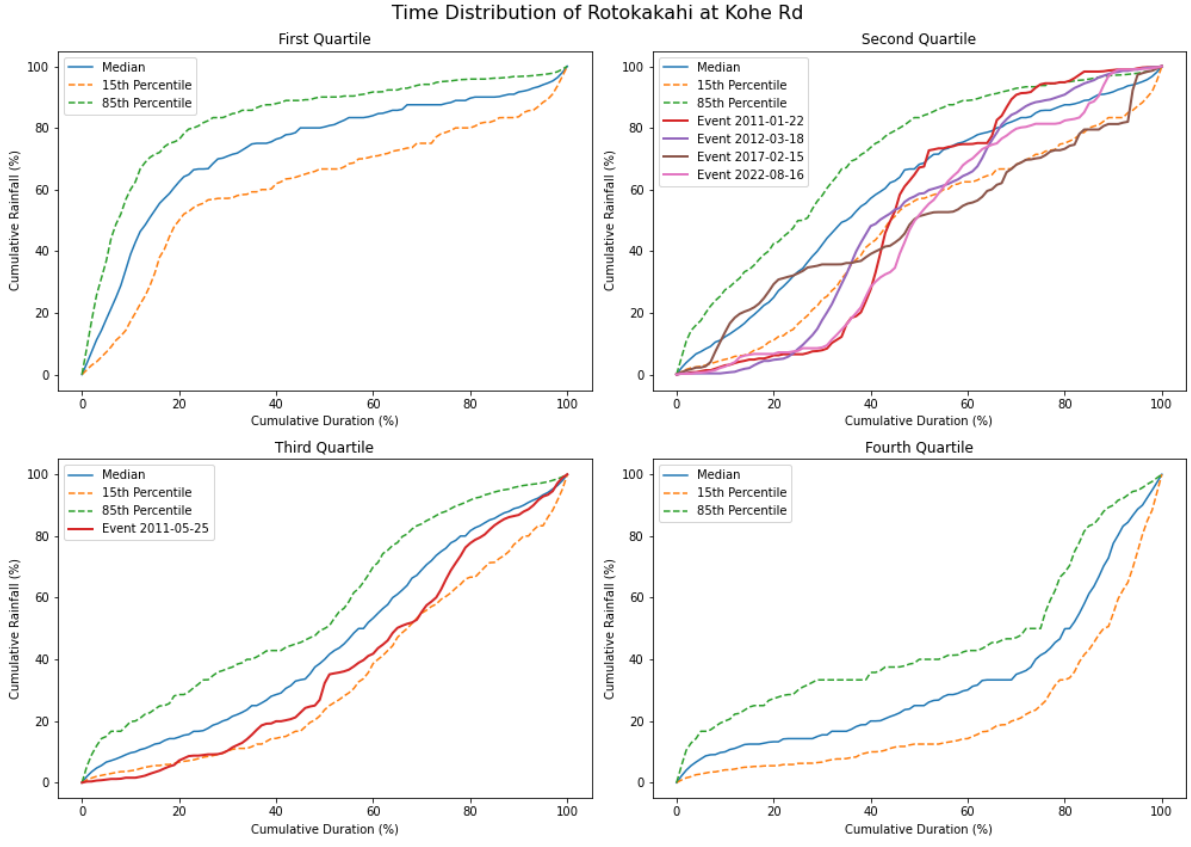
Time Distribution of Rotokakahi at Kohe Rd
First Quartile
Median
15th Percentile
85th Percentile
Second Quartile
Median
15th Percentile
85th Percentile
Event 2011-01-22
Event 2012-03-18
Event 2017-02-15
Event 2022-08-16
Third Quartile
Median
15th Percentile
85th Percentile
Event 2011-05-25
Fourth Quartile
Median
15th Percentile
85th Percentile
Cumulative Rainfall (%)
Cumulative Duration (%)

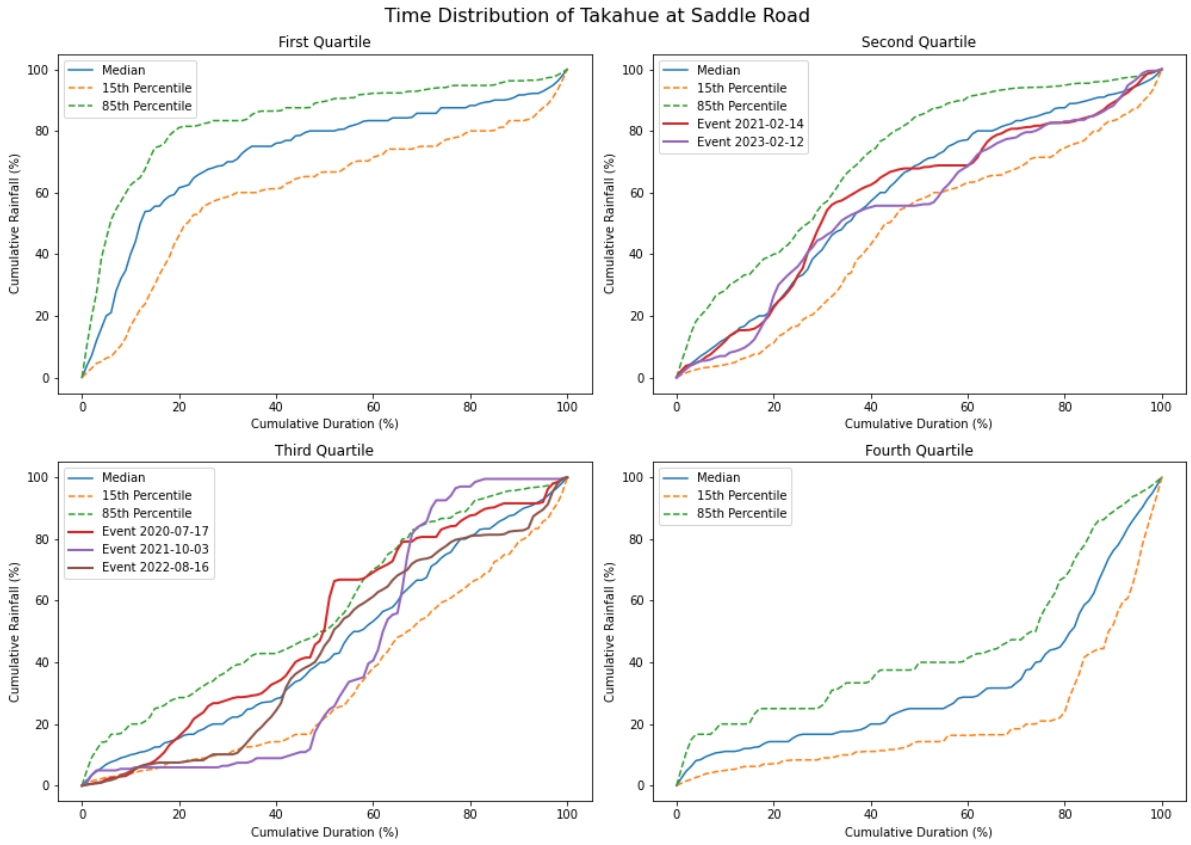
Time Distribution of Takahue at Saddle Road
First Quartile
Second Quartile
Third Quartile
Fourth Quartile
Median
15th Percentile
85th Percentile
Event 2021-02-14
Event 2023-02-12
Event 2020-07-17
Event 2021-10-03
Event 2022-08-16
Cumulative Rainfall (%)
Cumulative Duration (%)

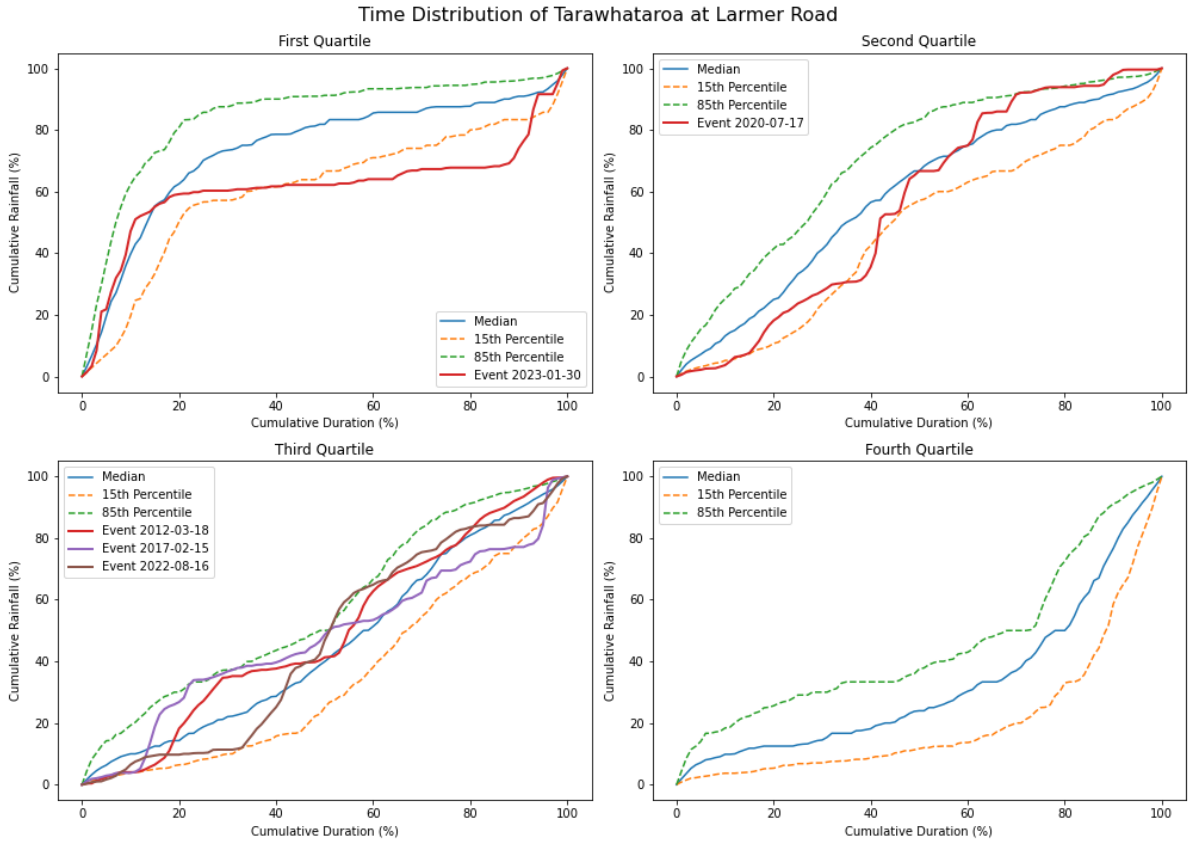
Time Distribution of Tarawhataroa at Larmer Road
First Quartile
Second Quartile
Third Quartile
Fourth Quartile
Median
15th Percentile
85th Percentile
Event 2023-01-30
Event 2020-07-17
Event 2012-03-18
Event 2017-02-15
Event 2022-08-16
Cumulative Rainfall (%)
Cumulative Duration (%)

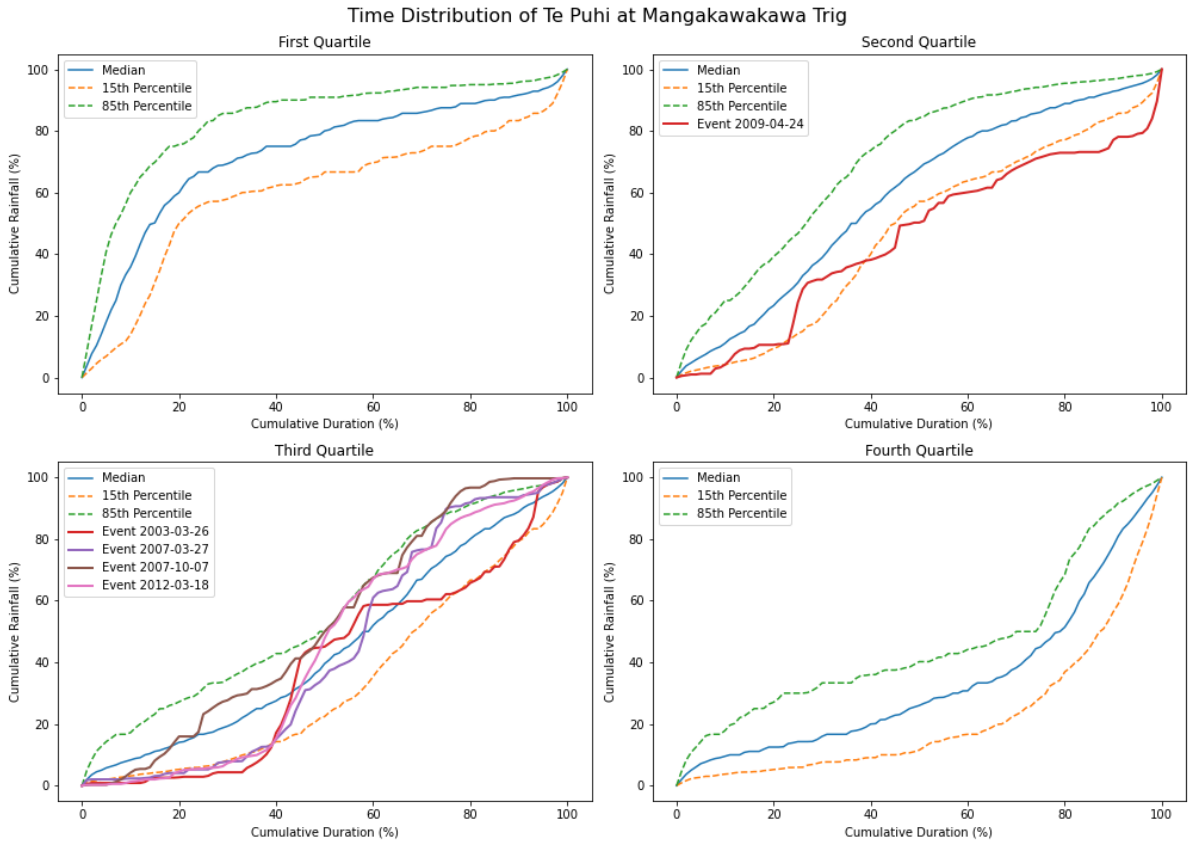
Time Distribution of Te Puhi at Mangakawakawa Trig
First Quartile
Second Quartile
Third Quartile
Fourth Quartile
Median
15th Percentile
85th Percentile
Event 2009-04-24
Event 2003-03-26
Event 2007-03-27
Event 2007-10-07
Event 2012-03-18
Cumulative Rainfall (%)
Cumulative Duration (%)

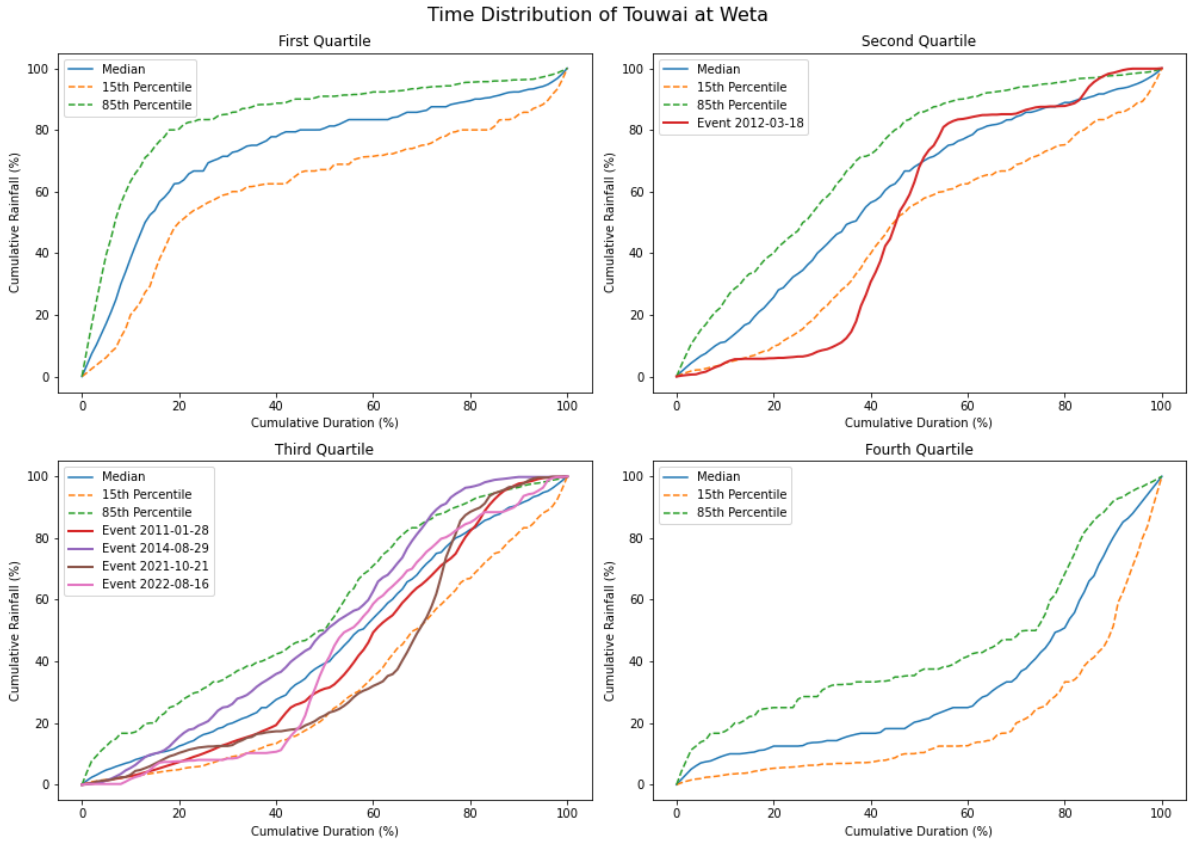
Time Distribution of Touwai at Weta
First Quartile
Second Quartile
Third Quartile
Fourth Quartile
Median
15th Percentile
85th Percentile
Event 2012-03-18
Event 2011-01-28
Event 2014-08-29
Event 2021-10-21
Event 2022-08-16
Cumulative Rainfall (%)
Cumulative Duration (%)

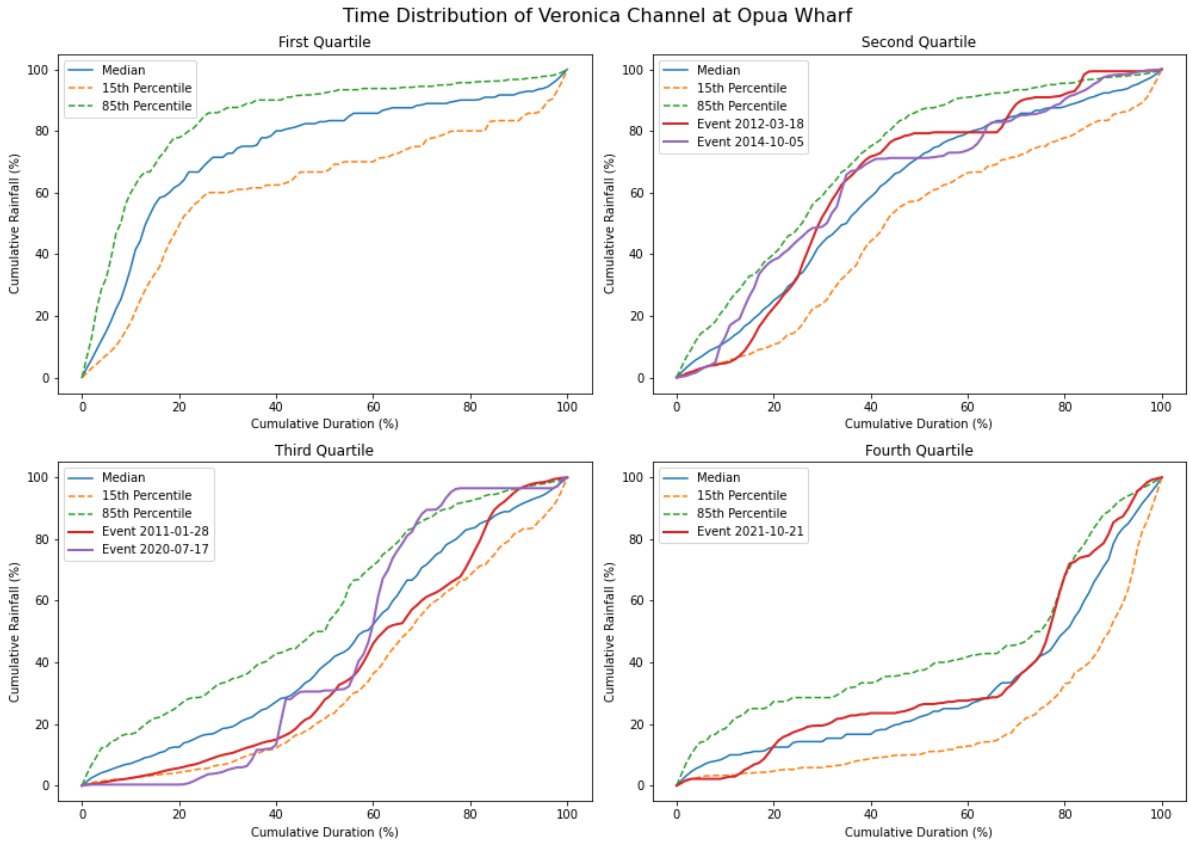
Time Distribution of Veronica Channel at Opua Wharf
First Quartile
Median
15th Percentile
85th Percentile
Second Quartile
Event 2012-03-18
Event 2014-10-05
Third Quartile
Event 2011-01-28
Event 2020-07-17
Fourth Quartile
Event 2021-10-21
Cumulative Rainfall (%)
Cumulative Duration (%)

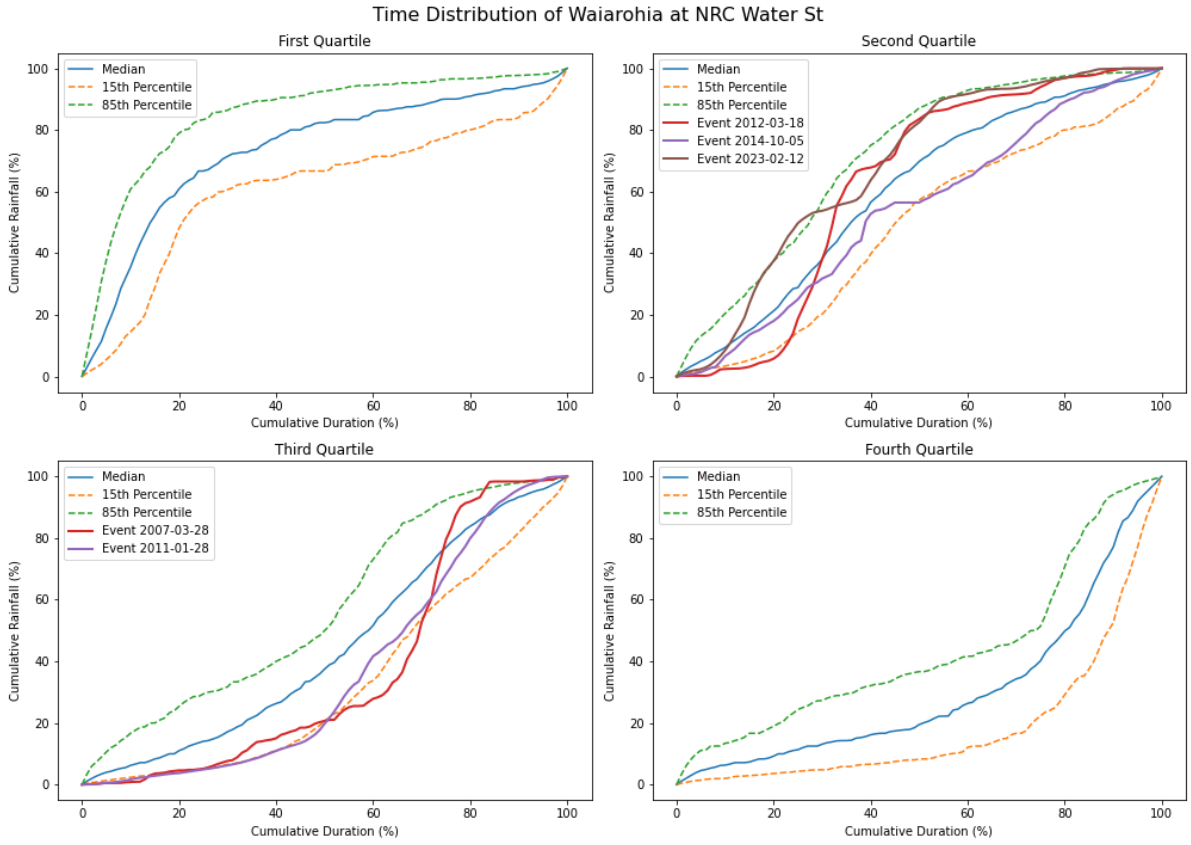
Time Distribution of Waiarohia at NRC Water St
First Quartile
Median
15th Percentile
85th Percentile
Second Quartile
Event 2012-03-18
Event 2014-10-05
Event 2023-02-12
Third Quartile
Event 2007-03-28
Event 2011-01-28
Fourth Quartile
Cumulative Rainfall (%)
Cumulative Duration (%)

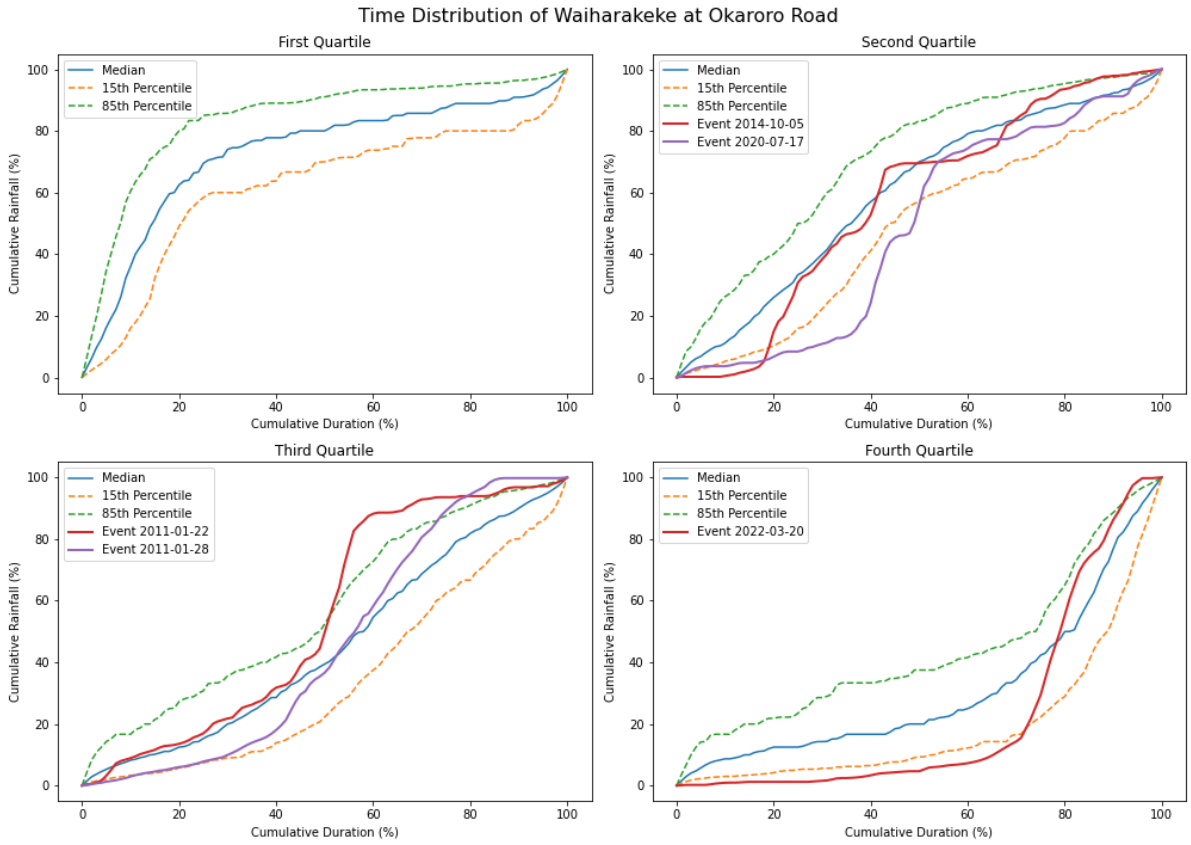
Time Distribution of Waiharakeke at Okaroro Road
First Quartile
Second Quartile
Third Quartile
Fourth Quartile
Median
15th Percentile
85th Percentile
Event 2014-10-05
Event 2020-07-17
Event 2011-01-22
Event 2011-01-28
Event 2022-03-20
Cumulative Rainfall (%)
Cumulative Duration (%)

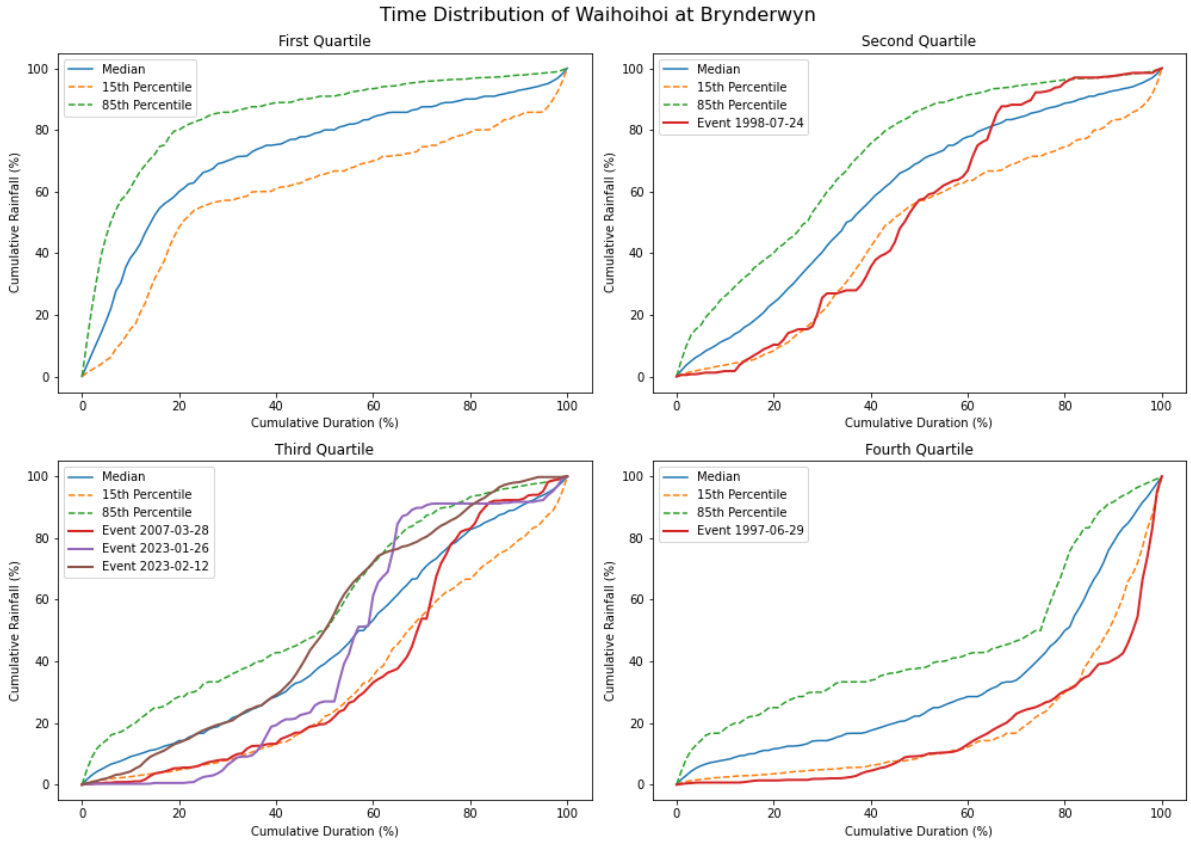
Time Distribution of Waihoihoi at Brynderwyn
First Quartile
Second Quartile
Third Quartile
Fourth Quartile
Median
15th Percentile
85th Percentile
Event 1998-07-24
Event 2007-03-28
Event 2023-01-26
Event 2023-02-12
Event 1997-06-29
Cumulative Rainfall (%)
Cumulative Duration (%)

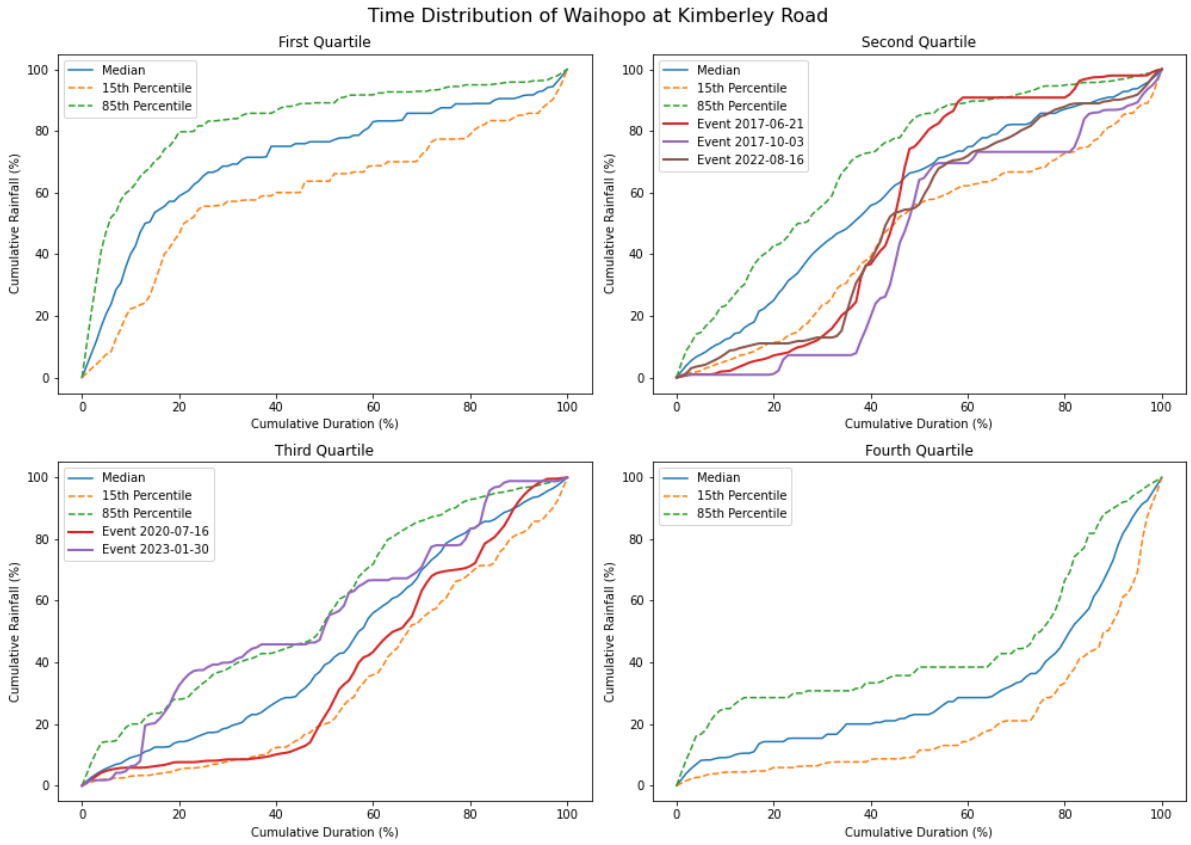
Time Distribution of Waihopo at Kimberley Road
First Quartile
Second Quartile
Third Quartile
Fourth Quartile
Median
15th Percentile
85th Percentile
Event 2017-06-21
Event 2017-10-03
Event 2022-08-16
Event 2020-07-16
Event 2023-01-30
Cumulative Rainfall (%)
Cumulative Duration (%)

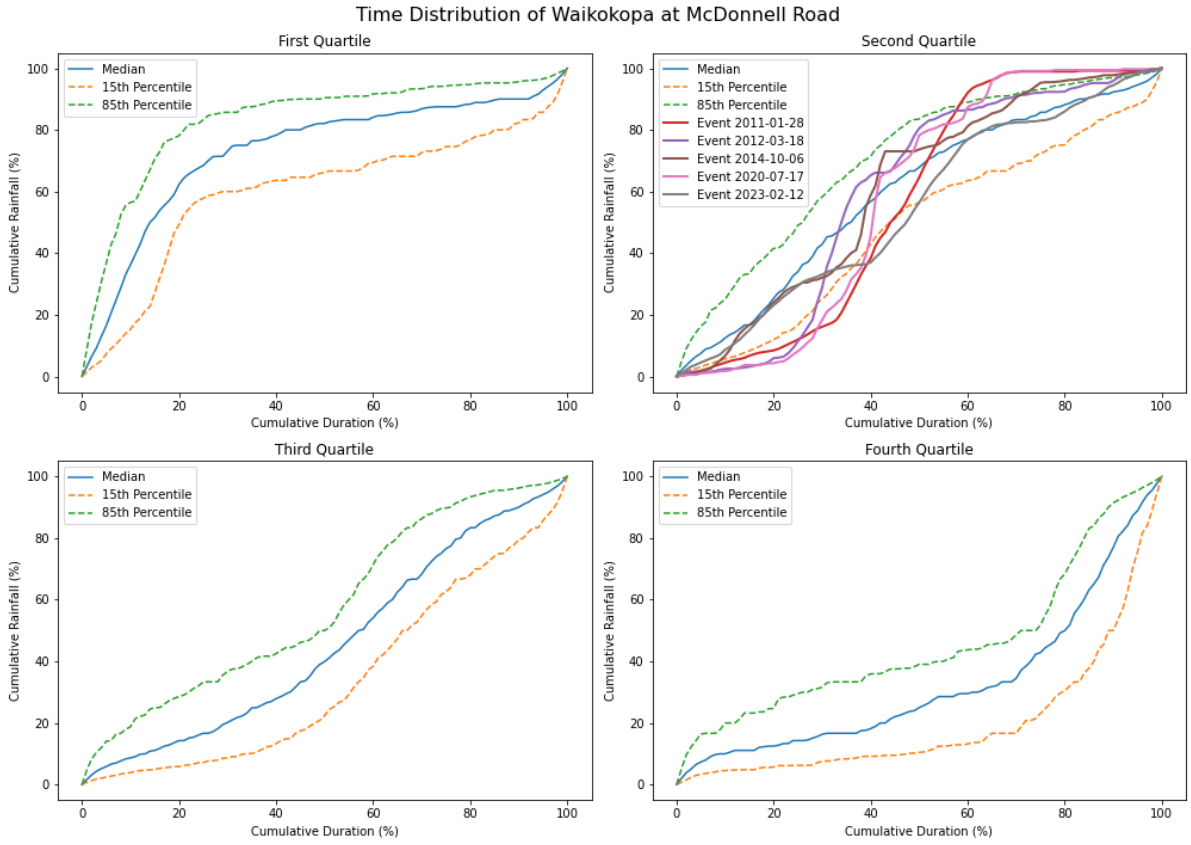
Time Distribution of Waikokopa at McDonnell Road
First Quartile
Second Quartile
Third Quartile
Fourth Quartile
Median
15th Percentile
85th Percentile
Event 2011-01-28
Event 2012-03-18
Event 2014-10-06
Event 2020-07-17
Event 2023-02-12
Cumulative Rainfall (%)
Cumulative Duration (%)

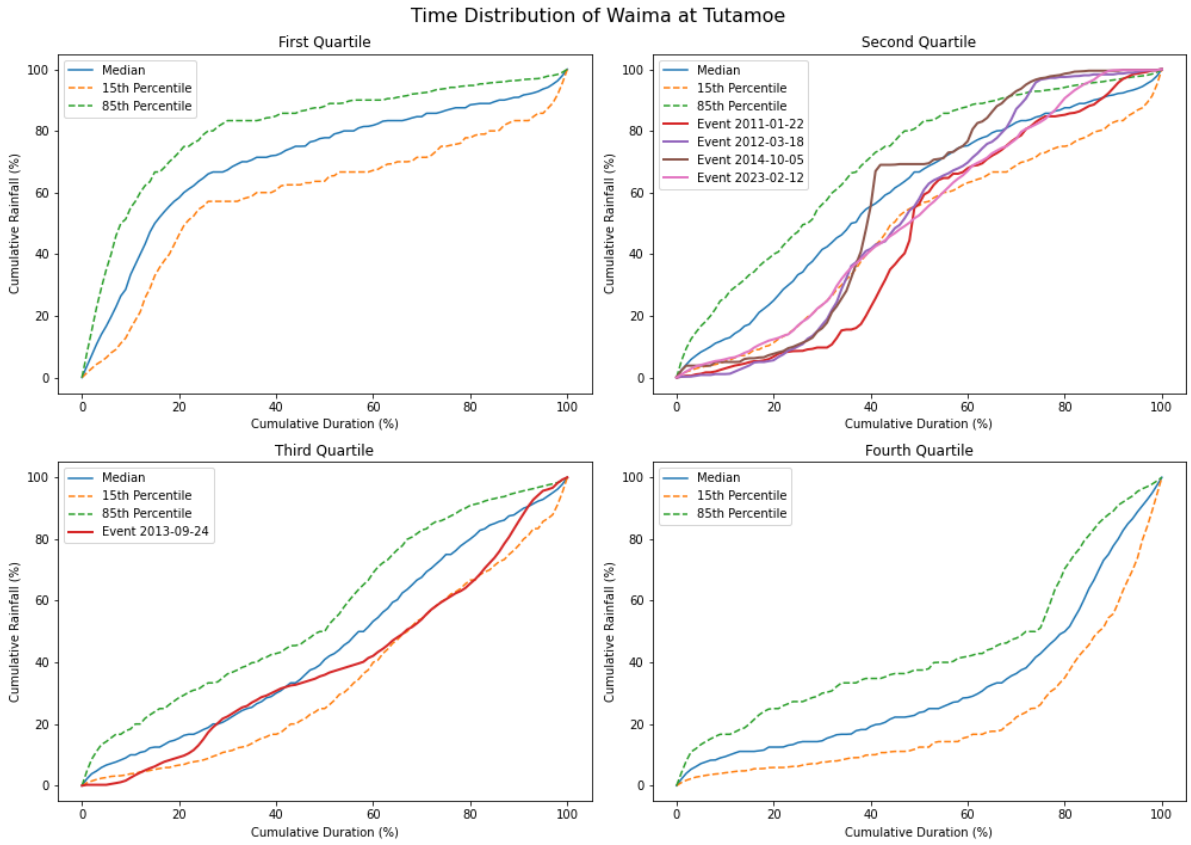
Time Distribution of Waima at Tutamoe
First Quartile
Median
15th Percentile
85th Percentile
Second Quartile
Median
15th Percentile
85th Percentile
Event 2011-01-22
Event 2012-03-18
Event 2014-10-05
Event 2023-02-12
Third Quartile
Median
15th Percentile
85th Percentile
Event 2013-09-24
Fourth Quartile
Median
15th Percentile
85th Percentile
Cumulative Rainfall (%)
Cumulative Duration (%)

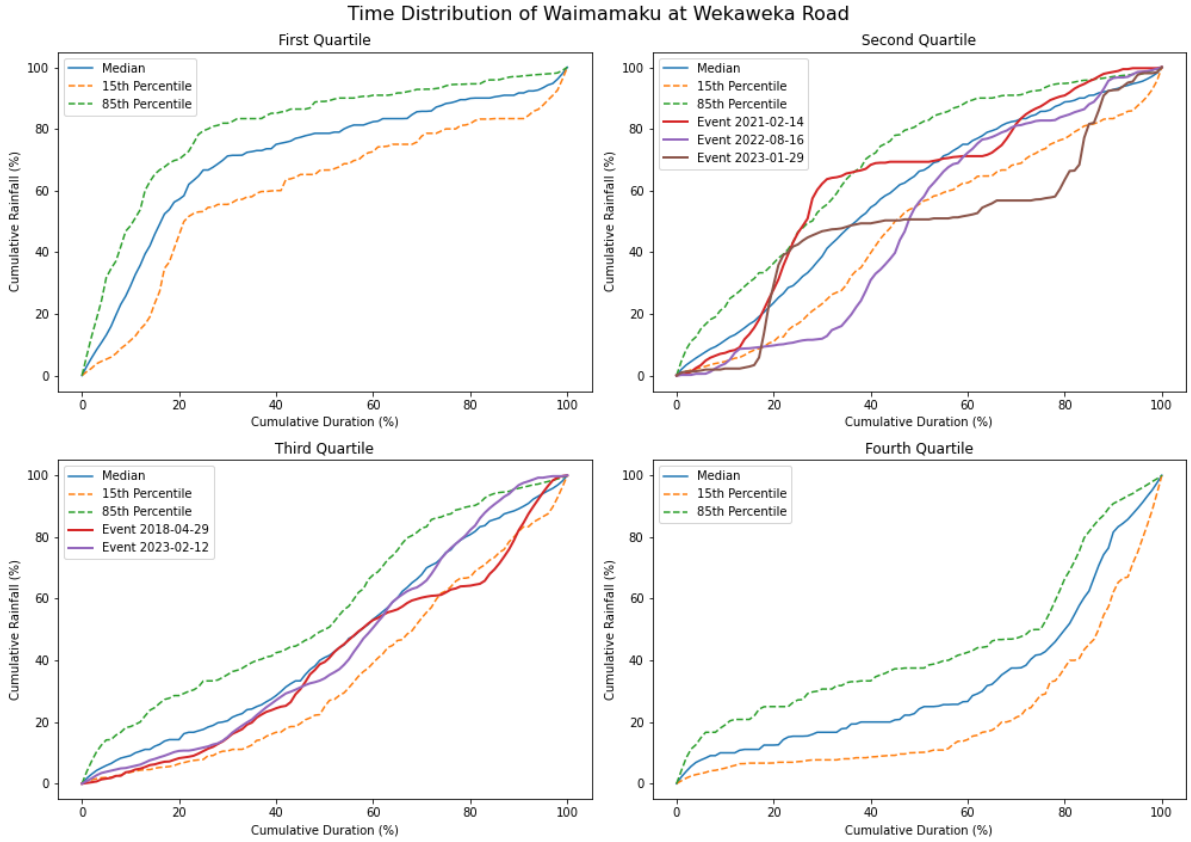
Time Distribution of Waimamaku at Wekaweka Road
First Quartile
Median
15th Percentile
85th Percentile
Second Quartile
Median
15th Percentile
85th Percentile
Event 2021-02-14
Event 2022-08-16
Event 2023-01-29
Third Quartile
Median
15th Percentile
85th Percentile
Event 2018-04-29
Event 2023-02-12
Fourth Quartile
Median
15th Percentile
85th Percentile
Cumulative Rainfall (%)
Cumulative Duration (%)

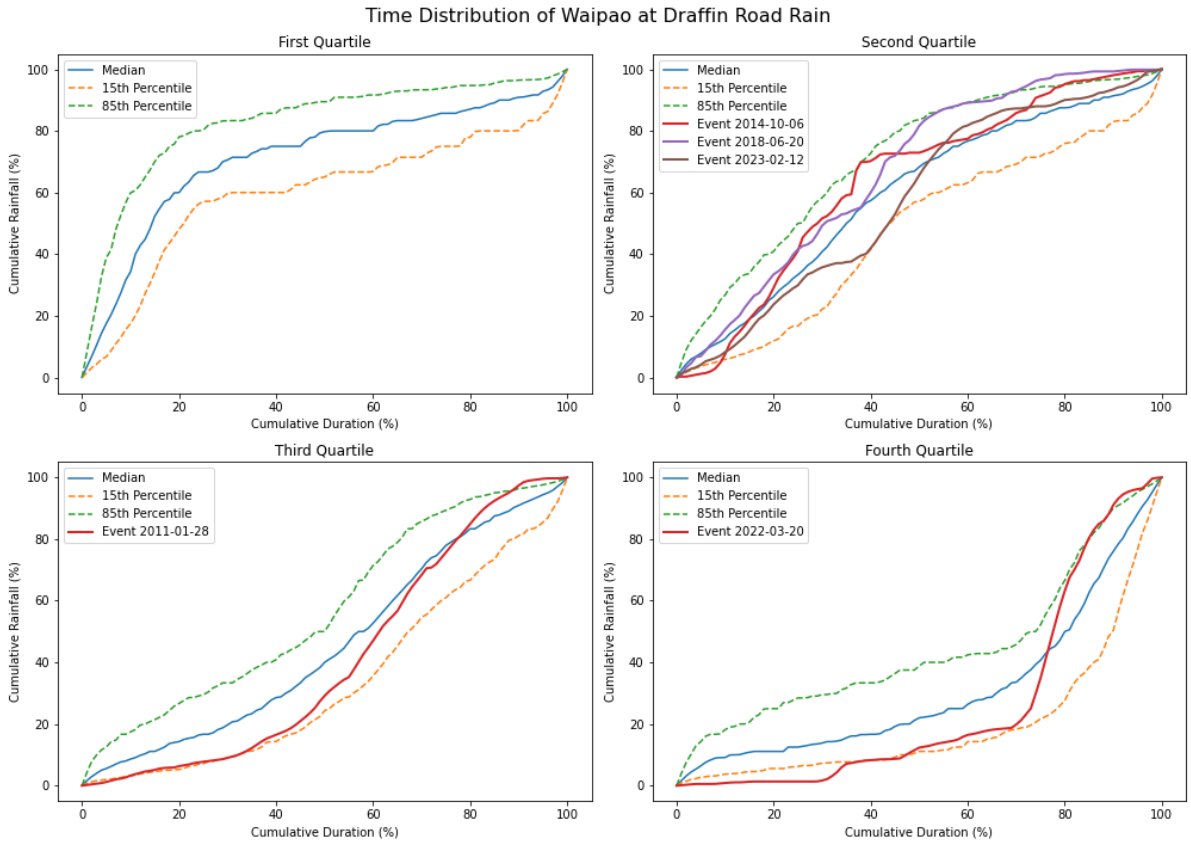
Time Distribution of Waipao at Draffin Road Rain
First Quartile
Median
15th Percentile
85th Percentile
Second Quartile
Median
15th Percentile
85th Percentile
Event 2014-10-06
Event 2018-06-20
Event 2023-02-12
Third Quartile
Median
15th Percentile
85th Percentile
Event 2011-01-28
Fourth Quartile
Median
15th Percentile
85th Percentile
Event 2022-03-20
Cumulative Rainfall (%)
Cumulative Duration (%)

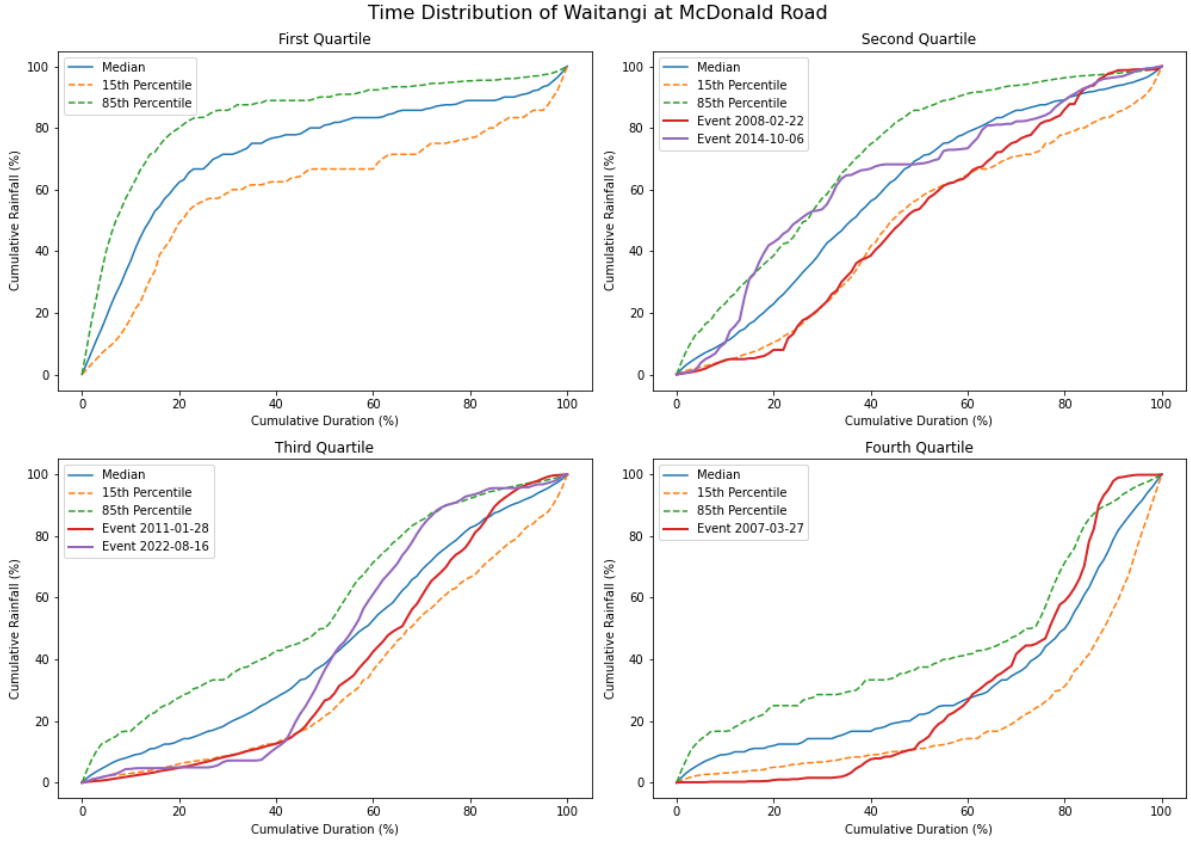
Time Distribution of Waitangi at McDonald Road
First Quartile
Median
15th Percentile
85th Percentile
Second Quartile
Median
15th Percentile
85th Percentile
Event 2008-02-22
Event 2014-10-06
Third Quartile
Median
15th Percentile
85th Percentile
Event 2011-01-28
Event 2022-08-16
Fourth Quartile
Median
15th Percentile
85th Percentile
Event 2007-03-27
Cumulative Rainfall (%)
Cumulative Duration (%)

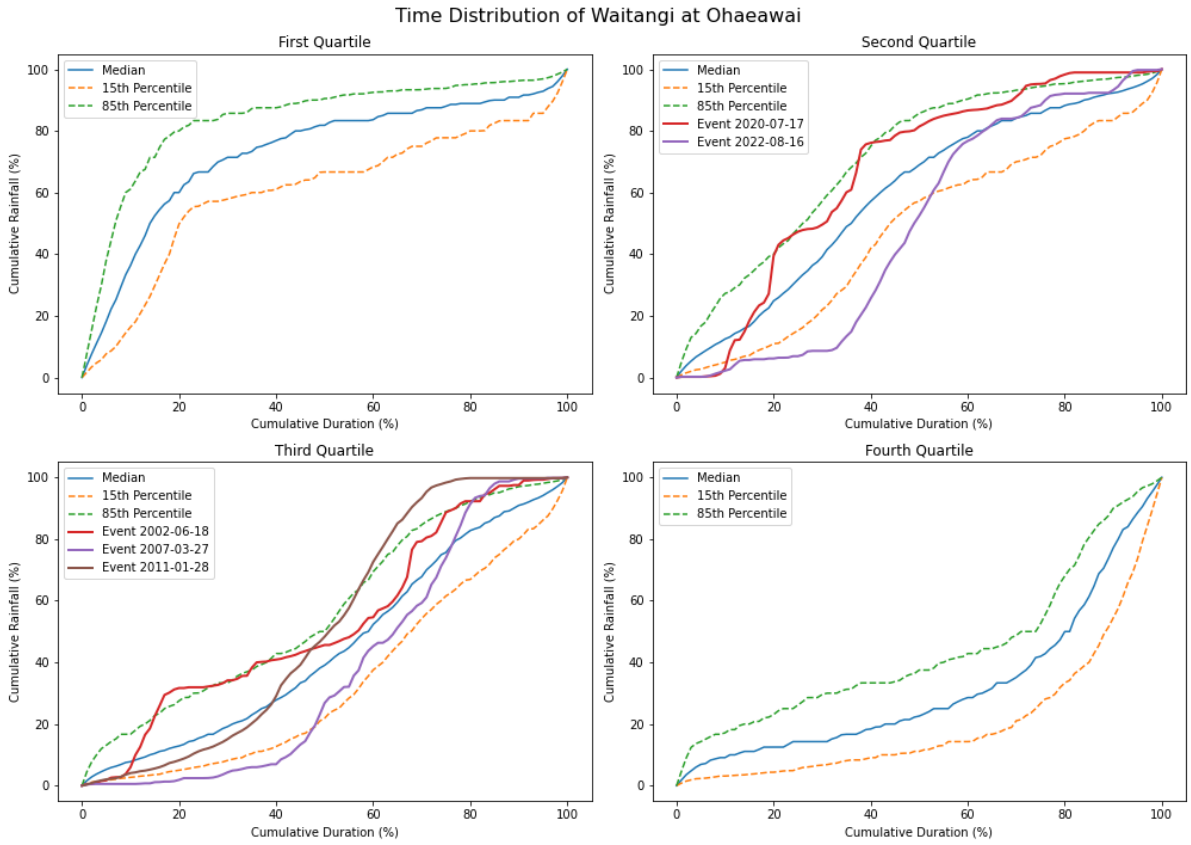
Time Distribution of Waitangi at Ohaeawai
First Quartile
Median
15th Percentile
85th Percentile
Second Quartile
Median
15th Percentile
85th Percentile
Event 2020-07-17
Event 2022-08-16
Third Quartile
Median
15th Percentile
85th Percentile
Event 2002-06-18
Event 2007-03-27
Event 2011-01-28
Fourth Quartile
Median
15th Percentile
85th Percentile
Cumulative Rainfall (%)
Cumulative Duration (%)

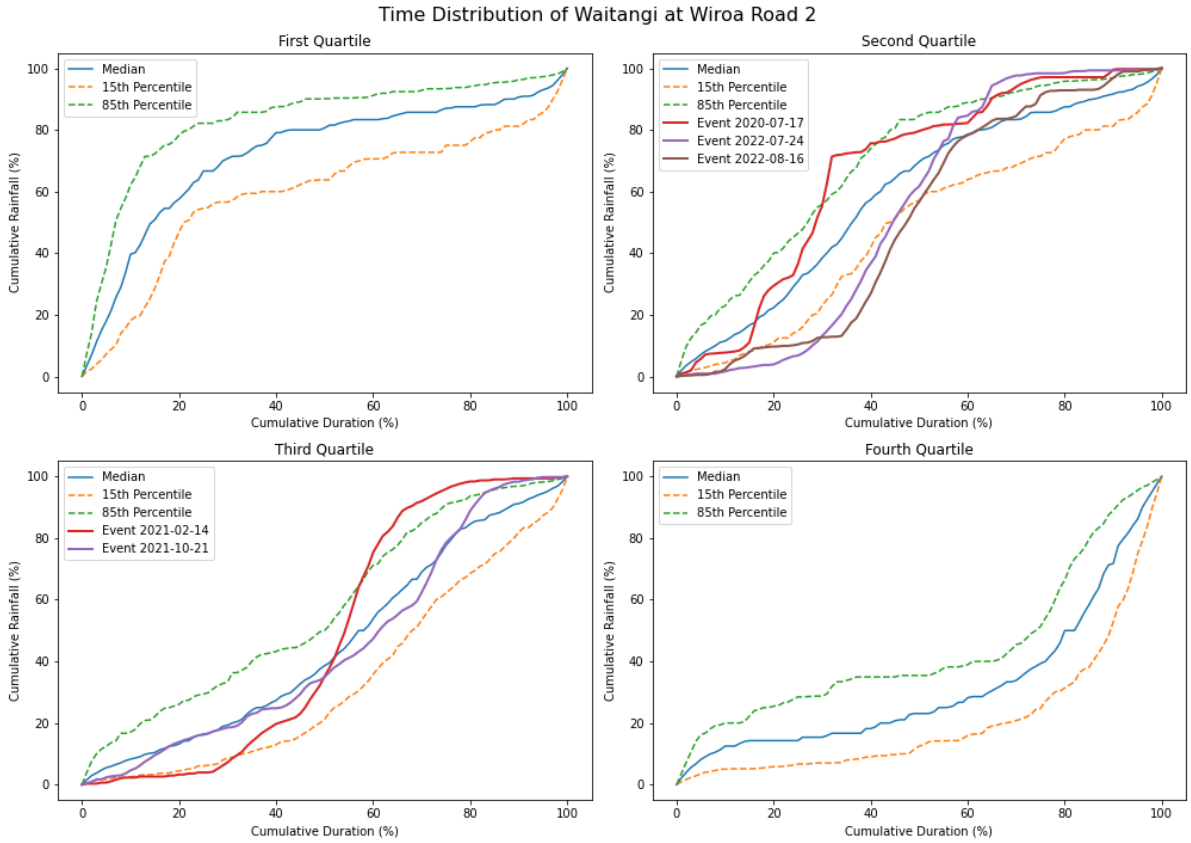
Time Distribution of Waitangi at Wiroa Road 2
First Quartile
Median
15th Percentile
85th Percentile
Second Quartile
Median
15th Percentile
85th Percentile
Event 2020-07-17
Event 2022-07-24
Event 2022-08-16
Third Quartile
Median
15th Percentile
85th Percentile
Event 2021-02-14
Event 2021-10-21
Fourth Quartile
Median
15th Percentile
85th Percentile
Cumulative Rainfall (%)
Cumulative Duration (%)

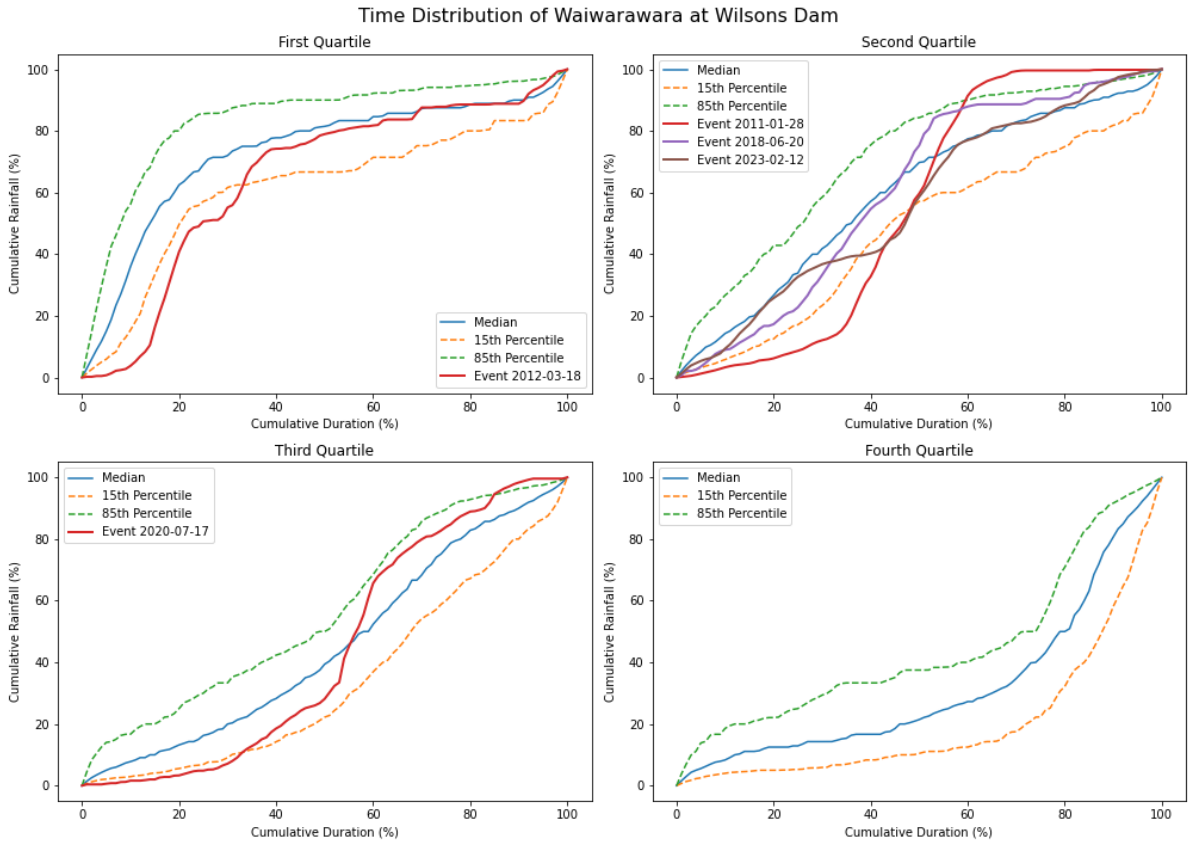
Time Distribution of Waiwarawara at Wilsons Dam
First Quartile
Second Quartile
Third Quartile
Fourth Quartile
Cumulative Rainfall (%)
Cumulative Duration (%)
Median
15th Percentile
85th Percentile
Event 2012-03-18
Event 2011-01-28
Event 2018-06-20
Event 2023-02-12
Event 2020-07-17

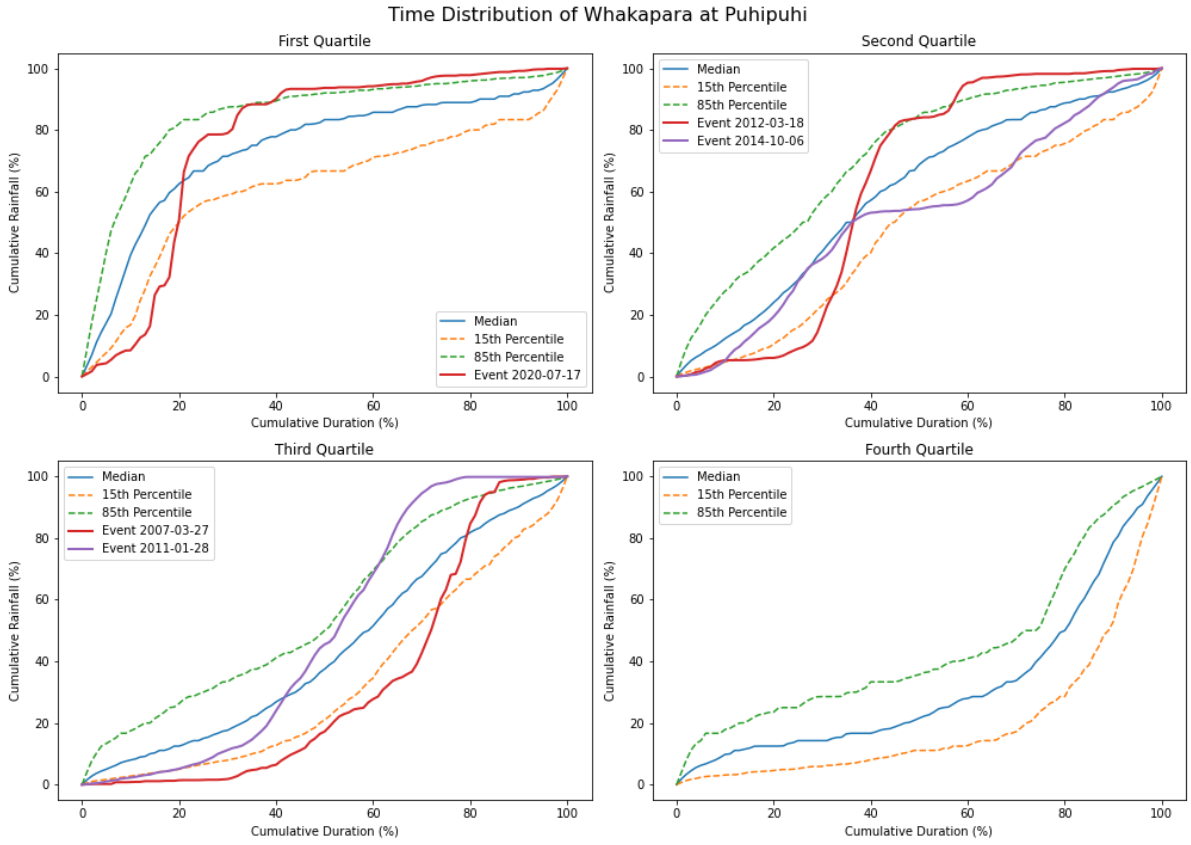
Time Distribution of Whakapara at Puhipuhi
First Quartile
Second Quartile
Third Quartile
Fourth Quartile
Cumulative Rainfall (%)
Cumulative Duration (%)
Median
15th Percentile
85th Percentile
Event 2020-07-17
Event 2012-03-18
Event 2014-10-06
Event 2007-03-27
Event 2011-01-28

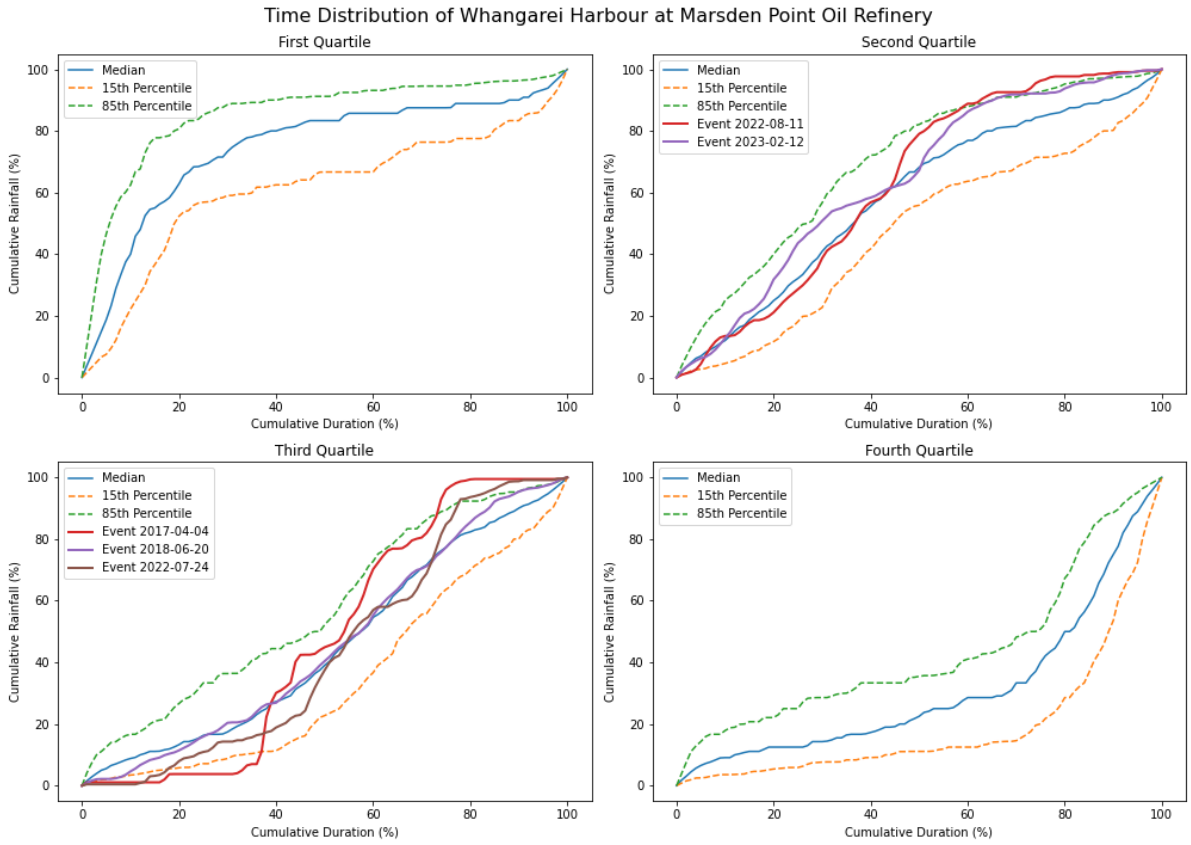
Time Distribution of Whangarei Harbour at Marsden Point Oil Refinery
First Quartile
Median
15th Percentile
85th Percentile
Second Quartile
Median
15th Percentile
85th Percentile
Event 2022-08-11
Event 2023-02-12
Third Quartile
Median
15th Percentile
85th Percentile
Event 2017-04-04
Event 2018-06-20
Event 2022-07-24
Fourth Quartile
Median
15th Percentile
85th Percentile
Cumulative Rainfall (%)
Cumulative Duration (%)

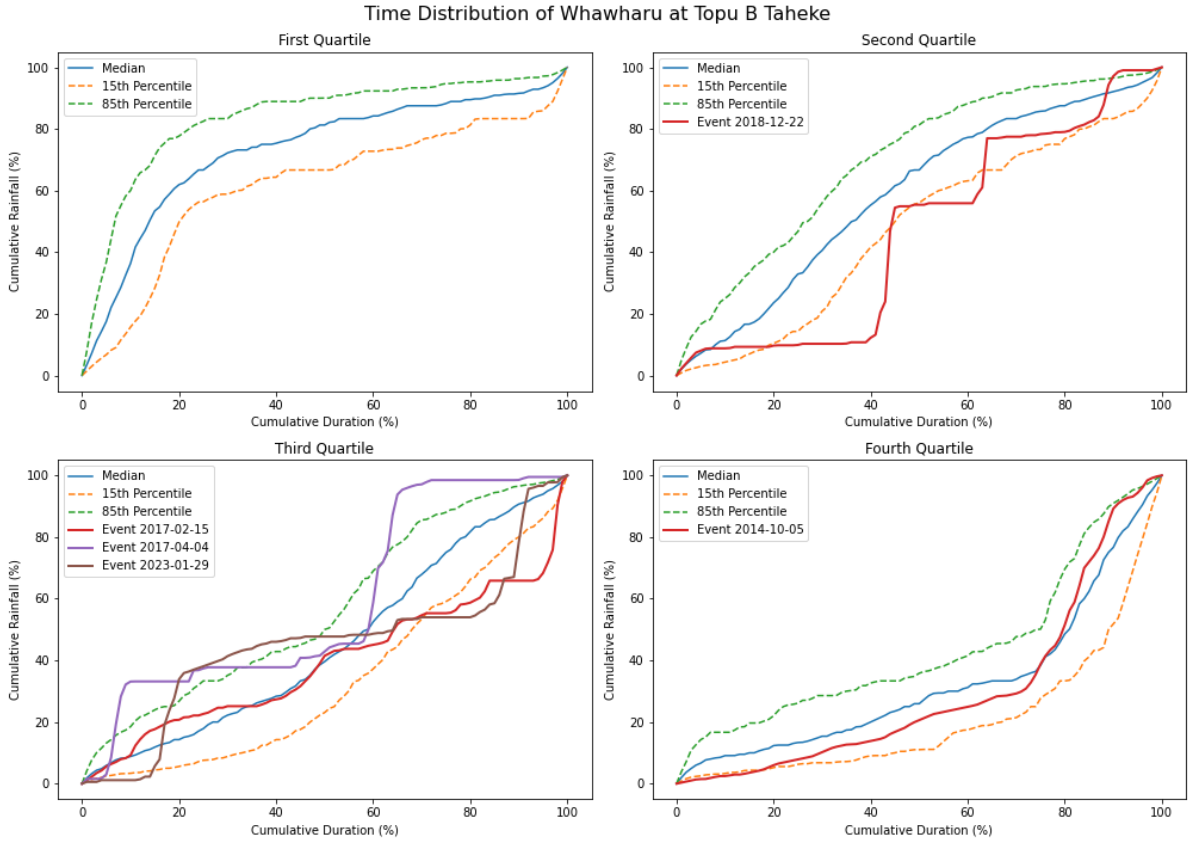
Time Distribution of Whawharu at Topu B Taheke
First Quartile
Median
15th Percentile
85th Percentile
Second Quartile
Median
15th Percentile
85th Percentile
Event 2018-12-22
Third Quartile
Median
15th Percentile
85th Percentile
Event 2017-02-15
Event 2017-04-04
Event 2023-01-29
Fourth Quartile
Median
15th Percentile
85th Percentile
Event 2014-10-05
Cumulative Rainfall (%)
Cumulative Duration (%)

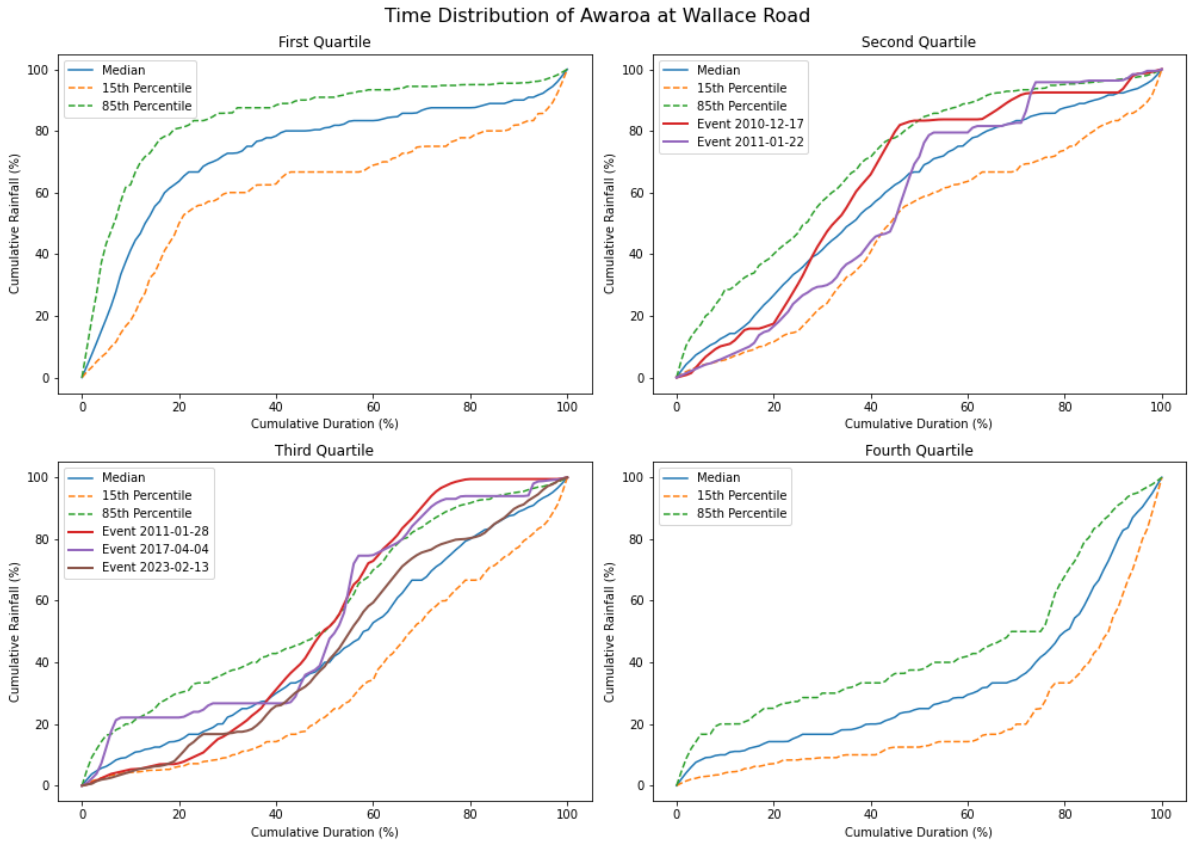
Time Distribution of Awaroa at Wallace Road
First Quartile
Second Quartile
Third Quartile
Fourth Quartile
Median
15th Percentile
85th Percentile
Event 2010-12-17
Event 2011-01-22
Event 2011-01-28
Event 2017-04-04
Event 2023-02-13
Cumulative Rainfall (%)
Cumulative Duration (%)

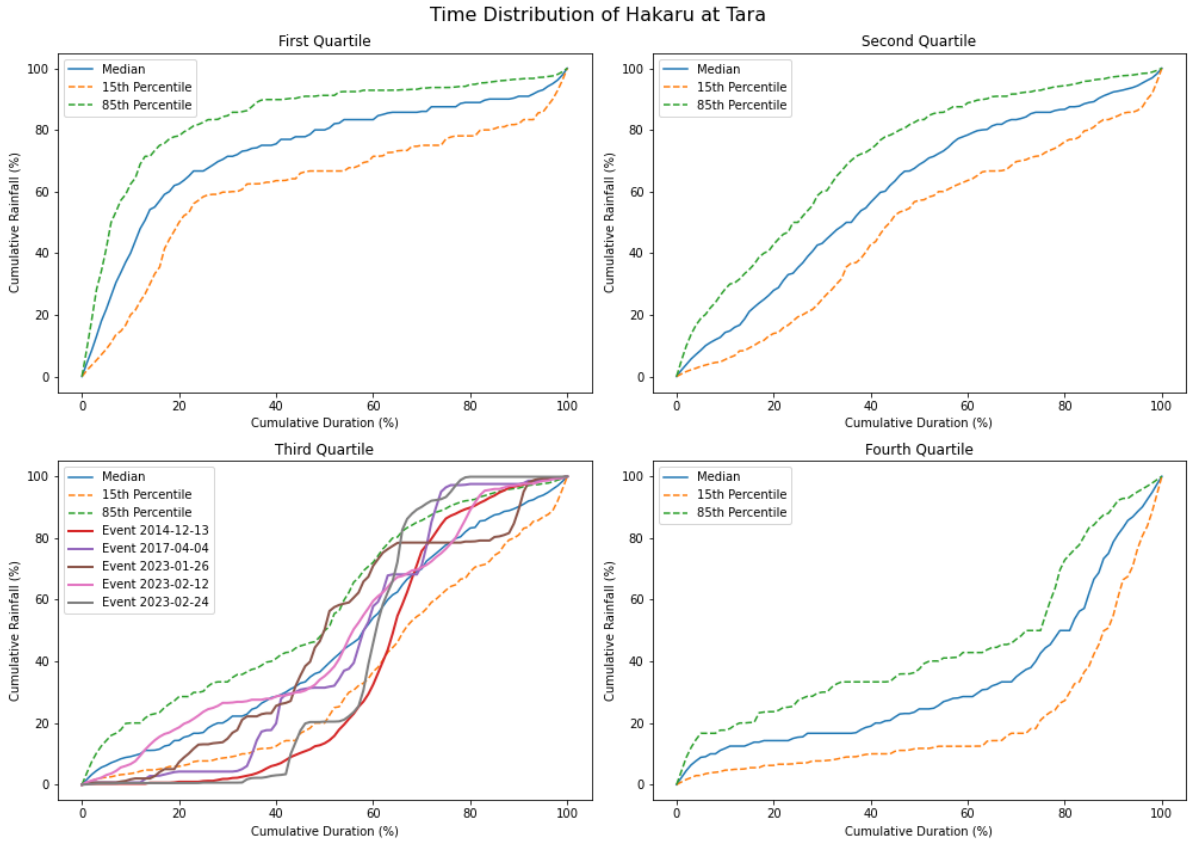
Time Distribution of Hakaru at Tara
First Quartile
Second Quartile
Third Quartile
Fourth Quartile
Median
15th Percentile
85th Percentile
Event 2014-12-13
Event 2017-04-04
Event 2023-01-26
Event 2023-02-12
Event 2023-02-24
Cumulative Rainfall (%)
Cumulative Duration (%)

APPENDIX 3: Hourly rainfall and river flow at stations during cyclone Gabrielle in February 2023.

Blue bars represent rainfall depth (mm), and the red line shows river flow rate (m^3/s).

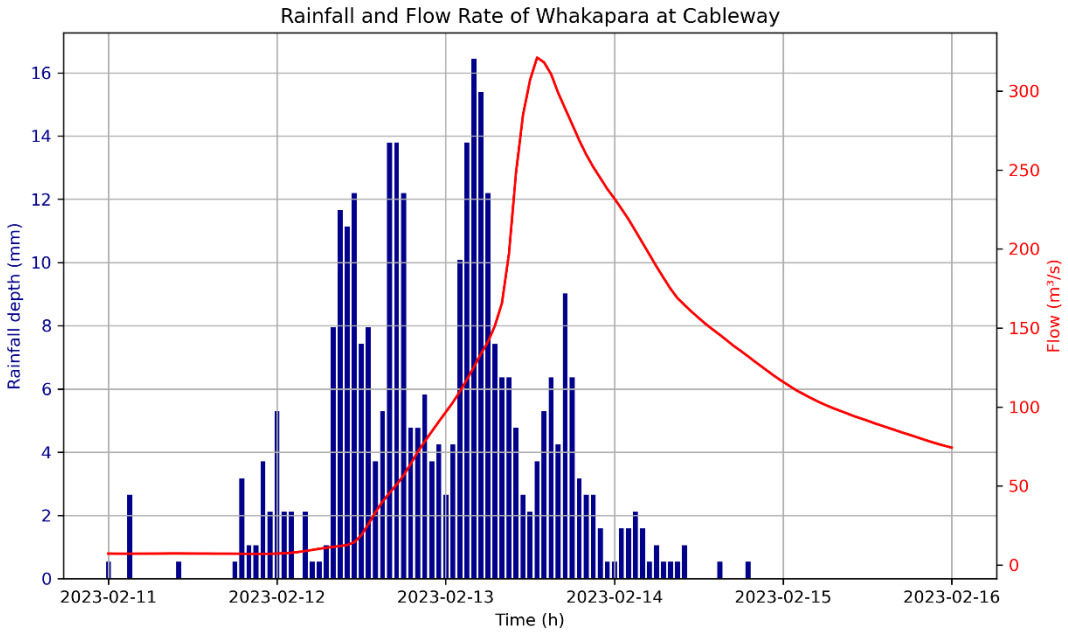

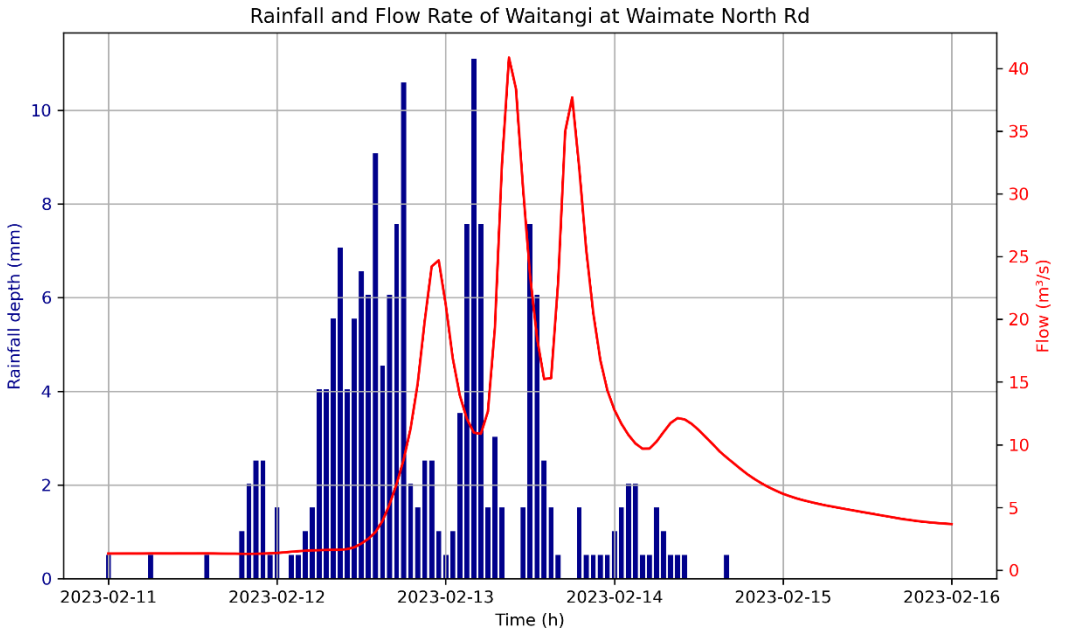

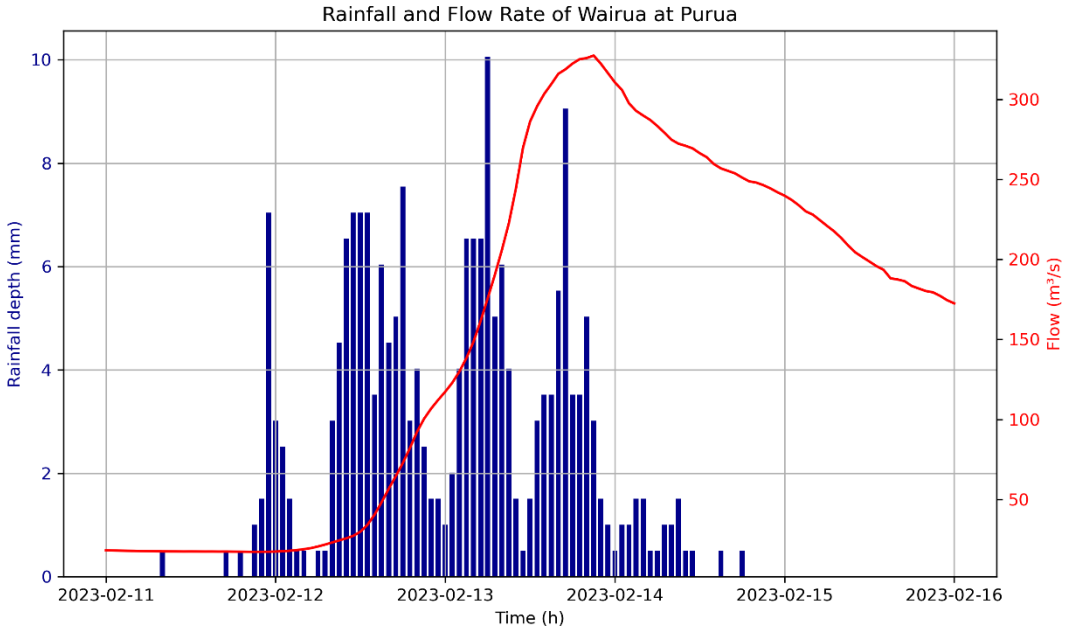
Rainfall and Flow Rate of Wairua at Purua
Rainfall depth (mm)
Flow (m³/s)
Time (h)
0
2
4
6
8
10
50
100
150
200
250
300
2023-02-11
2023-02-12
2023-02-13
2023-02-14
2023-02-15
2023-02-16

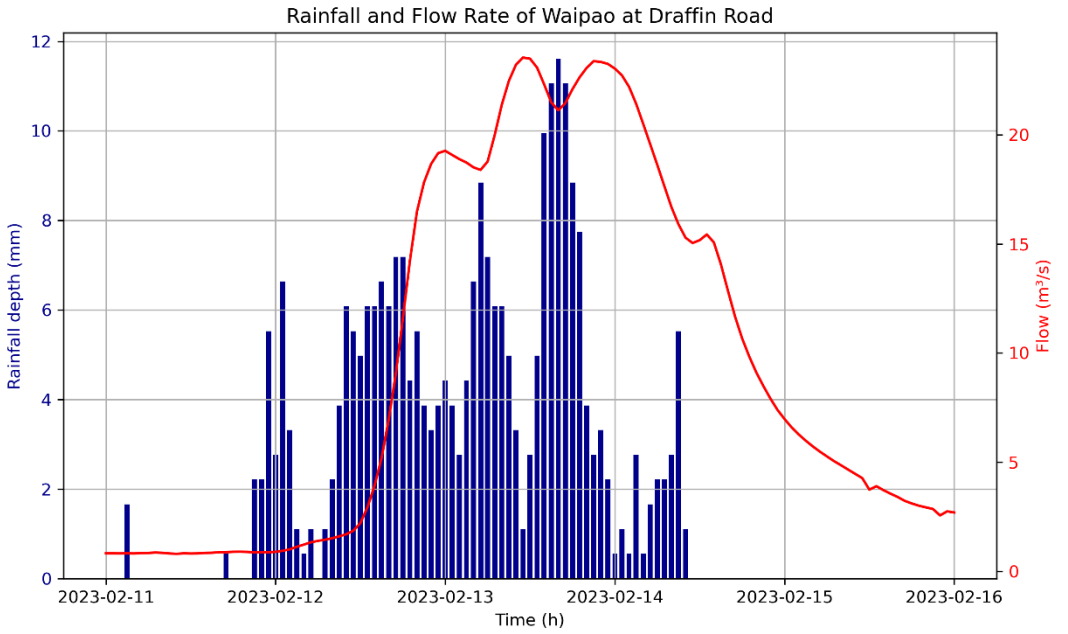
Rainfall and Flow Rate of Waipao at Draffin Road
Rainfall depth (mm)
Flow (m³/s)
Time (h)
0
2
4
6
8
10
12
0
5
10
15
20
2023-02-11
2023-02-12
2023-02-13
2023-02-14
2023-02-15
2023-02-16

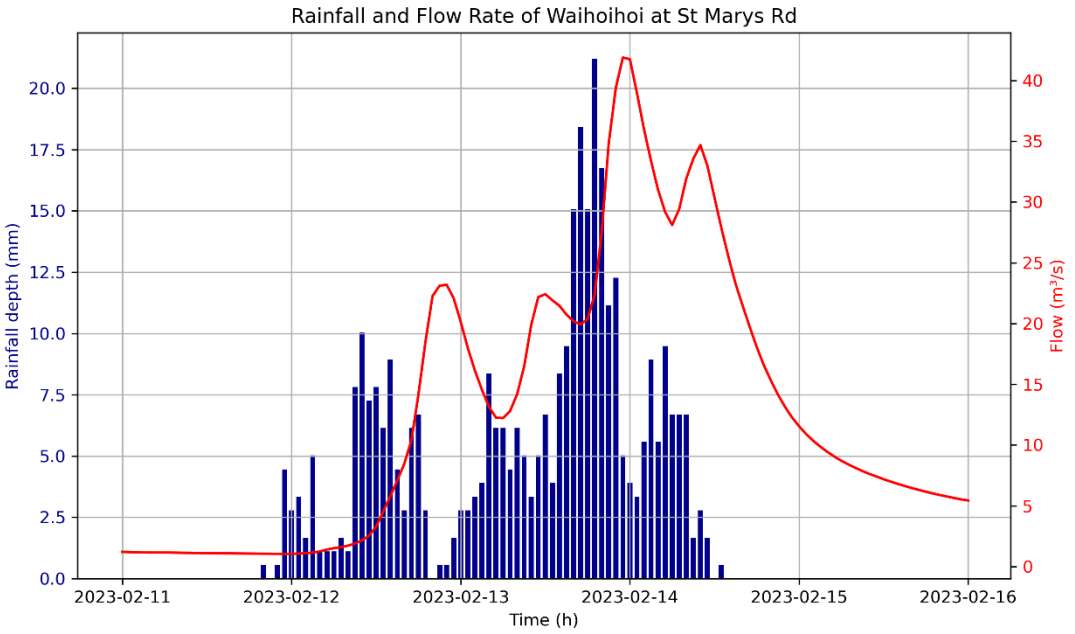
Rainfall and Flow Rate of Waihoihoi at St Marys Rd
Rainfall depth (mm)
Flow (m³/s)
Time (h)
2023-02-11
2023-02-12
2023-02-13
2023-02-14
2023-02-15
2023-02-16

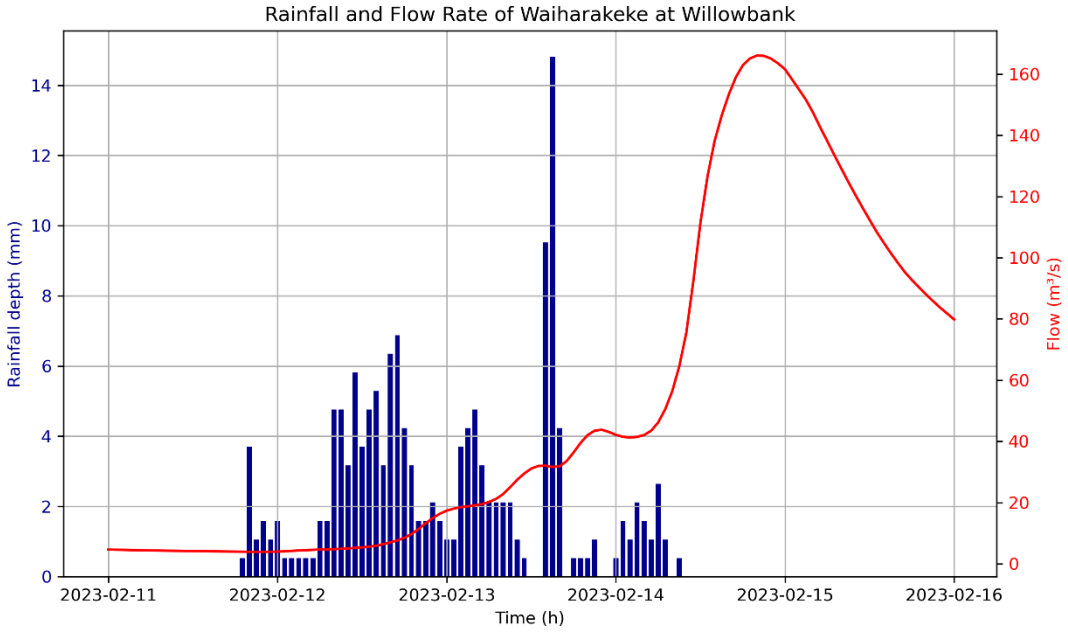
Rainfall and Flow Rate of Waiharakeke at Willowbank
Rainfall depth (mm)
Flow (m³/s)
Time (h)
2023-02-11
2023-02-12
2023-02-13
2023-02-14
2023-02-15
2023-02-16

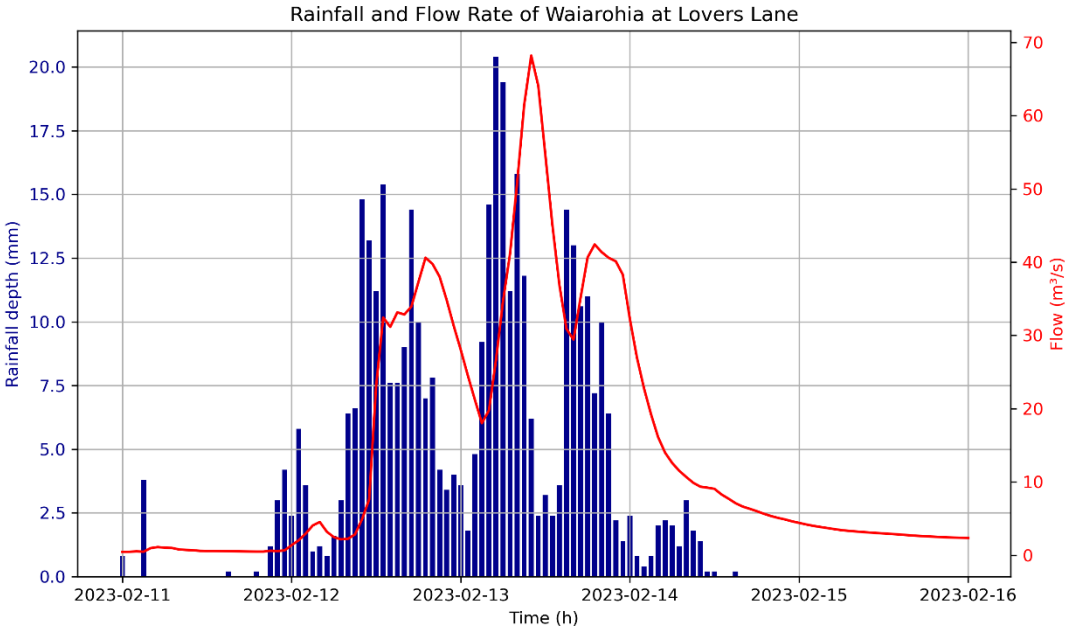
Rainfall and Flow Rate of Waiarohia at Lovers Lane
Rainfall depth (mm)
Flow (m³/s)
Time (h)
0.0
2.5
5.0
7.5
10.0
12.5
15.0
17.5
20.0
0
10
20
30
40
50
60
70
2023-02-11
2023-02-12
2023-02-13
2023-02-14
2023-02-15
2023-02-16

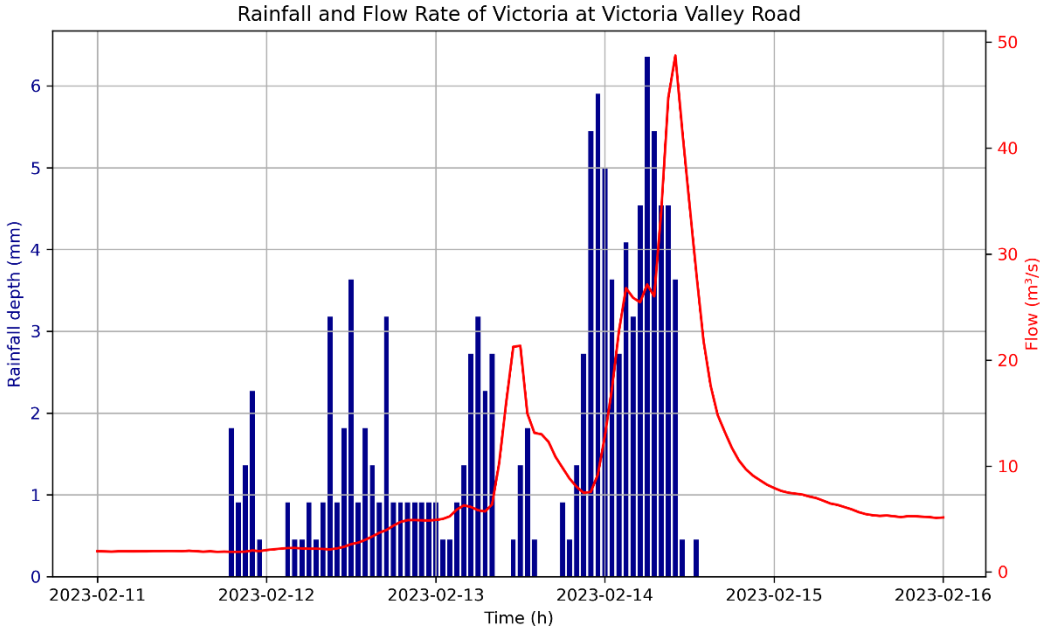
Rainfall and Flow Rate of Victoria at Victoria Valley Road
Rainfall depth (mm)
Flow (m³/s)
Time (h)
0
1
2
3
4
5
6
0
10
20
30
40
50
2023-02-11
2023-02-12
2023-02-13
2023-02-14
2023-02-15
2023-02-16

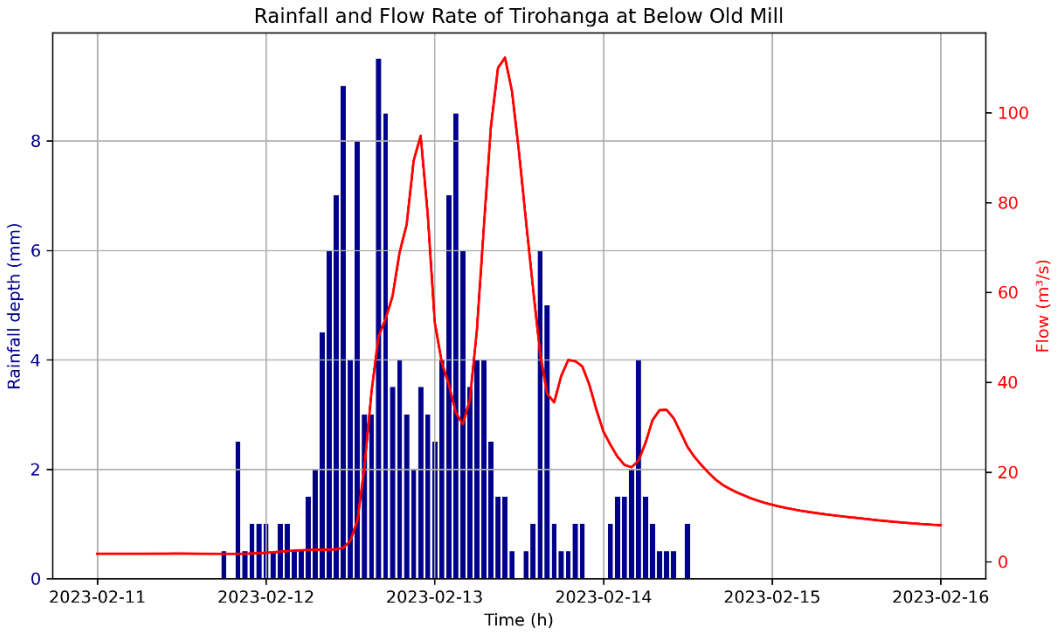
Rainfall and Flow Rate of Tirohanga at Below Old Mill
Rainfall depth (mm)
Flow (m³/s)
Time (h)
0
2
4
6
8
0
20
40
60
80
100
2023-02-11
2023-02-12
2023-02-13
2023-02-14
2023-02-15
2023-02-16

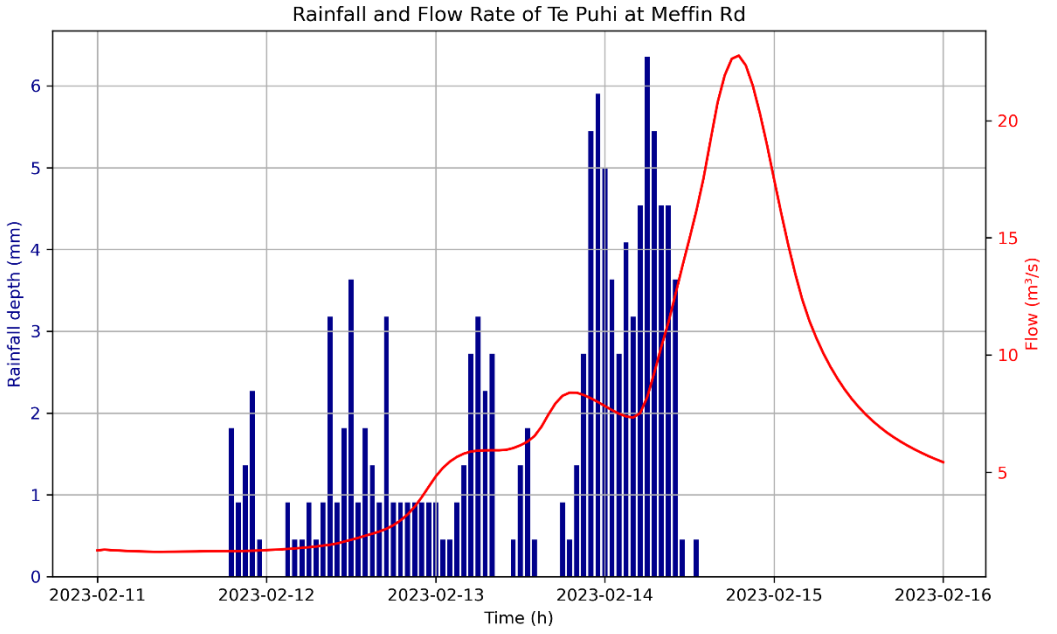
Rainfall and Flow Rate of Te Puhi at Meffin Rd
Rainfall depth (mm)
Flow (m³/s)
Time (h)
0
1
2
3
4
5
6
5
10
15
20
2023-02-11
2023-02-12
2023-02-13
2023-02-14
2023-02-15
2023-02-16

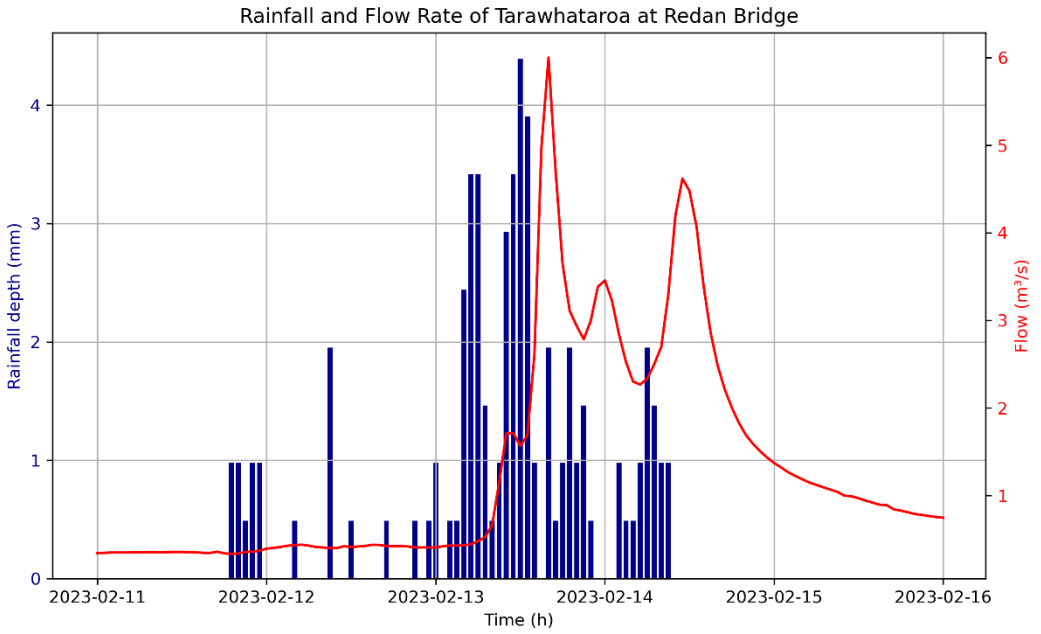
Rainfall and Flow Rate of Tarawhataroa at Redan Bridge
Rainfall depth (mm)
Flow (m³/s)
Time (h)
2023-02-11
2023-02-12
2023-02-13
2023-02-14
2023-02-15
2023-02-16

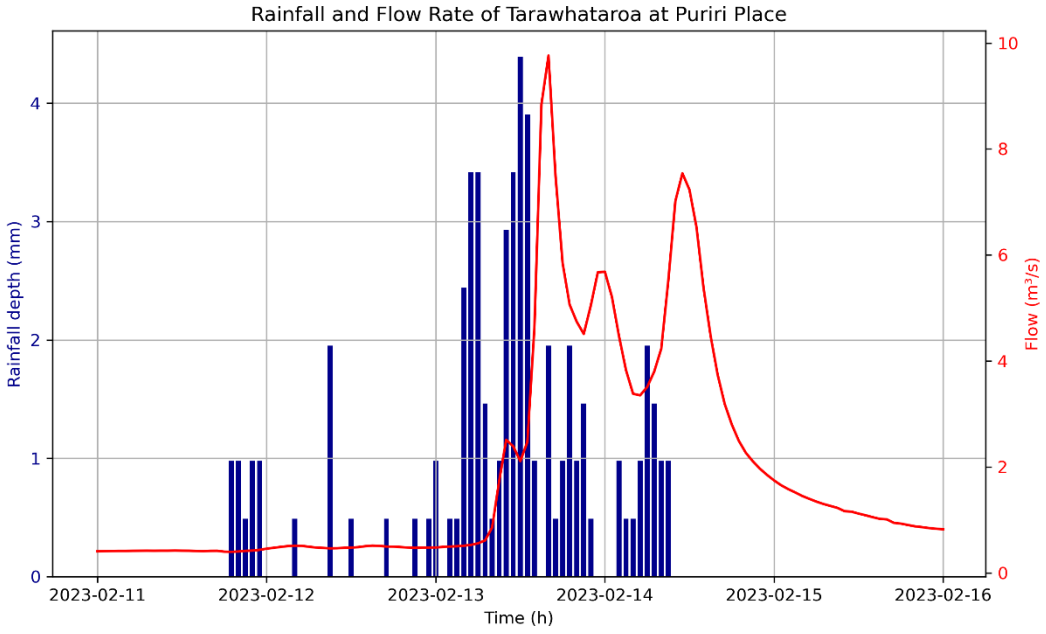
Rainfall and Flow Rate of Tarawhataroa at Puriri Place
Rainfall depth (mm)
Flow (m³/s)
Time (h)
2023-02-11
2023-02-12
2023-02-13
2023-02-14
2023-02-15
2023-02-16

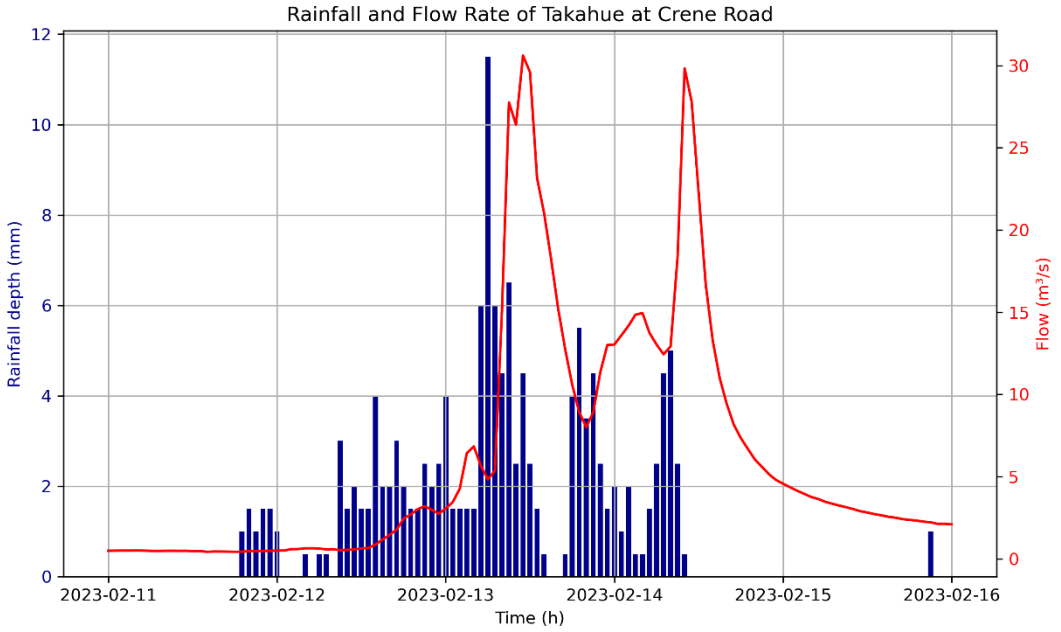
Rainfall and Flow Rate of Takahue at Crene Road
Rainfall depth (mm)
Flow (m³/s)
Time (h)
2023-02-11
2023-02-12
2023-02-13
2023-02-14
2023-02-15
2023-02-16

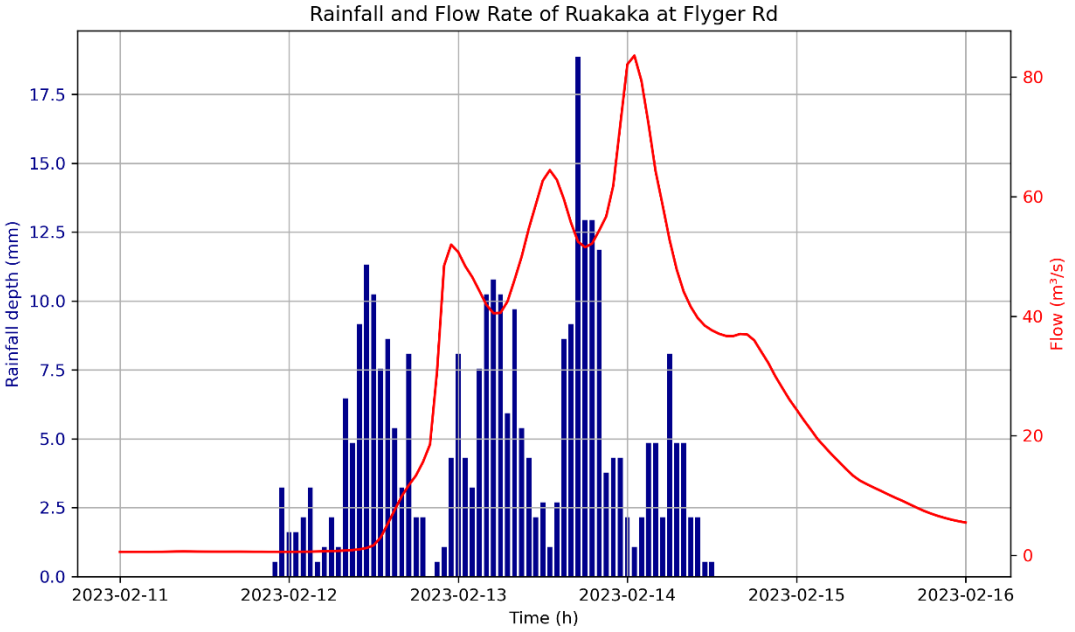
Rainfall and Flow Rate of Ruakaka at Flyger Rd
Rainfall depth (mm)
Flow (m³/s)
Time (h)
2023-02-11
2023-02-12
2023-02-13
2023-02-14
2023-02-15
2023-02-16

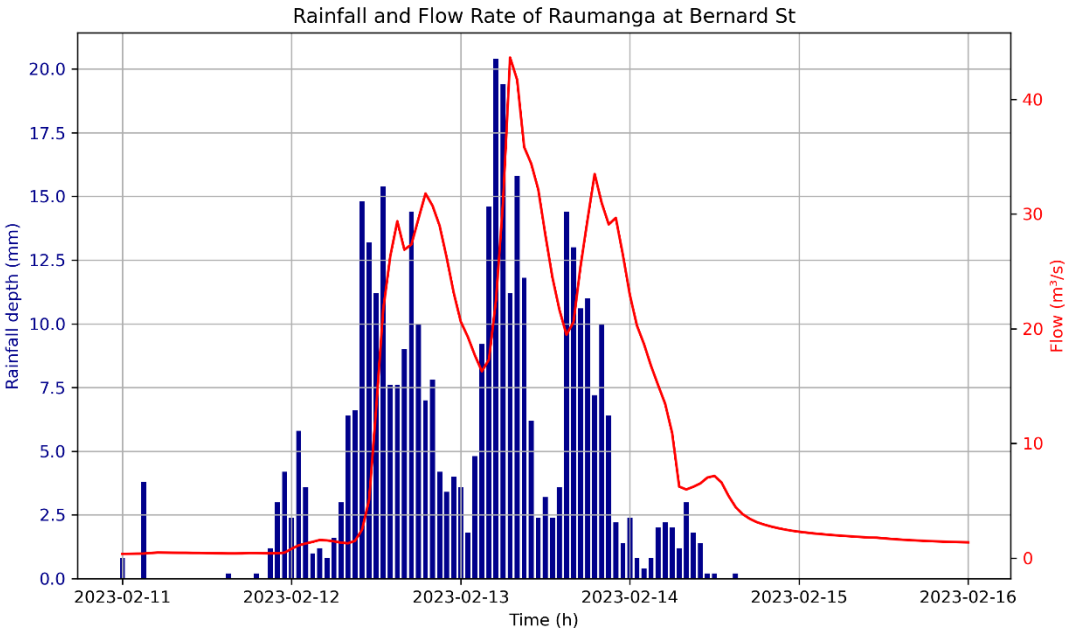
Rainfall and Flow Rate of Raumanga at Bernard St
Rainfall depth (mm)
Flow (m³/s)
Time (h)
2023-02-11
2023-02-12
2023-02-13
2023-02-14
2023-02-15
2023-02-16

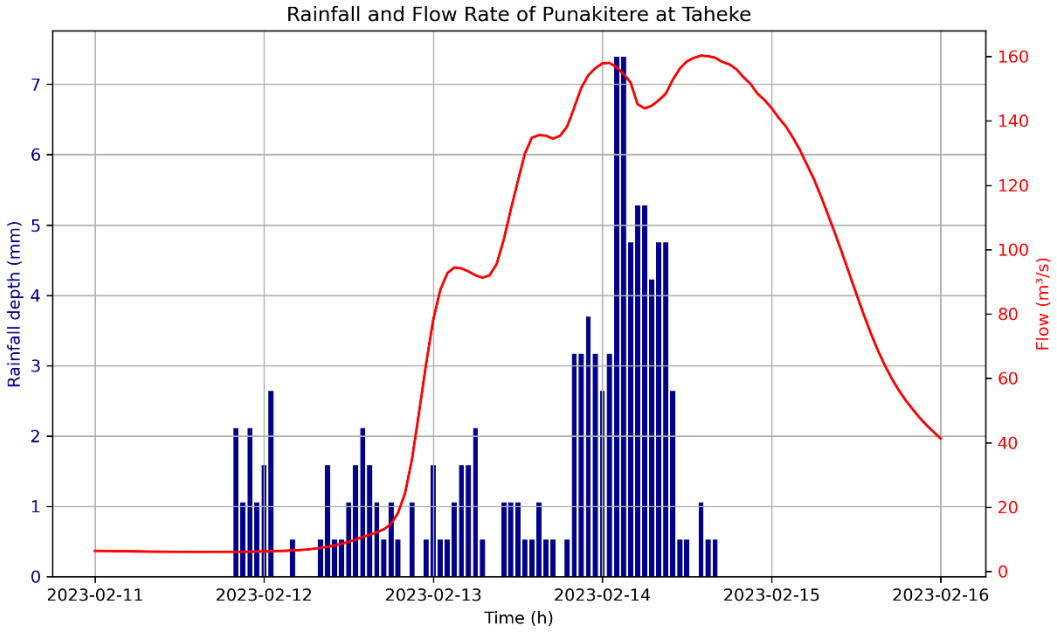
Rainfall and Flow Rate of Punakitere at Taheke
Rainfall depth (mm)
Flow (m³/s)
Time (h)
2023-02-11
2023-02-12
2023-02-13
2023-02-14
2023-02-15
2023-02-16

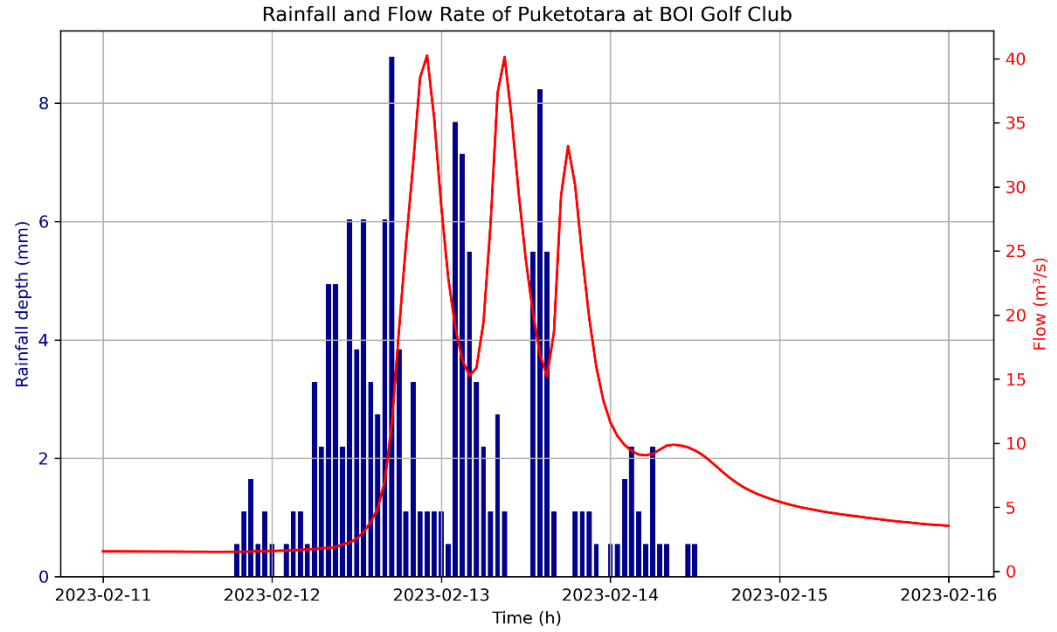
Rainfall and Flow Rate of Puketotara at BOI Golf Club
Rainfall depth (mm)
Flow (m³/s)
Time (h)
2023-02-11
2023-02-12
2023-02-13
2023-02-14
2023-02-15
2023-02-16

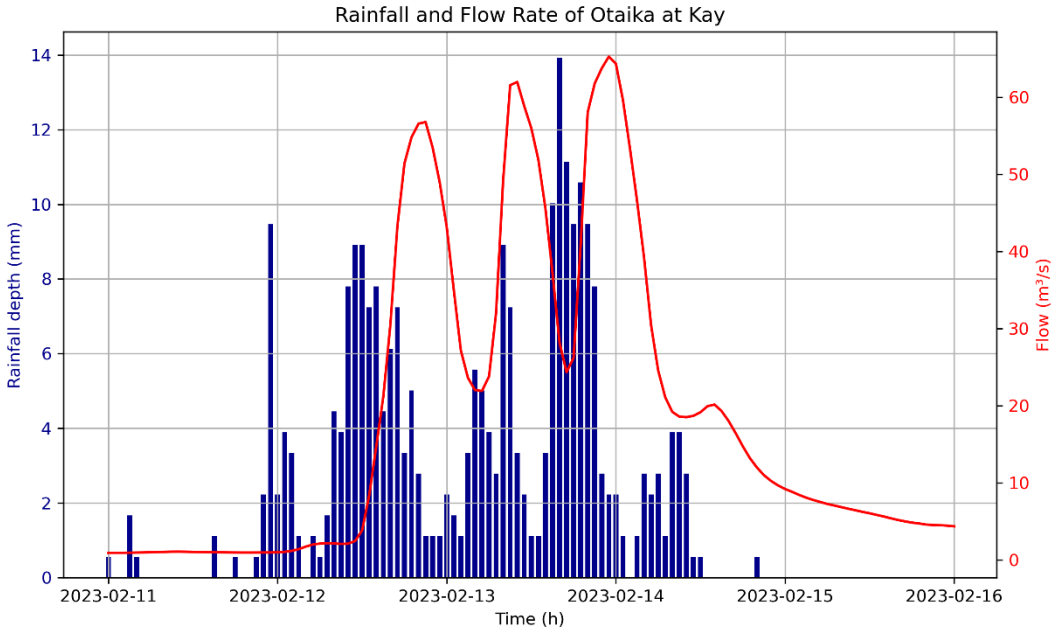
Rainfall and Flow Rate of Otaika at Kay
Rainfall depth (mm)
Flow (m³/s)
Time (h)
2023-02-11
2023-02-12
2023-02-13
2023-02-14
2023-02-15
2023-02-16

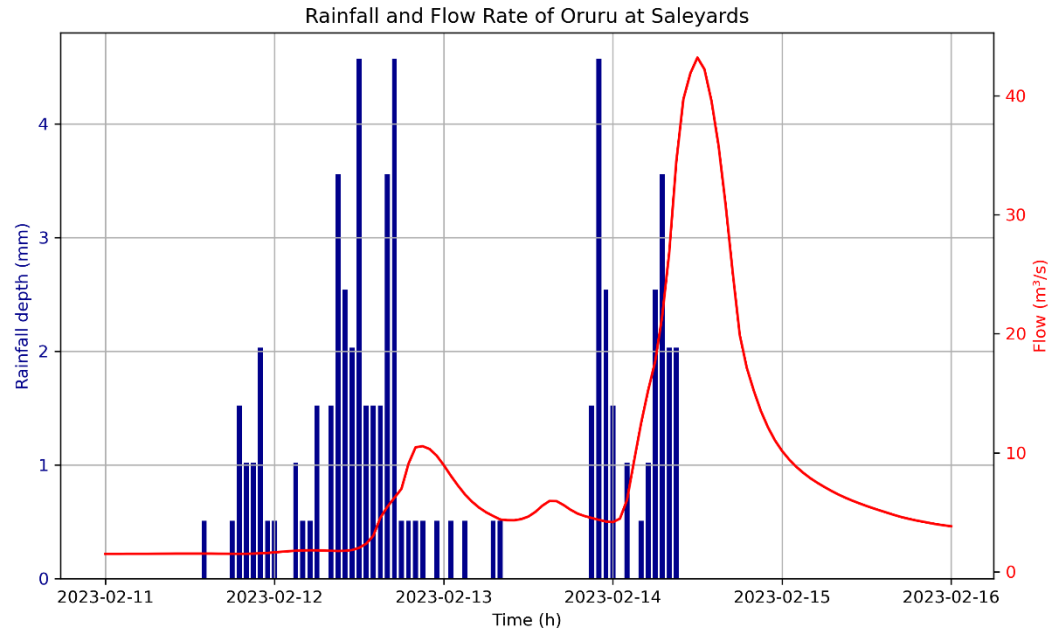
Rainfall and Flow Rate of Oruru at Saleyards
Rainfall depth (mm)
Flow (m³/s)
Time (h)
2023-02-11
2023-02-12
2023-02-13
2023-02-14
2023-02-15
2023-02-16

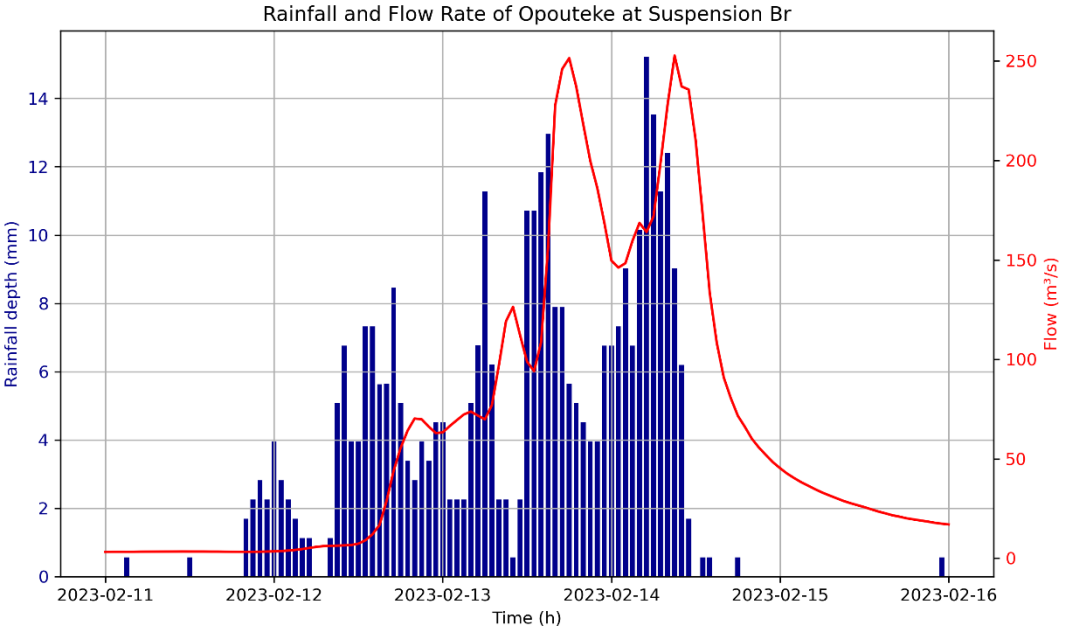
Rainfall and Flow Rate of Opouteke at Suspension Br
Rainfall depth (mm)
Flow (m³/s)
Time (h)
2023-02-11
2023-02-12
2023-02-13
2023-02-14
2023-02-15
2023-02-16

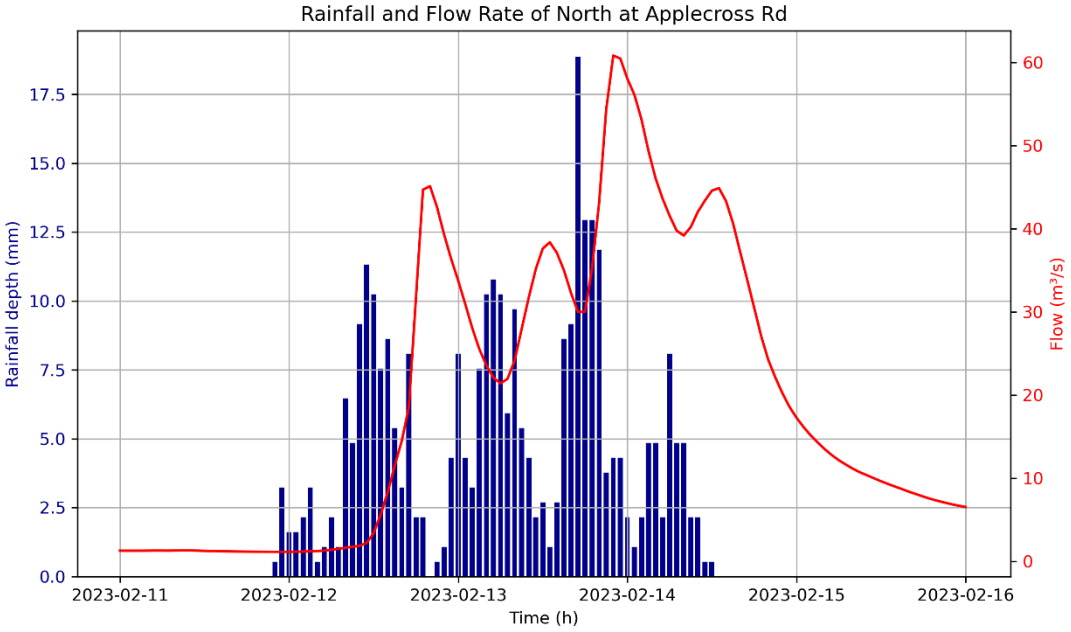
Rainfall and Flow Rate of North at Applecross Rd
Rainfall depth (mm)
Flow (m³/s)
Time (h)
0.0
2.5
5.0
7.5
10.0
12.5
15.0
17.5
0
10
20
30
40
50
60
2023-02-11
2023-02-12
2023-02-13
2023-02-14
2023-02-15
2023-02-16

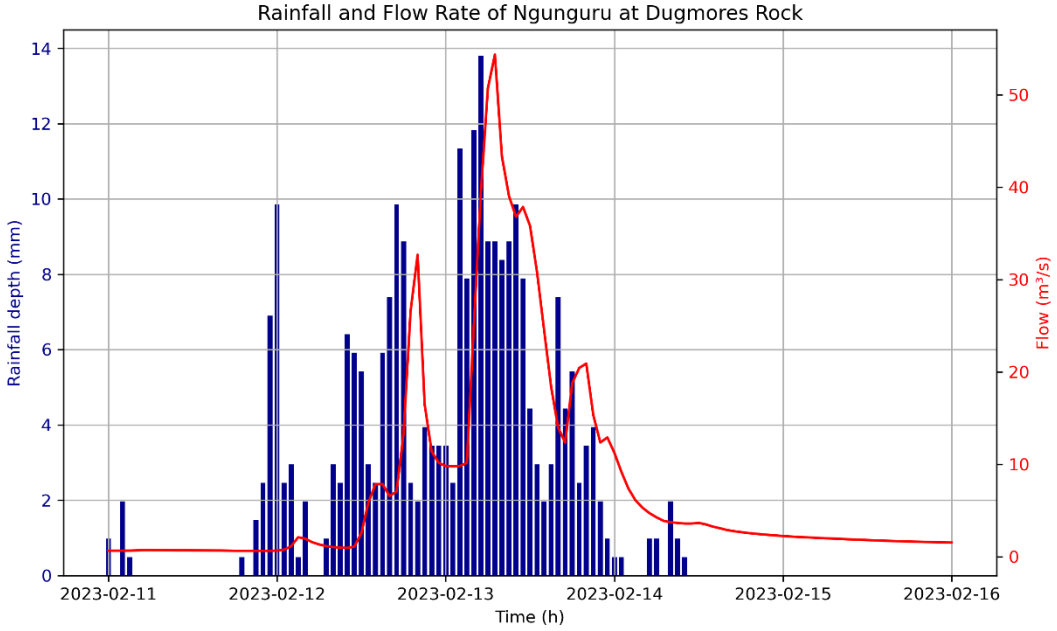
Rainfall and Flow Rate of Ngunguru at Dugmores Rock
Rainfall depth (mm)
Flow (m³/s)
Time (h)
0
2
4
6
8
10
12
14
0
10
20
30
40
50
2023-02-11
2023-02-12
2023-02-13
2023-02-14
2023-02-15
2023-02-16

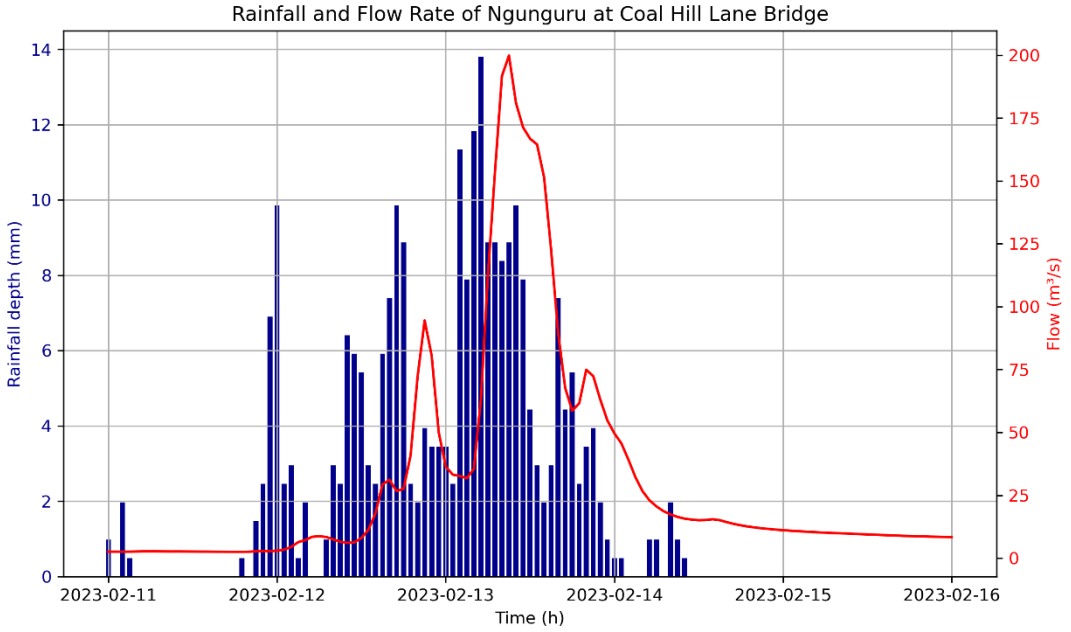
Rainfall and Flow Rate of Ngunguru at Coal Hill Lane Bridge
Rainfall depth (mm)
Flow (m³/s)
Time (h)
2023-02-11
2023-02-12
2023-02-13
2023-02-14
2023-02-15
2023-02-16

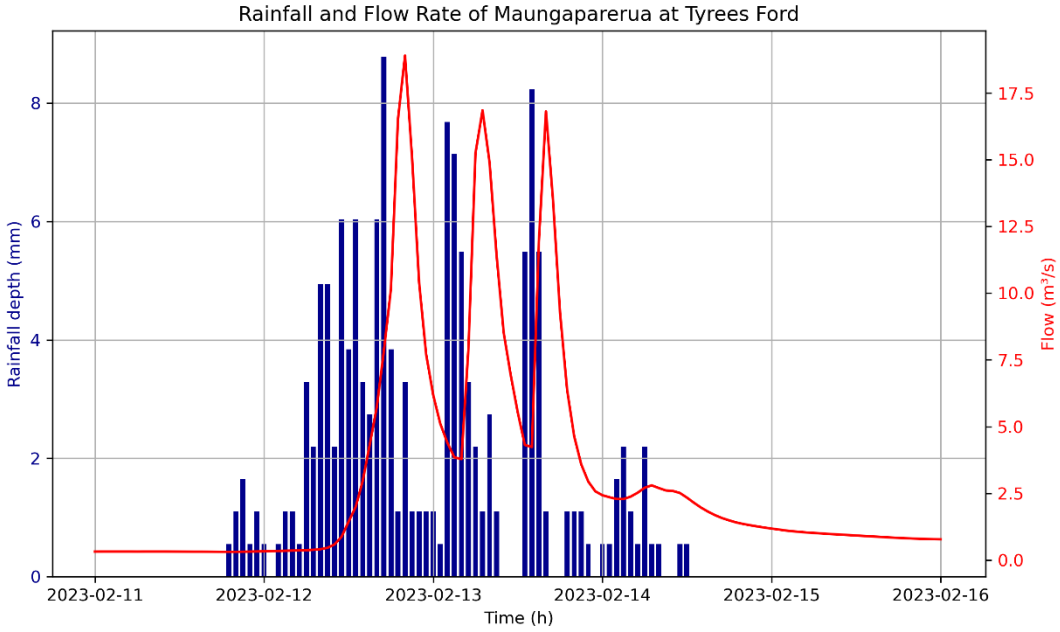
Rainfall and Flow Rate of Maungaparerua at Tyrees Ford
Rainfall depth (mm)
Flow (m³/s)
Time (h)
2023-02-11
2023-02-12
2023-02-13
2023-02-14
2023-02-15
2023-02-16

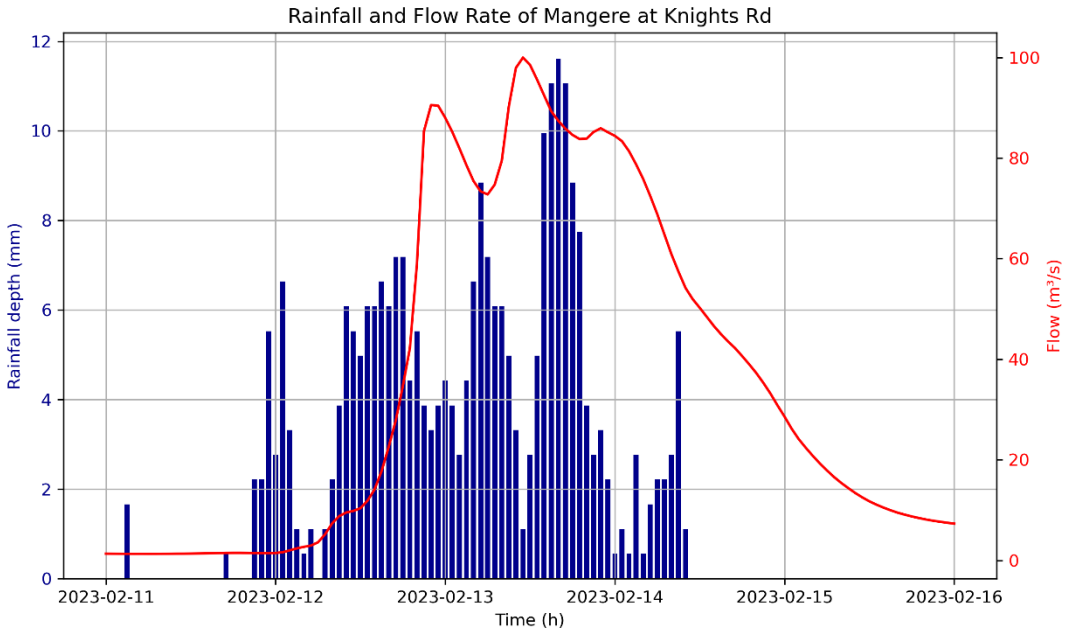
Rainfall and Flow Rate of Mangere at Knights Rd
Rainfall depth (mm)
Flow (m³/s)
Time (h)
2023-02-11
2023-02-12
2023-02-13
2023-02-14
2023-02-15
2023-02-16

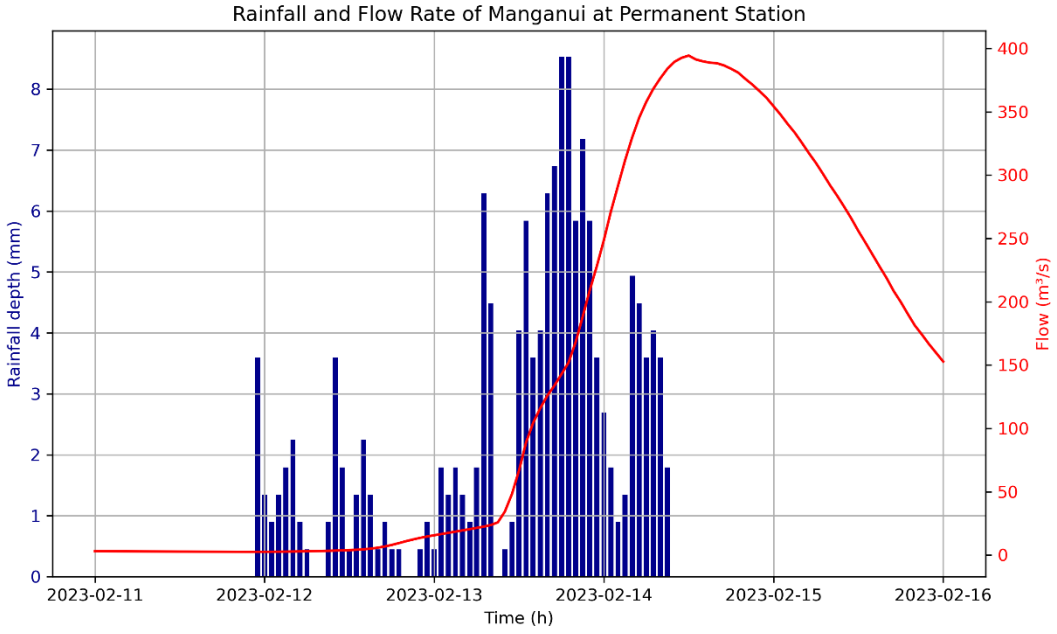
Rainfall and Flow Rate of Manganui at Permanent Station
Rainfall depth (mm)
Flow (m³/s)
Time (h)
2023-02-11
2023-02-12
2023-02-13
2023-02-14
2023-02-15
2023-02-16

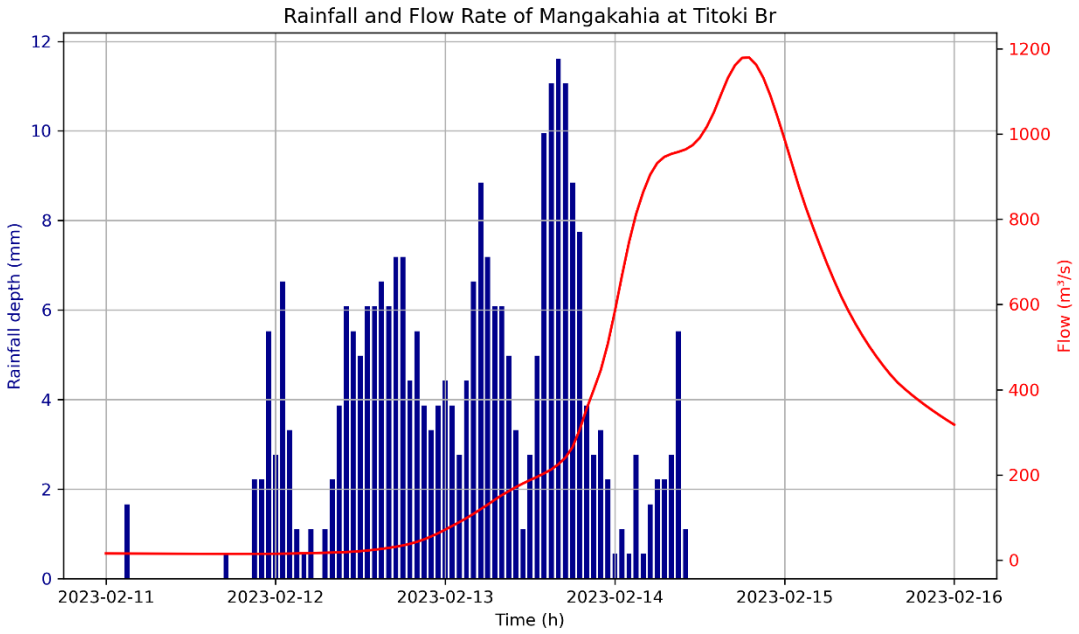
Rainfall and Flow Rate of Mangakahia at Titoki Br
Rainfall depth (mm)
Flow (m³/s)
Time (h)
0
2
4
6
8
10
12
0
200
400
600
800
1000
1200
2023-02-11
2023-02-12
2023-02-13
2023-02-14
2023-02-15
2023-02-16

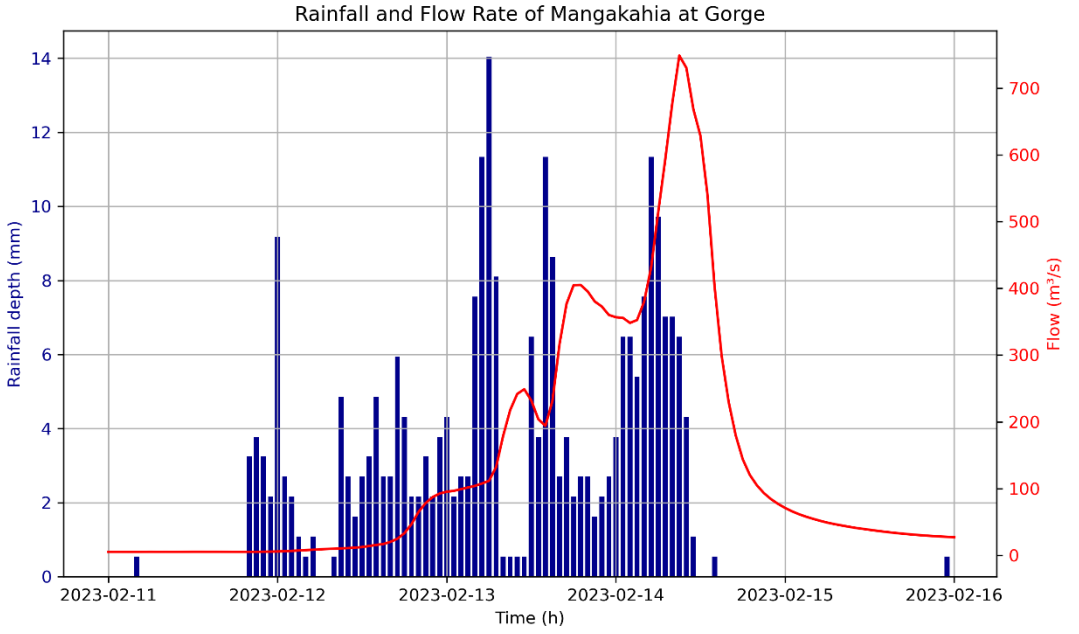
Rainfall and Flow Rate of Mangakahia at Gorge
Rainfall depth (mm)
Flow (m³/s)
Time (h)
0
2
4
6
8
10
12
14
0
100
200
300
400
500
600
700
2023-02-11
2023-02-12
2023-02-13
2023-02-14
2023-02-15
2023-02-16

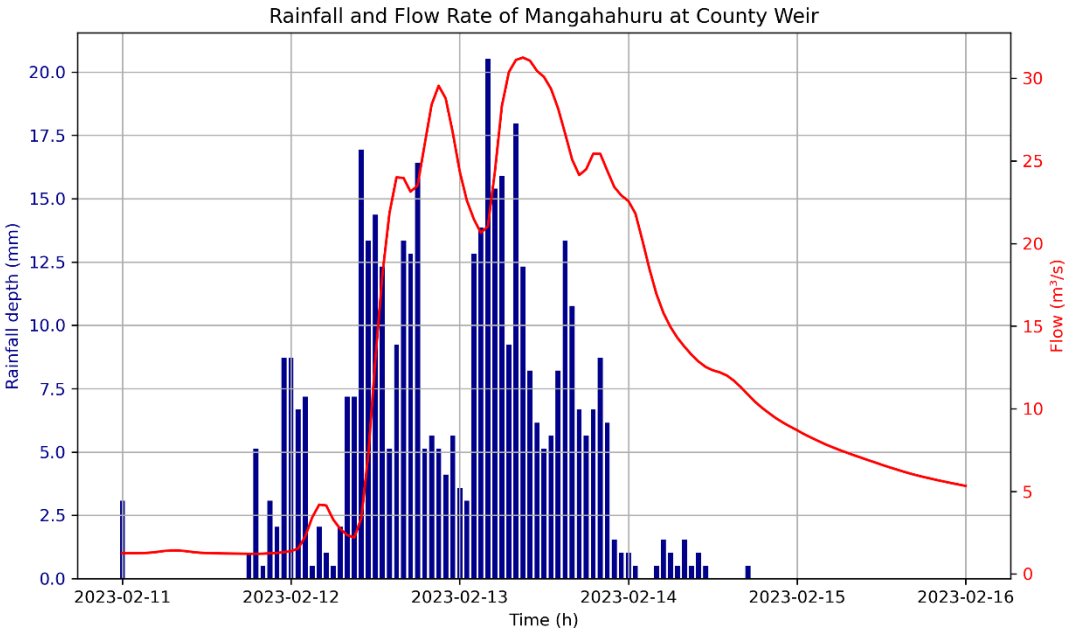
Rainfall and Flow Rate of Mangahahuru at County Weir
Rainfall depth (mm)
Flow (m³/s)
Time (h)
0.0
2.5
5.0
7.5
10.0
12.5
15.0
17.5
20.0
0
5
10
15
20
25
30
2023-02-11
2023-02-12
2023-02-13
2023-02-14
2023-02-15
2023-02-16

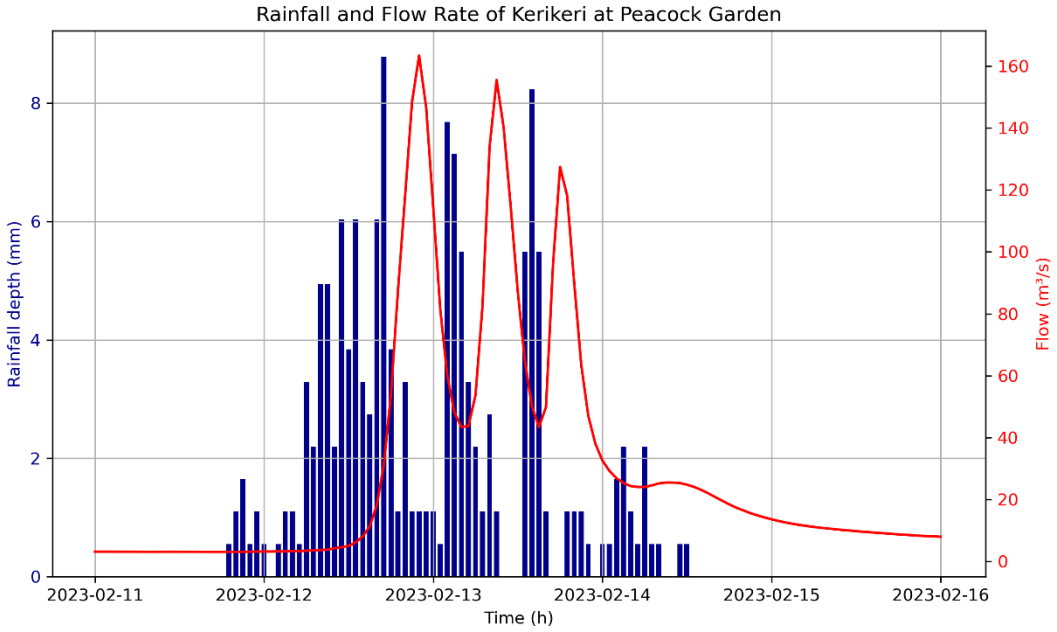
Rainfall and Flow Rate of Kerikeri at Peacock Garden
Rainfall depth (mm)
Flow (m³/s)
Time (h)
0
2
4
6
8
0
20
40
60
80
100
120
140
160
2023-02-11
2023-02-12
2023-02-13
2023-02-14
2023-02-15
2023-02-16

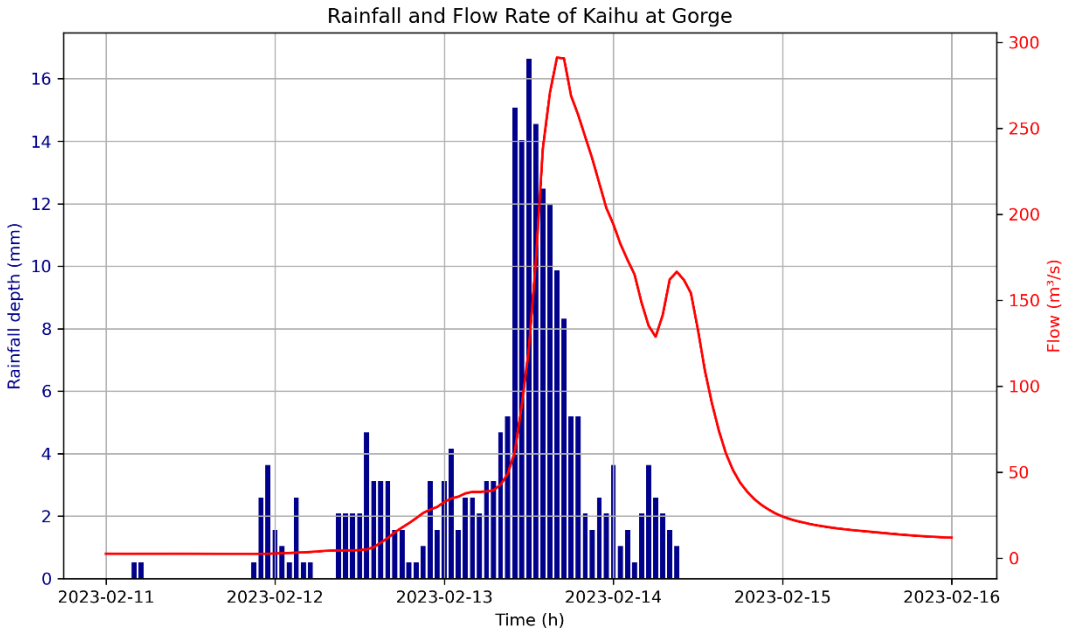
Rainfall and Flow Rate of Kaihu at Gorge
Rainfall depth (mm)
Flow (m³/s)
Time (h)
2023-02-11
2023-02-12
2023-02-13
2023-02-14
2023-02-15
2023-02-16

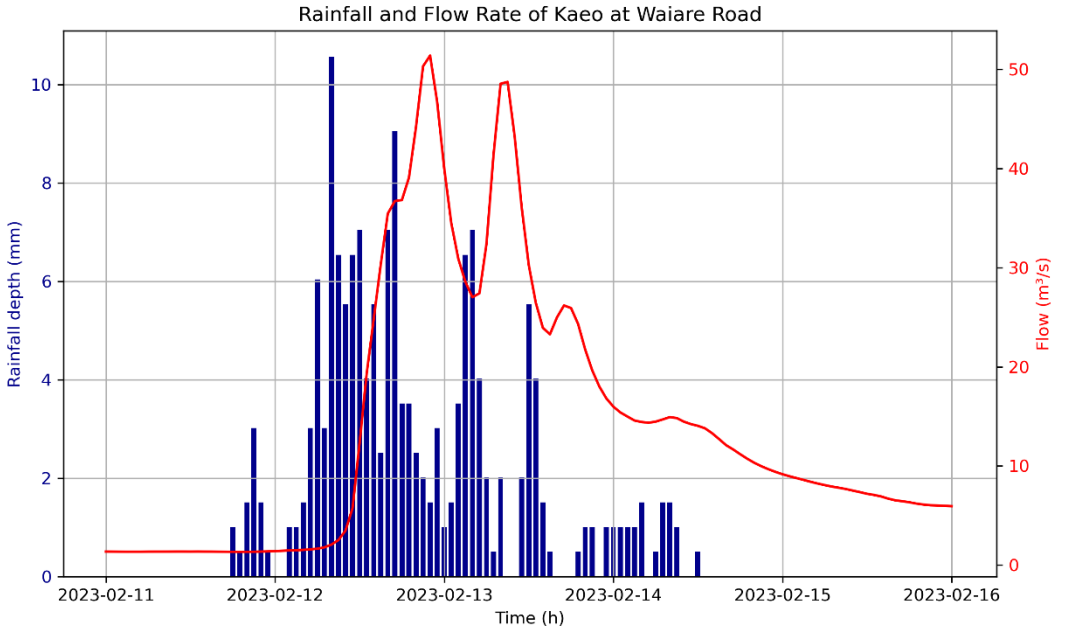
Rainfall and Flow Rate of Kaeo at Waiare Road
Rainfall depth (mm)
Flow (m³/s)
Time (h)
2023-02-11
2023-02-12
2023-02-13
2023-02-14
2023-02-15
2023-02-16

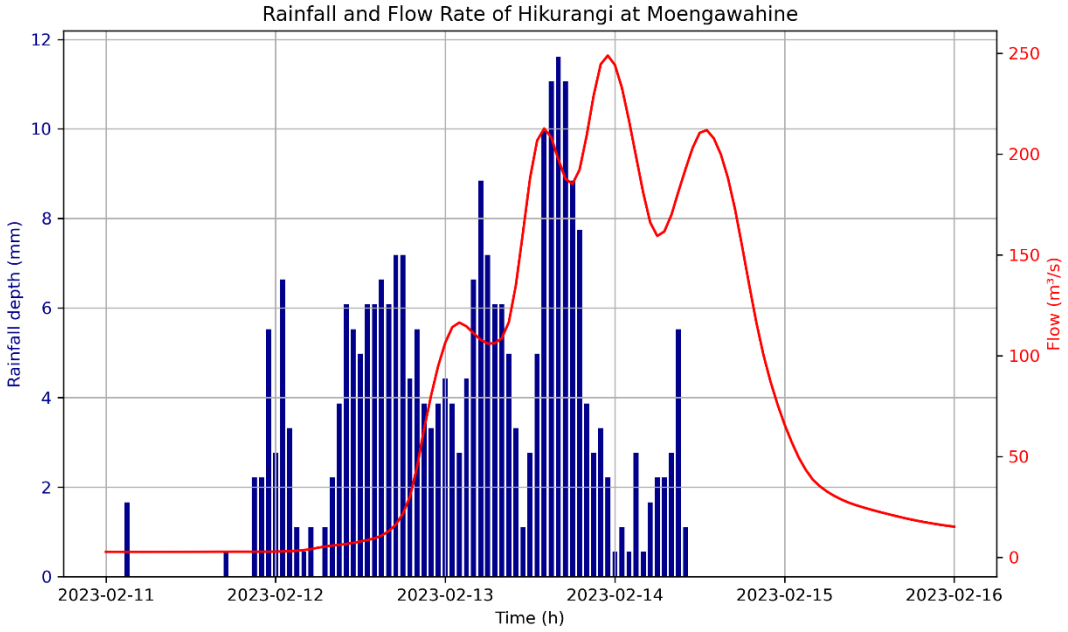
Rainfall and Flow Rate of Hikurangi at Moengawahine
Rainfall depth (mm)
Flow (m³/s)
Time (h)
0
2
4
6
8
10
12
0
50
100
150
200
250
2023-02-11
2023-02-12
2023-02-13
2023-02-14
2023-02-15
2023-02-16

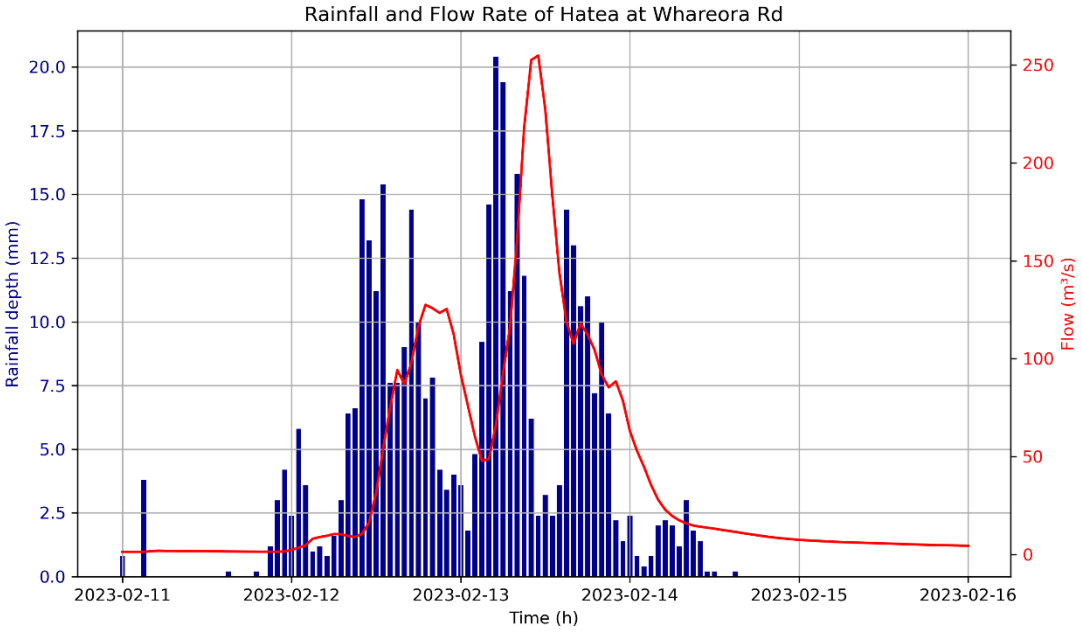
Rainfall and Flow Rate of Hatea at Whareora Rd
Rainfall depth (mm)
Flow (m³/s)
Time (h)
0.0
2.5
5.0
7.5
10.0
12.5
15.0
17.5
20.0
0
50
100
150
200
250
2023-02-11
2023-02-12
2023-02-13
2023-02-14
2023-02-15
2023-02-16

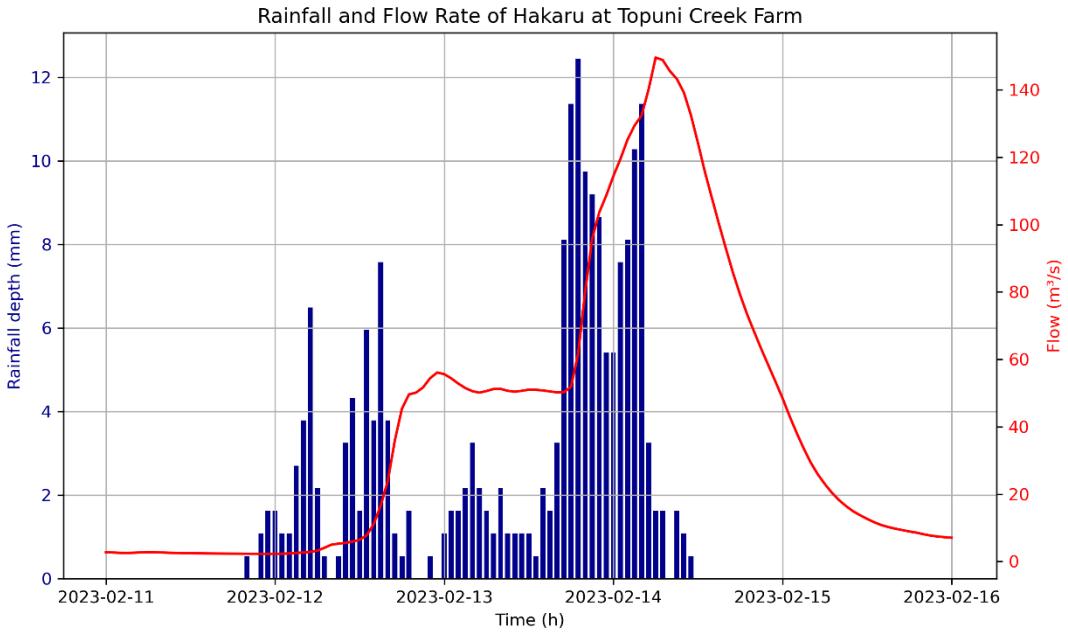
Rainfall and Flow Rate of Hakaru at Topuni Creek Farm
Rainfall depth (mm)
Flow (m³/s)
Time (h)
2023-02-11
2023-02-12
2023-02-13
2023-02-14
2023-02-15
2023-02-16

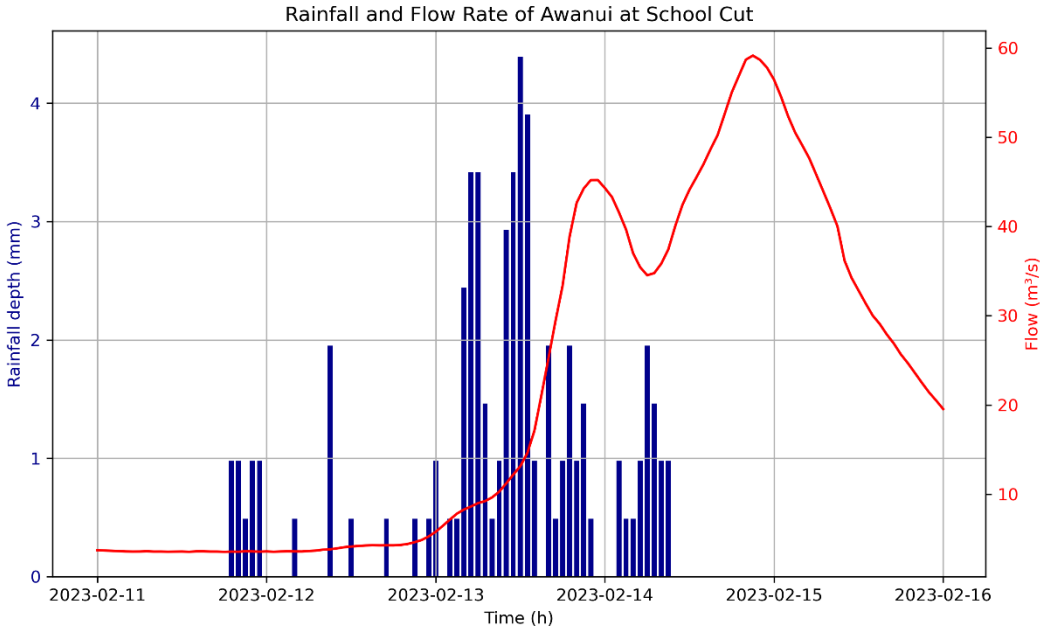
Rainfall and Flow Rate of Awanui at School Cut
Rainfall depth (mm)
Flow (m³/s)
Time (h)
2023-02-11
2023-02-12
2023-02-13
2023-02-14
2023-02-15
2023-02-16

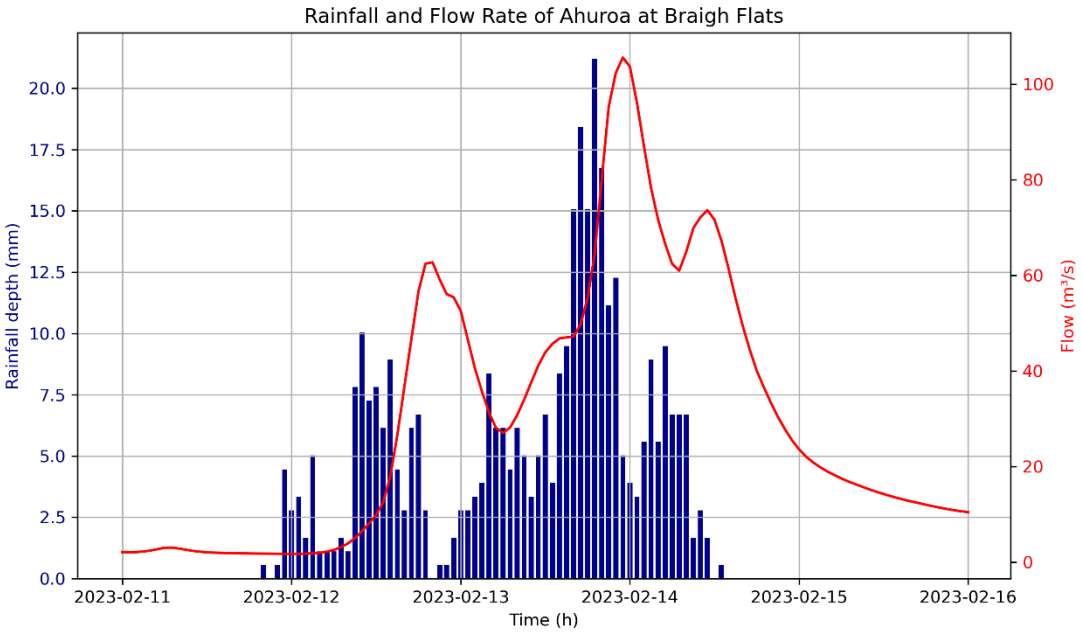
Rainfall and Flow Rate of Ahuroa at Braigh Flats
Rainfall depth (mm)
Flow (m³/s)
Time (h)
0.0
2.5
5.0
7.5
10.0
12.5
15.0
17.5
20.0
0
20
40
60
80
100
2023-02-11
2023-02-12
2023-02-13
2023-02-14
2023-02-15
2023-02-16

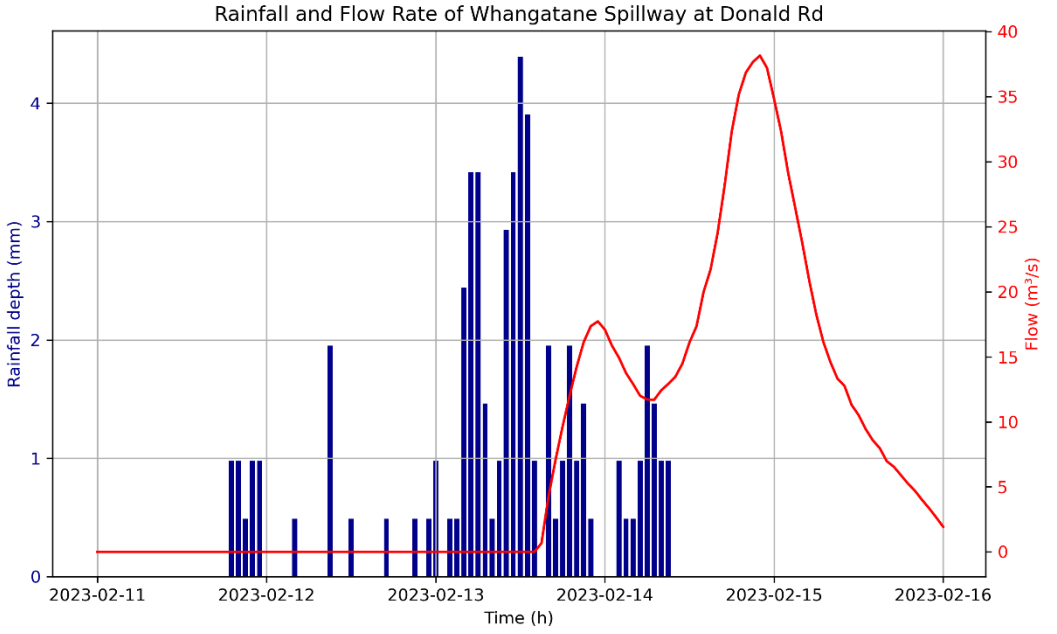
Rainfall and Flow Rate of Whangatane Spillway at Donald Rd
Rainfall depth (mm)
Flow (m³/s)
Time (h)
0
1
2
3
4
0
5
10
15
20
25
30
35
40
2023-02-11
2023-02-12
2023-02-13
2023-02-14
2023-02-15
2023-02-16